THEORETICAL STUDIES ON WHISTLER MODE WAVE-PARTICLE INTERACTIONS IN THE MAGNETOSPHERIC PLASMA

by

Hiroshi MATSUMOTO

December 1972

Department of Electrical Engineering
Kyoto University, Kyoto, Japan

THEORETICAL STUDIES ON
WHISTLER MODE WAVE-PARTICLE INTERACTIONS
IN THE MAGNETOSPHERIC PLASMA

by

Hiroshi MATSUMOTO

December 1972

Department of Electrical Engineering
Kyoto University, Kyoto, Japan

ACKNOWLEDGEMENTS

The author wishes to express his sincere and hearty appreciation to Professor Iwane Kimura for his continual guidance, inspiration and stimulating supervision throughout the present work and for his careful reading of the manuscript and to Professor Ken-ichi Maeda for his enthusiastic interest, helpful advice and encouragement.

The author also wishes to express his deep appreciation to Professors Susumu Kato, Toru Ogawa and Tatsuzo Obayashi, now Professor of University of Tokyo, for their useful discussion and enlightening criticism on the attitude and methods of a research during the course of the present work.

The author is grateful to Drs. Hiroshi Oya, Kazuaki Takao and Atsuhiro Nishida for their many discussion and stimulating suggestions.

The author is deeply grateful to Dr. Tetsuya Sato for his questions and comments which stimulated the investigation of a quasilinear cyclotron instability.

The author is indebted to all his associates in the Department of Electronics and Electrical Engineering, particularly to Mr. Takeo Matsumoto for his discussion and co-works of the computation in Chapter III, and to Messrs. Kaoru Mamiya, Sadao Miyatake, Kozo Hashimoto and Yoshiji Yamazaki for their discussion and co-studies including their master thesis investigations. He is also profited from Messrs. Shogo Yokoi and Makoto Kawai and is grateful for their assistance of some part of numerical calculations.

Thanks are also due to discussion with colleagues in the Department of Electrical Engineering and the Ionosphere Research Laboratory of Kyoto University, especially to discussion and assistance by Messrs. Toshiro Matsuo, Akira Nagao and Akira Kanemasa in drawing a part of the figures.

Numerical computations in the present work were all performed at the Data Processing Center of Kyoto University, Kyoto, Japan.

PREFACE

Within the last two decades, there has been a considerable progress in the physics of the fourth state of matter ——— Plasmas. Our present knowledge of the subject has been brought by many sources. It comes, in part, from the enthusiastic researches of plasma physicists and engineers after the realization of the controlled release of the thermonuclear energy as power sources for human life in the coming ages. It is also the results of tremendous theoretical and experimental studies of space science workers, including radio scientists, geophysicists and astronomers, in the quest for the better understanding of the environmental space of our mother planet, Earth. It is because the most matter in the universe is in the highly ionized state, i.e., the plasma state.

Before the advent of the space age, the activities of mankind were limited on the essentially two-dimensional husk of the earth against our desire and dream of space traveling and life therein. Since the satellite era, however, of the space age started on October 4 in 1957 when U.S.S.R. launched the Sputonik I, a rapidly increasing knowledge has been acquired about the physical properties of the extraterrestrial environment of the earth. Progressive experimental and theoretical studies refined the picture of our environmental space plasma. Now is it the well established concept that the earth's atmosphere extends upward in height from the basic ionosphere around 100 km to a more tenuous but more highly ionized plasma ——— the magnetosphere, and merges, smoothly or abruptly, with the interplanetary solar wind plasma beyond.

The magnetosphere ——— the region between the ionosphere and the outer boundary "magnetopause" ——— is filled with the highly ionized plasma pervaded with the strong magnetic field of the earth. Not only plays this region the role of the intermediate buffer defensive realm for our mild circumstances of the earth from the bombardment of the high energy solar corpuscular streams, but also is the treasure

house of the plasma instabilities containing plenty kinds of the fascinating plasma waves and their interactions with plasma particles.

Among these waves, VLF electromagnetic waves are most well known owing to the properties of being observable both on satellites and on the ground. The VLF electromagnetic waves are classified mainly into two kinds; one of them are those caused by the lightning discharges and well known as "whistlers"; the others are those which are believed to be produced by the wave-particle interactions in the magnetosphere and termed as "VLF emissions". The propagation characteristics of these VLF waves are now rather well understood by the established linear theories of the wave propagations in plasmas. The generation mechanisms of these VLF emissions, however, have been less well understood quantitatively so far because of their nonlinear characteristics and still offer one of the most incentive problems not only in the physics of the magnetosphere but also in the nonlinear theories of the plasma instabilities. In the past twenty years, we have progressed a long way in the space research, which has, fortunately, been accompanied with the development of the plasma physics. Both the space and plasma physics have really been quite complementary each other. We can see this, as an example, also in the problem of the VLF emissions. The established theories of the radiation from charged particles and of the instabilities were applied in understanding the phenomena, while, on the other hand, the VLF phenomena have been instructive, inspirative and ideal stimuli for the development of the theories of the propagation and instabilities of the electromagnetic mode in plasmas because the electromagnetic waves and their relevant instability phenomena are difficult to be realized in the laboratory plasma experiments due to many restrictions.

The aim of this thesis is to present theoretical investigations on the linear and nonlinear behavior of the cyclotron interaction which takes place between the whistler mode electromagnetic waves and charged particles, especially electrons, in a magneto-active plasma. As their applications, also given are the theoretical considerations of the generation mechanisms of the VLF emissions emanating from the magnetosphere.

This work was first initiated as an extension of the VLF theoretical

research which has been promoted by Kimura whose works had made constitute one of the main cores of the world VLF researches. At the early stage of the investigation, a linear theory of the whistler mode cyclotron instability was re-examined. Though one often heard that the era of the linear treatments of the plasma instabilities had been over, many quantitative problems were found to be left for the investigations of the VLF emissions. Attention was then concentrated on the nonlinear behaviors of those plasma instabilities. Although general nonlinear treatments had been developed by the plasma physicists by a rather sophisticated approaches, the nonlinear study of the concrete VLF problems had hardly been performed. This is because that such nonlinear phenomena of the electromagnetic waves were rather less known to laboratory plasma physicists and, on the other hand, the VLF workers have the disadvantage (or advantage) of having too many, complex and various data of emissions. Under such a background, the rest part of the present work was taken up with the studies of certain aspects of the nonlinear behaviors of the electromagnetic whistler mode cyclotron interactions and with their applications to the nonlinear phenomena of the VLF emissions. Before the author, there were not too many VLF data fortunately (or unfortunately) to construct theories, which makes him free in theoretical considerations from many restrictions brought by too much sophisticated phenomena.

We hope that the present theoretical study on the whistler mode wave-particle interactions in both linear and nonlinear regimes will more or less contribute to the advance of space probing by a whistler mode electromagnetic wave in the future. It is also an unexpected pleasure if the present work should stimulate the further theoretical studies on the more interesting and complex problems of the wave excitation and propagation in a plasma.

All equations and quantities are in the rationalized MKS systems of units unless otherwise mentioned.

LIST OF ILLUSTRATIONS

LIST OF TABLES

SYMBOLS AND NOMENCLATURES

f	: frequency
$\omega \equiv 2\pi f$ $\equiv \omega_r + j\omega_i$ $\equiv \omega_r + j\gamma$	: angular frequency
ω_r	: real part of ω; angular frequency
ω_i	: growth or damping rate
γ, γ_k	: growth or damping rate
k, $\vec{k}$	: wave number, wave number vector
$n = ck/\omega$	: refractive index
ω_c	: characteristic frequency
κ_A	: Attenuation constant
$f_p = \Pi_e/2\pi$	: electron plasma frequency
$f_H = \Omega_e/2\pi$	: electron cyclotron frequency
f_{Ho}	: electron cyclotron frequency at the equator
$\Pi_s = (N_s q_s^2/m_s \varepsilon_o)^{\frac{1}{2}}$	: plasma (angular) frequency for charged particles of kind s (s = e, i)
$\Omega_s = \lvert q_s \rvert B_o/m_s$	: cyclotron (angular) frequency for charged particles of kind s (s = e, i)
N	: number density of plasma particles
N_s	: number density of the s-th plasma particles (s=e for electrons and s=i for ions)
$\vec{B}_o$	: external magnetic field
m_s	: mass of the s-th particle
q_s	: charge of the s-th particle
ε_s	: sign of charge of charged particles of kind s
$\varepsilon_o = 8.854 \times 10^{-12}$ F/m	: permittivity of free space
$\mu_o = 1.257 \times 10^{-6}$ H/m	: permeability of free space
$\kappa = 1.381 \times 10^{-23}$ J/°K	: Boltzmann constant
r_L	: Larmor radius of electrons
λ_D	: Debye (shielding) length
ν_{en}	: collision frequency between electrons and neutral particles
ν_{ei}	: collision frequency between electrons and ions

$P \equiv f_p/f_H = \Pi_e/\Omega_e$	: plasma parameter
$T_\perp$	: temperature in the perpendicular direction to $\vec{B}_o$
$T_\parallel$	: temperature in the parallel direction to $\vec{B}_o$
$A \equiv T_\perp/T_\parallel$	: temperature anisotropic factor
$D(\omega,k)$	: algebraic expression which gives a dispersion equation $D(\omega,k) = 0$.
R_o, L_o, S_o, D_o and P_o	: conventional notations corresponding to the popular R, L, S, D, and P in the textbook by Stix[25]
$\vec{v}$, $\vec{V}$	: velocity
$V_\perp$, $v_\perp$	: velocity component perpendicular to $\vec{B}_o$
V_z, v_z	: velocity component parallel to $\vec{B}_o$
V_{ph}	: phase velocity
V_g	: group velocity
V_s	: signal velocity
V_D	: drift velocity of the instability region
V_T	: thermal velocity
V_R	: resonance velocity
ΔV_R	: velocity spread of resonance
ϕ	: Larmor phase angle
ζ	: Larmor phase angle
$\alpha = \tan^{-1}(V_\perp/V_z)$	: pitch angle
θ	: angle between $\vec{k}$ and $\vec{B}_o$; $\theta \equiv \omega t - kz$
t	: time
T_B	: bunching time
$\gamma_o = (1-V^2/c^2)^{-\frac{1}{2}}$	: relativistic factor
$s(t,z)$	: wave intensity at a time t and a position z
$\vec{B}$, $\vec{B}_w$	: wave magnetic field
$\vec{E}$, $\vec{E}_w$	: wave electric field
W_p	: kinetic energy density of particles
ΔW_p	: increment of W_p
$\langle W_p \rangle$	: mean value of W_p over the distribution function
$W_{p\parallel}$	: kinetic energy density of particles in the direction parallel to $\vec{B}_o$
$W_{p\perp}$	: kinetic energy density of particles in the direction perpendicular to $\vec{B}_o$

$W_w = \varepsilon_{wave} + \varepsilon_T$: wave energy density

ε_{wave} : wave field energy density

ε_T : kinetic energy density of thermal plasma particles associated with a wave

$\varepsilon_k = \frac{1}{2}\varepsilon_o |E_k|^2$: electric field energy density

ε_{rz} : kinetic energy density of resonant electrons in the direction parallel to $\vec{B}_o$

$\varepsilon_{r\perp}$: kinetic energy density of resonant electrons in the direction perpendicular to $\vec{B}_o$

$E_R = \frac{1}{2} m V_R^2$: kinetic energy corresponding to V_R

$F_a(\vec{V},\vec{r},t)$: velocity distribution function of the ambient plasma

$F_b(\vec{V},\vec{r},t)$: velocity distribution function of beam electrons

$F_s(\vec{V},\vec{r},t)$: velocity distribution function of the s-th plasma particles (s=e,i)

$f_s(\vec{V},\vec{r},t)$: perturbation of the velocity distribution function

$g_s(\vec{V},t)$: background (zero order) velocity distribution function of the s-th plasma particles (s=e,i)

$h_s(V_\perp)$: arbitrary distribution function in the perpendicular direction

$F_o(V_z) \equiv \int_0^\infty V_\perp dV_\perp F(V_z,V_\perp)$: averaged velocity distribution over $V_\perp$

$g_o(V_z) \equiv \int_0^\infty V_\perp dV_\perp g(\vec{V},t)$: averaged velocity distribution function over $V_\perp$

$G(\alpha_o) \equiv F(V_R - \alpha_o/k, V_\perp)$

$G_o(\alpha_o) \equiv \int_0^\infty V_\perp dV_\perp G(\alpha_o)$

G_s : $\equiv \frac{\partial g_s}{\partial V_\perp} + \frac{k}{\omega}\left(V_\perp \frac{\partial g_s}{\partial V_z} - V_z \frac{\partial g_s}{\partial V_\perp} \right)$

V_B, V_{Bz} : parallel velocity component of beam electrons

$V_{B\perp}$: perpendicular velocity component of beam electrons

η_j : ratio of the j-th particle density to the total density

n_o, n_j : index of enhanced anisotropy of the loss cone distribution function

α_L : loss cone angle

∇_v : $\equiv \frac{\partial}{\partial V_\perp} - \frac{kV_\perp}{\epsilon_s \Omega_s} \frac{\partial}{\partial V_z}$

$\delta(x)$: Dirac's delta function

$\hat{x},\hat{y},\hat{z},\hat{r},\hat{\phi}$: unit vectors

$\vec{J}$: current density

R_E : mean radius of the earth = 6371 km

L : McIlwain's L-value

K_p : index of geomagnetic activity

R : geocentric distance

Φ : geomagnetic latitude

CONTENTS

Chapter I

GENERAL INTRODUCTION

As a general introduction of the present thesis, we begin in this chapter with a short review of the materials of the investigation. Recently developed knowledge of the magnetospheric plasma surrounding the earth is first briefly described as a background medium of the wave-particle interactions of the present interest. Electromagnetic waves, especially the whistler mode waves, in the magnetosphere are then briefly described paying a special attention to triggered VLF emissions. A general and quick review of the previous theories of the VLF emissions is then presented as well.

§1. The Magnetosphere

The magnetosphere is the surrounding volume space of our earth and is filled with both neutral hydrogens and ionized particles, mainly protons and electrons (King et. al.[1]; Carovillano et. al.[2]; Williams et. al.[3]; McCormac[4]; Obayashi[5]). This region is pervaded with an earth's magnetic dipole field, the static energy of which is strong compared with the plasma kinetic energy so that the distribution and behavior of the plasma constituents are under the dominant control of the magnetic field. It extends from the top of the ionosphere to the outer boundary "magnetopause". The outer boundary is variable and complicated and has a maximum and minimum length along the earth-sun line. In the solar direction, the geocentric distance is roughly 10 earth radii but the length in the anti-solar direction is unknown and is estimated to range from hundreds of earth radii to some astronomical units. We can now find out many artist drawings of the magnetosphere inferred from the satellite data in the literatures[1~5]. We present here one of the most typical model drawings (Ness[6]) in Fig.1 for the sake of a better understanding of the physical situation of the present concern.

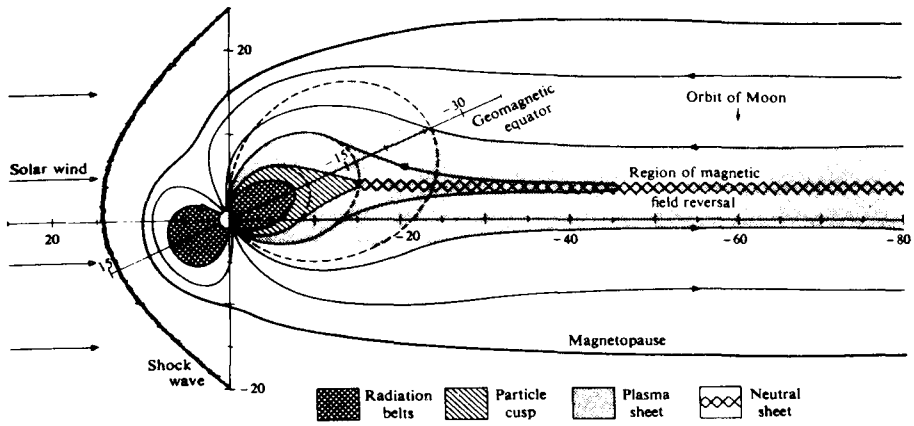

Fig.1 An Artist Drawing of the Model Magnetosphere
(from Ness[6])

Necessary physical quantities that should be kept in mind in considering theories of the whistler mode wave-particle interactions are in the followings; (1) the magnetic field intensity (or the electron cyclotron frequency), (2) the thermal electron density and temperature (including the anisotropy factor $A \equiv T_{\perp} / T_{\parallel}$), (3) the distribution function of suprathermal particles, especially electrons, and (4) the collision frequency of electrons with neutral particles and ions, etc.. We could not, of course, give a complete representative map of those quantities at the present stage due to the lack of data, but we discuss and present here plausible models of the distributions and profiles of those quantities in the magnetosphere in preparation for the following chapters.

1.1 Magnetic Field

As seen in Fig.1, the earth's magnetic field is compressed and deformed from a dipole field by the interaction with a continuously flowing plasma in the interplanetary space, the solar wind. An average magnetic field configuration in the outer magnetosphere is shown in Fig.2 (Fairfield[7]). Inside the geocentric distance 5 R_E (earth radii), however, the geomagnetic field is well approximated to be dipolar, which is illustrated in Fig.3 with contours of the corresponding cyclotron frequencies (Helliwell[8]). It is convenient to use the L-shells and invariant latitudes proposed by McIlwain[9] for a description of the magnetic field lines in this dipolar region. The electron cyclotron frequency

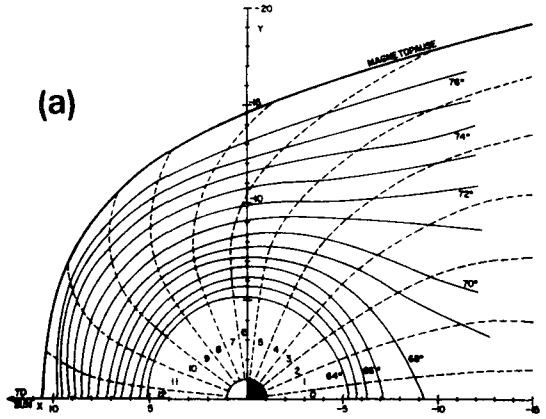

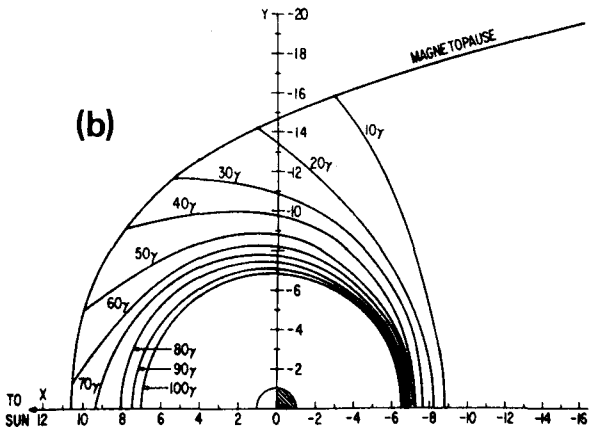

Fig.2 Contours of the Magnetic Field of the Earth in the Equatorial Plane. In the above figure (a), solid lines designate the latitude of origin of the field lines through that location, while the dashed lines show the local time of the foot of the blown field lines. The lower figure (b) indicates the contours of constant magnitude in the equatorial plane. (from Fairfield[7]).

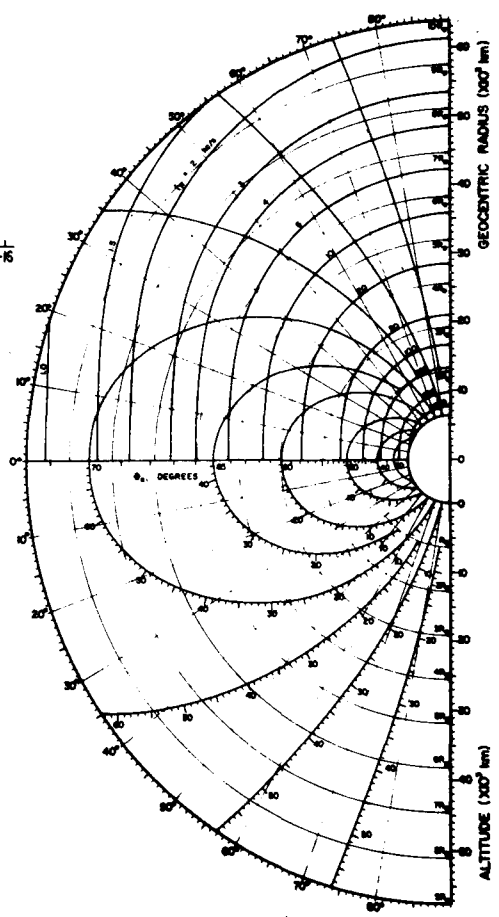

Fig.3 A Dipole Field of the Earth in the Noon-Midnight Cross Section. (from Helliwell[8])

f_H in this region is expressed as

$$f_H = f_{Heq}(R_E/ R)^3(1 + 3\sin^2\Phi)^{\frac{1}{2}} , \qquad (1.1)$$

where f_{Heq}, R and Φ are the electron cyclotron frequency on the surface of the earth in the equator, the geocentric distance and the geomagnetic latitude, respectively.

1.2 Density and Temperature of Thermal Plasma

The extensive studies (Carpenter[10]; Angerami & Carpenter[11]; Carpenter[12]) of the whistler knee provided the electron density profiles in the equatorial plane and clarified the existence of a boundary called "plasmapause", which divides the magnetosphere into two regions. An inner region is filled with a relatively quiet and high density plasma which can be described by a diffusive equilibrium model along the geomagnetic field lines. This region has a form of distorted torus and is called the "plasmasphere". We know at present that the electron density decreases

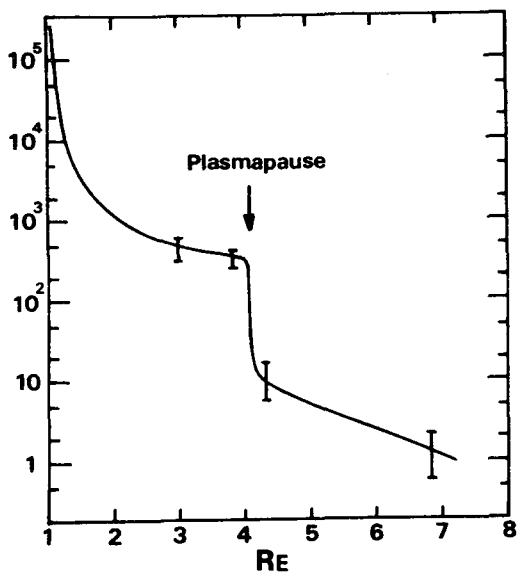

Fig.4 Equatorial Electron Density Profile as a Function of Geocentric Distance Deduced from Whistler Data (combined from Smith[13] and Angerami[14]).

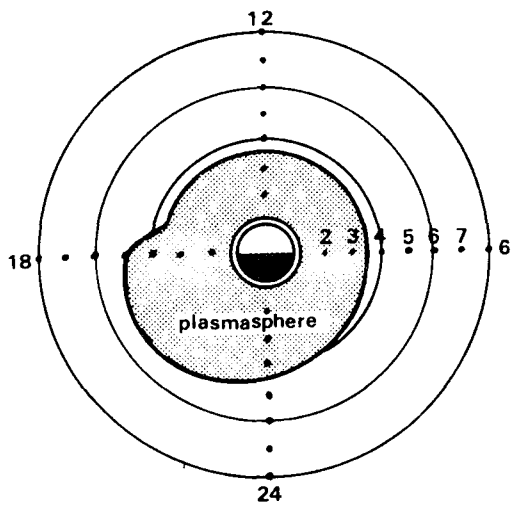

Fig.5 Projection on the Equatorial Plane of the Plasmapause (from Carpenter[12]).

in proportion to $R^{-3\sim-4}$ in this region up to the plasmapause. Beyond the plasmapause, the plasma density falls down abruptly from $10^2/cm^3$ to $1 \sim 10/cm^3$. This region is called the "plasmatrough". A typical equatorial electron density profile and the projection on the equatorial plane of the plasmapause deduced from the whistler data are illustrated in Fig.4 (Smith[12]; Angerami[14]) and in Fig.5 (Carpenter[12]) respectively.

These whistler data have recently been substantiated by a plenty of in situ measurements by the ion retarding potential analyzer (RPA) and the ion mass spectrometers. An example of the ion density distribution observed by the in situ measuements is given in Fig.6 (Harris et. al.[15]).

With regard to the electron temperature in the magnetosphere, we have not yet ample data compared with the data of the electron densities. Reviews of the ionospheric temperature measurements are given in detail by Gringauz[16] and Evans[17]. The in situ measurements of the magnetospheric temperature, however, were performed only by the ion RPA on IMP-1 and 2 (Serbu & Maier[18]). Fig.7 is an illustration of the typical temperature profiles both on the dayside and the nightside in the magnetosphere, which is re-arranged from Fig.4 in Serbu & Maier[18]. As seen in the figure, the electron (and ion) temperature increases as L increases with an approximate functional relation $T_e \propto L^2$ (Serbu & Maier[19]) until an abrupt and large temperature increase occurs within less than $0.1R_E$ at the plasmapause up to the order of 10^5°K by a factor of 5 to 10. It is also apparent that the temperature on the darkside is lower than that on the dayside by a factor of 2 or 3. A problem should, however, be kept in mind whether the quantity of the "temperature", which is determined from the characteristics of the ion RPA by assuming the velocity distribution function as the Maxwellian or the sums of the Maxwellians (i.e., from the simple application of the Langmuir theory), is proper or not for the theoretical studies of the wave-particle interactions in the plasma outside the plasmapause.

Temperature anisotropy factor $A \equiv T_\perp/T_{||}$ has not unfortunately been measured successfully, where $T_\perp$ and $T_{||}$ are the temperatures in the perpendicular and the parallel directions to the geomagnetic field, respectively. In this context, the study of the wave-particle interactions comes to have its meanings of the prediction and supplementation of these

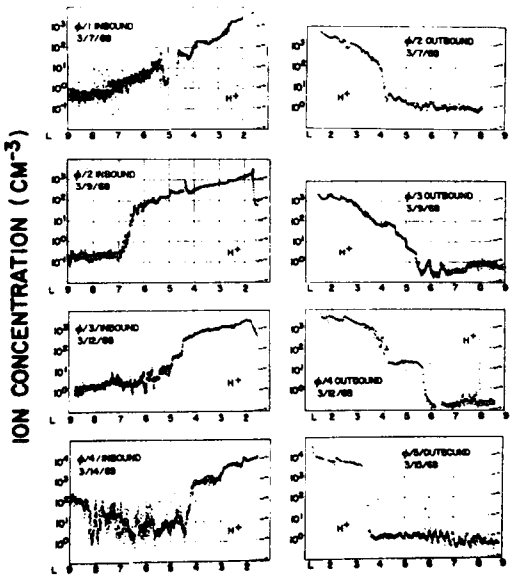

Fig.6 Ion Concentration Profiles Deduced from the Ion Spectrometer of OGO-5 (from Harris et. al.[15]).

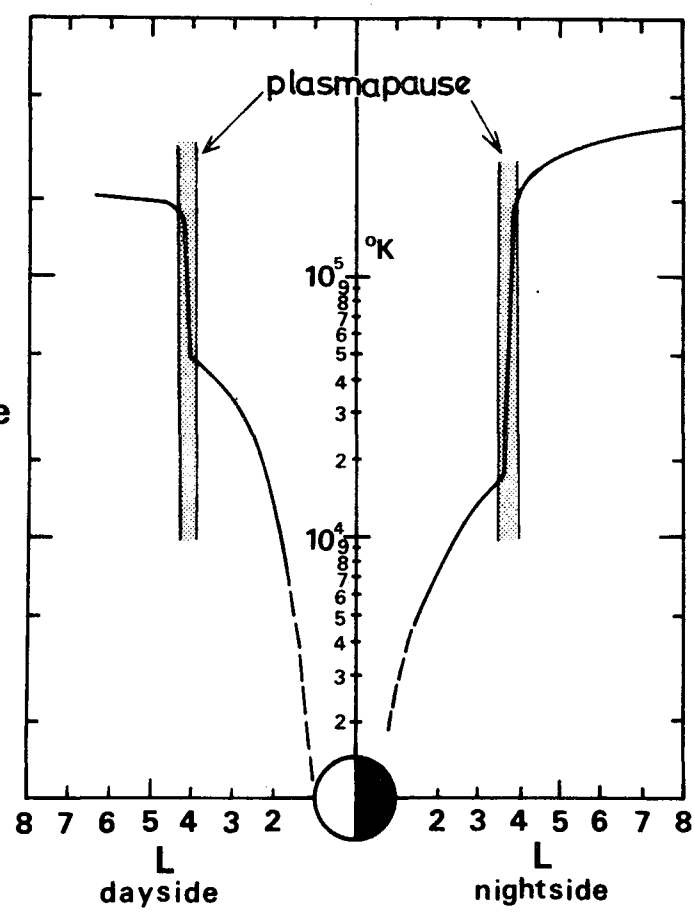

Fig.7 Temperature Profiles near the Equatorial Plane in the Magnetosphere. (rearranged from Fig.4 in Serbu & Maier[18])

observations.

1.3 Suprathermal Particles

It was the first surprise at the early stage of the space research to discover the existence of the suprathermal charged particles (i.e., the Van Allen belt) in and around our magnetosphere. At present, however, a comprehensive concept of various high energy particles is established and the inter-relations between different domains of high energy particles are now well understood (O'Brien[20]; Obayashi[5]; Hess[21]). Three dimensional distributions of the high energy particles in and around the magnetosphere are presented in Fig.8 (from Obayashi[5]).

The region of the present interest of the whistler mode wave-particle interactions lies around the plasmapause. Recently, a relation between the plasmapause, the plasmasheet and the Van Allen belt was investigated (Schield & Frank[22]; Frank[23]). The differential electron fluxes from

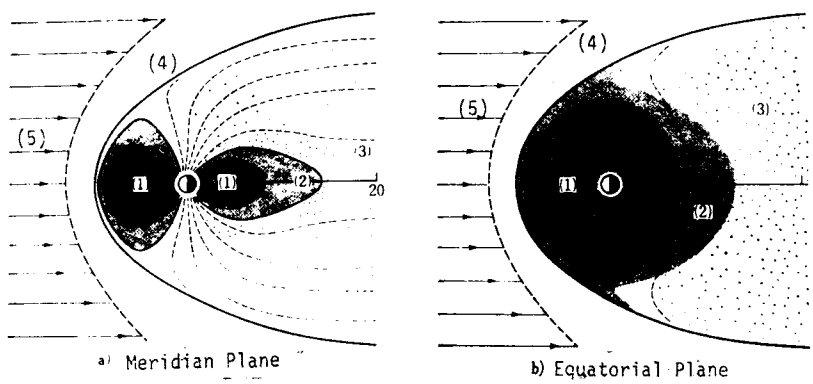

Fig.8 Distribution and Classification of High Energy Particles in and around the Magnetosphere. (from Obayashi[5]) (1) Van Allen particles (Trapped particles), (2) Auroral particles (Quasi-trapped particles), (3) Plasma sheet particles, (4) Magnetosheath particles, and (5) Solar Wind particles.

inside the plasmapause to the plasmasheet were observed by the electrostatic analyzers aboard the OGO-3. Their results are illustrated in Fig.9. The uppermost figure shows the directional differential intensities of electrons in each channel as a function of the magnetic shell parameter L. We can know from the middle panel that the earthward edge of the plasmasheet is characterized by exponential decrease in electron energy densities with decreasing L. An interesting feature can be

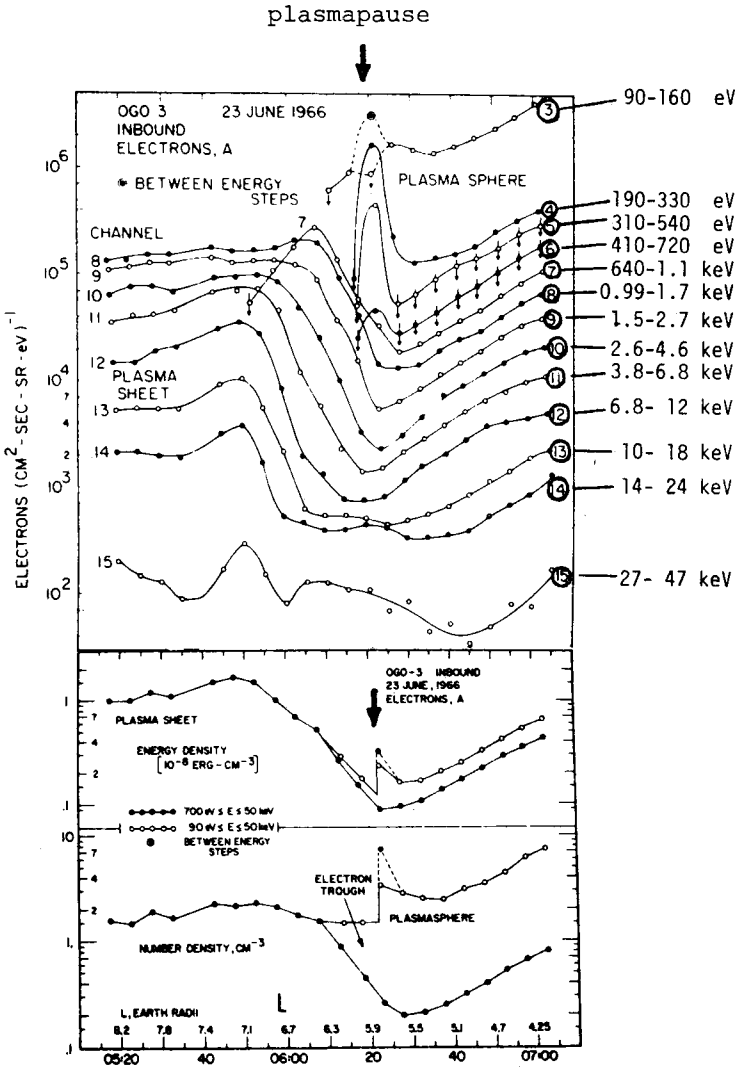

Fig.9 Directional, Differential Flux Intensities, Energy Density and Number Density of the High Energy Electrons in the Magnetosphere from L=8.2 to 4.2 by OGO-3. (from Schield & Frank[22])

derived from the lower two panels that although the electron intensities between 90 to 700 eV contribute negligibly to the energy density, these electrons are sufficiently much to maintain an almost constant number density of $N \sim 1/cm^3$ in the region inside $L \sim 6.4$. It is also very much interesting from the view point of the whistler mode wave-particle interactions that there is a dramatic increase of lower energy electrons with peak intensity around 100eV just around the plasmapause (see Fig.9; uppermost figure). This characteristic will be mentioned in some

detail in Chapter II in conjunction with the linear cyclotron instability in the whistler mode.

1.4 Other Plasma Parameters

We cast a spotlight here on the necessary plasma parameters in considering the whistler mode wave-particle interactions in the magnetosphere. We have seen hitherto the model distributions of B_o, N_e, T_e and the suprathermal particles, especially of electrons. From these informations are available almost all of the necessary parameters such as the electron plasma frequency f_p, the electron cyclotron frequency f_H, the ratio of f_p to f_H ——— we call this quantity a "plasma parameter" ——— $P \equiv f_p / f_H$, the Debye length λ_D and the electron Larmor radius r_L by the following practical formulae;

$$f_p = 8.98 \sqrt{N_e} \quad \text{(kHz)} , \tag{1.2}$$

$$f_H = 2800\, B_o \quad \text{(kHz)} , \tag{1.3}$$

$$P = 3.2 \frac{\sqrt{N_e}}{B_o} \times 10^{-3} , \tag{1.4}$$

$$\lambda_D = 6.9 \sqrt{T_e / N_e} \times 10^{-2} \quad \text{(m)} , \tag{1.5}$$

$$r_L = 3.1 \frac{\sqrt{T_e}}{B_o} \times 10^{-4} \quad \text{(m)} , \tag{1.6}$$

where N_e, T_e and B_o are measured in conventional units of [cm^{-3}], [°K] and [Gauss] respectively.

Other than these, a collision frequency is an important parameter that should be kept in mind. Since the number density of the neutral particles (mainly hydrogens) in the magnetosphere is no larger than the ion density, the electron-neutral collisions are negligible compared with the long-range Coulomb electron-ion collisions. Actually ν_{en} becomes less than ν_{ei} above the altitude of 300 km. ν_{ei} is determined by the following Nicholet[24] formula :

$$\nu_{ei} = \left(34 + 8.36 \log_{10} \frac{T_e^{\frac{3}{2}}}{\sqrt{N_e}} \right) N_e T_e^{-\frac{3}{2}} \quad [\sec^{-1}] \quad . \qquad (1.7)$$

Profiles of these parameters in the equatorial plane are calculated using Figs.2, 3, 4 and 7 and are illustrated in Figs.10 and 11. As seen in the figure, the plasma characteristics change drastically at the boundary of the plasmasphere, the plasmapause. Also are tabulated these typical parameters in Table 1.

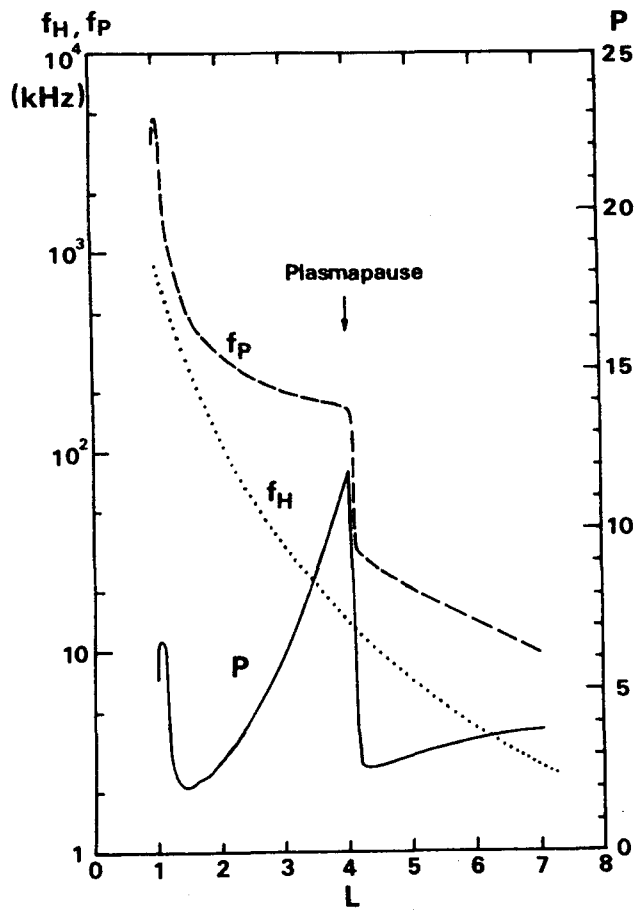

Fig.10 Equatorial Profiles of f_p, f_H and P as a Function of L.

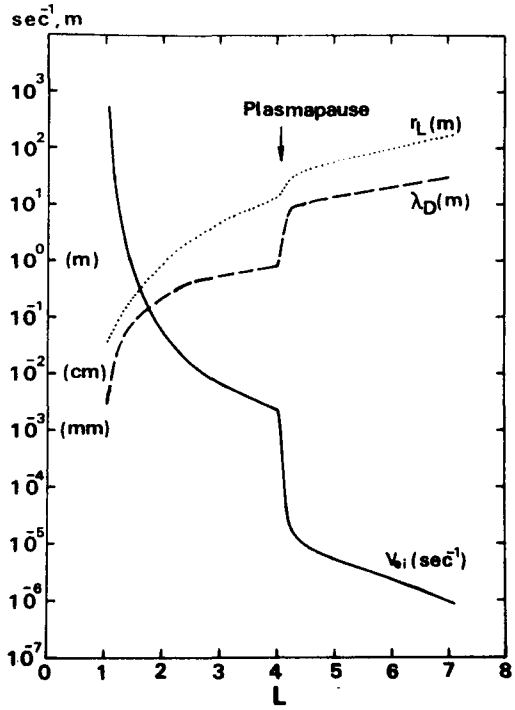

Fig.11 Equatorial Profiles of ν_{ei}, λ_D and r_L as a Function of L.

Table 1. Typical Magnetospheric Plasma Parameters.

R	N_e	T_e	T_e	<v>	B_o	f_H	f_p	P	ν_{ei}	λ_D	r_L
[R_E]	[cm^{-3}]	[°K]	[eV]	[km/s]	[Gauss]	[kHz]	[kHz]		[sec^{-1}]	[m]	[m]
1.05	3.0×10^{5}	1.0×10^{3}	0.09	174	2.72×10^{-1}	762	4920	6.46	4.6×10^{2}	0.0040	0.036
1.10	1.8×10^{5}	1.5×10^{3}	0.13	213	2.36×10^{-1}	661	3810	5.76	1.6×10^{2}	0.0063	0.051
1.15	5.0×10^{4}	1.7×10^{3}	0.15	227	2.07×10^{-1}	580	2010	3.47	3.9×10^{1}	0.013	0.062
1.20	2.2×10^{4}	2.0×10^{3}	0.17	246	1.82×10^{-1}	510	1330	2.61	1.4×10^{1}	0.021	0.077
1.30	9.0×10^{3}	2.7×10^{3}	0.23	286	1.43×10^{-1}	401	852	2.12	3.9×10^{0}	0.038	0.11
1.40	5.0×10^{3}	3.8×10^{3}	0.33	339	1.15×10^{-1}	322	635	1.97	1.4×10^{0}	0.060	0.17
1.50	3.3×10^{3}	5.0×10^{3}	0.43	389	9.31×10^{-2}	261	516	1.98	6.1×10^{-1}	0.085	0.24
1.60	2.6×10^{3}	6.0×10^{3}	0.52	427	7.67×10^{-2}	215	458	2.13	3.8×10^{-1}	0.11	0.32
1.80	1.6×10^{3}	9.4×10^{3}	0.81	534	5.39×10^{-2}	151	359	2.38	1.2×10^{-1}	0.17	0.56
2.00	1.3×10^{3}	1.3×10^{4}	1.12	628	3.93×10^{-2}	110	324	2.95	6.4×10^{-2}	0.22	0.91
2.50	7.0×10^{2}	2.3×10^{4}	1.98	835	2.01×10^{-2}	56.3	238	4.23	1.5×10^{-2}	0.40	2.4
3.00	5.0×10^{2}	3.3×10^{4}	2.84	1000	1.16×10^{-2}	32.5	201	6.18	6.6×10^{-3}	0.56	4.9
3.50	4.0×10^{2}	4.1×10^{4}	3.53	1110	7.33×10^{-3}	20.5	180	8.78	3.9×10^{-3}	0.70	8.7
4.00	3.2×10^{2}	4.8×10^{4}	4.14	1210	4.91×10^{-3}	13.8	161	11.7	2.5×10^{-3}	0.85	14.0
4.10	5.0×10^{1}	7.0×10^{4}	6.03	1460	4.56×10^{-3}	12.8	63.5	4.96	2.4×10^{-4}	2.6	18.2
4.20	1.2×10^{1}	1.2×10^{5}	10.3	1910	4.24×10^{-3}	11.9	31.1	2.61	2.7×10^{-5}	6.9	25.6
4.30	1.0×10^{1}	1.7×10^{5}	14.7	2270	3.95×10^{-3}	11.1	28.4	2.56	1.4×10^{-5}	9.0	32.6
4.40	9.0×10^{0}	1.8×10^{5}	15.5	2340	3.69×10^{-3}	10.3	26.9	2.61	1.1×10^{-5}	9.8	36.0
4.50	8.0×10^{0}	1.9×10^{5}	16.4	2400	3.45×10^{-3}	9.7	25.4	2.62	9.3×10^{-6}	10.6	39.6
4.60	7.0×10^{0}	2.0×10^{5}	17.2	2460	3.23×10^{-3}	9.0	23.8	2.64	7.6×10^{-6}	11.7	43.3
4.80	6.0×10^{0}	2.1×10^{5}	18.1	2520	2.84×10^{-3}	8.0	22.0	2.75	6.1×10^{-6}	12.9	50.5
5.00	5.2×10^{0}	2.1×10^{5}	18.1	2520	2.51×10^{-3}	7.0	20.5	2.93	5.3×10^{-6}	13.9	57.0
5.50	3.5×10^{0}	2.2×10^{5}	19.0	2580	1.89×10^{-3}	5.3	16.8	3.17	3.4×10^{-6}	17.3	77.7
6.00	2.5×10^{0}	2.3×10^{5}	19.8	2640	1.46×10^{-3}	4.1	14.2	3.46	2.3×10^{-6}	20.9	103
6.50	1.7×10^{0}	2.4×10^{5}	20.7	2700	1.14×10^{-3}	3.2	11.7	3.66	1.5×10^{-6}	25.9	134
7.00	1.1×10^{0}	2.5×10^{5}	21.5	2750	9.16×10^{-4}	2.6	9.40	3.62	8.9×10^{-7}	32.9	171

§2. Electromagnetic Waves in the Magnetospheric Plasma

It is well known that there exist mainly two different types of waves in the plasma; the electrostatic and the electromagnetic waves. In the early days of the plasma physics in the laboratory, the electrostatic waves attracted much attention, whilst the electromagnetic waves did not have a spotlight of the investigation because the former are much more easily excited and observed than the latter in the bounded laboratory plasma. On the contrary, the leading mode of the waves in space was the electromagnetic mode, especially the whistler mode. Progressive satellite and ground-based observations revealed that the electromagnetic waves, both whistlers and VLF emissions, can be drastically influenced by high energy resonant electrons through the wave-particle interactions in the midst of the magnetosphere. It should be, however, mentioned that recent advances of the space probing technique using the effective electric field sensors make it possible to find out the electrostatic waves in a warm magneto-active plasma in and around the magnetosphere.

In this section, we first present a brief review on whistlers and the whistler mode propagation. Characteristics of the VLF emissions, both spontaneous and triggered emissions, are then summarized limiting to the intrinsically important features to the present theoretical works.

2.1 Whistlers and Whistler Mode Propagation

With regard to whistlers which are well known to be originated from the lightnings and the whistler mode propagation, both the experimental and theoretical works were extensively performed and now the subjects are well understood and documented (Helliwell[8]).

In the present work, most of the mode of the treated waves will be the "whistler mode" of propagation. This mode is identified as the elliptically polarized waves with a rotating magnetic (or electric) vector of the same rotational sense as that of electrons, i.e., the R-mode waves which exist at frequencies below the electron cyclotron frequency f_H. In a cold, homogeneous, collisionless and infinite plasma, the refractive index n for R-mode waves is given by (Stix[25])

$$n^2 = \frac{R_o L_o \sin^2\theta + P_o S_o (1+\cos^2\theta) \pm [(R_o L_o - P_o S_o)^2 \sin^4\theta + 4P_o^2 D_o^2 \cos^2\theta\,]^{\frac{1}{2}}}{2(\,S_o \sin^2\theta + P_o \cos^2\theta\,)}\,, \tag{1.8}$$

where

$$S_o = \frac{1}{2}(\,R_o + L_o\,), \qquad D_o = \frac{1}{2}(\,R_o - L_o\,)\,, \tag{1.9}$$

$$R_o = 1 - \sum_s \frac{\Pi_s^2}{\omega^2}\left(\frac{\omega}{\omega + \varepsilon_s \Omega_s}\right)\,, \tag{1.10}$$

$$L_o = 1 - \sum_s \frac{\Pi_s^2}{\omega^2}\left(\frac{\omega}{\omega - \varepsilon_s \Omega_s}\right)\,, \tag{1.11}$$

$$P_o = 1 - \sum_s \frac{\Pi_s^2}{\omega^2}\,, \tag{1.12}$$

where Π_s and Ω_s are the angular plasma and cyclotron frequencies for the s-th species of particles and ε_s is a positive or negative unity according to whether the s-th particles are positively or negatively charged. Eq.(1.8) is identical with the famous Appleton-Hartree formula, but is written by the Stix expression for the consistency with the dispersion equations used in the following chapters.

2.2 VLF Emissions

In addition to whistlers, there was discovered another type of naturally occurring electromagnetic waves in the VLF range which propagate also in the whistler mode in the magnetosphere and exhibit more attractive and diversified musical tones to the listners than whistlers. These phenomena have gathered much attention in both theoretical and experimental investigations but are less well understood than whistlers. Though the generation mechanisms of these emissions are still opaque, they are believed to be closely related to the wave-particle interactions in the magnetopshere.

A comprehensive review on the subject, especially on the characteristics and features of the observed emissions, was made by Helliwell[8] and recently also by Kimura[26]. Although we can find out detailed descriptions on the matter in these literatures, we believe we had better

present a short summary on the necessary characteristics of the VLF emissions which are related to the present work.

2.2.1 Classification of VLF Emissions

VLF emissions show surprisingly various forms in the spectrograms. They are, however, put in order and classified into several groups as tabulated in Table 2 (Helliwell[8]). VLF emissions may be divided into two classes; (1) hiss with steady nature durable up to several hours which shows a wide band spectrum of the order of several kHz with some exceptional hiss extending up to several hundred kHz, and (2) discrete emissions with a transient nature of the duration of a few seconds or less. Discrete emissions are further classified into rising tones, falling tones, hooks, inverted hooks and their complex combinations by their spectral forms. A special type of discrete emissions with a multitude of closely spaced or overlapped rising tones is called "chorus" which usually appear below 5kHz in the spectrograms. In addition to these apparently spontaneous emissions, there exists another class of emissions which are clearly triggered by whistlers or other emissions or man-made signals. They are specially termed as "triggered emissions".

General properties and characteristics of these VLF emissions are as follows: (1) The intensity of these VLF emissions is comparable to that of whistlers with a typical electric field intensity of 100 μV/m to 1 mV/m. (2) The band width of discrete emissions is about 30Hz to 50Hz, while those of hiss are usually as high as a few tens of kHz. (3) They are most commonly observed at middle and high latitudes. (4) The location of their generation is thought to lie around the equatorial plane though there is an exception observed by satellites for some type of emissions that must be produced in the ionosphere. (5) They show interesting diurnal and seasonal variations as well as K_p-dependence which, however, are not mentioned here.

2.2.2 Characteristics of Triggered VLF Emissions

Amongst various VLF emissions, triggered emissions are most incentive in the sense that their sources or at least catalyzers in the process of their generation are clear. They are available as a clue of

Table 2. A Classification of VLF Emissions (from Helliwell[8])

Type and Name	Model Spectral Form
I. Hiss	
II. Discrete Emissions	
A. Rising Tone	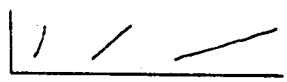
B. Falling Tone	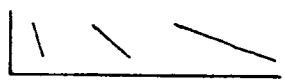
C. Hook	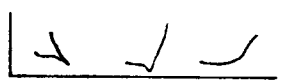
D. Combinations	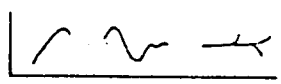
III. Periodic Emissions	
A. Dispersive	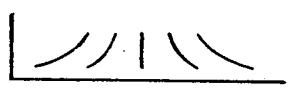
B. Non-dispersive	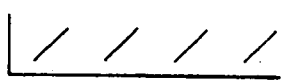
C. Multiphase	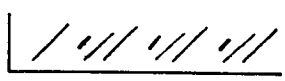
D. Drifting	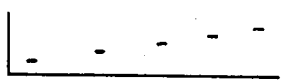
IV. Chorus	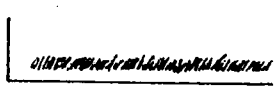
V. Quasi-periodic Emissions	
VI. Triggered Emissions	
A. Whistler Triggered Emissions (WTE)	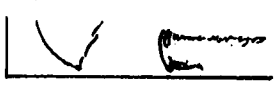
B. Artificially Stimulated Emissions (ASE)	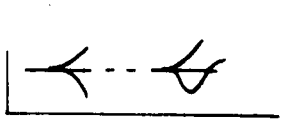

(a) Whistler Triggered Emissions (WTE)

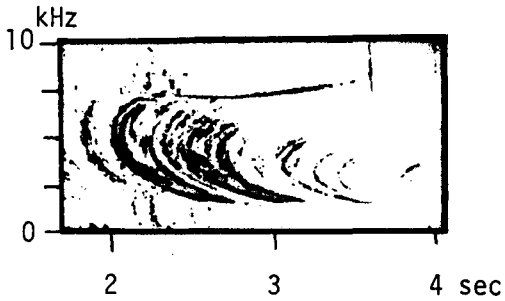

(b) Artificially Stimulated Emissions (ASE)

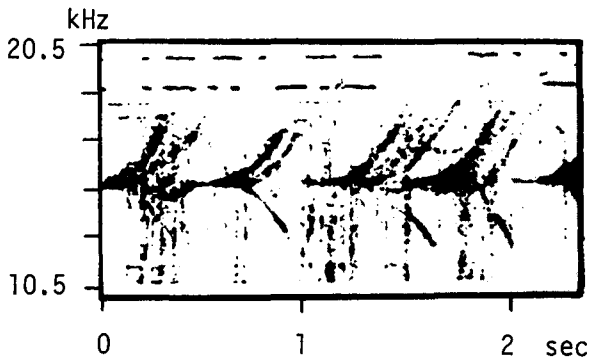

Fig.12 Typical Examples of the Spectrograms of Triggered VLF Emissions.

the theoretical investigations on the nonlinear process in triggering of the instabilities. Therefore, we focus our attention on the discrete VLF emissions triggered by whistlers and the artificially stimulated emissions i.e., ASE. Typical examples of triggered emissions are given in Fig.12.

Whistler triggered emissions (shortly WTE) are classified into two types as schematically illustrated in Fig.13. One of them is emissions triggered just around the whistler cutoff frequency and the other triggered around the whistler tails. The former is conveniently called WTE-H (high), the latter WTE-L (low) in the present thesis. An occurrence histogram of these WTE is made using spectrograms involved in Helliwell's textbook[8] (Matsumoto[27]) and shown in Fig.14. A more accurate histogram about WTE-H was made by Carpenter[28] The determination of the minimum cyclotron frequency f_{Ho} (f_{Hmin} in Fig.14) at the equator along the propagation path is made by the use of the nose frequency measurement. These statistical studies indicate that WTE-H have an occurrence peak around $f_{Ho}/2$ and WTE-L around $f_{Ho}/6$. A clear explanation on these magic numbers 1/2 and 1/6 has not been given so far.

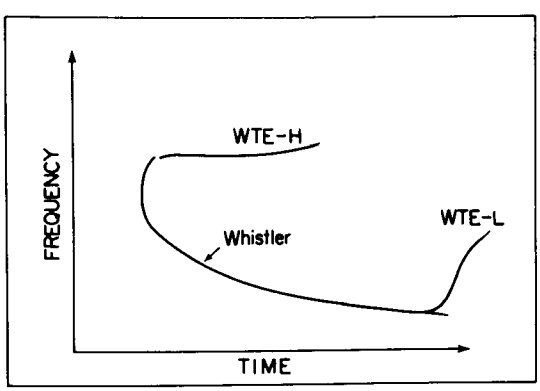

Fig.13 Schematic Illustration of Two Types of Whistler Triggered Emissions.

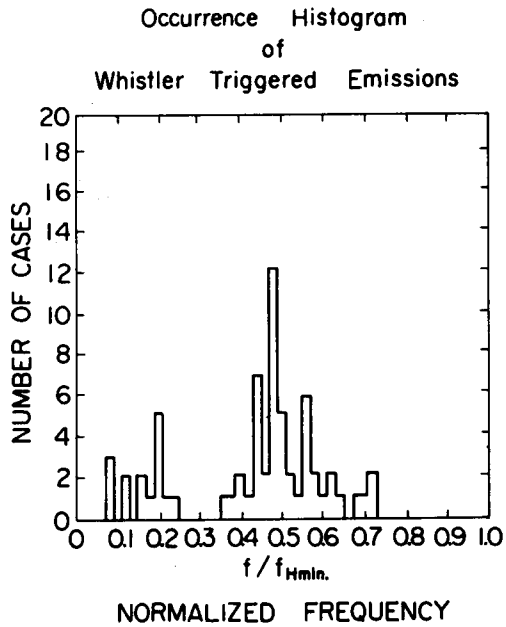

Fig.14 Occurrence Histogram of Whistler Triggered Emissions.

The most prominent difference of these two types of WTE except the difference in the emission frequency is the frequency-time behavior. WTE-L show a rapid frequency change indicating their generation may be due to radiations from something like a moving oscillator in the inhomogeneous medium. As regards the generation mechanism of these WTE-L, Helliwell[29], Kimura[26] and Matsumoto et. al.[30] proposed their theories. The detailed theoretical calculations and explanations by Kimura[26] and Matsumoto et. al.[30] will be described in Chapter II. On the other hand, WTE-H will be explained by the linear and quasilinear cyclotron instability caused by the temperature anisotropy in Chapter II and III.

Artificially stimulated emissions (ASE) are another interesting phenomenon in the triggered VLF emissions which also stimulate a theoretical interest. They are emissions that are produced by VLF signals of constant frequency with a certain duration propagating in the magnetosphere, which are transmitted by the ground-based transmitter. Details of ASE are given by Kimura[26] and Helliwell[29].

Characteristics of WTE and ASE are summarized in the followings:

WTE-H

(1) Frequency of emissions is nearly equal to $f_{Ho}/2$.
(2) Emissions are triggered just around or a little below the whistler cutoff frequency f_c, i.e., $f \lesssim f_c$.
(3) Emissions have a narrow band structure of the order of 50Hz.
(4) Frequency hardly changes with time and the frequency-time curves show an almost constant or a little rising tone.
(5) Emissions sometimes endure for a long time (up to 20 sec.).

WTE-L

(1) Frequency of emissions is nearly equal to $f_{Ho}/6$.
(2) Emissions are triggered at the end of the whistler tails.
(3) Spectral forms resemble to spontaneous emissions, especially rising tones and hooks.
(4) The bandwidth of emissions is usually as narrow as 50Hz.
(5) Frequency usually changes rapidly to much extent.

ASE

(1) Emissions are most easily triggered when the frequency of triggering signal satisfies (Carpenter[28])

$$f \sim \frac{1}{2} f_{Ho} \quad . \tag{1.13}$$

(2) Emissions are triggered with a certain time delay after the incoming of the triggering waves.

(3) Even a low power transmitter ($\sim$ 100W) can trigger ASE when the signal duration long enough (Kimura[31]). The time delay of the excitation of emissions after the incoming of triggering waves is strongly dependent on the intensity of the triggering wave.

(4) Emissions have a tendency to be triggered at a little higher frequency than that of the triggering signal ("offset phenomenon").

(5) Frequency-time spectrum often shows a peculiar pattern of "rise and fall" (or a "branching spectrum"), which cannot be found in the spontaneous emissions. Falling tones are often observed but their curvature is positive, while that of spontaneous emissions is negative.

The characteristics of the triggered VLF emissions itemized here will be discussed from the view point of the linear and quasilinear cyclotron instability and of the nonlinear whistler mode wave-particle interactions in the following chapters.

§3. Background of the Present Work

3.1 Previous Theoretical Works on VLF Emissions

Since the present work deals with theoretical investigations on the whistler mode wave-particle interactions, and their application to the theoretical explanation of VLF emissions, a review of the previous theoretical works on the VLF emissions will well describe a background of the present work.

The problem of the theoretical explanation of the natural VLF phenomena had been attracting many scientific pioneers for a long time since the first theoretical work was published in 1957. A historical

review on plenty of theoretical works until 1964 is summarized in detail by Bell[41] and that until 1967 is made by Kimura[26] classifying the theories into three categories.

Among them, the works which played a fuse to the present work are as follows; works by Kimura[32,26] and Neufeld & Wright[31~35] on a beam cyclotron instabilities and amplifications; works by Brice[38,39], Bell & Buneman[40] and Bell[41] on a transverse instability (i.e., a cyclotron instability), the last of which gives us a hint and clue of the investigation in Chapter IV; a pioneering phenomenological work by Helliwell[29] on the theories of discrete VLF emissions; and a work by Kennel & Petschek[42] on the generation of the continuous waves and the particle precipitation. Of course, all the other references given in the last part of the present thesis gave more or less influence to us. Especially many papers regarding with a general mathematical and physical treatment of the linear and nonlinear theories of the instabilities became nourishing to us, amongst which Briggs[43] and Drummond & Pines[44] were the most influential at the early stage of the present investigation. Almost all of our knowledge on the characteristics of the VLF emissions come from the textbook by Helliwell[8].

The works contained in the present thesis have almost been performed during a period from 1967 to 1971 so that excellent recent works have been published partly during the period and partly more recently. They are listed up here for references: Das[45]; Sudan & Otto[46] ; Dysthe[47] ; Nunn[48]; and Brinca[49]. All of them aim at the theoretical explanation of the triggered emissions, especially ASE. Their principles and methods for the theoretical construction differ from each other and from those in the present thesis. However, we could not determine which theory is right or wrong at the present stage and further experimental studies on the subject would be necessary.

3.2 Contribution of the Present Work

In Chapter II, we are concerned with the studies of certain quantitative aspects of the linear characteristics of the whistler mode cyclotron instability and with their applications to some sorts of the spontaneous VLF emissions. The whistler mode cyclotron instability is clas-

sified into two types due to its causative free energies brought by departures from the Maxwellian of the distribution function of the plasma particles. One is the whistler mode cyclotron instability caused by the beam kinetic energy and the other is that due to the anisotropic temperature or more rigorously to the anisotropic velocity distribution.

With regard to the former type of the instability, two specific problems were considered. One of them is the study of the properties of the beam cyclotron instability ——— convective or absolute ———, which enables us to estimate the moving velocity of the instability region along the magnetic field. A generation mechanism of the spontaneous discrete VLF emissions is proposed using a moving oscillator model due to the convective cyclotron instability (Matsumoto, Miyatake & Kimura[30]). Regarding with the beam cyclotron instability, there is a question "With what velocity does a signal propagate in an abnormally dispersive medium where the group velocity exceeds the light speed in a certain frequency range ?". A Fourier-Laplace inverse transformation technique is applied to the present problem instead of the Sommerfeld-Brillouin method. Numerical computations of the real time-space responses in a plasma-beam system were carried out to yield a few interesting results (Yamazaki[51]; Matsumoto, Kimura & Yamazaki[52]).

The latter type of the whistler mode cyclotron instability due to the temperature anisotropy was then investigated relating to the characteristics of the VLF emissions. Various kinds of the distribution functions including an appropriate distribution function inferred from the satellite data about the magnetospheric plasma were taken into account in the numerical calculations of the growth rate of the instability. Some characteristics of the VLF emissions are successfully explained by the inferred distribution function (Matsumoto & Kimura[50]).

In Chapters III and IV, we are concerned with the nonlinear treatment of the whistler mode cyclotron instability as an extension of the linear analyses in Chapter II. A quasilinear approach to the problem is developed starting from the Vlasov equation in Chapter III. For a weak interaction for waves with a frequency spread, the quasilinear treatment is permissible which uses a delta-functional resonance description. Since it had been shown that a mode-mode coupling (i.e., a wave-wave interaction) does not play an important role for the whistler mode

waves, a main nonlinear effect comes from the quasilinear effect of the resonant wave-particle interaction. First in Chapter III, a physical consideration on the quasilinear instability is made and a basic set of the quasilinear equations for a description of the evolution of the distribution function is derived not mathematically but physically. A mathematical derivation of the set of equations for the quasilinear whistler mode cyclotron instability is then presented. A physical consideration on the characteristics of the electromagnetic whistler mode instability on the quasilinear stage leads us to an explanation on the slow frequency change of the excited waves in WTE-H and to understand a triggering process of the instability in ASE. Following the above physical consideration, extensive numerical computations of the quasilinear change of the instability are carried out aiming at a simulation of triggered emissions, both WTE and ASE. Satisfactory results are obtained to explain the characteristics of these emissions, which makes us confirm that a quasilinear effect is important and essential not only in the triggering process of the emissions but also in the successive frequency change of the emissions (Matsumoto & Kimura[50]). In the last part of Chapter III, a short description is given on the emissions responsible to the quasilinear steady cycle of the whistler mode wave-particle interactions proposed by Kennel & Petschek[42]. Characteristics of the quasilinear KP cycle are compared with the observed morphological features of VLF waves and precipitated particles (Matsumoto & Kimura[53]).

In Chapter IV, we discuss more subtle but interesting phenomena of triggering of emissions by a wave train with a monochromatic frequency. We progressed from the quasilinear Vlasov treatment of the instability, which is effective only for waves with rather wide band spectra, to a nonlinear treatment of the wave-particle interaction between a monochromatic whistler mode wave and nearly resonant electrons. In this chapter, attention is concentrated on the phase bunching of nearly resonant electrons in a given field on the nonlinear stage. In the end, we pointed out that the so far overseen phase bunching process different from the Brice type[38,39] of the phase bunching is much more important in the nonlinear process under consideration (Matsumoto, Hashimoto & Kimura[54]).

Chapter V is devoted to a summary of the present thesis. Suggestions of the experimental investigation of the subject, in which the

author himself takes part, are also presented together with recommendations for the further theoretical works on the subject in the future.

Chapter II

LINEAR ANALYSES OF WHISTLER MODE CYCLOTRON INSTABILITY AND THEIR APPLICATION TO VLF EMISSIONS

§1. Introduction

In this chapter, we are concerned with the studies of certain aspects of the linear characteristics of the whistler mode cyclotron instability bearing in mind their applications to the VLF emission problem.

Since in the space of our interest, the magnetosphere, in which the number of particles N_D in a Debye sphere is typically of the order of $10^8 \sim 10^9$/cc (at the equatorial plane near $L \simeq 4$) and is much greater than unity, the behavior of the plasma can be well described by the Vlasov equation. The plasma in the magnetosphere is slowly varying spatially and hence the propagation and instability characteristics of electromagnetic waves in the homogeneous plasma are applicable locally. In the case of whistler mode waves which are our present concern, the wave growth of the low frequency waves (Kennel[78]) and the propagation vector in a ducted mode are known to be confined in a relatively narrow cone of the wave normals around the static magnetic field. Therefore we limit our treatment to the whistler mode waves propagating along the external magnetic field lines in an infinite, collision-free and magneto-active plasma.

Within the linear treatment of the whistler mode wave-particle interaction, there have been historically two distinct approaches; one is to treat the interaction in a cold plasma-beam system; the other is to describe the problem in terms of the velocity distribution functions. Of course, the former can be included in the latter, if we regard a cold

plasma-beam system as that described by a δ-functional form of the distribution function. In the latter treatment, there appears an instability even if the plasma does not contain a beam, i.e., even if the distribution function has no bump in the tail. This situation resembles the difference between the "two-stream instability" which is described by the MHD equations, and the "Landau instability" which is described by the Poisson-Vlasov equations. In this context, the whistler mode cyclotron instability is classified conventionally into two types by its causative free energies which are brought by departure from the equilibrated Maxwellian of the distribution function. One is called a "whistler mode beam cyclotron instability" which is caused essentially by the beam kinetic energy. The other is simply called a "whistler mode cyclotron instability" which is caused by an anisotropic velocity distribution.

Before entering into a concrete and quantitative discussion, we present a general argument of the physical pictures of the cyclotron instability in Section 2.

The beam cyclotron instability was first investigated extensively by Neufeld & Wright[31~35]. Importance and consequence of the beam cyclotron instability were stressed by Bell & Buneman[40] and Bell[41] comparing with the Landau instability in the case of the whistler mode problem in the magnetosphere. Thenceforth, there was a blank historically in the development of the quantitative argument on the subject until Helliwell[29] and Kimura[26] rebegan a new research. Helliwell[29] considered a moving oscillator model combining the concept of the beam cyclotron instability with a single particle aspect analysis. He explained the mechanism of the drift of the moving oscillator by an energy balance between waves and particles in the interaction region. Kimura[26] also considered a moving interaction model but he attributed the drift mechanism to convective characteristics of the instability determined by the local dispersion equation. It was such a period when we began to investigate the quantitative characteristics of the beam cyclotron instability. We take up two specific problems. One is to investigate the property of the instability ——— convective or absolute ———. The other is to study a propagation velocity of a signal in such an abnormally dispersive and unstable medium as the plasma-beam system under consideration.

Section 3 is devoted to the study of the instability characteristics

——— convective or absolute ——— in the case of the whistler mode beam cyclotron instability. Then a similar but essentially different explanation of the discrete VLF emissions from Helliwell's theory (Helliwell[29]) is given by applying the concept of the drift of the instability region due to the convective instability. In Section 4, another problem regarding with the beam cyclotron instability is investigated which arose from the following question relating to the experimental design of the satellite experiment CIE* (Cyclotron Instability Experiment) on a Japanese scientific satellite REXS*. "With what velocity does an applied signal or a newly generated wave propagate for frequencies around which a group velocity exceeds the light speed ?" Actually a dispersion curve of the whistler mode beam cyclotron instability shows an abnormal region in the ω-k diagram near the intersection between the unperturbed whistler mode curve and a beam mode straight line. Numerical computations were performed on the time-space response of the plasma-beam system which shows an abnormal and unstable dispersion. In this procedure, we adopted a Fourier-Laplace inverse transformation technique instead of the famous Sommerfeld-Brillouin method. Results and discussion are also given there.

The latter type of the whistler mode cyclotron instability caused by the anisotropic distribution function had also been investigated in parallel to the study of the beam cyclotron instability, relating to the magnetospheric whistler mode problems (Scarf[55]; Liemohn & Scarf[56]; Guthart[57]). They investigated a behavior of the instability quantitatively by assuming that the distribution function is an anisotropic Maxwellian and/or a double-humped Maxwellian with a temperature anisotropy. The distribution function, however, in the magnetopshere is not a simple Maxwellian in almost all cases. In Section 5, therefore, a more general study of this type of the instability is made for arbitrary distribution functions removing the restriction of the Maxwellian distribution. A comparison of the results of numerical computations on the growth and damping rates with some sort of VLF emissions, especially WTE-H. A consideration on the location of the generation region of the emissions in the magnetosphere is also made in the same section.

---

* About CIE and REXS, an explanation is given in Chapter IV.

§2. Physical Picture of the Whistler Mode Cyclotron Instability

The usual method for the treatment of the plasma instability is based upon the Vlasov and Maxwell equations which are solved to yield a dispersion equation $D(\omega,k) = 0$. A growth or damping rate is calculated from the dispersion equation by assuming a proper distribution function. This description is, however, accompanied with some mathematical complications which prevent us from understanding the underlying physical process of the instability.

There is an alternative method to reduce the expression of the growth or damping rate by using the equations of motion for individual particles, which yields an easy insight into the physical process of the instability or damping. The single-particle aspect analysis of the plasma instability was first made by Stix[25] in the problem of the physical interpretation of the Landau damping. With regard to the cyclotron instability (or damping) in the electromagnetic mode (including the whistler mode), first attempts were made by Kimura[32,58] and Brice[38,39] with a physical consideration of the energy transfer between the whistler mode wave and a single particle. Though they were rather qualitative investigations, they gave a straight and elegant explanation of the fundamental behavior of the individual particles in the process of the cyclotron wave-particle interaction. Bell[41] reduced a growth rate expression from the single-particle equations of motion by calculating a power transfer from the wave to particles, i.e., by calculating $P_w = (\mathrm{Re}\, \vec{E}) \cdot (\mathrm{Re} \langle \vec{j} \rangle)$ where $\langle \vec{j} \rangle = \int d\vec{j}$, $d\vec{j} = -e\{ F(\vec{V}) V_\perp dV_\perp dV_z d\phi \cdot \vec{v} + \Delta N \vec{V} \}$, in which ΔN is a perturbation in $F(\vec{V}) V_\perp dV_\perp dV_z d\phi$ determined by the continuity equation. Terashima[59] also attempted a similar calculation using the equation of motion and the continuity equation but attained a little different result because of the neglect of a part of the second order quantities. Lutomirski[60] paralleled the method employed by Stix[25] and reduced the same expression of the growth (or damping) rate as obtained from the Vlasov-Maxwell equations in a rather elegant way.

All methods using the single-particle equations of motion mentioned above are based upon the calculation of the energy change (or transfer) with the use of the energy conservation law. A claim, however, is opposed to the above methods by Hollweg & Völk[61], who appointed out that

a full dispersion equation cannot be derived without the simultaneous use of the law of the momentum conservation in addition to the energy conservation law. Their argument is quite accurate mathematically and is especially important in a case that the growth or damping rate ω_i is so large that the dispersion relation between the real frequency ω_r and the wave number k cannot be approximated by the cold plasma dispersion equation. A quantitative estimation, however, of the effective frequency range of the usual method is computed by Kawai[62] comparing with the rigorous method by Hollweg & Völk[61]. It was clarified that the difference between the two does not become conspicuous for the whistler mode waves with frequencies below $0.85f_H$ in the case of typical magnetospheric plasma parameters.

In this section, a brief but sufficient survey on the physical pictures of the cyclotron instability is made. Some physical considerations are given for a better understanding of the following discussion on the subject. A fundamental treatment of the pitch angle diffusion of the individual particles is first explained in Section 2.1 after Brice[38]. Thenceforth a single-particle aspect calculation is given along the Stix[25] and Lutomirski[60] lines in Section 2.2. Physical consideration and explanation of the cyclotron instability are given in Section 2.3.

2.1 Pitch Angle Diffusion of Resonant Electrons in the Cyclotron Interaction with Whistler Mode Waves

Let us consider an energy change of an individual resonant electron in a whistler mode plane wave which propagates along the external magnetic field $\vec{B}_o$ in a homogeneous, collisionless and infinite plasma. We see a change ΔW_p of the particle kinetic energy W_p of the electron, i.e.,

$$\Delta W_p = \Delta\{ \frac{1}{2} m(V_\perp^2 + V_z^2)\} = mV_\perp \Delta V_\perp + mV_z \Delta V_z$$

$$\equiv \Delta W_{p\perp} + \Delta W_{p\parallel} \quad , \tag{2.1}$$

where $\Delta W_{p\perp} \equiv mV_\perp \Delta V_\perp$, $\Delta W_{p\parallel} \equiv mV_z \Delta V_z$, $V_\perp$ and V_z are the kinetic energy incre-

ments and velocity components in the perpendicular and parallel direction to $\vec{B}_o$, respectively. In the wave frame which moves along the $\vec{k}$ (and $\vec{B}_o$) direction with the wave phase velocity V_{ph}, the apparent electric field disappears as the Lorentz transformation shows

$$\vec{E}' = \gamma_o (\vec{E} + \vec{V}_{ph} \times \vec{B}) = \gamma_o (\vec{E} + \vec{V}_{ph} \times \frac{\vec{V}_{ph} \times \vec{E}}{V_{ph}^2}) = 0 , \qquad (2.2)$$

where the primed and unprimed quantities are in the wave frame and the rest (laboratory) frame respectively. γ_o is the relativistic factor defined by $\gamma_o = (1 - V_{ph}^2/c^2)^{-1/2}$. As there is no electric field in the wave frame, the energy of an electron in this frame is conserved so that

$$\frac{1}{2} m V_\perp^2 + \frac{1}{2} m (V_z - V_{ph})^2 = \text{constant} . \qquad (2.3)$$

Therefore combining Eqs.(2.1) and (2.3),

$$\Delta W_p = m V_{ph} \Delta V_z . \qquad (2.4)$$

Thus we see the following relations,

$$\frac{\Delta W_{p\parallel}}{\Delta W_p} = \frac{k V_z}{\omega_r} , \qquad (2.5)$$

$$\frac{\Delta W_{p\perp}}{\Delta W_p} = 1 - \frac{\Delta W_{p\parallel}}{\Delta W_p} = \frac{\omega_r - k V_z}{\omega_r} , \qquad (2.6)$$

where ω_r and k are the wave angular frequency and the wave number respectively. For an electron with nearly resonance velocity, i.e.,

$$V_z \simeq V_R \equiv \frac{\omega_r - \Omega_e}{k} < 0 , \qquad (2.7)$$

we get

$$\frac{\Delta W_{p\parallel}}{\Delta W_p} < 0 \quad \text{and} \quad \frac{\Delta W_{p\perp}}{\Delta W_p} > 0 , \qquad (2.8)$$

which yields a conclusion that the transverse energy decreases while the longitudinal energy is increased if the electron loses energy by the

interaction and vice versa.

It should be noticed, however, that the energy of an individual electron does not necessarily increase even when the energy change of the wave ΔW_w is negative, i.e., the wave is damped out. The above discussion, therefore, does not include the explanation of the instability condition. The instability or damping should be determined by the energy change of total resonant electrons, though a portion of them loses its energy and the other gains.

2.2 Derivation of the Growth Rate Expression from the Single-Particle Equations of Motion

In order to see the physical process of the instability as simply as possible, we consider a wave-particle interaction between nearly resonant electrons and a whistler mode wave with a frequency ω_r and a wave number k which propagates along the external magnetic field $B_o\hat{z}$ in a collisionless, infinite and homogeneous plasma. We also make an important and essential assumption that the dispersion relation between ω_r and k is well described by the cold plasma theory. Namely, the contribution of the resonant electrons to the wave propagation characteristics is assumed to be negligible. This assumption corresponds to the condition of $|\omega_i| \ll \omega_r$.

As seen in Eq.(2.4), the energy change of a single electron is computable if we know the velocity change ΔV_z in the $\vec{k}$-direction. In calculating the energy increment, we should inquire after not only the first order quantities but also the second order quantities if we take a perturbation scheme because the energy is essentially a second order quantity. A most simple way, that is contrived by Lutomirski[60], is to solve the equations of motion in the wave frame, partly because the electric field disappears in this frame and partly because the wave magnetic field seems to be a time-independent stationary spatial helix.

In the wave frame, the equations of motion of an electron are

$$\frac{dv'_x}{dt} = -\frac{e}{m}\left(B\, v'_z \sin kz + v'_y B_o \right) \tag{2.9}$$

$$\frac{dv'_y}{dt} = -\frac{e}{m}\left(B\, v'_z \cos kz - v'_x B_o \right) , \tag{2.10}$$

$$\frac{dv'_z}{dt} = \frac{eB}{m}\left(v'_x \sin kz + v'_y \cos kz \right) , \tag{2.11}$$

where the wave magnetic field $\vec{B}$ = (Bcoskz, -Bsinkz, 0), and velocities in the wave frame are denoted by attached primes. In order to solve the above equations, the usual perturbation method is adopted as follows:

$$v'_i = v'_{i0} + v'_{i1} + v'_{i2} + \cdots\cdots\cdots , \quad (i = x, y, z) \tag{2.12}$$

$$z = z_0 + v_{z0} t + \int_0^t v_{z1} dt + \int_0^t v_{z2} dt + \cdots\cdots . \tag{2.13}$$

The zero and first order solutions are easily obtained under the initial conditions;

$$v'_{x0} = V'_\perp \cos\phi', \quad v'_{y0} = V'_\perp \sin\phi', \quad v'_{z0} = V'_z , \tag{2.14}$$

$$v'_{x1} = v'_{y1} = v'_{z1} = 0 . \tag{2.15}$$

The results are

$$v'_{x0} = V'_\perp \cos(\Omega_e t+\phi'), \quad v'_{y0} = V'_\perp \sin(\Omega_e t+\phi'), \quad v'_{z0} = V'_z , \tag{2.16}$$

$$v'_{x1} = -\frac{e}{m}\frac{BV'_z}{kV'_z+\Omega_e}\{ \cos(kz_0-\Omega_e t) - \cos(kz_0+kV'_z t) \} , \tag{2.17}$$

$$v'_{y1} = +\frac{e}{m}\frac{BV'_z}{kV'_z+\Omega_e}\{ \sin(kz_0-\Omega_e t) - \sin(kz_0+kV'_z t) \} , \tag{2.18}$$

$$v'_{z1} = -\frac{e}{m}\frac{BV'_\perp}{kV'_z+\Omega_e}[\cos\{(kV'_z+\Omega_e)t+kz_0+\phi'\} - \cos(kz_0+\phi')] , \tag{2.19}$$

where $V'_\perp$, V'_z and ϕ' are the velocity components of the electron at the pre-state of the interaction.

The perturbation method for the equations of motion, (2.9) to (2.11), gives to the second order

$$\frac{dv'_{z_2}}{dt} = \frac{eB}{m}\{ v'_{x_1}\sin(kz_0+kV'_z t) + v'_{y_1}\cos(kz_0+kV'_z t)$$

$$+ kv'_{x_0}\int_0^t v'_{z_1}dt\cos(kz_0+kV'_z t) - kv'_{y_0}\int_0^t v'_{z_1}dt\sin(kz_0+kV'_z t)\} . \tag{2.20}$$

Substituting Eqs.(2.16) to (2.19) into Eq.(2.20),we obtain

$$\frac{dv'_{z_2}}{dt} = -\frac{e^2B^2}{m^2}[\frac{V'_z}{kV'_z+\Omega_e}\sin(kV'_z+\Omega_e)t + \frac{kV'^2_\perp}{kV'_z+\Omega_e}\{\frac{\sin(2kz_0+2\phi'+2kV'_z t+2\Omega_e t)}{kV'_z+\Omega_e}$$

$$+ \frac{\sin(kV'_z+\Omega_e)t - \sin(2kz_0+2\phi'+kV'_z t+\Omega_e t)}{2(kV'_z+\Omega_e)}$$

$$- t\frac{\cos(2kz_0+2\phi'+kV'_z t+\Omega_e t) + \cos(kV'_z+\Omega_e)t}{2}\}] . \tag{2.21}$$

Rewriting dv_{z_1}/dt and dv_{z_2}/dt by the rest frame quantities,

$$\frac{dv_{z_1}}{dt} = -\frac{e}{m}BV_\perp\sin(\alpha_o t-kz_0-\phi) , \tag{2.22}$$

$$\frac{dv_{z_2}}{dt} = -\frac{e^2B^2}{m^2}[(V_z-V_{ph})\frac{\sin\alpha_o t}{\alpha_o} - \frac{kV^2_\perp}{\alpha_o}\{\frac{\sin(2\alpha_o t-2kz_0-2\phi)}{\alpha_o}$$

$$+ \frac{\sin\alpha_o t-\sin(\alpha_o t-2kz_0-\phi)}{2\alpha_o} - t\frac{\cos(\alpha_o t-2kz_0-2\phi)+\cos\alpha_o t}{2}\}] , \tag{2.23}$$

where $\alpha_o = \omega_r - kV_z - \Omega_e$ which corresponds to α in Stix[25]. If it is assumed that the distribution function of the electrons is uniform over ϕ from 0 to 2π around $\vec{B}_o$, only the nonperiodic terms in Eqs.(2.22) and (2.23) survive after an average process over ϕ. The results are

$$\left\langle\frac{dv_{z_1}}{dt}\right\rangle_\phi = 0 , \tag{2.24}$$

$$\left\langle\frac{dv_{z_2}}{dt}\right\rangle_\phi = \frac{e^2B^2}{m^2}\frac{\omega_r}{k^2}[(\alpha_o+\Omega_e)\frac{\sin\alpha_o t}{\alpha_o} + \frac{1}{2}k^2V^2_\perp\frac{\sin\alpha_o t}{\alpha_o^2} - \frac{1}{2}k^2V^2_\perp\frac{t\cos\alpha_o t}{\alpha_o}] , \tag{2.25}$$

where < > indicates the averaged quantity over the suffix. Combining Eq.(2.4) with Eqs.(2.24) and (2.25), we find the expression of the rate of the energy change of electrons after a further averaging operation over $V_\perp$ and V_z as

$$\left\langle \frac{dW_p}{dt} \right\rangle_{\phi,V_\perp,V_z} = \frac{2\pi e^2}{m} B^2 \frac{\omega_r}{k^2} \int_0^\infty V_\perp dV_\perp \int_{-\infty}^\infty dV_z \, F(V_z,V_\perp)$$

$$\left[\sin\alpha_o t + \Omega_e \frac{\sin\alpha_o t}{\alpha_o} + \frac{1}{2} k^2 V_\perp^2 \frac{\sin\alpha_o t}{\alpha_o^2} - \frac{1}{2} k^2 V_\perp^2 t \frac{\cos\alpha_o t}{\alpha_o} \right] , \qquad (2.26)$$

where $F(V_z,V_\perp)$ is the velocity distribution function. Introducing $G(\alpha_o)$ by

$$G(\alpha_o) \equiv F(V_R - \frac{\alpha_o}{k}, V_\perp) \equiv F(V_z,V_\perp) , \qquad (2.27)$$

quite a similar estimation of the integration in Eq.(2.26) is possible in parallel to the Stix[25] description (page 134 to 135). The first and the fourth terms become zero after integration and the rest terms yield a result of

$$\left\langle \frac{dW_p}{dt} \right\rangle_{\phi,V_\perp,V_z} = 2\pi^2 \frac{e^2}{m} B^2 \frac{\omega_r}{k^3} \int_0^\infty V_\perp dV_\perp \left[\Omega_e F(V_z,V_\perp) - \frac{1}{2} kV_\perp^2 \frac{\partial F(V_z,V_\perp)}{\partial V_z} \right] \Big|_{V_z=V_R} , \qquad (2.28)$$

and a further integration by parts over $V_\perp$ gives

$$\left\langle \frac{dW_p}{dt} \right\rangle_{\phi,V_\perp,V_z} = - \frac{\pi^2 e^2}{m} E^2 \frac{\Omega_e}{\omega_r k} \int_0^\infty V_\perp^2 dV_\perp \left[\left(\frac{\partial}{\partial V_\perp} + \frac{kV_\perp}{\Omega_e} \frac{\partial}{\partial V_z} \right) F(V_z,V_\perp) \right] \Big|_{V_z=V_R} , \qquad (2.29)$$

or equivalently

$$\left\langle \frac{dW_p}{dt} \right\rangle_{\phi,V_\perp,V_z} = - \frac{\pi^2}{N} \varepsilon_o E^2 \frac{\Pi_e^2 \Omega_e}{\omega_r} \int_0^\infty V_\perp^2 dV_\perp \delta(\omega_r - kV_z - \Omega_e) \left(\frac{\partial F}{\partial V_\perp} + \frac{kV_\perp}{\Omega_e} \frac{\partial F}{\partial V_z} \right) , \qquad (2.30)$$

where $E = \omega_r B/k$ is the wave electric field intensity. On the other hand, the sum of the wave electric and magnetic field energy densities and the oscillatory kinetic energy of the thermal plasma particles

associated with the wave is expressed by

$$W_w \equiv \frac{1}{2}\varepsilon_o E^2 + \frac{1}{2}\mu_o H^2 + \frac{1}{2} N m v_T^2 \quad . \tag{2.31}$$

Noting that the kinetic velocity v_T of the oscillatory part of the thermal plasma is simply calculated from the linearized equations of motion as

$$v_T^2 = \frac{e^2}{m^2\varepsilon_o}\frac{\varepsilon_o E^2}{(\omega_r - \Omega_e)^2} \quad , \tag{2.32}$$

Eq.(2.31) can be expressed as

$$W_w = \frac{1}{2}\varepsilon_o E^2\{\, 1 + \frac{c^2k^2}{\omega_r^2} + \frac{\Pi_e^2}{(\omega_r - \Omega_e)^2}\,\} \quad . \tag{2.33}$$

Since there is a relation as

$$\frac{dW_w}{dt} = 2\omega_i W_w \quad , \tag{2.34}$$

the growth (or damping) rate is given by

$$\omega_i = \frac{1}{2W_w}\frac{dW_w}{dt} = -\frac{1}{2W_w}\left\langle \frac{dW_p}{dt} \right\rangle_{\phi, V_\perp, V_z} \quad . \tag{2.35}$$

Combining Eq.(2.29) (or Eq.(2.30)) with Eq.(2.35), the final expression for ω_i becomes

$$\omega_i = \frac{\pi^2}{N}\frac{\Pi_e^2\Omega_e}{\omega_r k}\frac{\int_0^\infty V_\perp^2 dV_\perp \left(\frac{\partial F}{\partial V_\perp} + \frac{kV_\perp}{\Omega_e}\frac{\partial F}{\partial V_z} \right)\Big|_{V_z = V_R}}{2 + \Pi_e^2\Omega_e / \{\omega_r(\omega_r - \Omega_e)^2\}} \quad , \tag{2.36}$$

or

$$\omega_i = -\frac{\pi^2}{N}\frac{\Pi_e^2\Omega_e}{\partial D/\partial\omega_r}\int_{-\infty}^{\infty} dV_z \int_0^\infty V_\perp^2 dV_\perp \left(\frac{\partial F}{\partial V_\perp} + \frac{kV_\perp}{\Omega_e}\frac{\partial F}{\partial V_z} \right)\delta(\omega_r - kV_z - \Omega_e) \quad , \tag{2.37}$$

where the cold plasma dispersion relation

$$D(\omega_r, k) = c^2k^2 - \omega_r^2 + \frac{\Pi_e^2\omega_r}{\omega_r - \Omega_e} = 0 \quad , \tag{2.38}$$

is utilized. These expressions Eqs.(2.37) and (2.38) are the same as

Eqs.(2.136) and (2.135), respectively which are obtained from the usual Vlasov-Maxwell treatment as will be described in Section 5.

2.3 Physical Consideration

In the previous Section 2.2, we showed a process of calculating the growth (or damping) rate of the whistler mode cyclotron instability by solving the single-particle equations of motion to the second order. Though the result of the expression for ω_i is entirely coincident with that obtained by the usual Valsov-Maxwell method, the procedure reveals some underlying physical details of the instability.

One of the most prominent features that the final result Eq.(2.36) or (2.37) indicates is that the instability condition for a given frequency ω_r is dependent upon the local characteristics of the distribution function only at the resonance velocity $V_z = V_R \equiv (\omega_r - \Omega_e)/k(\omega_r)$. Such a $\delta(\omega_r - kV_z - \Omega_e)$-functional feature is always used to discuss the instability characteristics in the linear and the quasilinear treatment. We can find out in the process of the previous calculation how this prominent feature is introduced. It is instructive to know the background in using the δ-function not only in applying the result to the concrete VLF problem, but also in extending the theory into the nonlinear regimes.

We can see that the integration over V_z or equivalently over α_o in Eq.(2.26) gives

$$\left\langle \frac{dW_p}{dt} \right\rangle_{z_0, V_\perp} = \frac{2\pi e^2}{N} B^2 \frac{\omega_r}{k^3} \int_{-\infty}^{\infty} G_o(\alpha_o) \left[\Omega_e \frac{\sin\alpha_o t}{\alpha_o} + \frac{1}{2} k^2 \langle V_\perp^2 \rangle \frac{\sin\alpha_o t}{\alpha_o^2} \right] d\alpha_o$$

$$\equiv \frac{2\pi e^2}{N} B^2 \frac{\omega_r}{k^3} \left[\Omega_e I_2 + \frac{1}{2} k^2 \langle V_\perp^2 \rangle I_3 \right] , \qquad (2.39)$$

where $G_o(\alpha_o)$ is the transformed distribution function of $G(\alpha_o)$ [defined by Eq.(2.27)] integrated over $V_\perp$ as

$$G_o(\alpha_o) \equiv \int_0^\infty V_\perp dV_\perp G(\alpha_o) \equiv \int_0^\infty V_\perp dV_\perp F(V_z, V_\perp) , \qquad (2.40)$$

and the survival integrations I_2 and I_3 are difined by

$$I_2 = \int_{-\infty}^{\infty} \frac{\sin\alpha_o t}{\alpha_o} G_o(\alpha_o) d\alpha_o = \int_{-\infty}^{\infty} G_o(\frac{x}{t}) \frac{\sin x}{x} dx \quad , \tag{2.41}$$

and

$$I_3 = \int_{-\infty}^{\infty} \frac{\sin\alpha_o t}{\alpha_o^2} G_o(\alpha_o) d\alpha_o = t\int_{-\infty}^{\infty} G_o(\frac{x}{t}) \frac{\sin x}{x^2} dx \quad , \tag{2.42}$$

in which $\alpha_o \equiv \omega_r - kV_z - \Omega_e$ and $x \equiv \alpha_o t$. It should be, however, noticed that the other two terms of the integrand in Eq.(2.26) become zero by integration only if the transformed distribution function G(x/t) can be regarded as a very slowly varying function compared with a trigonometric function of x [see Fig.7-1 in Stix[25]]. As time elapses, G(x/t) becomes more and more slowly varying function so that these two diminishing terms approach zero only some time after the beginning of the interaction. The restriction, however,on the time brought about by the above is generally less severe compared with the restriction brought about by the δ-functional feature mentioned before. We can see this in the following.

Since $G_o(x/t)$ is generally slowly varying function of x compared with sinx as assumed in the above, the main contribution to the integral in Eqs.(2.41) and (2.42) is determined by the sampling function sinx/x. The contribution comes mainly from the range of $|x| \leq 2\pi$ which corresponds to the velocity range of

$$V_R - \Delta V_R \leq V_z \leq V_R + \Delta V_R \quad , \tag{2.43}$$

where

$$\Delta V_R = \frac{2\pi}{kt} \quad , \tag{2.44}$$

is the velocity spread of the cyclotron resonance. The resonance width $2\Delta V_R$ is a function of time t and becomes narrower and narrower as time elapses after the beginning of the interaction. Therefore the distribution function $G_o(\alpha_o)$ becomes to be well approximated by the first two terms of the Taylor expansion around $\alpha_o = 0$ as

$$G_o(\frac{x}{t}) = G_o(0) + \frac{x}{t}\frac{\partial G_o}{\partial \alpha_o}(0) \quad , \qquad \text{for} \quad |x| \leq 2\pi \quad , \tag{2.45}$$

or equivalently

$$F_o(V_z) = F_o(V_R) + (V_z - V_R)\frac{\partial F_o}{\partial V_z}(V_R), \quad \text{for} \quad |V_z - V_R| \leq \Delta V_z \quad , \tag{2.46}$$

where

$$F_o(V_z) \equiv \int_0^\infty V_\perp dV_\perp F(V_z, V_\perp) \quad . \tag{2.47}$$

Such a procedure reduced the result of Eq.(2.28) from Eq.(2.26), i.e., introduced a δ-functional feature. Therefore, the result of Eq. (2.36), which is expressed by the δ-function, is effective only when the distribution function is approximated by the linear equation (2.46). Thus we can estimate a time limit t_o after when Eq.(2.36) is effective as

$$t_o = \frac{2\pi}{k\Delta V_z} \quad , \tag{2.48}$$

where ΔV_z is the velocity range in which the distribution function is well described by the first two terms of the Taylor expansion in Eq. (2.46). The limiting time t_o is thus dependent upon the property of the distribution function around the resonance velocity. If it is a well smooth function, it does not need to elapse much time until the growth (or damping) rate can be described by Eq.(2.36) or (2.37) with a δ-functional feature. On the contrary, however, if the distribution function changes quickly within a small velocity range in such a case of a δ-function beam with the resonance velocity, the expression Eq. (2.36) or (2.37) for ω_i cannot be used for a finite time.

For time $t \geq t_o$, the integrations in Eqs.(2.41) and (2.42) become

$$I_2 \simeq G_o(0) \int_{-\infty}^{\infty} \frac{\sin x}{x} dx = \pi G_o(0) = \pi F_o(V_R) \quad , \tag{2.49}$$

$$I_3 \simeq \frac{\partial G_o(0)}{\partial \alpha_o} \int_{-\infty}^{\infty} \frac{\sin x}{x} dx = \pi \frac{\partial G_o}{\partial \alpha_o}(0) = -\frac{\pi}{k} \frac{\partial F_o}{\partial V_z}(V_R) \quad , \tag{2.50}$$

after remaining the even functions in the integrands, which show that the integrated values are functions of the local information of the distribution function at $V_z = V_R$.

Thus we could find a time limit t_o until when the δ-functional description, Eq.(2.36) or (2.37), for ω_i loses its basis.

Another interesting feature of the cyclotron instability can be extracted from the previous argument by the single-particle equations of motion. It is now clear that the electrons which take part in the

interaction with the wave are not only those with a rigorous resonance velocity, i.e., $V_z = V_R$, but also those with $V_z \simeq V_R$, even though the result for ω_i is described by $\delta(\omega_r - kV_z - \Omega_e)$. The point lies, then, in whether the causative energy of the cyclotron instability is brought about by the electrons with $|V_z| > |V_R|$ or by those with $|V_z| < |V_R|$. In order to see it, the two terms of the multiplicand of the weighting distribution function in the integrand in Eq.(2.39) are illustrated in Fig.15. It is easy to see that the first and the second terms are the results of the acceleration of v_{z_2} by the $-e\vec{v}_{\perp 1} \times \vec{B}_1$ - Lorentz force and

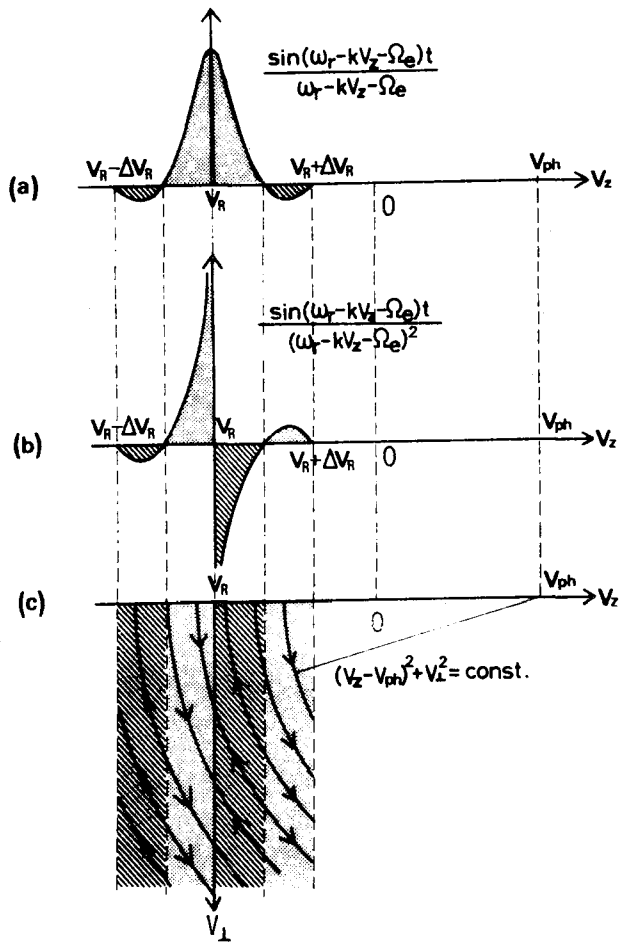

Fig.15 Schematic Illustration of the Two Terms of the Integrand in Eq.(2.39). (a) and (b) correspond to the first and second terms in the bracket in Eq (2.39), repectively. (c) is an illustration of the diffusion in the $V_\perp$-V_z velocity space for the case of the instability.

by the $-e\vec{V}_\perp \times \vec{B}_2$-Lorentz force respectively as understood by Eq.(2.20). In other words, the first term is the result of the acceleration of $v_{\perp 1}$, while the second term is a manifestation of a change of v_{z1}, which, in turn, affects the second order change of the wave magnetic field $\vec{B}_2$ through Eq.(2.13). As seen in Fig.15, the change of the electron kinetic energy $\langle dW_p/dt\rangle_{\phi,V_\perp}$ due to the change of $v_{\perp 1}$ is symmetric around $V_z = V_R$ and almost positive (which is a sense of the increase of the electron kinetic energy). Thus the change of $v_{\perp 1}$ contributes only in the cyclotron damping regardless of the gradient of the distribution function at $V_z = V_R$. On the contrary, the change of v_{z1} leads to the change of the electron kinetic energy $\langle dW_p/dt\rangle_{\phi,V_\perp}$ in such a way that the integrand is an odd function of V_z around V_R. Therefore, the net energy due to this term after the integration over V_z is positive, zero or negative according to the derivative $\partial F_o/\partial V_z(V_R)$ is negative, zero or positive. Thus we know that the necessary condition for the instability is $\partial F_o/\partial V_z(V_R) > 0$ or $\partial F/\partial V_z(V_R) > 0$.

Consequently the causative energy of the cyclotron instability comes from the kinetic energy of electrons with V_z that satisfies

$$V_z \sim V_R \qquad \underline{\text{and}} \qquad |V_z| < |V_R| \ . \tag{2.51}$$

It is interesting to note that the Landau instability is brought about by particles with V_z that is contrarily a little larger than the phase velocity, i.e.,

$$V_z \sim V_{ph} \qquad \underline{\text{and}} \qquad |V_z| > |V_{ph}| \ . \tag{2.52}$$

It should be noticed that the pitch angle diffusion on both sides of V_R is quite reverse in the case of the instability for a monochromatic wave as shown in Fig.15(c). Such a micro-process within the resonance width is usually nonsense when we use a δ-functional description, i.e., a zero resonance width description, but becomes important when the resonance width becomes conspicuous in such a case of the nonlinear problem of a strong monochromatic wave.

§3. Convective Beam Cyclotron Instability and Spontaneous VLF Emissions[30]

The beam cyclotron instability was first proposed in order to explain the insufficiency of the emission intensity by a single-particle radiation theory and was thought to be compatible with the observed intensity. It was, however, pointed out that the cyclotron instability was a result of a feedback mechanism as in the backward oscillator, and hence the instability region was thought to stand at a fixed point in space. Therefore this mechanism was not regarded as being able to reproduce the observed frequency change of the discrete VLF emissions within the linear theory. It becomes, then, necessary to make the interaction region of the cyclotron instability move by any means in order to comprehend the three following characteristics of the discrete VLF emissions, i.e., the intensity, the wave-triggering process and the spectral forms. An idea was proposed by Helliwell[29] assuming the "consistent wave condition", which explained the "inverted hooks" and "oscillatory tones" that had not been understood by the previous works. As a driving mechanism of the interaction region in Helliwell's theory, an extent of balance between the input and output energies was thought to play an important role.

In this section, another idea of the "moving oscillator" is given which also is able to explain the "inverted hooks" and the "oscillatory tones". It has been pointed out by Kimura[26] that the beam cyclotron instability, which was thought heretofore to be an absolute instability fixed in space, is really a convective instability which moves spatially with a certain velocity determined by the medium. Therefore, without any assumption upon the wave condition as contrived by Helliwell[29], we get the idea of the moving interaction region. In this section, characteristics of this convective beam cyclotron instability in the whistler mode are investigated in some detail and its applications to the magnetospheric plasma as a generation mechanism of discrete VLF emissions are also discussed by taking account of the inhomogeneity of the magnetospheric plasma.

3.1 Convective Beam Cyclotron Instability in the Magnetosphere

3.1.1 Model and Basic Equations

The magnetosphere is filled with a neutral plasma imbedded in the geomagnetic field which is approximately a centered dipole subject to perturbations and distortion due to various solar effects. The magnetospheric plasma parameters vary with both time and space but, in the present analysis, the medium is approximated by a quiescent plasma as the average immersed in the centered dipole magnetic field. Since the plasma parameters are slowly varying spatially in the sense that the wavelength of the present interest is short enough compared with a characteristic length of the variation of the medium, the usual following assumptions will be made. The wave we consider propagates in the whistler mode along a uniform magnetic field. The plasma is assumed to be collisionless and to consist of an ambient stationary cold plasma and a small fraction of electron beam. The distribution function $F(V_z,V_\perp)$ is then expressed as a sum of two kinds of delta-function as follows.

$$F(V_z,V_\perp) = F_a(V_z,V_\perp) + F_b(V_z,V_\perp) , \tag{2.53}$$

where

$$F_a(V_z,V_\perp) = \frac{N}{2\pi} \frac{\delta(V_\perp)}{V_\perp} \delta(V_z) , \tag{2.54}$$

$$F_b(V_z,V_\perp) = \frac{N\eta}{2\pi} \frac{\delta(V_\perp - V_{B\perp})}{V_\perp} \delta(V_z - V_{Bz}) , \tag{2.55}$$

in which η indicates the ratio of the beam density to the ambient plasma density N. $V_{B\perp}$ and V_{Bz} are the velocity components of the electron beam perpendicular and parallel to the external magnetic field $B_o\hat{z}$, respectively.

In this case, the dispersion equation of a complex form is simply given by (see, for example, Bell & Buneman[40])

$$c^2k^2 - \omega^2 + \frac{\Pi_e^2\omega}{\omega-\Omega_e} + \frac{\Pi_i^2\omega}{\omega+\Omega_i} + \Pi_b^2 \left\{ \frac{\omega-kV_{Bz}}{\omega-kV_{Bz}-\Omega_e} + \frac{\frac{1}{2}k^2V_{B\perp}^2}{(\omega-kV_{Bz}-\Omega_e)^2} \right\} = 0 , \tag{2.56}$$

where Π_s and Ω_s (s=i,e,b) denote the plasma and cyclotron frequency of

the kind s-th particle and subscripts e, i, and b correspond to the ambient electrons, ions and beam electrons respectively. Contribution of the helical beam to the dispersion is represented by the last term of Eq.(2.56). It is noticed that the beam distribution function in the perpendicular direction is not necessarily a δ-function as in Eq.(2.55). If it is given by other arbitrary distribution functions, the quantity $V_{B\perp}^2$ in the second term in the brackets in Eq.(2.56) is to be replaced by $\langle V_{B\perp}^2 \rangle$. It is easily expected from Eq.(2.56) that the instability in the whistler mode may arise in the vicinity of a point where the whistler mode branch crosses the beam mode branch line on the ω-k diagram as shown in Fig.16. It should be noticed that the another instability is excited at the same time in the above plasma-beam system. It is known as a "beam mode cyclotron instability", though the former is continuously connected with the latter (Neufeld & Wright[34]; Kimura[26]).

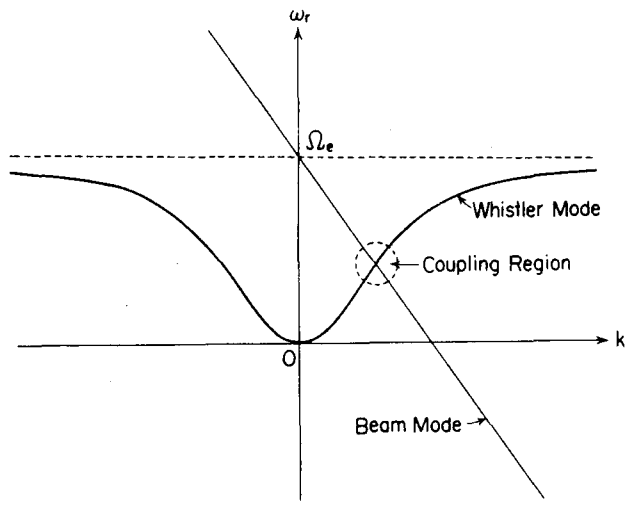

Fig.16 Resonance Condition between the Whistler and the Beam Modes.

3.1.2 Characteristics of the Beam Cyclotron Instability

Complex frequency $\omega = \omega_r + j\omega_i$ for a given real wave number k is determined by the dispersion equation (2.56). An example of the resulting ω-k diagram is illustrated in Fig.17. It is noted that both ω and k are normalized as $\omega^* = \omega/\Omega_e$ and $k^* = 2\pi/3\times(ck/\Omega_e)$ for convenience. It can be seen that unstable solutions exist in two different modes, the whistler mode and the beam mode. The cyclotron instability in the whistler mode has larger values of the growth rate than in the beam cyclotron mode and hence clearly overcomes the beam cyclotron instability in the asymptotic time limit. In the following, therefore, we pay atten-

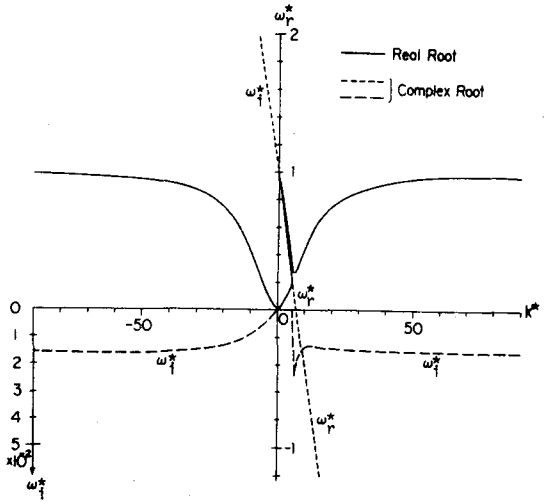

Fig.17 Typical Example of ω-k Diagram of the Plasma-Beam System.

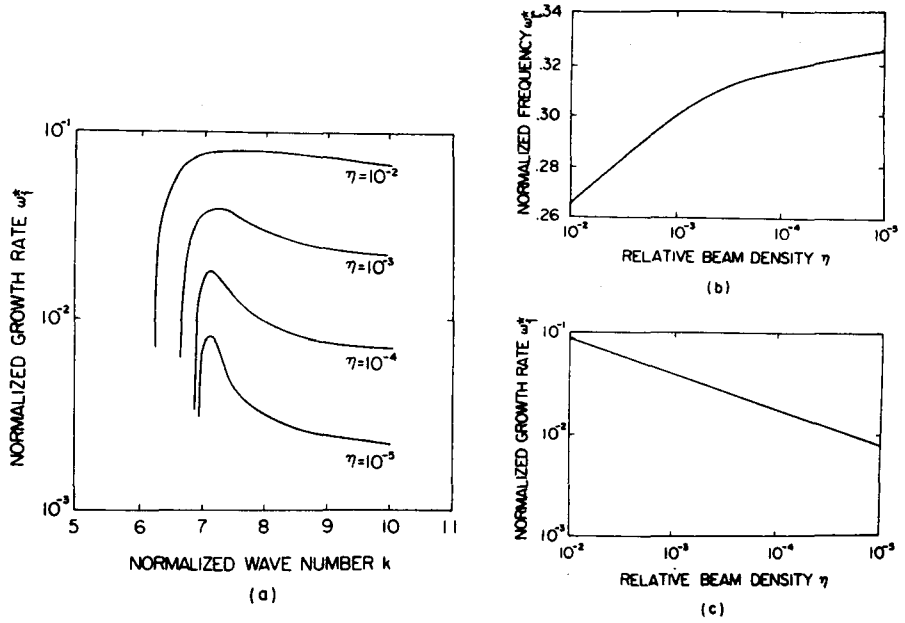

Fig.18 Dependence of the Growth Rate and the Frequency of the Whistler Mode Beam Cyclotron Instability upon the Relative Beam Density.

tion only to the whistler mode cyclotron instability in this plasma-beam system. It is also interesting to note that there exists a peculiar region in the ω-k diagram in Fig.17, in which the usual group velocity $\partial\omega_r/\partial k$ exceeds the light speed c, in the vicinity of the intersection of the whistler mode and the beam mode. This abnormal property, however, will be discussed in the next Section 4. A careful attention must be paid in a discussion of the energy transfer in such an instability region.

Though it is believed that suprathermal electrons exist as a beam in the magnetosphere, its relative density to the background thermal (cold) plasma is still unknown. Therefore it is useful and full of information to check the dependence of the instability characteristics upon the beam relative density η. Figs.18(a) and (b) show the dependence upon the relative beam density η of a real and an imaginary part of ω near the instability frequency respectively, where $10^{-2} \sim 10^{-5}$ are chosen as a plausible quantity for η. Fig.18(a) shows the relation between the growth rate of the instability and the wave number k with parameters of the relative density η. It can be easily seen that the less the beam relative density is, the clearer the whistler mode instability character can be distinguished from the beam mode instability and the corresponding frequency band becomes narrower around the frequency of the maximum growth rate. The corresponding real part of ω is shown as a function of η in Fig.18(b). The plot of the maximum growth rate vs. η is illustrated in Fig.18(c). It is found that the maximum growth rate ω_{imax} is increasing in proportion to the cubic root of η, which agrees well with the result obtained by Bell & Buneman[40].

The next interesting feature of the instability is the pitch angle dependence of the growth rate. This becomes important when we survey a behavior of the instability for a beam which travels along the geomagnetic field line with changing its pitch angle under the first magnetic invariant. For the pitch angles from 0 to $\pi/2$ of the beam particles with a constant kinetic energy, the maximum growth rate ω_{imax} and the corresponding real frequency ω_r change as shown in Figs.19(a) and (b). It is found that the quantity ω_{imax} changes slowly except the limits of $\alpha \to 0$ or $\alpha \to \pi/2$. In the limit of $\alpha \to 0$, the reduction of ω_{imax} is due to the reduction of the transverse energy as a supply of the energy source of

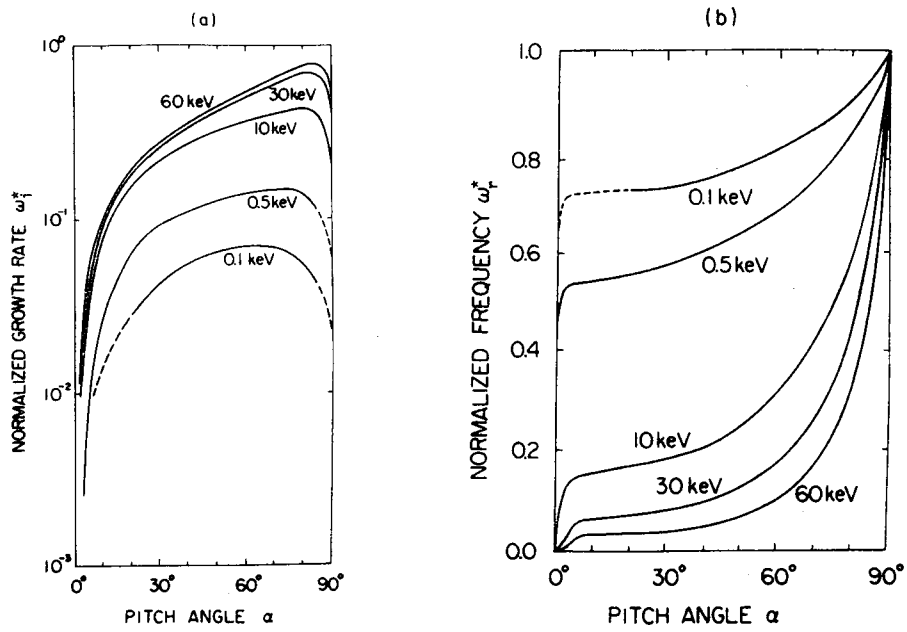

Fig.19 Dependence of the Growth Rate and the Frequency of the Whistler Mode Beam Cyclotron Instability upon the Beam Pitch Angle α.

the instability. However it should be noticed that in the limit of $\alpha \to \pi/2$, the corresponding real frequency ω_r tends toward the cyclotron frequency Ω_e so that the resonance character shown by the thermal plasma must begin to play a more important role than the beam coupling. Therefore the growth or damping rate cannot be described accurately by the simple calculation mentioned here.

3.1.3 The Moving Oscillator

In the application of the mechanism of the whistler mode beam cyclotron instability to the generation theory of VLF emissions in the magnetosphere, a crucial discussion arises whether or not the instability (or interaction) region moves along the geomagnetic field line of force, because the frequency-time characteristics of some types of the discrete VLF emissions can be simply explained if the instability region drifts along the geomagnetic field line. Helliwell[29] discussed this point with some physical insight about the wave-beam interaction. His discussion, however, on the "consistent-wave condition" is rather intuitive

and its physical meaning is obscure. Historically, the cyclotron instability was defined to be one of the class of the absolute instabilities, the region of which does not move spatially. In order to avoid the discrepancy between the moving oscillator and the absolute instability, the idea of the consistent-wave condition might have possibly been contrived by Helliwell[29]. At first Brice[39] and Bell & Buneman[40] considered that the beam-cyclotron instability in the whistler mode was an absolute instability because it resulted from a feedback mechanism. A simple application of the Sturrock[63] criterion for determining the type of the instability from the ω-k diagram showed that the beam-cyclotron instability was a type of the absolute instability. However, the whistler mode beam cyclotron instability is not a result of a coupling between two modes but among three modes, i.e., a whistler mode and two beam cyclotron modes. Therefore, we should use the Polovin[64] or Briggs[43] criterion in place of the Sturrock criterion which is valid only for the two mode coupling.

In the present section, we examine the instability characteristics ——— absolute or convective ——— after the Briggs criterion. The solutions of the dispersion equation (2.56) for complex k are plotted in Fig.20 where only an imaginary part ω_i of ω is varied from $-\infty$ to 0, keeping the real part ω_r of ω to fixed values. This picture shows that for some values of ω_r, the locus of the complex wave number k crosses the real k-axis in the k-plane for some complex value in the lower half ω-plane (No.4 and No.5 solid lines in Fig.20), which means that there exists an instability in this system. No locus, however, in the complex k-plane crosses each other which means that there appears no saddle point in the complex k-plane. Consequently, according to the Briggs criterion, the beam-cyclotron instability in the whistler mode should be regarded as a convective instability rather than an absolute instability.

The drift velocity of the instability region (or interaction region) can be estimated from the value of $\partial\omega_r/\partial k$ at $k = k_o$ for which the maximum growth rate is attained. An approximate analytical expression for the drift velocity can be derived from the dispersion equation (2.56) as follows. Since we are concerned with a frequency region in which the resonance condition $\omega_r - kV_{Bz} - \Omega_e = 0$ is nearly satisfied, we can well approximate ω by

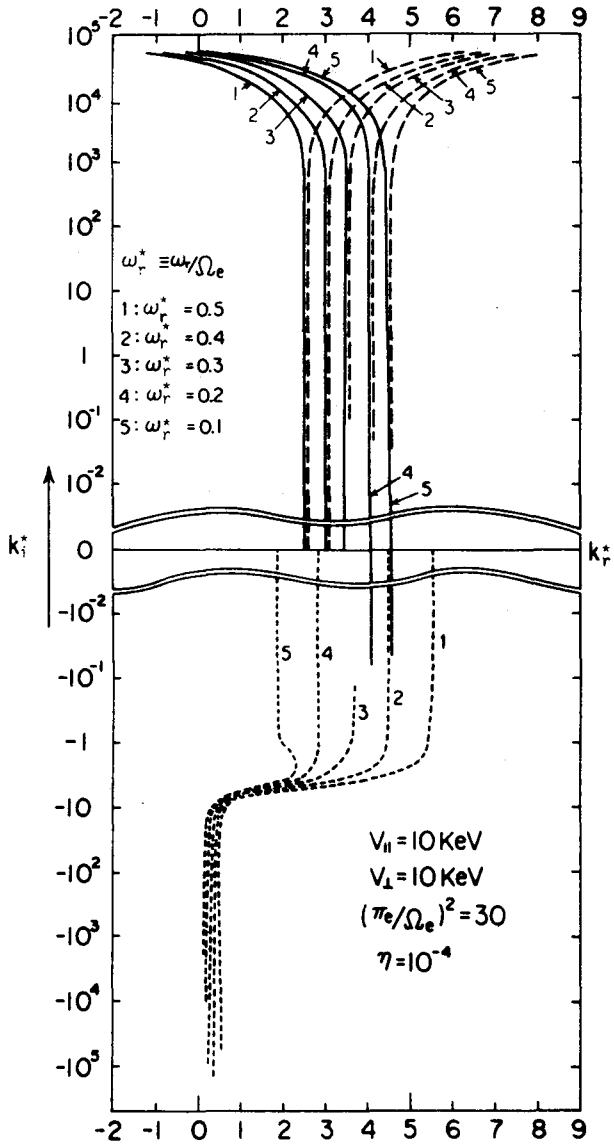

Fig.20 Mapping of the Solution of the Dispersion Equation (2.56) for a Criterion of the Instability.
The solid, dashed and dotted lines show different modes in the solutions. This mapping shows that the present plasma-beam system is free from an absolute instability.

$$\omega = \omega_L + \delta \ ,$$
$$\omega_L = kV_{Bz} + \Omega_e \ , \tag{2.57}$$

with a small complex quantity δ. Substituting Eq.(2.57) into Eq.(2.56), we get the following equation for the real part of δ with an assumption of

$$|\delta| << \frac{\frac{1}{2} k^2 V_{B\perp}^2}{\Omega_e} \ , \tag{2.58}$$

after an appropriate Taylor expansion around $\omega = \omega_L$.

$$\eta \Pi_e^2 k^2 V_{B\perp}^2 \frac{\partial F_{p1}}{\partial \omega} = 4\delta_r \left(F_{p1} + 2 \frac{\partial F_{p1}}{\partial \omega} \delta_r \right)^2 \ , \tag{2.59}$$

where

$$F_{p1} = c^2k^2 - \omega^2 + \frac{\Pi_e^2 \omega}{\omega - \Omega_e} \Big|_{\omega=\omega_L} \ . \tag{2.60}$$

It is noted that ions are considered as an immobile background in the above procedure. Differentiation of Eq.(2.59) with k then gives

$$\frac{\partial \delta_r}{\partial k} = \frac{\eta \Pi_e^2 k^2 V_{B\perp}^2 \frac{\partial^2 F_{p1}}{\partial \omega \partial k} + 2\eta \Pi_e^2 k V_{B\perp}^2 \frac{\partial F_{p1}}{\partial \omega} - 8\delta_r \left(F_{p1} + 2\frac{\partial F_{p1}}{\partial \omega}\delta_r\right)\left(\frac{\partial F_{p1}}{\partial k} + 2\frac{\partial^2 F_{p1}}{\partial \omega \partial k}\delta_r\right)}{4\left(F_{p1} + 2\frac{\partial F_{p1}}{\partial \omega}\delta_r\right)\left(F_{p1} + 6\frac{\partial F_{p1}}{\partial \omega}\delta_r\right)} \ . \tag{2.61}$$

Drift velocity of the interaction region is defined by $V_{Bz} + (\partial \delta_r / \partial k)\big|_{\delta_i = \delta_{imax}}$ and hence adopting an approximate result for δ_{imax} and δ_{rmax} obtained by Bell & Buneman[40] as

$$\delta_{imax} = 0.69 \left(- \frac{\eta \Pi_e^2 k^2 V_{B\perp}^2}{\partial F_{p1} / \partial \omega} \right)^{\frac{1}{3}} \ , \tag{2.62}$$

$$\delta_{rmax} = 0.50 \left(- \frac{\frac{1}{2} \eta \Pi_e^2 k^2 V_{B\perp}^2}{\partial F_{p1} / \partial \omega} \right)^{\frac{1}{3}} \ , \tag{2.63}$$

we finally get the following expression for the drift velocity V_D of the

interaction region with some approximations as

$$V_D \equiv \frac{\partial \omega_r}{\partial k}\Big|_{k=k_o} = V_{Bz} + \frac{\partial \delta_r}{\partial k}\Big|_{\delta_i=\delta_{imax}}$$

$$= V_{Bz} - \frac{\sqrt[3]{4}}{6} \frac{\eta^{\frac{2}{3}} \Pi_e^{\frac{2}{3}} V_{B\perp}^{\frac{2}{3}} (3kV_{Bz} + \Omega_e)}{k^{\frac{1}{3}} (\partial F_{p_1}/\partial \omega)^{\frac{4}{3}}} , \qquad (2.64)$$

where k should be determined from Eqs.(2.57) and $F_{p_1} = 0$.

It is then clarified that the whistler mode beam cyclotron instability is of a convective type, meaning physically that the instability region moves along the geomagnetic field line. Thus the concept of the "moving oscillator" of not a single particle but of the instability, is established without any other conditions. The generation mechanisms of some types of the discrete VLF emissions are now possibly attributed to the present convective beam cyclotron instability in the whistler mode.

3.2 Generation Mechanism of Some Sort of Discrete VLF Emissions

In the previous section 3.1, the dispersion equation for an infinite and uniform system composed of a stationary cold magnetoactive plasma and a helical electron beam has been investigated. In order to apply the previous calculation to the magnetospheric VLF problem, a particular plasma column along a geomagnetic field line with a shell parameter of $L \simeq 4$ will be selected. In each part of the column, the plasma may be treated electromagnetically as uniform and infinite in the sense that the wavelength of interest is much smaller than the scale of medium non-uniformity. Therefore, an inquiry is attempted into the generation mechanism of a certain type of the discrete VLF emissions by applying the results of the previous section.

The situation of the present interest is schematically shown in Fig.21. It is well known that the VLF emission activity in the magnetosphere lies around the magnetic shells between L = 3 and 5, and hence we investigate, for the sake of reality, the convective beam cyclotron instability in the region along such a field line. A component of electromagnetic waves with some frequency ω_o transmitted from the point T on the

ground or just below the ionosphere propagates along a line of force of the geomagnetic field and is received at the conjugate point R on the opposite hemisphere. An electron beam is assumed to travel in the direction opposite to that of the wave of interest. It is indicated that the plasma-beam system in such a case should yield an instability for waves in the whistler mode.

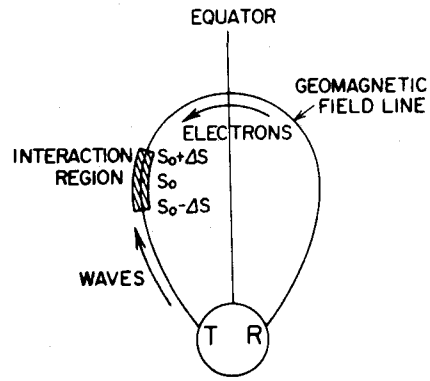

Fig.21 Schematic Illustration of the Beam-Wave Coupling in the Magnetosphere

Since the magnetospheric plasma changes its plasma parameters along the field line, though it is slowly varying, we can find a region where the growth rate becomes maximum for the frequency ω_o. We call this region conventionally the "interaction region". When the wave transmitted from T passes through this interaction region between $S_o - \Delta S$ and $S_o + \Delta S$, as schematically shown in Fig.21, for a time period from t_o to $t_o + \Delta t$, the situation appears as if a disturbance with a frequency of ω_o is applied as a pulse-modulated source in the vicinity of S_o. Since the plasma-beam system in our case is free from an absolute instability, the initial switch-on of the "oscillator" is thus made. The oscillator begins to drift with a velocity of $V_D = \partial\omega_r/\partial k \,|_{k=k_o}$ defined by Eq.(2.64) which is uniquely determined by the plasma parameters at the local region around S_o.

It is noticed in the above discussion that the frequency of the wave excited by the instability does not change with time even when the interaction region drifts, if the background plasma-beam system is uniform. A slow change, however, of the magnetospheric plasma parameters along the field line makes it possible to explain the varying frequency-time spectra in a manner to be mentioned below.

The instability region which lies initially around the point S_o at $t = t_o$ begins to drift with the velocity V_D and arrives at an adjacent point S_1 after a time increment Δt where the plasma parameters change to some extent. At this adjacent place, the frequency corresponding to the maximum growth rate shifts to ω_1 which is slightly different from ω_o. The energy component of ω_1 is contained in the wave packet coming from S_o

since the energy spectrum of the wave excited at the initial point S_o has a spread around ω_o. Therefore the wave of a frequency ω_1 grows up and becomes the most prominent component in the instability region which now arrives at S_1. By a similar procedure, the convective beam cyclotron instability propagates along the system with slowly varying parameters. Thus the observer far away from the instability region can receive the waves whose frequency changes with time. This successive triggering of the instability by the moving oscillator in the slowly varying inhomogeneous plasma is schematically depicted in Fig.22. Fig.22(a) shows the spectral change of the most unstable frequency. At any location, the excited spectrum as well as the most rapidly growing frequency is determined. An illustration is given in Fig.22(b) of the time-evolution of the instability for various frequencies. It can

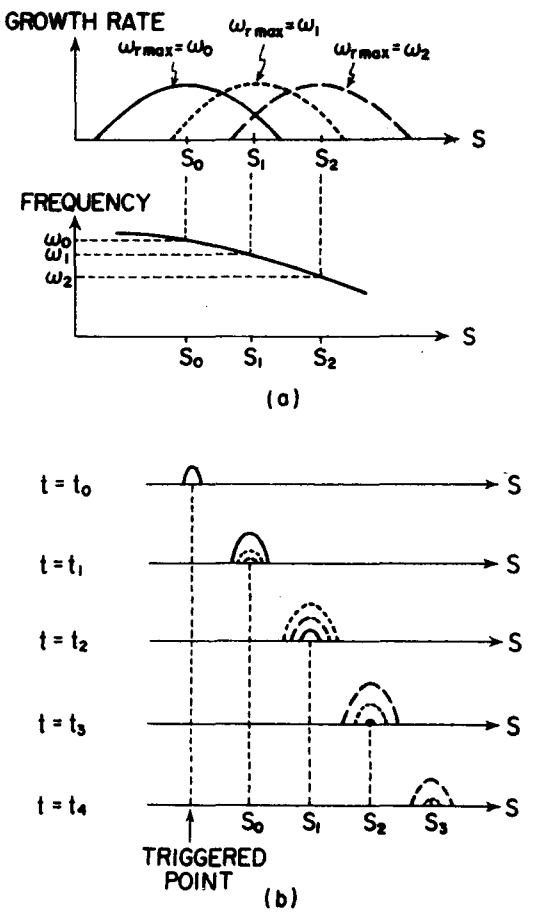

Fig.22 An Illustration of Explaining the Successive Triggering of the Convective Beam Cyclotron Instability in Slowly Varying Inhomogeneous Plasma.

be well understood how wave packets can be successively excited by the convective beam cyclotron instability even in a slightly inhomogeneous plasma. It is, therefore, concluded that, in this mechanism, the termination of the emission depends upon the condition of whether the energy density of the frequency of the maximum growth rate supplied as a "seed" of the instability comes into the interaction region or not from the previous adjacent point.

It is now demonstrated that the convective beam cyclotron instability in the whistler mode exhibits the time varying frequency characteristics due to the slowly varying plasma parameters along a geomagnetic field line in the magnetosphere. We then concern ourselves in the explanation of various types of discrete VLF emissions by the present idea throughout the remainder of this section.

Since the main factor which controls the most rapidly growing frequency is the local cyclotron frequency in the interaction region, the excited wave must have the lowest frequency when the instability region lies on the equator. The "risers" or the "falling tones" can be generated when the convective instability drifts down to the earth or moves upwards the equator, respectively. If the condition of successive triggering (i.e., successive drift of the instability region) is satisfied so as to continue to drift over the equator, one observes a "hook" at the receiving point R. All of them have been well explained by the previous theories so far proposed (Gallet & Helliwell[65]; Dowden[66]; Helliwell[29] etc.), though the drift mechanisms of the oscillator (or radiator in case of the single particle theory) in those theories were quite different from the present theory. However, the most difficult but most fascinating types of spontaneous emissions which nature shows us are "inverted hooks" and "oscillatory tones".

Helliwell[29] first explained the oscillatory tones by the oscillator moving back and forth around the equator in his theory. Our present analysis, however, on the drift velocity of the interaction region never shows such a piston motion around the equator. Therefore, such an oscillatory tone seems not to be attributed to such a wandering interaction region around the equator. In the present theory, they are explained as follows.

When the convective instability region drifts toward the mirror

point, the backward emission propagates toward and over the equator. After passing the equator, the emission suffers a great time delay when the local cyclotron frequency approaches the frequency of the emission, which yields the slow change of the observed frequency at the observing point at the hemisphere. One example of the time-delay due to the dispersion is illustrated in Fig.24. We can see that an almost constant frequency is observed even when the frequency changes quickly at the generated point. Therefore, an energy of an almost constant single frequency is supplied continuously to the plasma for some time at the hemisphere. If the duration of supply is moderately long, the instability may be triggered first at the conjugate point with respect to the equator, since the instability condition is similar there with the highest possibility. The new oscillator, then, goes up toward the equator, while the emitted wave travels down from the oscillator to the observer on the ground. One cannot distinguish the newly generated wave by the new instability region (daughter instability) from the triggering wave by the original (mother) instability at the conjugate point. Thus we can observe the "inverted hooks" as a continuous tone on the ground. Furthermore, if such a new instability region continues to drift to the region around the opposite mirror point after having passed the equator and triggers again the successive new instability at the conjugate point, the "oscillatory tone" could be generated. Such a process of the generation of the inverted hooks and the oscillatory tones is schematically explained in Fig.23 as well as that for the risers and the falling tones. We should notice, however, that the condition for sustaining such a long-run successive triggering is very severe so that the oppotunity for generation of such type of emissions as the oscillatory tones may be very few. Necessary conditions for such successive triggering of the new instability at the conjugate point are;

1) symmetrical distribution of the electron beam around the equator,
2) strong intensity of the emitted wave from the mother instability region

and

3) enough duration of time of a constant frequency wave which depends mainly upon both the drift velocity of the convective instability around the mirror point of the electron beam and the plasma para-

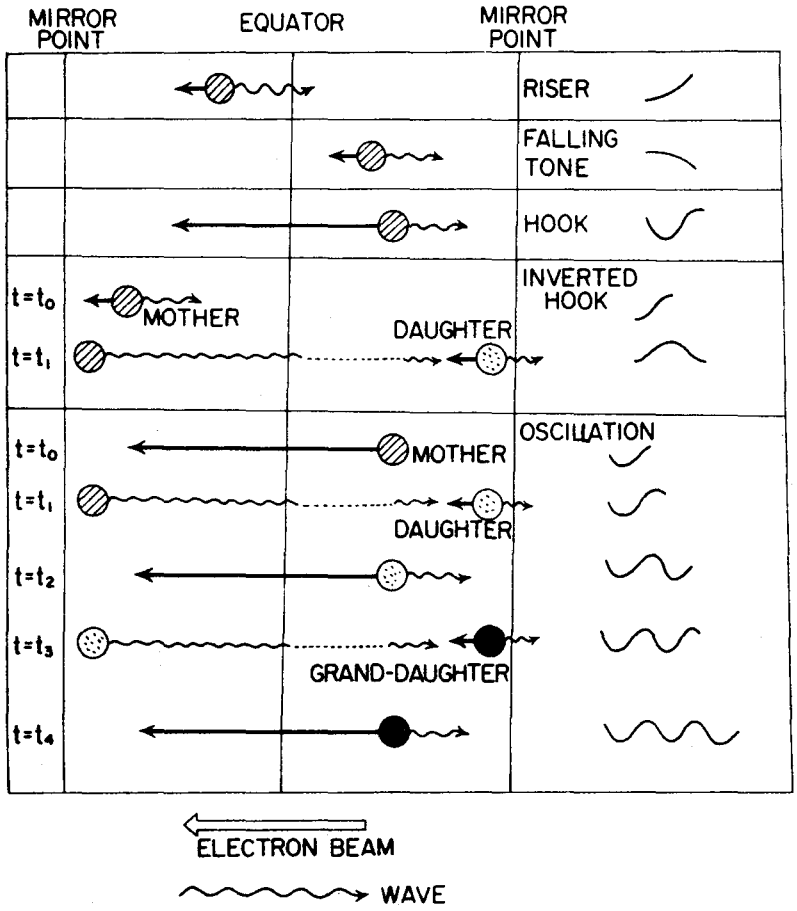

Fig.23 Speculative Illustration of the Explanation of Various Types of the Discrete VLF Emissions by the Convective Beam Cyclotron Instability in the Whistler Mode.

meters around the conjugate point.

All of the above conditions should be satisfied for the appearance of the "inverted hooks" and "oscillatory tones". Fig.23 gives a speculative illustration of the generation of various types of the discrete emissions. Therefore, once a numerical calculation has been made on the motion of the convective instability region from a mirror point to the conjugate mirror point along a given field line, it is possible to acquire a theoretical spectrum for any type of emissions quantitatively by combining the numerical result with the speculative illustration in Fig.23. A typical example of the frequency-time characteristics generated by such a traveling convective instability, i.e., by the "moving oscillator",

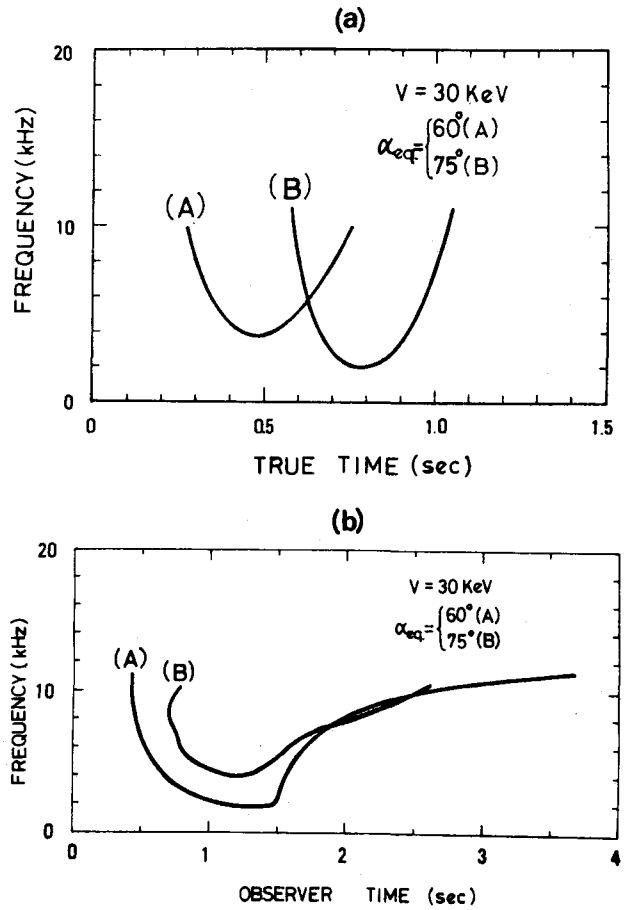

Fig.24 A Calculated Frequency-Time Spectrum of a Discrete VLF Emission Generated by the Convective Beam Cyclotron Instability; (a) the frequency spectrum at the generated point, (b) the frequency spectrum at the observing point.

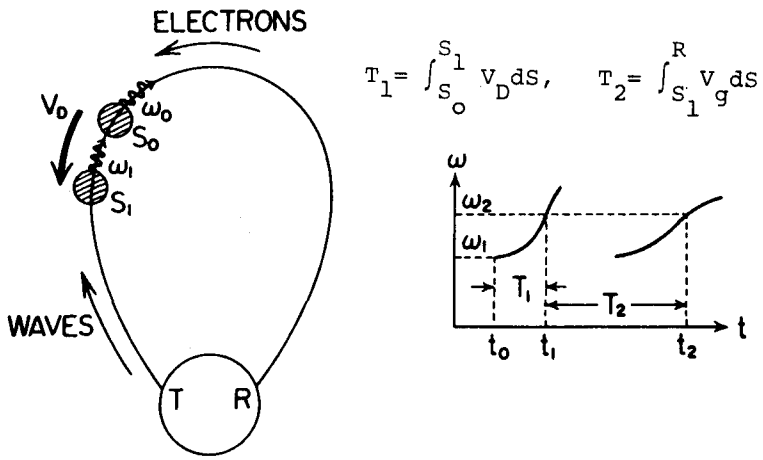

Fig.25 Deducing Method of the Observed Spectrum Fig.24(b) from the Generated Spectrum Fig.24(a).

which travels from a mirror point to the conjugate mirror point, is shown in Fig.24. Fig.24(a) shows a frequency-time characteristic at a generated place on the field line (L ≃ 4 in this case). The frequency-time spectrum at the observing point on the ground is also calculated and depicted in Fig.24(b). The latter observed spectrum was deduced from the former by calculating the propagation time along the field line as schematically illustrated in Fig.25, because a wave generated at the instability region can propagate in the normal whistler mode along the plasma column outside the interaction region. In the present calculation, the plasma parameters along a plasma column of L ≃ 4 are calculated from Angerami's diffusive equilibrium model[14] for the plasma density and from a centered dipole model for the magnetic field intensity.

The difference between Helliwell's[29] and the present theory[30] becomes clear. In the Helliwell theory, the "moving oscillator" was assumed to move due to the "consistent-wave condition", but its driving mechanism was rather obscure physically. In the present theory, on the other hand, a single "moving oscillator" cannot generate all types of emissions by itself but its driving mechanism is clear, and yet it is possible to explain various types of VLF emissions by considering a successive triggering of the other similar oscillators.

3.3 Discussion and Conclusions

A wide-band type of VLF emissions is now thought to be related to the diffusion and precipitation of the high-energy particles in the magnetospheric plasma. On this point, we will discuss in Chapter III. These emissions such as "hiss" are clearly the manifestation of rather incoherent characteristics of the magnetospheric plasma. On the other hand, discrete emissions show more coherent features of the wave-particle interactions occurring in the magnetosphere and are clearly related to the high energy beams in the particle distributions. According to the observations of spontaneously triggered discrete emissions, they can be classified into two types; one of which shows a rapid frequency change, the other hardly shows a frequency change with time. As the generation mechanism of the first type of the discrete emissions with a rapid frequency change, we investigated the convective beam cyclotron instability

in the whistler mode as a candidate of the generation mechanism by considering the application of the instability to the magnetospheric plasma which varies slowly along the geomagnetic field line. This attempt explained in success the spectral forms of the "inverted hooks" and "oscillatory tones" as well as other popular types of discrete VLF emissions without any assumption upon a wave condition. Instead of the wave-condition, we introduced the idea of the successive triggering of the instability.

The theory, however, developed in this section is within the linear theory and hence the most important and interesting problem of a quantitative triggering process of the instability has not been mentioned. The switch-on of the instability is simply thought to be brought by a "seed" of the incoming wave produced by the other sources. The triggering problem and its successive relevant nonlinear evolution of the instability will give an important key to the solution of the ASE phenomenon and of the generation process of the other type of discrete VLF emissions with almost constant frequency which is often triggered just above the cutoff frequency of nose whistlers. These problems will be postponed in the nonlinear treatment in Chapter III and IV and were not discussed here.

§4. Propagation Velocities of Waves in Anomalous Media of Beam-Cyclotron Instability[52]

4.1 Description of the Problem

It is difficult to define precisely the velocity of a signal passing through a dispersive medium which has the spread of a frequency spectrum. First scalpel was plunged by Lord Rayleigh[67] who established the concept of the "group velocity". He showed that the main energy accompanied with a wave packet is carried by the "group velocity", while the phase propagates by the "phase velocity". This is really a case for the wave propagations in normally dispersive media. In the case of abnormally dispersive media in which an infinitely large value of the group velocity is apparently given from the ω-k diagram, a detailed investgation was

performed by Sommerfeld[68] and Brillouin[69,70]. Sommerfeld introduced a "terminated wave" which continues from t = 0 to t = ∞ in order to determine the velocity of the propagation of a signal. He examined how the wave front of the terminated wave propagates in such an abnormally dispersive medium by the use of the complex integral and found that the group velocity $\partial\omega_r/\partial k$ loses the meaning of signal velocity in such a case. Brillouin investigated more quantitatively the velocities of propagation by the usual saddle point method for the analytical solution of the complex integral and showed that a signal velocity can never exceed the light speed c even when the group velocity is greater than c. Recently Hines[71~74] again attacked the same problem by comparing the Sommerfeld-Brillouin method with that of the Poynting flux vectors. He also concludes that the main part of the wave energy is carried by the so-called group velocity $\partial\omega_r/\partial k$ insofar as the medium is normally dispersive.

Thus it is now well established that the group velocity which exceeds the light speed loses its meaning of the propagation velocity of the wave energy or of the signal. In such a case, however, it has not yet been established quantitatively by what quantity the propagation velocity of the wave energy or of the signal is then determined. Hence in order to know the actual velocity of the signal propagation in such a case, we should inquire numerically after the solution case by case.

It is one of such problems what we have discussed briefly in the introduction and the previous section of this chapter. In Fig.17, we saw a region in the ω-k diagram where the group velocity exceeds the light speed. A more detailed illustration of the ω-k diagram around the interaction point is given in Fig.26. This is the ω-k diagram for

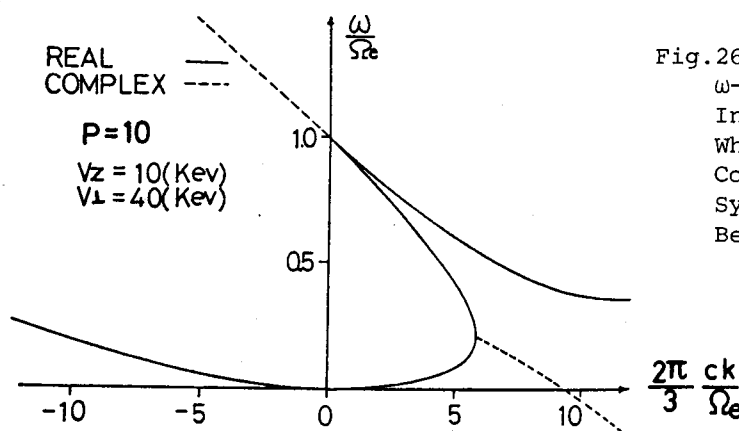

Fig.26 Typical Example of the ω-k Diagram around the Interaction Region in the Whistler Mode for the Collisionless Plasma-Beam System with a δ-functional Beam.

$\eta = 10^{-2}$

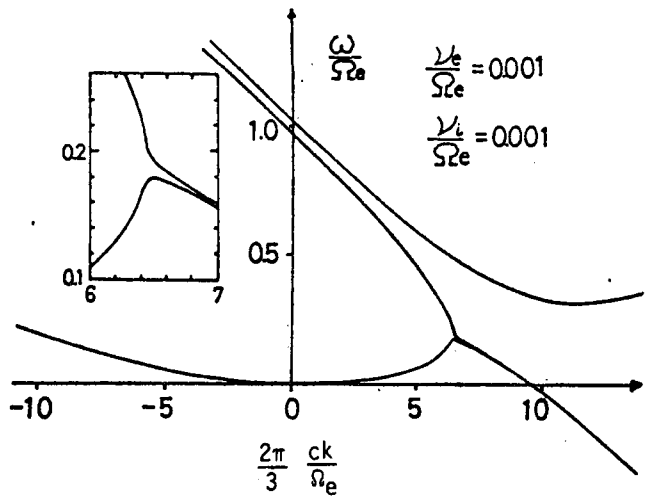

Fig.29 Typical Example of the ω-k Diagram around the Interaction Region in the Whistler Mode for the Collisional Plasma-Beam System with a δ-functional Beam. The parameters used in the calculations are the same as in Fig.26.

in the plasma-beam system which manifests a beam convective instability. Therefore, whenever we discuss the wave propagation in such a system, a careful attention should be paid. A simple calculation of the group velocity leads to an erroneous result. In the remainder of this section, we will discuss how to determine the propagation velocity of the main signal in such anomalous media, and will show a result of a numerical approach.

4.2 Method for Determining the Signal Velocity

4.2.1 Sommerfeld-Brillouin Method

In this section, we will briefly review a classical method for analysis of the wave propagation in the dispersive medium in order to compare the Fourier-Laplace method that will be used in the present paper.

As mentioned before, the "terminated wave" which initiates at t = 0 is usually considered in investigating the propagation of the wave. This terminated wave with a frequency ω_o is expressed mathematically by

$$s(t) = \frac{1}{2\pi} \mathrm{Re} \int_{Br} e^{-j\omega t} \frac{d\omega}{\omega-\omega_o} , \tag{2.67}$$

where Br denotes a Bromwich's integral path, and Re indicates to take the real part of the following quantity. The signal s(t,z) after passing through a dispersive medium is expressed as

$$s(t,z) = \frac{1}{2\pi} \mathrm{Re} \int_{Br} e^{-j(\omega t-kz)} \frac{d\omega}{\omega-\omega_o} . \tag{2.68}$$

The validity of the above expression is not given in the original literature, but its physical meaning would be that the signal intensity at a time t and a position z can be expressed as a sum of the waves with a phase of $\exp\{-j(\omega t-kz)\}$ since the phase at z is different from that at z = 0 by $\exp(-jkz)$. Sommerfeld and Brillouin used the above equation, (2.68), for solving the propagation in the dispersive medium which is characterized by the following dispersion equation

$$k^2 = \frac{\omega^2}{c^2} \left(1 + \frac{\Pi_e^2}{\omega_c^2 - 2j\rho\omega - \omega^2} \right) , \tag{2.69}$$

where ω_c is a characteristic frequency of the medium, and ρ is an attenuation constant. We can see that the integrand of the integral in Eq. (2.68) has the following five singular points: One of them is a pole at $\omega = \omega_o$ which comes from the denominator of the integrand in Eq.(2.68), and the others are the branch points which come from the exponential term of the integrand in Eq.(2.68). They are determined from Eq.(2.69) by letting k = 0 or ∞ as

$$\begin{aligned} \omega &= -j\rho \pm \sqrt{\omega_c^2 - \rho^2} \qquad \text{when} \quad k = \infty , \\ \omega &= -j\rho \pm \sqrt{\omega_c^2 + \Pi_e^2 - \rho^2} \quad \text{when} \quad k = 0 . \end{aligned} \tag{2.70}$$

Therefore the five singular points are mapped by "×" as shown in Fig.30. Since $k \to \omega/c$ when $|\omega| \to \infty$, the integral in Eq.(2.68) can be estimated by deforming the Bromwich integral path "u" into a path in the upper half ω-plane "a" as shown in Fig.30 to yield

$$s(t,z) = 0 \qquad \text{for} \quad t < \frac{z}{c} . \tag{2.71}$$

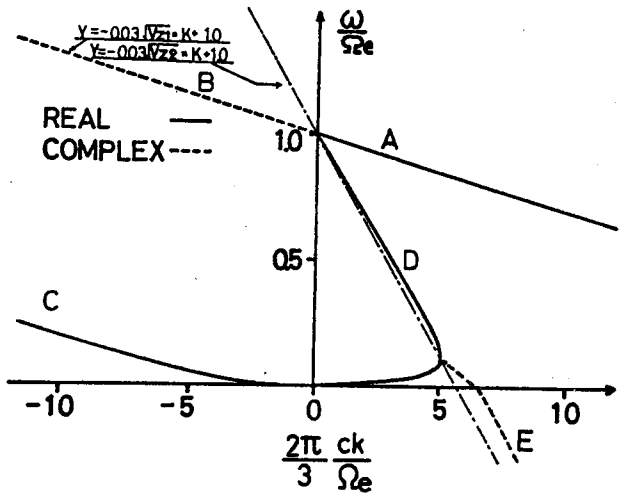

Fig.27 Typical Example of the ω-k Diagram around the Interaction Region in the Whistler Mode for the Plasma-Beam System with a Beam of the Square Distribution. The parameters used in the calculation are;

$P \equiv \Pi_e/\Omega_e = 10$, $V_{z_1} = 1\text{keV}$, $V_{z_2} = 29\text{keV}$,

$\eta = 10^{-2}$, $\langle V_{B\perp} \rangle = 40\text{keV}$.

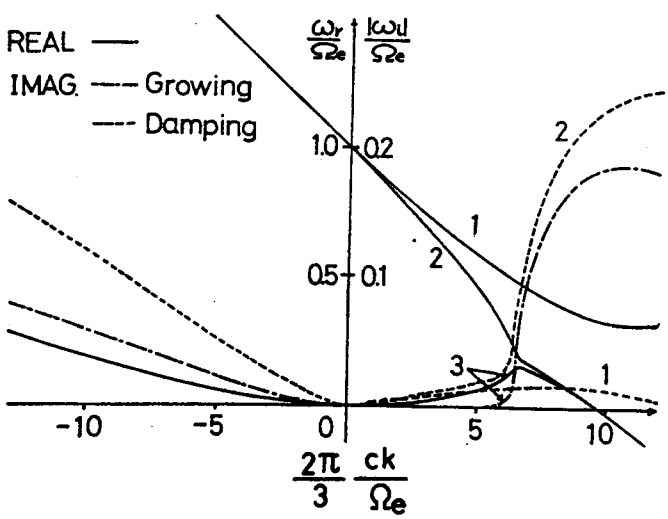

Fig.28 Typical Example of the ω-k Diagram around the Interaction Region in the Whistler Mode for the Plasma-Beam System with a Beam of the Cauchy Distribution. The parameters used in the calculation are;

$P \equiv \Pi_e/\Omega_e = 10$, $\langle V_{B\perp} \rangle = 40\text{keV}$, $V_{Bz} = 10\text{keV}$,

$\eta = 10^{-2}$, $V_T = 0.01\text{keV}$

the plasma-beam system composed of a cold background plasma and a cold beam which is described by the δ-functional distribution function. An anomalous dispersion around $\omega_r/\Omega_e \simeq 0.2$ is seen in Fig.26. It is, however, supposed that the anomaly depends wholly upon an artificial assumption of the distribution function for the beam such as the δ-function. In order to check it, other distribution functions which are supposed more realistic were assumed. One of them is a "square distribution function" which has a spread in the particle velocity parallel to the external magnetic field and is expressed as

$$F_b(V_z,V_\perp) = \frac{N\eta}{2\pi} h_b(V_\perp) \frac{1}{|V_{z_2}-V_{z_1}|} , \qquad \text{for } -V_{z_2} \leq V_z \leq -V_{z_1} ,$$

$$= 0 , \qquad \text{for } V_z > -V_{z_1} \text{ and } V_z < -V_{z_2} , \tag{2.65}$$

where $h_b(V_\perp)$ is an arbitrary function. The other is the well known Cauchy distribution function which is expressed by

$$F_b(V_z,V_\perp) = \frac{V_T}{2\pi} \frac{1}{(V_z+V_{Bz})^2+V_T^2} h_b(V_\perp) , \tag{2.66}$$

where V_T is a measure of the thermal spread of the beam distribution around V_{Bz}. Typical examples of the ω-k diagrams for these distribution functions are illustrated in Figs.27 and 28. For a beam with the square distribution, there still remains an anomalous region, as seen in Fig.27. While, for the Cauchy distribution which may be more realistic, there is no region where the group velocity becomes infinity as seen in Fig.28. There, however, exists a region near the interaction point where the group velocity exceeds the light speed. This tendency becomes distinct when the thermal spread V_T in the beam approaches to zero. A similar situation is realized even for the δ-functional beam, if the effect of collision is taken into account. An example of this case is shown in Fig.29. As seen in the figure, there still remains a frequency range where the anomalous group velocity which does not, however, become infinity, is found.

As discussed above, an anomalous frequency region appears essentially

When $t > \frac{z}{c}$, on the other hand, the Bromwich integral can be replaced by another deformed path, labeled "b" in Fig.30. As we can reduce the integral on the lines "b_1" and "b_2" to zero, the integral in Eq.(2.68) can be estimated by the residue around ω_o and the integrals along "b_4" and "b_5" around the branch cuts. The result is formally written by

$$s(t,z) = e^{-\frac{2\pi\kappa_A}{\lambda}z} \sin 2\pi\left(\frac{t}{\tau_o} - \frac{z}{\lambda}\right) + BR, \quad \text{for} \quad t > \frac{z}{c}, \qquad (2.72)$$

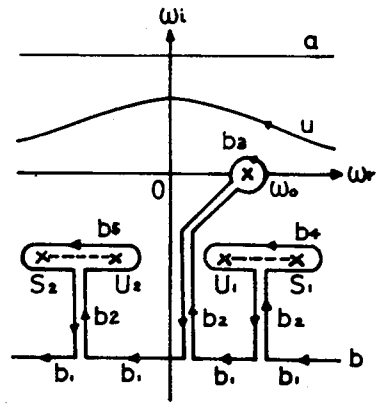

Fig.30 Singular Points and Deformed Integral Paths in the ω-Plane (after Fig.6 in Brillouin[70]). Dashed lines indicate the branch cuts.

where τ_o, λ and κ_A are a period of the given frequency ω_o (i.e., $\tau_o = 2\pi/\omega_o$), the distance z between the adjacent points of the same phase and the logarithmic decrement of the amplitude as the wave moves through one wavelength, and BR indicates a contribution from the integrals along "b_4" and "b_5". The first term corresponds to the forced oscillation by the input wave, while the rest term BR comes from a free transient motion of the constituents of the medium.

If we take only the first term in Eq.(2.72), we know that a wavy motion with a finite amplitude suddenly begins at t = z/c and propagates with a phase velocity $V_{ph} = \lambda/\tau_o = \omega_o/k_o$. Such a sudden commencement of a signal is, however, impossible due to a transient characteristic of the medium. Brillouin[70] put this point into a quantitative calculation by estimating BR by the "saddle point method" of the complex integral. He obtained the following result.

" It was found that after penetrating to a certain depth in the medium, the signal changes. The first forerunners arrive with a velocity c; their originally very small period increases continuously, their amplitude increases and, taking the damping into account, then decreases, until the period is equal to the characteristic period of oscillating electrons.

The second forerunners arrive with the velocity $c\omega_c/\sqrt{\omega_c^2+\Pi_e^2} < c$ determined by the dielectric constants; their period is at first very large and then decreases, while their amplitude behaves in a manner similar to that of the first forerunners. These two forerunners can partly overlap. In general, their amplitude is very small but increases rapidly as their period approaches that of the signal."

The time variation of the forerunners and the signal is schematically shown by him and is re-illustrated in Fig.31, here. He defined the signal velocity V_s as a velocity with which the main signal arrives, though it is not defined accurately. A more detailed examination by Brillouin yielded that V_s coincides with V_g when ω_o is much far from the characteristic frequency ω_c but V_s becomes incoincident with the group velocity V_g when ω_o approaches ω_c. The famous result obtained by Brillouin about the c/V_{ph}, c/V_g and c/V_s is re-depicted in Fig.32. As seen in the figure, V_s never exceeds the light speed c even in a frequency region where the group velocity exceeds c or even becomes negative.

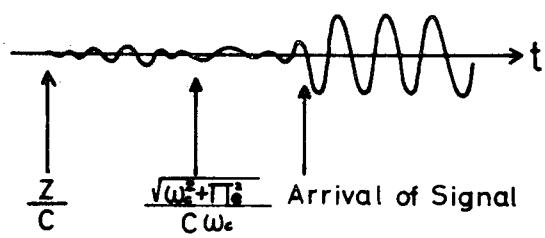

Fig.31 Schematic Illustration of the Arrival of the Two Forerunners and the Signal. (after Fig.20 in Brillouin[70])

Fig.32

Brillouin's Result of the Relation between the Signal Velocity, Group Velocity and the Phase Velocity.

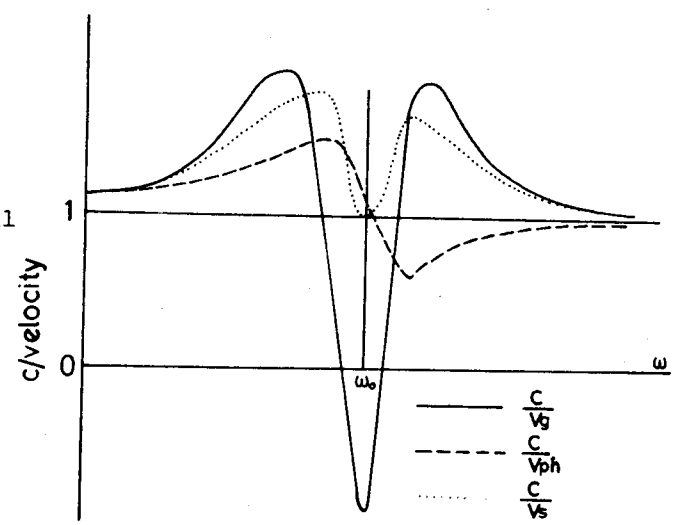

In the above, we briefly followed the famous method by Sommerfeld-Brillouin shortly. In the case that the singular points such as a branch point are not found easily, the Sommerfeld-Brillouin method is not so effective in comparison with the numerical Fourier-Laplace inverse transformation method.

4.2.2 Inverse Fourier-Laplace Transformation Method

A more basic method to acquire the response of a signal in a medium in the real time and space is to calculate the inverse Fourier-Laplace transformation of the signal.

Let us consider a case in which the system under consideration is well described by the following linear equation for the one-dimensional quantity $\vec{E}(t,z)$ in space as

$$\begin{bmatrix} L_{xx} & L_{xy} & L_{xz} \\ L_{yx} & L_{yy} & L_{yz} \\ L_{zx} & L_{zy} & L_{zz} \end{bmatrix} \begin{bmatrix} E_x \\ E_y \\ E_z \end{bmatrix} = \begin{bmatrix} e_x \\ e_y \\ e_z \end{bmatrix} , \tag{2.73}$$

where e_x, e_y and e_z are the disturbances imposed upon the system and L_{ij}'s $(i,j = x,y,z)$ indicate the linear operator which is a function of $\partial/\partial t$, $\partial^2/\partial t^2, \cdots$; $\partial/\partial z$, $\partial^2/\partial z^2$ $\cdots$. If the system under consideration is uniform in both space z and time t, the solution of Eq.(2.73) is formally given by

$$\vec{E}(t,z) = \int_0^t dt' \int_{-\infty}^{\infty} dz' \, [G_r(t-t',z-z')] \, \vec{e}(t',z') \quad , \tag{2.74}$$

where $[G_r(t,z)]$ is a Green's function. The Fourier-Laplace transformation of Eq.(2.74) gives

$$\tilde{\vec{E}}(\omega,k) = [\tilde{G}_r(\omega,k)] \, \tilde{\vec{e}}(\omega,k) \quad , \tag{2.75}$$

by the use of the convolution theorem, where ~ denotes the transformed quantity defined by

$$\tilde{\vec{E}}(\omega,k) = \int_0^{\infty} dt \int_{-\infty}^{\infty} dz \, \vec{E}(t,z) \, e^{-j(\omega t - kz)} \quad , \tag{2.76}$$

and

$$\vec{E}(t,z) = \frac{1}{(2\pi)^2} \int_{Br} d\omega \int_{-\infty}^{\infty} dk \, \tilde{\vec{E}}(\omega,k) \, e^{j(\omega t - kz)} \quad . \tag{2.77}$$

Therefore, if we could get a transformed equation (2.75), a solution for the response in real time and space can be obtained by a calculation of Eq.(2.77).

In a problem of a wave propagation in a plasma-beam system which manifests the whistler mode beam cyclotron instability, a transformed relation in a form of Eq.(2.75) can be obtained by the usual well established method. The basic equations are the Maxwell equations

$$\nabla \times \vec{E} = - \frac{\partial \vec{B}}{\partial t} \quad , \tag{2.78}$$

$$\nabla \times \vec{B} = \mu_o (\vec{J} + \vec{J}_s) + \frac{1}{c^2} \frac{\partial \vec{E}}{\partial t} \quad , \tag{2.79}$$

and the Vlasov equation

$$\frac{\partial f}{\partial t} + \vec{V} \cdot \frac{\partial f}{\partial \vec{r}} - \frac{e}{m} (\vec{E} + \vec{V} \times \vec{B}) \cdot \frac{\partial g}{\partial \vec{V}} - \frac{e}{m} (\vec{V} \times \vec{B}_o) \cdot \frac{\partial f}{\partial \vec{V}} = 0 \quad , \tag{2.80}$$

where $f(\vec{V},\vec{r},t)$ is a perturbation of the velocity distribution function $F(\vec{V},\vec{r})$ and $\vec{E}$ and $\vec{B}$ are the wave field intensities. $\vec{J}$ and $\vec{J}_s$ are defined by

$$\vec{J} = - e \int f \vec{V} d\vec{V} \quad , \tag{2.81}$$

$$\vec{J}_s = \delta(z) \, e^{j\omega_o t} \, H(t) \, \hat{s} \quad , \tag{2.82}$$

namely, $\vec{J}$ is a current density formed by the plasma particles and $\vec{J}_s$ denotes an imposed current source to the system, where $\delta(z)$, $H(t)$ and $\hat{s}$ are the delta-function, Heaviside's step function and a unit vector in the direction of $\vec{J}_s$. Under the following assumptions

$$\begin{aligned} 1^\circ \quad & \vec{E}(t=0,z) = 0, \quad \partial\vec{E}/\partial t(t=0,z) = 0, \\ & \vec{B}(t=0,z) = 0, \quad \partial\vec{B}/\partial t(t=0,z) = 0, \end{aligned} \tag{2.83}$$

$$2^\circ \quad B(t,z=\infty) = B(t,z=-\infty) = 0 \quad , \tag{2.84}$$

we obtain the well-known relation as

$$\tilde{\vec{E}}(\omega,k) = \frac{1}{\varepsilon_o\omega^2}\,\frac{1}{P_o\{(S_o-n^2)^2-D_o^2\}}\begin{bmatrix} P_o(S_o-n^2) & jP_oD_o & 0 \\ -jP_oD_o & P_o(S_o-n^2) & 0 \\ 0 & 0 & (S_o-n^2)^2-D_o^2 \end{bmatrix}\tilde{\vec{a}}\,, \tag{2.85}$$

where n is a refractive index and S_o, D_o, P_o are the extended Stix notations in order to include the beam term, and $\tilde{\vec{a}}$ is a Fourier-Laplace transformation of a source current in a form of

$$\tilde{\vec{a}} = \int_0^\infty dt \int_{-\infty}^{\infty} dz\, \frac{\partial \vec{J}_s}{\partial t}\, e^{-j(\omega t-kz)} \quad . \tag{2.86}$$

For the source current given by Eq.(2.82), $\tilde{\vec{a}}$ becomes

$$\tilde{\vec{a}} = \frac{\omega_o}{\omega-\omega_o}\,\hat{s} \quad . \tag{2.87}$$

In the problem of a propagation of a purely transverse whistler mode wave in the plasma-beam system such as that considered in the previous Section 3, Eq.(2.85) is simply written as

$$\begin{bmatrix} \tilde{E}_x \\ \tilde{E}_y \end{bmatrix} = \frac{1}{\varepsilon_o\omega^2}\,\frac{1}{(S_o-n^2)^2-D_o^2}\begin{bmatrix} S_o-n^2 & jD_o \\ -jD_o & S_o-n^2 \end{bmatrix}\begin{bmatrix} \omega_o/(\omega-\omega_o) \\ 0 \end{bmatrix}, \tag{2.88}$$

where the direction of the source current is taken in the x-direction, and

$$S_o = 1 - \frac{1}{\omega^2}\left[\frac{\omega^2\Pi_e^2}{\omega^2-\Omega_e^2} + \frac{(\omega-kV_{Bz})^2\Pi_b^2}{(\omega-kV_{Bz})^2-\Omega_e^2} + \frac{\frac{1}{2}k^2\langle v_{B\perp}^2\rangle\{(\omega-kV_{Bz})^2+\Omega_e^2\}\Pi_b^2}{\{(\omega-kV_{Bz})^2-\Omega_e^2\}^2}\right], \tag{2.89}$$

$$D_o = \frac{1}{\omega^2}\left[\frac{\omega\Omega_e\Pi_e^2}{\omega^2-\Omega_e^2} + \frac{\Omega_e(\omega-kV_{Bz})\Pi_b^2}{(\omega-kV_{Bz})^2-\Omega_e^2} + \frac{k^2\langle v_{B\perp}^2\rangle\Omega_e(\omega-kV_{Bz})\Pi_b^2}{\{(\omega-kV_{Bz})^2-\Omega_e^2\}^2}\right]. \tag{2.90}$$

Thus a space-time response in the plasma-beam system to the imposed terminated source current, which initiates suddenly at t = 0, can be obtained

by an inverse Fourier-Laplace transformation as

$$E_x(t,z) = \frac{1}{(2\pi)^2} \int_{-\infty}^{\infty} dk \int_{Br} d\omega \, \tilde{E}_x(\omega,k) \, e^{j(\omega t - kz)} . \qquad (2.91)$$

In the next sub-section 4.3, we will perform a numerical calculation of Eq.(2.91).

4.2.3 Comparison between Sommerfeld-Brillouin Method and Inverse Fourier-Laplace Transformation Method

In this section, we make a brief insight into a difference between the Sommerfeld-Brillouin method (hereafter S-B method for short) and the inverse Fourier-Laplace transformation method (I-F-L method for short) for the real space and time response in the dispersive medium.

Respective mathematical expressions of the S-B and I-F-L methods are written in the general form as

$$s(t,z) = \frac{1}{2\pi} \mathrm{Re} \int_{Br} \frac{1}{\omega-\omega_o} e^{-j\{\omega t - k(\omega) z\}} \, d\omega , \qquad \text{(S-B)} \qquad (2.92)$$

and

$$s(t,z) = \frac{1}{2\pi} \mathrm{Re} \int_{Br} d\omega \, \frac{e^{-j\omega t}}{\omega-\omega_o} \left[\frac{1}{2\pi} \int_{-\infty}^{\infty} dk \, \frac{N(\omega,k)}{D(\omega,k)}\right], \qquad \text{(I-F-L)} \qquad (2.93)$$

where $s(t,z)$ is the response at time t and space z to the applied source at $z = 0$ with the form of the "terminated wave disturbance" defined by Eq.(2.67). In the S-B method, $k = k(\omega)$ is a function of ω through the the functional relation of the dispersion equation

$$D(\omega,k) = 0 . \qquad (2.94)$$

On the contrary, the wave number k in the I-F-L method (Eq.(2.93)) is an integral variable which is independent of ω.

In order to compare the two expressions Eq.(2.92) and Eq.(2.93), we deform the latter by integrating over k as

$$s(t,z) = \frac{1}{2\pi} \int_{Br} d\omega \, \frac{e^{-j\omega t}}{\omega-\omega_o} \sum_{\substack{s \\ \mathrm{Im}(k_s)>0}} \frac{N(\omega,k_s(\omega))}{A_s(\omega)} e^{jk_s(\omega) z} , \quad \text{for } z > 0 ,$$

$$= \frac{1}{2\pi} \int_{Br} d\omega \, \frac{e^{-j\omega t}}{\omega-\omega_o} \sum_{\substack{s \\ Im(k_s)<0}} \frac{N(\omega,k_s(\omega))}{A_s(\omega)} e^{jk_s(\omega)z} \quad , \text{ for } z < 0 \, , \tag{2.95}$$

where

$$A_s(\omega) = \frac{\partial D}{\partial k} \{ k - k_s(\omega) \}\Big|_{k=k_s} \, . \tag{2.96}$$

Comparing Eq.(2.92) and Eq.(2.95), the difference is clear between the two methods. The conclusion is that the S-B method can only be used in the special case that the solution of $k = k_s(\omega)$ of the dispersion equation is uniquely determined in each half complex-k plane and yet the condition

$$\frac{N(\omega,k_s(\omega))}{A_s(\omega)} \equiv 1 \, , \tag{2.97}$$

is satisfied regarding with the amplitude of the normal mode $\exp\{-j\omega t+jk_s(\omega)z\}$. Therefore, we had better use the I-F-L method for general problems which manifest the multivalued solutions in the complex-k plane of the dispersion equation.

4.3 Numerical Computation of Signal Propagation Velocity in the Beam Cyclotron Instability

4.3.1 Method of Computation

In this section, we describe a method of numerical computation of the signal propagation velocity in the whistler mode beam cyclotron instability. Basic equations which describe the problem were given by Eqs.(2.88) to (2.91). Substituting Eqs.(2.89) and (2.90) into Eq.(2.88), the expression of the inverse F-L transformation for the response in real space and time is given by

$$E_x(t,z) = \frac{\omega_o}{(2\pi)^2\varepsilon_o} \int_{-\infty}^{\infty} dk \int_{Br} d\omega \, \frac{(\omega-kV_{Bz})^2-\Omega_e^2}{\prod_{\ell=0}^{10}(\omega-\omega_\ell)} e^{j(\omega t-kz)}$$

$$\times \, [(\omega^2-c^2k^2)(\omega^2-\Omega_e^2)\{(\omega-kV_{Bz})^2-\Omega_e^2\} - \omega^2\Pi_e^2\{(\omega-kV_{Bz})^2-\Omega_e^2\}$$

$$- \Pi_b^2 (\omega - kV_{Bz})^2 (\omega^2 - \Omega_e^2) \{ (\omega - kV_{Bz})^2 - \Omega_e^2 \}$$

$$- \frac{1}{2} k^2 \langle V_{B\perp}^2 \rangle \Pi_b^2 \{ (\omega - kV_{Bz})^2 + \Omega_e^2 \} (\omega^2 - \Omega_e^2)] \quad , \qquad (2.98)$$

where ω_ℓ (ℓ=1∿5) are the solutions of the dispersion equation for the R-waves satisfying

$$c^2 k^2 - \omega^2 + \frac{\Pi_e^2 \omega}{\omega - \Omega_e} + \frac{\Pi_b^2 (\omega - kV_{Bz})}{\omega - kV_{Bz} - \Omega_e} + \frac{\frac{1}{2} k^2 \langle V_{B\perp}^2 \rangle \Pi_b^2}{(\omega - kV_{Bz} - \Omega_e)^2} = 0 \quad , \qquad (2.99)$$

and ω_ℓ (ℓ=6∿10) are the solutions of the dispersion equation for the L-waves satisfying

$$c^2 k^2 - \omega^2 + \frac{\Pi_e^2 \omega}{\omega + \Omega_e} + \frac{\Pi_b^2 (\omega - kV_{Bz})}{\omega - kV_{Bz} + \Omega_e} + \frac{\frac{1}{2} k^2 \langle V_{B\perp}^2 \rangle \Pi_b^2}{(\omega - kV_{Bz} + \Omega_e)^2} = 0 \quad . \qquad (2.100)$$

Method of estimating the double integrations in Eq.(2.98), adopted in our computation, was to estimate the complex ω-integration first by residue calculations for a given real k and then to compute a real integration over k by the Simpson formula. In this procedure, however, we made the following simplifications in order to reduce the machine time and to reject responses other than the whistler mode. Namely, we estimate an integrand of the k-integral by picking up only residues of poles in the integrand of Eq.(2.92) which drop in the frequency range from $\omega_r = 0$ to $\omega_r = \Omega_e$. Therefore, an appearance of the so-called "forerunners" is excluded by such a procedure, but it is sufficient to trace the response in the whistler mode. The infinite integral over real k is replaced by the finite integral over $-M \leq k \leq M$ where such an M is selected that the integrand becomes negligibly small for $|k| > M$.

In order to check the numerical procedure, a propagation of whistler mode waves in a cold plasma was solved numerically by the above mentioned method and compared with the well known analytically reduced propagation velocities ——— phase and group velocities ——— by Yamazaki[51]. The results showed a good agreement between these two approaches so that the numerical method of I-F-L will be guarantied.

4.3.2 Results of Numerical Computations

Responses in real space and time are computed for the whistler mode waves in a plasma-beam system which manifests the beam cyclotron instability. As the first case, the plasma and beam parameters are chosen as

$$P = \frac{\Pi_e}{\Omega_e} = 3, \quad V_{Bz} = 10\text{keV}, \quad V_{B\perp} = 40\text{keV}, \qquad (2.101)$$

$$\eta = N_b/N_e = 10^{-4} .$$

The dispersion curve for the above plasma-beam system is illustrated in Fig.33. We can see in the figure an abnormal dispersion which shows

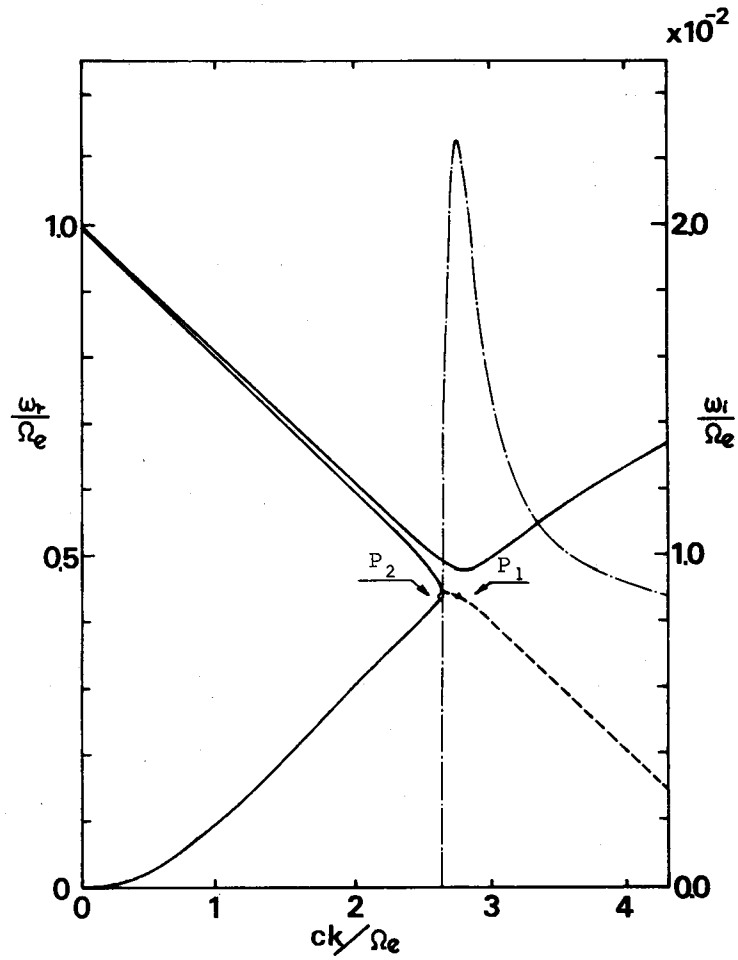

Fig.33 Dispersion Curve in the Whistler Mode for the Selected Plasma-Beam System for the Numerical Computation of the Wave Propagations in Figs.34 and 35.

$|\partial\omega_r/\partial k| > c$. Eight different frequencies are selected of the source current which is imposed at $z = 0$ as described by Eq.(2.82). They are $\omega_o/\Omega_e = 0.2$, 0.3, 0.4, 0.5, 0.6, 0.7, 0.8 and 0.9, while the frequency of the maximum growth rate is $\omega_m/\Omega_e = 0.438$.

The corresponding responses in the Z-T space are depicted in Fig.34, in which Z and T are normalized quantities through

$$Z = \frac{2\pi\Omega_e}{3c} z \ ,$$
$$T = \frac{\Omega_e}{2\pi} t = \frac{t}{T_H} \ , \qquad (2.102)$$

where T_H is the period of the cyclotron motion of electrons. Gradient of the dashed lines indicates the phase velocity of the computed responses, i.e.,

$$V_{ph} = \frac{1}{3}\frac{Z}{T} c \quad . \qquad (2.103)$$

From these figures, we first realize the fact that the frequency of the response is constant even if the frequency of the current source is changed. This constant frequency is $0.438\Omega_e$ and is found to be coincident with the frequency ω_m at which the growth rate becomes maximum as seen in Fig.33. In the cases $\omega_o = 0.7\Omega_e$, $0.8\Omega_e$ and $0.9\Omega_e$, the wave form is distorted from a pure sinusoidal form. It is attributed to a beat phenomenon between the imposed wave with $\omega_r = \omega_o$ and the excited wave with $\omega_r = \omega_m$. Therefore, a response of the plasma-beam system which manifests a cyclotron instability does not show a temporal sinusoidal behavior of the imposed frequency but exhibits a growing sinusoidal behavior with a frequency corresponding to the maximum growth rate in the system. This is physically natural and understandable because the spectrum of a "terminated" source current is given by Eq.(2.87), which includes the spectrum component ω_m. Thus the most rapidly growing mode becomes eminent before the wave of the imposed frequency reaches a steady state.

All of the responses in Fig.34 indicate the same phase velocity, which is numerically

$$V_{ph} = 0.161 \ c \ . \qquad (2.104)$$

This phase velocity is coincident with that for the frequency of the

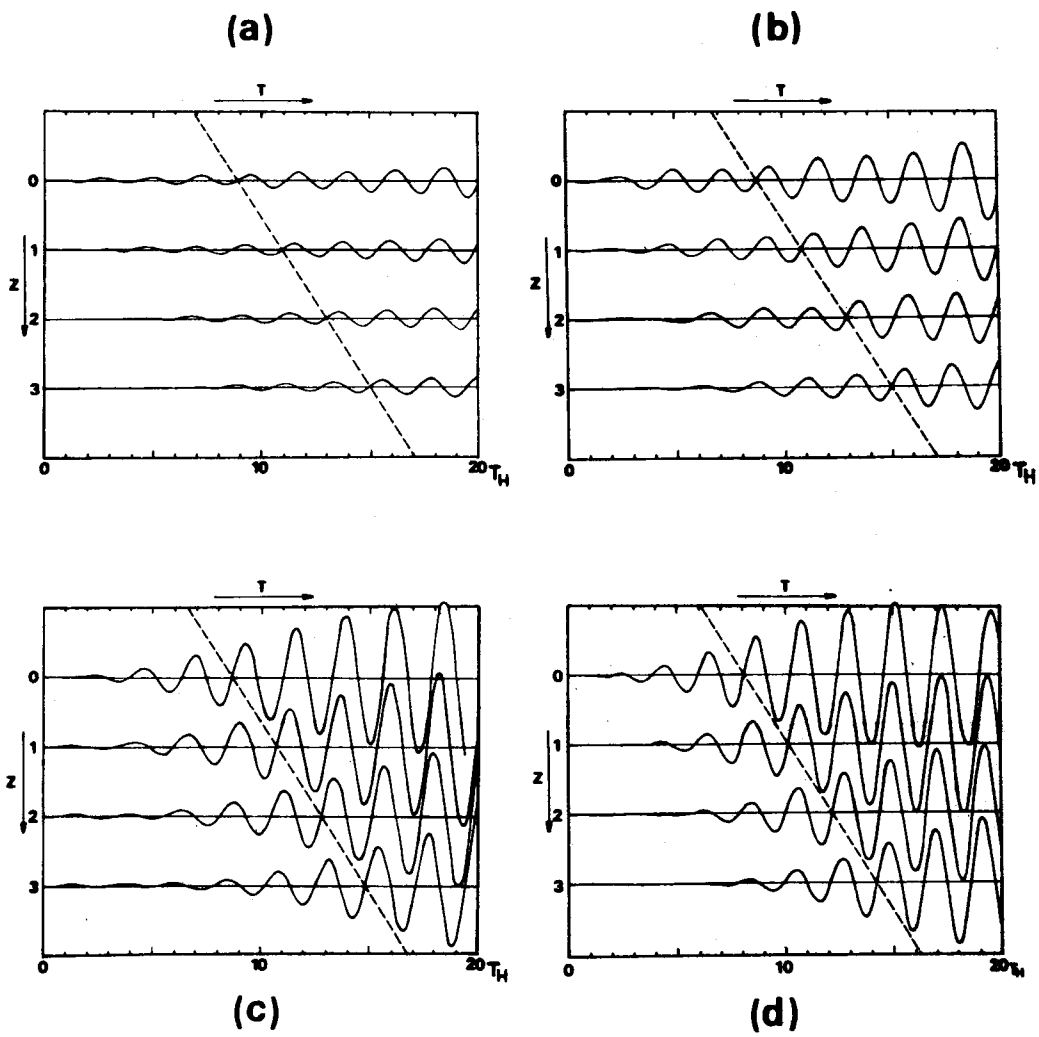

Fig.34 Computed Responses in Real Space and Time in an Unstable Plasma-Beam System. Eight figures correspond to the responses to the source current of eight different frequencies;

(a) $\omega_o^* = 0.2$, (b) $\omega_o^* = 0.3$, (c) $\omega_o^* = 0.4$, (d) $\omega_o^* = 0.5$,

(e) $\omega_o^* = 0.6$, (f) $\omega_o^* = 0.7$, (g) $\omega_o^* = 0.8$, (h) $\omega_o^* = 0.9$,

where $\omega_o^* \equiv \omega_o/\Omega_e$. The ordinate is an arbitrary same scale except (c) and (d) which are reduce to 1/2 from others.

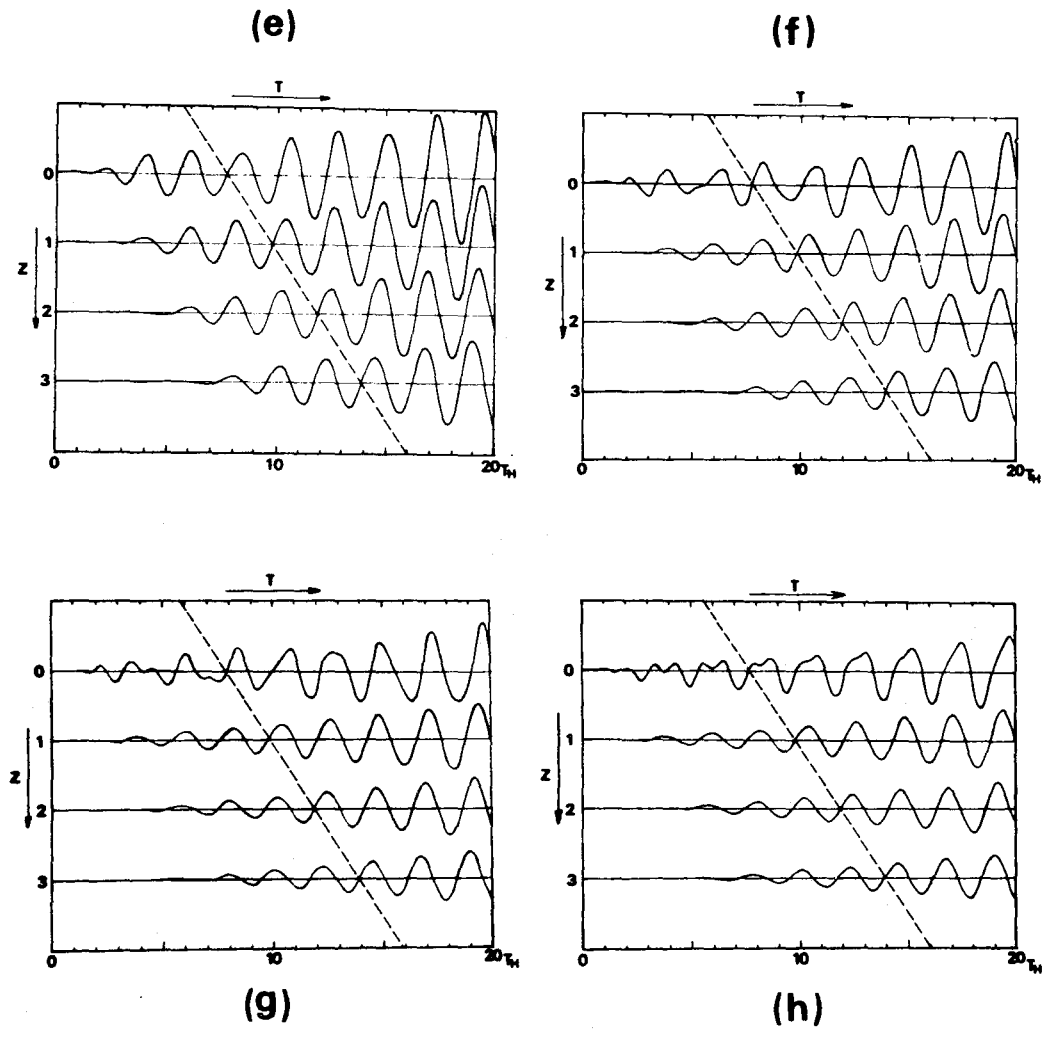
(e)
(f)
(g)
(h)
T
Z
0
1
2
3
10
20τH

maximum growth rate on the dispersion curves which is indicated by a point P_1 on the branch drawn by a dashed line, namely on the beam mode branch, in Fig.33. Therefore, with reference to the calculated phase velocity for given frequencies, it can be inferred that the plasma-beam system displays a growing whistler mode wave with the frequency of the maximum growth rate on the dispersion curve, whenever a "terminated" current source is imposed with an arbitrary frequency in the whistler mode frequency range. However, it should be noticed that the group velocity at that point indicated by P_2 in Fig.33 is negative so that the energy flow or the direction of the signal propagation should be negative. Our numerical results, however, do not show such a tendency as indicated in Fig.34.

What is the signal propagation velocity then? This velocity will be obtained from the amplitude vs. time at different Z positions. The amplitude of response at each point is plotted as a function of time in the semi-logarithmic graphs. Corresponding results to Fig.34 are illustrated in Fig.35. Figures are depicted in each case of different source frequency. In each figure in Fig.35, four traces at four different positions Z = 0, 1, 2, 3 are illustrated. From these figures, we can extract the following features.

Firstly, it is found that the amplitude itself shows a periodic change. The measured period is quite the same as $2\pi/(\omega_o-\omega_m)$, which shows that the amplitude of the growing wave with frequency $\omega_r = \omega_m$ is modulated by the imposed wave with $\omega_r = \omega_o$. Namely, a beat phenomenon is observed. Therefore, a simple sinusoidal growing wave with $\omega_r = \omega_m$ is not excited but a beat between those with $\omega_r = \omega_o$ and $\omega_r = \omega_m$ is excited and propagates along $\vec{B}_o$ direction. This phenomenon is clearly observed in the Z-T responses in cases of $\omega_o = 0.7\Omega_e$, $0.8\Omega_e$ and $0.9\Omega_e$ in Fig.34, but it is recognized from Fig.35 that this is true for all other frequencies of the imposed source current.

Secondly from Fig.35 it is clarified how the wave grows up with time. All figures in Fig.35 show a tendency to grow up with different three growth rate on three stages. The pattern of the wave growth is schematically depicted in Fig.36. Initially, the amplitude apparently grows up with a greater growth rate (indicated by the dashed line A). This

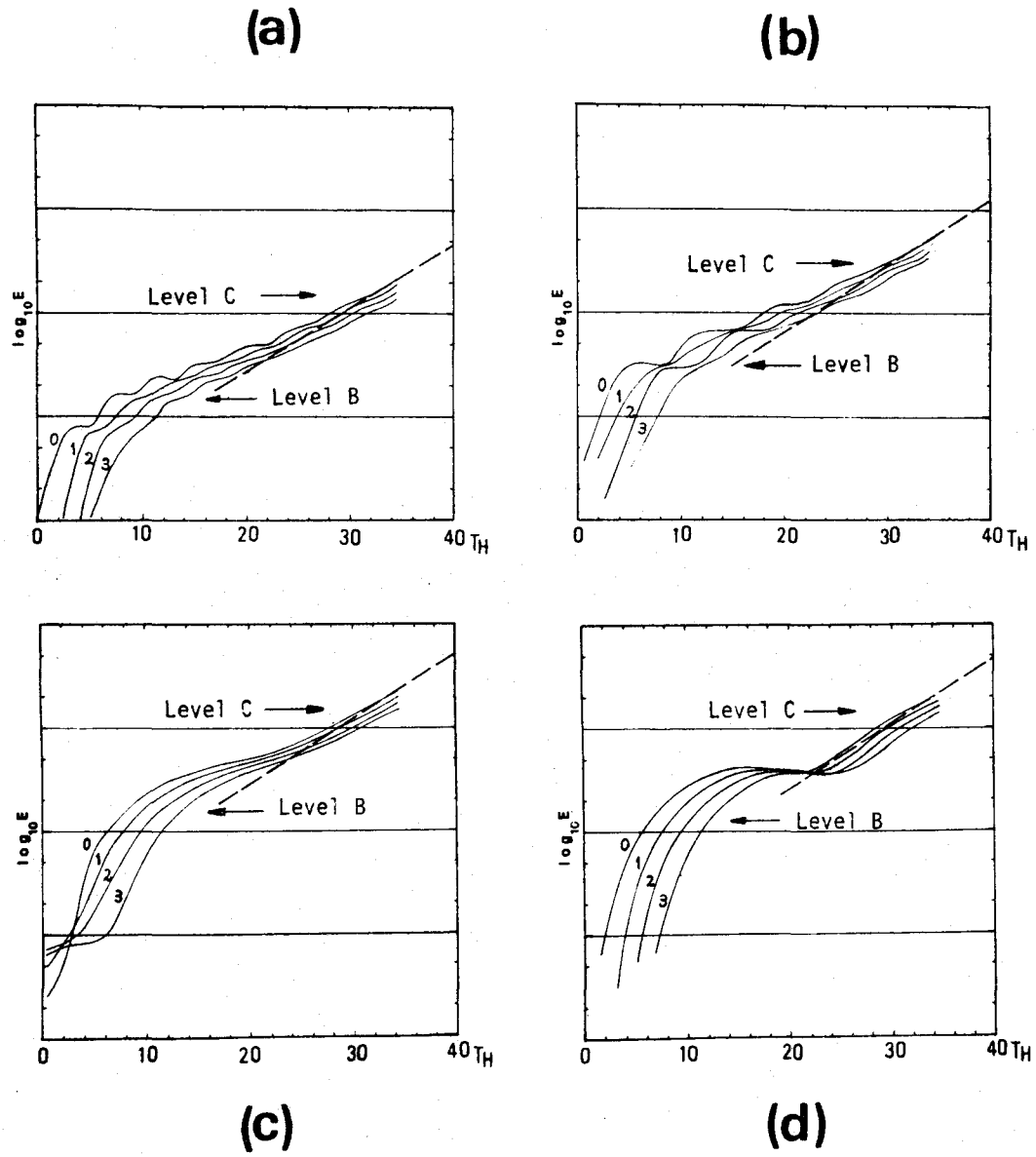

Fig.35 Amplitude Growth of the Responses Corresponding to Fig.34. The ordinate is measured in $\log_{10}\hat{E}$, where $\hat{E}$ is the amplitude of the responses. Numbers attached to curves in the figure show the normalized position Z.

(e)

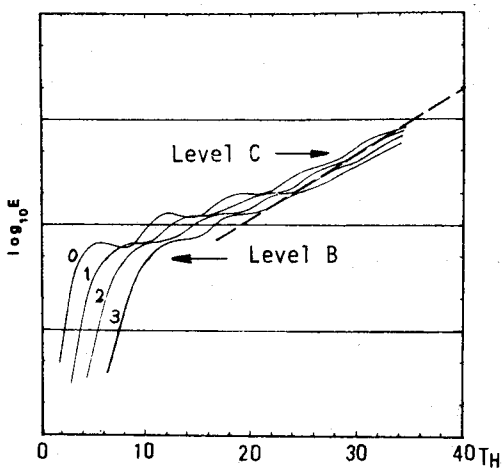
Level C
Level B
0
1
2
3
$\log_{10}E$
0
10
20
30
40 T_H

(f)

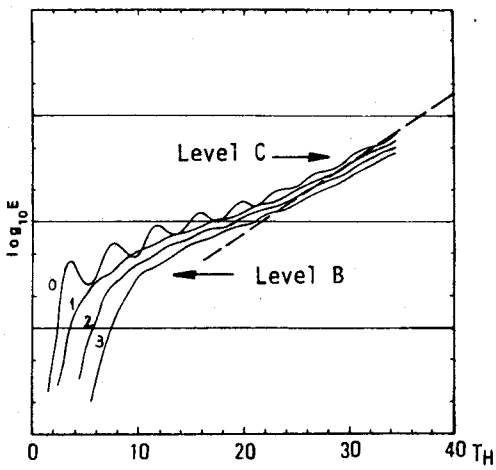
Level C
Level B
0
1
2
3
$\log_{10}E$
0
10
20
30
40 T_H

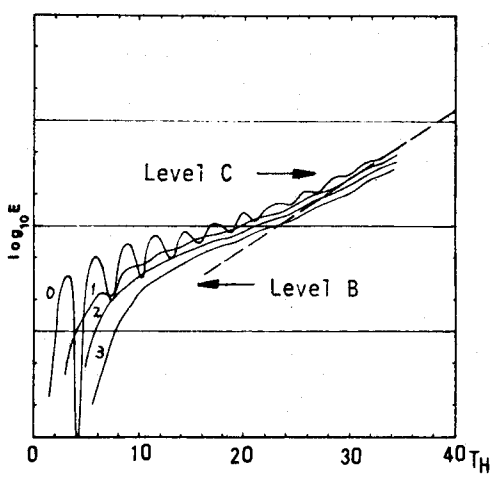
Level C
Level B
0
1
2
3
$\log_{10}E$
0
10
20
30
40 T_H

(g)

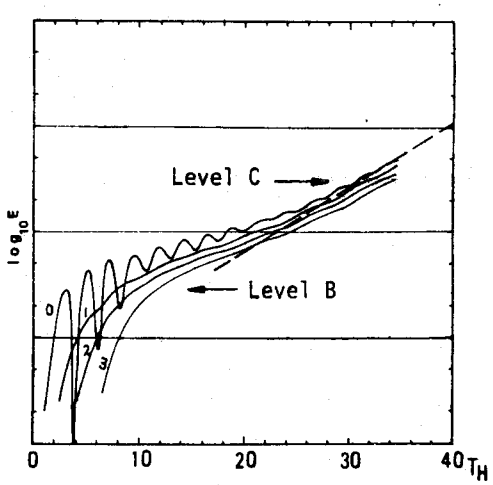
Level C
Level B
0
1
2
3
$\log_{10}E$
0
10
20
30
40 T_H

(h)

may be the process of the transition from a transient to steady state. Actually such a transient is also seen even for a whistler mode propagation in a stable cold plasma, as a result of an imposed current source as shown in Fig.37.(Yamazaki[51]). The second stage of the wave growth in Fig.36 shows a rather slow growing with a growth rate of $|\omega_i| < |\omega_{imax}|$ (indicated by a dashed line B). Finally the growth rate approaches to an asymptotic line C which shows a growth rate of $|\omega_i| = |\omega_{imax}|$ that corresponds to the maximum growth rate determined by the dispersion equation. The reason why the wave on the second stage grows with a growth rate smaller than the maximum growth rate, can be explained as follows. Using Eq.(2.91), the response E(t) is expressed as

$$E(t) \propto \int_{-\infty}^{\infty} F(k)\, e^{|\omega_i(k)|t}\, e^{j\omega_r(k)t}\, dk . \qquad (2.105)$$

This means that the time behavior of the response is expressed as a sum of many growing sinusoidal waves with a continuous spectrum from $\omega_r = 0$ to $\omega_r \simeq \omega_m$ because the contribution from $\omega_r = \omega_m$ to $\omega_r = \Omega_e$ becomes exponentially smaller as time elapses. Therefore, for a short time scale of the order of a period of the oscillation, we can estimate roughly a

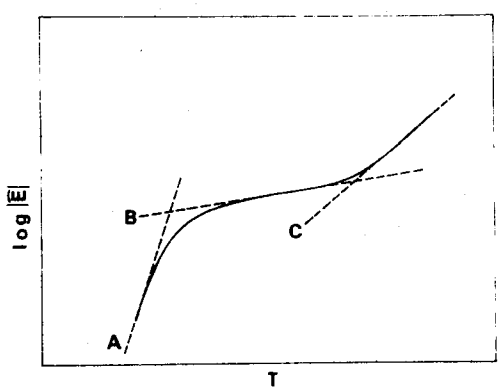

Fig.36 Schematic Illustration of the Whistler Mode Wave Growth due to the Imposed Terminated Current Source in the Plasma-Beam System Which Manifests a Whistler Mode Beam Cyclotron Instability.

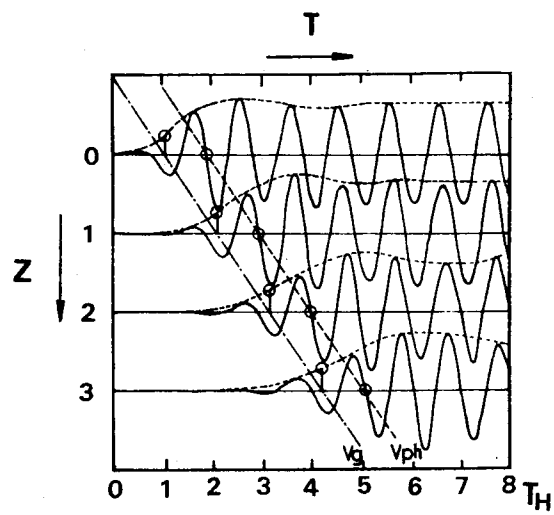

Fig.37 A Response of a Whistler Mode Propagation in a Cold Plasma to an Imposed Current Source with $\omega_o = 0.5\Omega_e$.
(Yamazaki[51])

period of the resultant oscillation as

$$E(t) \sim \int_0^{\omega_m} \cos\omega_r t \, d\omega_r \sim \sin\omega_m t \quad . \tag{2.106}$$

While the amplitude should be estimated for a longer time scale. The growth rate of the amplitude could not be given by $|\omega_i| = |\omega_{imax}|$ until the amplitude of the spectrum with $\omega_r = \omega_m$ grows up enough to predominate other spectra with smaller growth rates. The resultant growth rate may be given by an average of the growth rates of all unstable waves in the whistler mode.

Thirdly, the most important problem is how to estimate the signal propagation velocity (in this case, the wave excited by the cyclotron instability). In the case of growing signals, however, we could not rigorously define the signal velocity. We adopt here the following definition of the signal velocity, i.e.,

$$V_s\Big|_{\text{a certain level of amplitude}} = \frac{\Delta z}{\Delta t} \quad , \tag{2.107}$$

where Δt is a time interval between the times of arrival of the signal with a certain level of amplitude at two different points spatially separated by Δz. In the normalized coordinate in Fig.35,

$$V_s\Big|_{\text{level}} = \frac{1}{3}\frac{\Delta Z}{\Delta T} c \quad , \tag{2.108}$$

where the subscript "level" is short for "a certain level of amplitude". It should be noticed that the signal velocity V_s is not constant but depends on the level of the set amplitude.

From Fig.35, we estimated the above defined signal velocities at two different levels, i.e., level B and level C which correspond to the last two stages of the growing pattern described in Fig.36 and indicated by arrows in Fig.35. Averaging the measured time intervals, we estimated numerically the signal velocity as

$$V_s\Big|_{\text{level B}} = \frac{1}{3} \times \frac{1}{1.70} c = 0.20c \quad , \tag{2.109}$$

$$V_s|_{\text{level C}} = \frac{1}{3} \times \frac{1}{1.06} c = 0.31c \ . \qquad (2.110)$$

While, various velocities which are derived from the dispersion curves in Fig.34 or more rigorously from the dispersion equation (2.99) are as follows:

1) A beam velocity:

$$V_{Bz} = -0.199c \ . \qquad (2.111)$$

2) A group velocity at the point of the maximum growth rate on the beam mode branch indicated by P_1 in Fig.34:

$$V_{g1} = -0.084c \ . \qquad (2.112)$$

3) A group velocity at the point on the whistler mode branch where the frequency $\omega_r = \omega_m$, indicated by P_2 in Fig.34:

$$V_{g2} = 0.31c \ . \qquad (2.113)$$

4) A group velocity of the unperturbed whistler mode wave with a a frequency around ω_m in the case of no interaction with the beam:

$$V_{g3} = 0.20c \ . \qquad (2.114)$$

If we compare the signal velocities (Eqs.(2.109) and (2.110)) with the above various velocities, it is found that the signal velocity $V_s|_{\text{level B}}$ is determined by the group velocity V_{g3} which is the usual group velocity at the corresponding frequency in the unperturbed whistler mode waves in a beamless plasma. The signal velocity $V_s|_{\text{level C}}$ is determined by the group velocity V_{g2} defined above. The above inferred conclusion obtained from one numerical result for an example of plasma and beam parameters will be ascertained by another example of the plasma parameters. The plasma parameter P is changed from 3 to 8. The resultant dispersion curves, the Z-T responses and the amplitude plots in the logarithmic scale are given in Figs.38, 39 and 40, respectively.

From these figures, the same conclusion can be inferred as obtained previously. Quantities read from the numerical computations of the responses are

$$\begin{aligned} V_{ph} &= 0.046c \ , \\ V_s|_{\text{level B}} &= 0.084c \ , \\ V_s|_{\text{level C}} &= 0.123c \ . \end{aligned} \qquad (2.115)$$

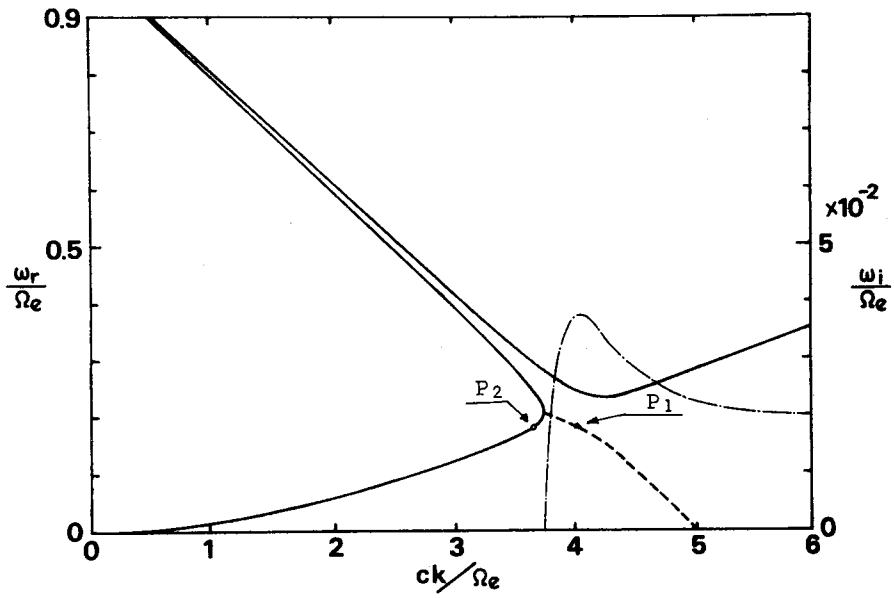

Fig.38 Dispersion Curve in the Whistler Mode for Another Plasma-Beam System for the Numerical Computation in Figs.39 and 40. Parameters used in the calculation are

$P = 8$, $\eta = 10^{-4}$, $V_{Bz} = 10\text{keV}$, $V_{Bl} = 40\text{keV}$

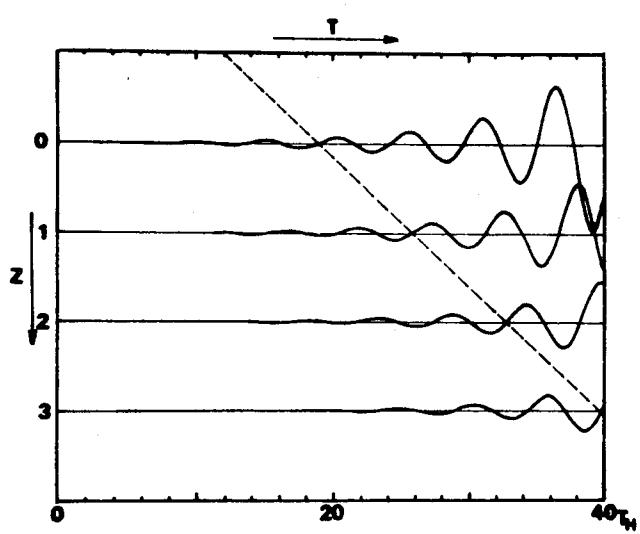

Fig.39 Computed Responses in Real Space and Time in a Plasma-Beam System. ($\omega_o^* = 0.2$)

While the quantities obtained from the dispersion equation are

$$V_{ph}|_{\text{at } P_1} = 0.046c \ ,$$
$$V_{Bz} = -0.199c \ ,$$
$$V_{g1} = -0.126c \ , \qquad (2.116)$$
$$V_{g2} = 0.126c \ ,$$
$$V_{g3} = 0.084c \ .$$

The quantity $V_s|_{\text{level C}}$ is a little different from V_{g2} not like the previous numerical example. This is due to the fact that the $V_s|_{\text{level C}}$ is not correctly measured in Fig.40 because the time T did not elapse enough for the growth rate of the wave to be well described by the maximum growth rate. Namely, the wave growth does not attain to the third stage C shown in Fig.36.

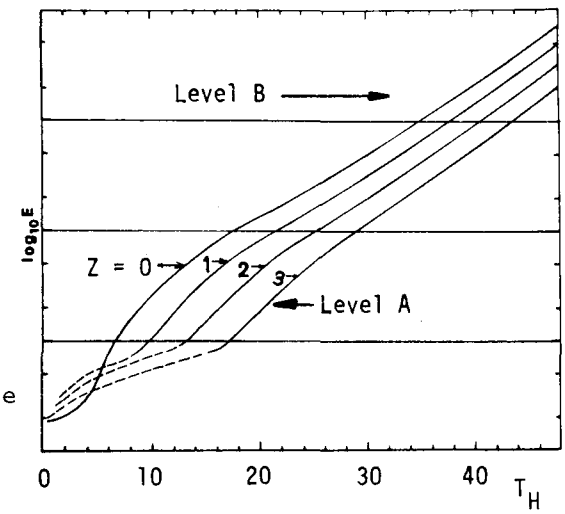

Fig.40 Amplitude Growth of the Responses Corresponding to Fig.39.

Another interesting problem is the wave propagation in the negative z direction, i.e., in the same direction as the beam streaming. The result of two cases of different source frequencies $\omega_o = 0.2\Omega_e$ and $0.5\Omega_e$ are illustrated in Figs.41 and 42. The plasma parameter was the same as the first computations, i.e., P = 3. As seen in Fig.41, a wave with frequency $\omega_r = \omega_m$ grows up at each position. The phase velocity of this wave is again coincident with the phase velocity at a point indicated by P_1 in Fig.34. The amplitude plottings in the logarithmic scale vs. time indicate an interesting result. In the initial stage, i.e., for small value of T, the wave amplitude attains to a certain level (for example level A in Fig.42) earlier at the position z nearer to the source. Therefore, the direction of the wave propagation is surely negative. However, as time elapses to some extent, the sequence of the times when the amplitude attains to another certain level (for example, level B in Fig.42) for different z positions becomes reversed. The grown up wave flows in the positive z direction even in the negative z region as in the positive z region. The measured signal velocity corresponding

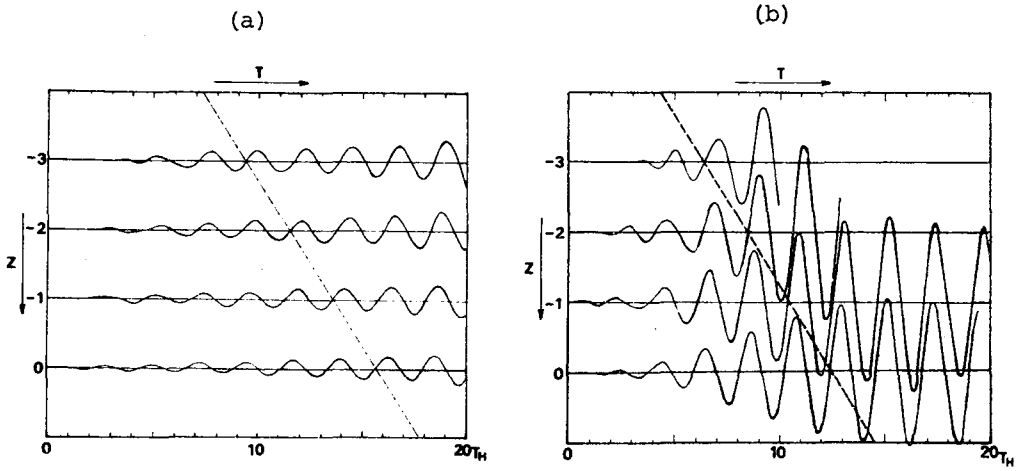

Fig.41 Computed Responses in the Negative z-Space.
(a) $\omega_o = 0.2\Omega_e$ (b) $\omega_o = 0.5\Omega_e$

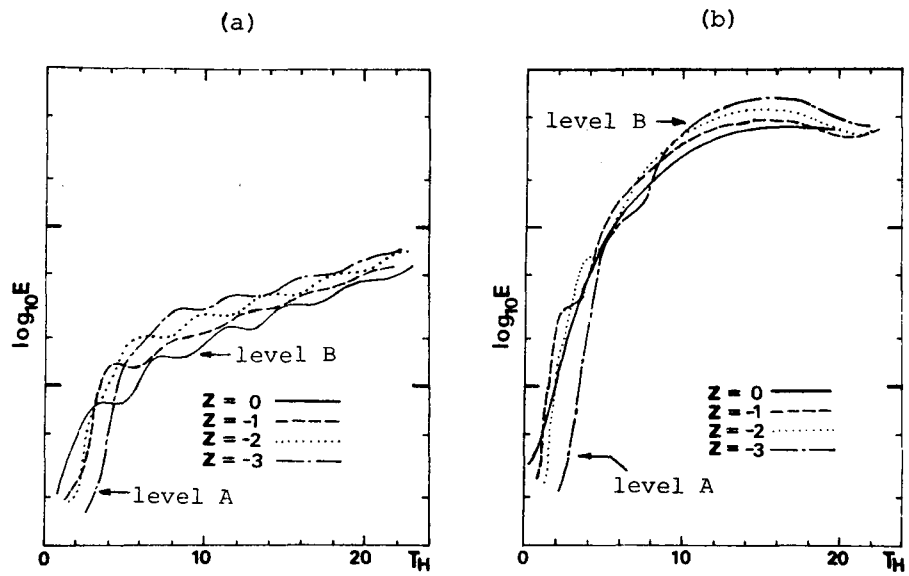

Fig.42 Amplitude Growth of the Responses Corresponding to Fig.41.
(a) $\omega_o = 0.2\Omega_e$ (b) $\omega_o = 0.5\Omega_e$

to the level B in Fig.36 is almost coincident with V_{g3} for the propagation to the positive z region.

This is physically explained as follows. When a "terminated" current source with a frequency of ω_o is imposed at z = 0, the various frequency components, which are included in the spectrum of the source, start to propagate also in the negative z-direction with a normal whistler mode as inferred from the dispersion curves in the negative k region (see for example Fig.26). On the other hand, the beam-wave interaction can take place even in the negative z region because the source current, Eq. (2.82), implies an initial spatial distribution of the electric field. Therefore the waves which interact with the counter-streaming electron beam start to grow up. These grown up waves should be described by the dispersion curves in the positive k region so that the same propagation in the positive z direction should take place even in the negative z region.

4.4 Discussion and Conclusions

In this section, we have investigated on the propagation velocity of waves in the whistler mode on the conditions of a beam cyclotron instability. In this case, a dispersion equation gives an abnormal group velocity which exceeds the light speed for some frequency range. The motivation of the present investigation was to investigate how a wave propagates in such an abnormally dispersive and unstable medium. Numerical computations were carried out on the responses of a signal in real time and space by the inverse Fourier-Laplace method, which is more rigorously proper than the Sommerfeld-Brillouin method. In the procedure of numerical computations, only the poles were picked up which dropped in a priori set frequency range in the whistler mode in estimating the complex ω-integral. This physically corresponds to a use of a filter for a receiver.

The problem of the wave propagation in such an abnormally dispersive and unstable medium, especially taking nonlinearity into consideration is much interesting, but it is beyond the scope of the present interest and will be left as a future problem.

The results obtained in this section will also be useful in the estimation of the frequency vs. time characteristics of the excited VLF emissions.

§5. Cyclotron Instability due to Temperature Anisotropy and Spontaneous VLF Emissions[50]

Many linear analyses have been made by many authors on the initial phase of instabilities in a magnetoactive plasma and on various conditions for instabilities of their relevant systems. In spite of the limitations, the linear analyses give a lot of information such as frequencies of the most unstable modes or on the most prominent instability amongst possible instabilities in the system, e.g., in the magnetosphere. In this section, therefore, the linear theory of the cyclotron instability in the whistler mode, which is caused mainly by the temperature anisotropy, is briefly reviewed for general and arbitrary distribution functions.

In the case of the Maxwell distribution of plasma particles, much work has been done (Fried & Conte[75]; Scharer & Trivelpiece[76] etc.) and cyclotron damping of whistlers in the magnetosphere has been explained qualitatively (Scarf[55]; Liemohn & Scarf[56]; Guthart[57]). It is, however, not necessarily proper to describe the distribution function of the magnetospheric plasma by the Maxwell distribution even when a two-temperature anisotropic characteristic is taken into account. Further, in the nonlinear analysis in the next chapter, time evolution of the distribution function itself plays an important role. Thus the distribution function changes its shape with time even if it is initially Maxwellian. The growth and/or damping rate of the whistler mode waves for an arbitrary distribution function are thus necessary to be obtained. It is possible to find out such an analytical expression for the growth and damping rate so long as these rates are sufficiently small. Though it has already been found in the literatures (e.g., Sudan[77]; Bell[41]; Kennel[78] etc.), it is re-described here briefly for completeness, including thermal corrections. The result will be made use of the discussion of the application to the spontaneous VLF emissions. A short discussion will also be made in this section of a case where the growth and/or damping rate is large enough to break the assumption $|\gamma_k| \ll \omega_r$.

5.1 Model and Basic Equations

We limit our treatment to the whistler mode waves propagating along the external magnetic field lines in an infinite, collision-free and magneto-active plasma (Fig.43).

Writing the distribution function of plasma particles of the s-th species with charge q_s and mass m_s as $F_s(\vec{V},\vec{r},t)$, the Vlasov equation is

$$\frac{\partial F_s}{\partial t} + \vec{V}\cdot\frac{\partial F_s}{\partial \vec{r}} + \frac{q_s}{m_s}\{\vec{E}+\vec{V}\times(\vec{B}_o+\vec{B})\}\cdot\frac{\partial F_s}{\partial \vec{V}} = 0 , \tag{2.117}$$

where $\vec{B}_o = B_o\hat{z}$ is the external magnetic field, and the self consistent wave fields $\vec{E}$ and $\vec{B}$ are, in turn, determined by the distribution function as

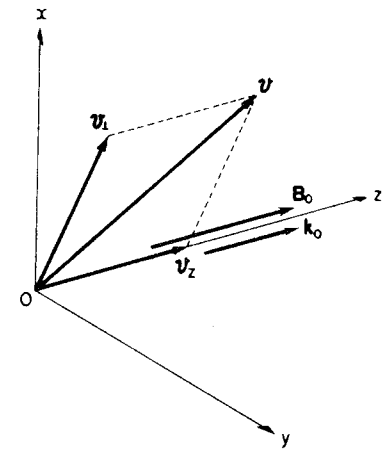

Fig.43 Coordinate Adopted in the Present Analysis.

$$\nabla \times \vec{E} = -\frac{\partial \vec{B}}{\partial t} , \tag{2.118}$$

$$\nabla \times \vec{B} = \mu_o \sum_s q_s \int \vec{V} F_s d\vec{V} + \frac{1}{c^2}\frac{\partial \vec{E}}{\partial t} , \tag{2.119}$$

where $\sum_s$ is taken over all species of the plasma particles. As is customarily made in the linear theory, we divide the particle distribution function into two parts; a rapidly oscillating perturbation $f_s(\vec{V},\vec{r},t)$ and a background homogeneous part $g_s(\vec{V})$ as

$$F_s(\vec{V},\vec{r},t) = g_s(\vec{V}) + f_s(\vec{V},\vec{r},t) . \tag{2.120}$$

Expanding f_s, E and B into Fourier series as a sum of normal modes in the form*,

$$\exp\{-j\omega(k)t + jkz\} , \tag{2.121}$$

we obtain the rapidly oscillating part of the distribution function after

---

* It should be noticed that the normal mode was $\exp(j\omega t - j\vec{k}\cdot\vec{r})$ in the previous section 4.

selecting out of Eq.(2.117) with the aid of the Maxwell equation (2.118) and (2.119) as follows (see Appendix A, Eq.(A-23)).

$$f_s = \sum_k f_{sk\omega} \exp\{-j\omega(k)t + jkz\} , \tag{2.122}$$

$$f_{sk\omega} = \frac{q_s}{jm_s}\Bigg[\frac{\dfrac{\partial g_s}{\partial V_z}}{\omega - kV_z} E_{kz} + \frac{(1-\dfrac{kV_z}{\omega})\dfrac{\partial g_s}{\partial V_\perp} + \dfrac{kV_\perp}{\omega}\dfrac{\partial g_s}{\partial V_z}}{\omega - kV_z + \varepsilon_s\Omega_s} \frac{e^{j\phi}}{\sqrt{2}} E_{k-}$$

$$+ \frac{(1-\dfrac{kV_z}{\omega})\dfrac{\partial g_s}{\partial V_\perp} + \dfrac{kV_\perp}{\omega}\dfrac{\partial g_s}{\partial V_z}}{\omega - kV_z - \varepsilon_s\Omega_s} \frac{e^{-j\phi}}{\sqrt{2}} E_{k+}\Bigg] , \tag{2.123}$$

where convenient variables $E_{k\pm} = (E_{kx} \pm jE_{ky})/\sqrt{2}$ are introduced and $\Omega_s = |q_s|B_o/m_s$ is the angular cyclotron frequency, $V_\perp$, V_z and ϕ are the velocity components perpendicular and parallel to the external magnetic field and the Larmor phase angle, respectively.

Thus the basic equations in the present section are prepared and are given by Eqs.(2.117) to (2.119), which can be linearized to give Eqs. (2.122) and (2.123).

5.2 Growth and Damping Rate Expression for Arbitrary Distribution Functions

Substituting Eqs.(2.122) and (2.123) into Eqs.(2.118) and (2.119) and using the Dirac-Plemelj formula

$$\lim_{y\to 0} \frac{1}{z-(x\pm jy)} = P\frac{1}{z-x} \pm \pi j\delta(z-x) \qquad (y > 0) , \tag{2.124}$$

where P implies the principal value and $\delta(z-x)$ is the usual delta function, we can find the dispersion equation and the expression for the growth and/or damping rate for the whistler mode waves. Since we are interested in the resonant interaction of electromagnetic waves with charged particles on the relatively high energy tail, the number of resonant particles and hence the growth and/or damping rate is small. Therefore, assuming $|\gamma_k| << \omega_r$ where $\omega(k) = \omega_r + j\gamma_k$, the dispersion equation and the expression of the growth and/or damping rate γ_k are obtained.

In the case of longitudinally propagating whistler mode waves, setting $E_{k+} = E_{kz} = 0$, we get after some manipulation (see Appendix A, Eqs.(A-40) and (A-41))

$$c^2k^2 - \omega_r^2 - \sum_s \frac{\pi\omega_r \Pi_s^2}{kN_s} \left[2P\int_{-\infty}^{\infty} dV_z \frac{H_{s1}(V_z)}{V_z - V_R} + \frac{k}{\omega_r} P\int_{-\infty}^{\infty} dV_z \frac{H_{s2}(V_z)}{V_z - V_R} \right] = 0, \quad (2.125)$$

and

$$\gamma_k = - \sum_s \frac{\pi^2 \Pi_s^2}{|k| N_s} \left[2H_{s1}(V_R) + \frac{k}{\omega_r} H_{s2}(V_R) \right]$$

$$\Big/ \left[2 + \sum_s \frac{\pi \Pi_s^2}{kN_s\omega_r} \left\{ 2P\int_{-\infty}^{\infty} dV_z \frac{H_{s1}(V_z)}{V_z - V_R} + \frac{2\omega_r}{k} P\int_{-\infty}^{\infty} dV_z \frac{H'_{s1}(V_z)}{V_z - V_R} \right.\right.$$

$$\left.\left. + P\int_{-\infty}^{\infty} dV_z \frac{H'_{s2}(V_z)}{V_z - V_R} \right\}\right], \quad (2.126)$$

where $N_s = \int g_s d\vec{V}$ is the number density of particles of the s-th species, $\Pi_s = (N_s q_s^2/m_s\varepsilon_o)^{1/2}$ is the angular plasma frequency and the function $H_{s1}(V_z)$ and $H_{s2}(V_z)$ are defined by

$$H_{s1}(V_z) = \int_0^{\infty} V_\perp g_s dV_\perp \ , \quad (2.127)$$

$$H_{s2}(V_z) = \int_0^{\infty} V_\perp^2 \left(V_z \frac{\partial g_s}{\partial V_\perp} - V_\perp \frac{\partial g_s}{\partial V_z} \right) dV_\perp \ . \quad (2.128)$$

The prime in Eq.(2.126) denotes the differentiation with respect to V_z and $V_R = (\omega_r + \varepsilon_s\Omega_s)/k$ is the resonance velocity. It is noticed that ω is assumed to have a small positive imaginary part to keep all the integrals being defined but solutions for which $\gamma_k \leqq 0$ is to be obtained by the usual analytic continuation in the complex ω-plane. Careful examination of the analytic continuation by deforming the integral contour in the complex V_z-plane together with the use of the Dirac-Plemelj formula (2.124) shows that the expression (2.126) is also effective even for $\gamma_k \leqq 0$ as far as the assumption $|\gamma_k| << \omega_r$ mentioned before is satisfied.

The principal values of the integrals in Eqs.(2.125) and (2.126) are then evaluated under the following customary assumptions as

(1) $g_s(\vec{V}) = o(V_\perp^{-n})$; $n > 2$ for large $V_\perp$,

(2) $g_s(\vec{V})$ is such that the contribution to the integral

$$P\int_{-\infty}^{\infty} dV_z \frac{H_{sl}(V_z)}{V_z - V_R}$$

in the range $|V_z| > |V_R|$ is negligibly small,

and

(3) $|V_R|$ is relatively greater than the mean velocity of the plasma particles.

Thus, we obtain the following dispersion equation and the expression of the growth and/or damping rate (of each harmonic) in the whistler mode (see Appendix A). They are given to the second order of $\langle V_\ell \rangle / V_R$ ($\ell = \perp, z$), in the coordinates where the plasma is at rest, by

$$D(\omega_r, k) - \sum_s \frac{k\varepsilon_s \Omega_s \Pi_s^2}{(\omega_r + \varepsilon_s \Omega_s)^3} \frac{K}{m_s} \left(T_{\parallel} - \frac{\omega_r + \varepsilon_s \Omega_s}{\varepsilon_s \Omega_s} T_{\perp} \right) = 0 \ , \tag{2.129}$$

and

$$\gamma_k = \frac{\sum_s \frac{\pi^2}{N_s} \frac{\varepsilon_s \Omega_s \Pi_s^2}{\partial D / \partial \omega_r} \int_{-\infty}^{\infty} dV_z \int_0^{\infty} dV_\perp V_\perp^2 \delta(\omega_r - kV_z + \varepsilon_s \Omega_s) \left(\frac{\partial g_s}{\partial V_\perp} - \frac{kV_\perp}{\varepsilon_s \Omega_s} \frac{\partial g_s}{\partial V_z} \right)}{1 - \frac{3}{\partial D / \partial \omega_r} \sum_s \frac{\varepsilon_s \Omega_s \Pi_s^2}{(\omega_r + \varepsilon_s \Omega_s)^2} \frac{K}{m_s V_R^2} \left(T_{\parallel} - \frac{2}{3} \frac{\omega_r + \varepsilon_s \Omega_s}{\varepsilon_s \Omega_s} T_{\perp} \right)} \ , \tag{2.130}$$

where

$$D(\omega_r, k) \equiv c^2 k^2 - \omega_r^2 + \sum_s \frac{\omega_r \Pi_s^2}{\omega_r + \varepsilon_s \Omega_s} \ , \tag{2.131}$$

and the temperature $T_{\parallel}$ and $T_{\perp}$ are defined by

$$T_{\parallel} = \frac{m_s \langle V_z^2 \rangle}{K} \ , \qquad T_{\perp} = \frac{m_s \langle V_\perp^2 \rangle}{2K} \ , \tag{2.132}$$

as usual, in which K is the Boltzmann constant and $\langle\ \rangle$ means the averaged quantity.

It is noticed that the first term D in Eq.(2.129) is just the same as that gives the cold dispersion equation

$$D(\omega, k) = 0 \ , \tag{2.133}$$

i.e., the dispersion equation for the zero temperature plasma which is well described by the distribution function of the form of

$$g_s(\vec{V}) = \delta(V_z)\delta(V_\perp)/2\pi V_\perp \ . \qquad (2.134)$$

The second term in Eq.(2.129) vanishes to the first order of $\langle V_\ell \rangle / V_R$ (ℓ= $\perp$,z), which means physcially that the relation between ω_r and k does not depend upon the shape of the distribution function insofar as the thermal velocity determined by the distribution function itself is much smaller than the absolute value of the resonance velocity of the whistler mode waves. This can also be understood by the MHD equations. In the MHD equations, temperature effect appears primarily only in the form of the pressure gradient in the direction of propagation, while the plasma motions associated with the longitudinally propagating whistler mode waves are essentially perpendicular to it. Therefore, the propagation characteristics, i.e., the dispersion equation is not affected primarily by the temperature effect at all. Figs.44 show the universal ω_r-k diagram for the cold plasma (Fig.44(a)) and the thermal effects on the refractive index of the whistler mode waves, in which the plasma parameters are chosen so as to fit the typical magnetospheric plasma. It follows from these figures that the thermal effects appear appreciably only in the frequency range of $f > 0.7f_H$ even when the plasma temperature is as high as 3×10^4°K. Influence of the thermal motions on the growth and/or damping rate is found from Eq.(2.130) to be very small and well described by the cold plasma limit $T_\ell \to 0$ ($\ell=\perp$ or z). In what follows, therefore, we shall neglect the thermal corrections on the dispersion equation and the growth (and/or damping) rate except in the case that $f \to f_H$. Then, Eqs.(2.129) and (2.130) are written in such a simple forms as

$$D \equiv c^2k^2 - \omega_r^2 + \sum_s \frac{\omega_r \Pi_s^2}{\omega_r + \varepsilon_s \Omega_s} = 0 \ , \qquad (2.135)$$

and

$$\gamma_k = \sum_s \frac{\pi^2}{N_s} \frac{\varepsilon_s \Omega_s \Pi_s^2}{\partial D/\partial \omega_r} \int_{-\infty}^{\infty} dV_z \int_0^{\infty} dV_\perp V_\perp^2 \delta(\omega_r - kV_z + \varepsilon_s\Omega_s) \nabla_v g_s \ , \qquad (2.136)$$

or

$$= \sum_s \frac{\pi}{2N_s} \frac{\varepsilon_s \Omega_s \Pi_s^2}{\partial D/\partial \omega_r} \int d\vec{V} V_\perp \delta(\omega_r - kV_z + \varepsilon_s\Omega_s) \nabla_v g_s \ , \qquad (2.136)'$$

where the operator ∇_v is defined by

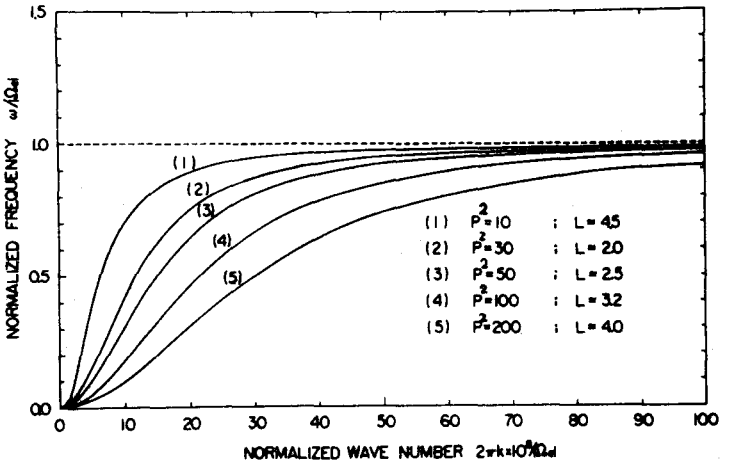

Fig.44(a) Universal Whistler Mode ω_r-k Diagram.

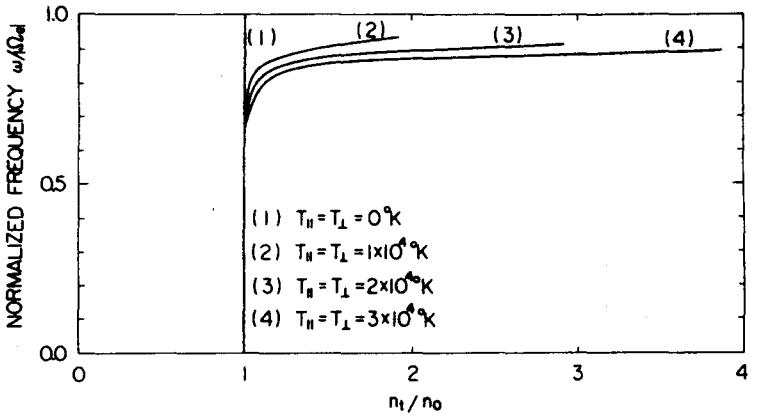

Fig.44(b) Thermal Effects on the Whistler Mode Dispersion.

The ratio of the refractive index n_t for finite temperature plasma to that n_o for cold plasma is shown vs. normalized frequency ω_r/Ω_e. The ratio of n_t/n_o is given by

$$\frac{n_t}{n_o} = \{1 - \sum_s \frac{K}{m_s c^2} \frac{\varepsilon_s \Omega_s \Pi_s^2}{(\omega_r + \varepsilon_s \Omega_s)^3} (T_{\parallel} - \frac{\omega_r + \varepsilon_s \Omega_s}{\varepsilon_s \Omega_s} T_{\perp})\}^{-1/2} \quad .$$

$$\nabla_v \equiv \frac{\partial}{\partial V_\perp} - \frac{kV_\perp}{\varepsilon_s \Omega_s} \frac{\partial}{\partial V_z} \quad . \tag{2.137}$$

Eq.(2.136) (or Eq.(2.136)') now enables us to estimate the growth rate of the cyclotron instability in the whistler mode for an arbitrary type of the distribution functions which satisfy the assumptions (1)∿(3) mentioned before. (p.88 ∿ p.89)

It should be, however, noted that Eq.(2.136) or Eq.(2.136)' is not applicable to the case of relatively large $|\gamma_k|$, such as the strong cyclotron damping of the whistler mode waves near the cyclotron frequency of plasma particles, but gives proper description only in the state of the plasma such that $|\gamma_k|$ is small enough. In cases where the growth and/or damping rate is so large that the assumption $|\gamma_k| \ll \omega_r$ is not satisfied, the method described above breaks down and either of the following two methods should be employed.

One is to take higher order terms γ_k/ω_r in the Taylor expansion when estimating the principal values of Eqs.(2.125) and (2.126) with repeated uses of the Dirac-Plemelj formula (2.124). The other is to do a numerical analysis of the dispersion equation having the integral form. The former method is only a modification of the case of small $|\gamma_k|$ and is not so effective. In the latter method, it is necessary to obtain the integral dispersion equation, which, in case of the whistler mode waves, is expressed as

$$c^2k^2 - \omega^2 + \sum_s \Pi_s^2 \{1 + Q_s(\omega,k)\} = 0 \ , \tag{2.138}$$

where

$$Q_s(\omega,k) = \begin{cases} \int_{-\infty}^{\infty} \dfrac{\Psi_s(V_z,k)}{V_z - V_R} dV_z & \text{for } \gamma_k > 0 \ , \quad (2.139) \\ \int_{-\infty}^{\infty} \dfrac{\Psi_s(V_z,k)}{V_z - V_R} dV_z + 2\pi j \left|\dfrac{k}{k}\right| \Psi_s(V_R,k) & \text{for } \gamma_k \leq 0 \ , \quad (2.140) \end{cases}$$

in which

$$\Psi_s(V_z,k) = \zeta_s(V_z) + \frac{\varepsilon_s \Omega_s}{k} \eta_s(V_z) \ , \tag{2.141}$$

$$\eta_s(V_z) = \frac{2\pi}{N_s}\int_0^\infty dV_\perp V_\perp g_s(V_\perp, V_z) \quad , \tag{2.142}$$

$$\zeta_s(V_z) = \frac{\pi}{N_s}\frac{\partial}{\partial V_z}\int_0^\infty dV_\perp V_\perp^3 g_s(V_\perp, V_z) \quad . \tag{2.143}$$

In a special case that the distribution function has the following form,

$$g_s(V_\perp, V_z) = N_s\sqrt{\frac{m_s}{2\pi\kappa T_{||}}}\exp[-\frac{m_s V_z^2}{\kappa T_{||}}]\, h(V_\perp) \quad . \tag{2.144}$$

Eq.(2,138) reduces to the well known dispersion equation described by the plasma dispersion function Z (Fried & Conte[75]; Scharer & Trivelpiece[76]) as

$$\frac{c^2k^2}{\omega^2} = 1 + \sum_s \frac{\Pi_s^2}{\omega k V_T}[\, Z(\Phi) - \frac{kV_T(1-A)}{\omega}\{1 + \Phi Z(\Phi)\}\,] \quad , \tag{2.145}$$

where

$$\Phi = \frac{\omega_r + \varepsilon_s\Omega_s}{kV_T} \quad , \qquad V_T = \sqrt{\frac{2\kappa T_{||}}{m_s}} \quad , \tag{2.146}$$

$$A = \frac{T_\perp}{T_{||}} = \frac{\pi m_s}{\kappa T_{||}}\int_0^\infty dV_\perp V_\perp^3 h(V_\perp) \quad . \tag{2.147}$$

Eqs.(2.138) to (2.143) enable us to examine the behavior of the rapidly growing or damping waves in the whistler mode for both instability problems (k:real, ω:complex) and amplifying problems (ω:real, k:complex).

Applications of the linear analyses of the cyclotron instability in the whistler mode due to the temperature anisotropy will be given in the following, using Eqs.(2.135) and (2.136) described in this section.

5.3 Location of the Instability in the Magnetosphere

Much information upon the properties of the cyclotron instability in the magnetosphere can be extracted from the results of the linear analysis e.g., from the expression for the growth or damping rate Eq.(2.136) or (2.136)'. At first, a general argument will be given on the location of the instability region in the magnetosphere.

It is reported (Helliwell[29]) that the wave growth is found to be almost confined to a region near the geomagnetic equator. This specific

feature of the wave growth, i.e., of the instability region is brought into light by referring the expression (2.136) for γ_k with the use of magnetospheric plasma parameters mentioned in Chapter I.

Expressing γ_k in terms of the resonance velocity V_R under the assumption that the real part of the refractive index is much greater than unity, we obtain

$$\gamma_k = -\text{sign}(k)\pi^2 V_R(\Omega_e-\omega_r) \int_{-\infty}^{\infty} dV_z \int_0^{\infty} dV_\perp V_\perp^2 \delta(V_z-V_R) \nabla_v \tilde{g}_e \ , \qquad (2.148)$$

where $\tilde{g}_e$ is the normalized distribution function and the resonance velocity V_R is expressed as

$$V_R = -c \ \text{sign}(k) \frac{(\Omega_e-\omega_r)^{3/2}}{\Pi_e\sqrt{\omega_r}} \ . \qquad (2.149)$$

The most influential factor on the magnitude of the maximum growth rate in Eq.(2.148) is the delta function $\delta(V_z-V_R)$ in the V_z-integral. This corresponds physically to the fact that the magnitude of the growth or damping rate primarily depends upon the number of resonant particles. Since the smaller the resonance velocity is, the more particles exist generally, it is concluded that the location of the minimum resonance velocity V_R becomes the most feasible region for the instability. On the other hand, the resonance velocity in the whistler mode is mainly controlled by a plasma parameter $P = \Pi_e/\Omega_e$; a measure of the plasma density to the magnetic field energy density as in the form of

$$V_R = - c \ \text{sign}(k) \ \frac{(1-x)^{3/2}}{P\sqrt{x}} \ , \qquad (2.150)$$

where $x = \omega_r/\Omega_e$.

Typical magnetospheric parameters <u>along</u> the $L \simeq 4$ field line are depicted in Fig.45, from which the resonance velocity in the whistler mode for various frequencies vs. the distance S from the ground along the field line is plotted in Fig.46. From these figures, we know immediately that the cyclotron instability of the whistler mode waves is most easily excited at the equator on each geomagnetic field line. As an example, the maximum growth rate for a simple loss cone distribution function

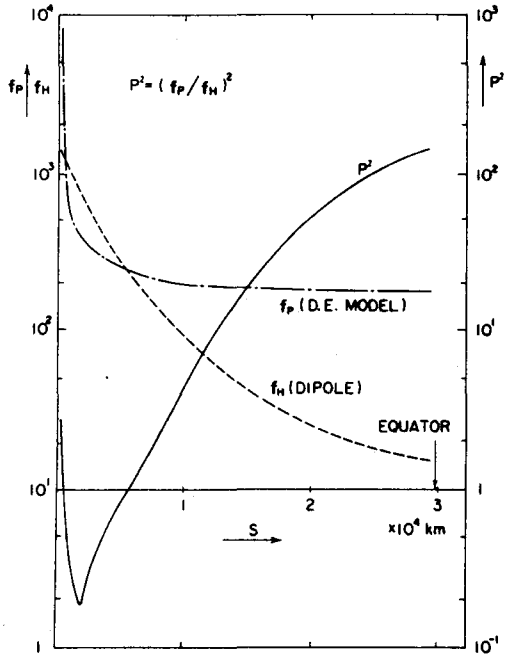

Fig.45 Typical Magnetospheric Plasma Parameters along L ≃ 4 Field Line.

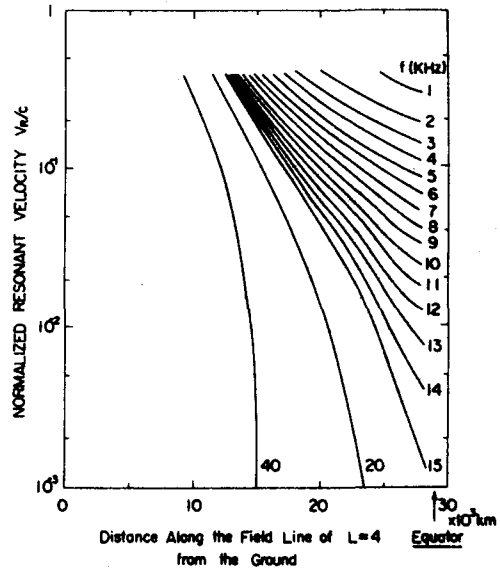

Fig.46 Resonance Velocity of Electrons with Whistler Mode Waves vs. Distance from the Ground along L ≃ 4 Field Line.

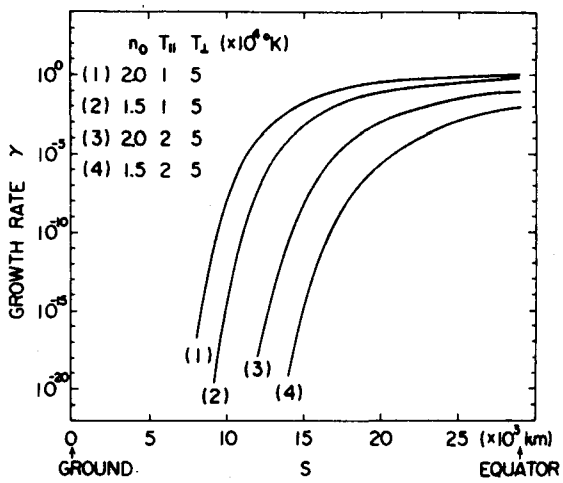

Fig.47 Maximum Growth Rate of Whistler Mode Cyclotron Instability vs. Distance from the Ground along L ≃ 4 Field Line for a Simple Loss Cone Distribution Function.

$$g_e(V_\perp,V_z) = \frac{1}{\pi\Gamma(n_o+1)}\sqrt{\frac{m_e}{2\pi\kappa T_{||}}}\left[\frac{m_e}{2\kappa T_\perp}\right]^{n_o+1} V_\perp^{2n_o} \exp\left(-\frac{m_e V_\perp^2}{2\kappa T_\perp} - \frac{m_e V_z^2}{2\kappa T_{||}}\right), \tag{2.151}$$

vs. distance S from the ground along the L ≃ 4 field line is illustrated in Fig.47, where $\Gamma(x)$ is a gamma function. Thus, we know that the main controlling factor on the magnitude of the maximum growth rate is the plasma parameter P which usually becomes maximum at the equator on each geomagnetic field line.

5.4 Growth and Damping Rate Calculation for Model Distribution Functions

A next possible investigation within the linear theory is a quantitative study of the growth and/or damping rate of the cyclotron instability as a function of wave frequency for various distribution functions. Such a computation will give some information for the actual distribution of the high energy part of the magnetospheric plasma around the resonance velocity by comparing the emission spectrum and the peak of the growth rate vs. frequency.

As tentative model distribution functions, the following three distribution functions are considered in this section. They are

(a) Maxwellian in the direction of the external magnetic field $\vec{B}_o$, but an arbitrary function $h_s(V_\perp)$ in the perpendicular direction, i.e.,

$$g_s(V_\perp,V_z) = N_s\sqrt{\frac{m_s}{2\pi\kappa T_{||}}}\, h_s(V_\perp) \exp\left(-\frac{m_s V_z^2}{2\kappa T_{||}}\right). \tag{2.152}$$

The loss cone distribution function Eq.(2.151) is one of the examples of the above expression.

(b) The modified Cauchy distribution along $\vec{B}_o$ but an arbitrary function $h_s(V_\perp)$ perpendicular to $\vec{B}_o$, i.e.,

$$g_s(V_\perp,V_z) = N_s \frac{2V_T^3}{\pi(V_z^2+V_T^2)^2} h_s(V_\perp), \tag{2.153}$$

where

$$V_T^2 = \frac{\kappa T_{||}}{m_s}. \tag{2.154}$$

and

(c) The modified Olbert distribution function: a distribution function of the power law which is extended to two-temperature anisotropic characters from the Olbert distribution (Vasyliunas[79]), i.e.,

$$g_s(V_\perp, V_z) = N_s \sqrt{\frac{m_s}{(2\lambda-3)\pi\kappa T_{\parallel}}} \frac{m_s}{(2\lambda-3)\pi\kappa T_\perp} \frac{\Gamma(\lambda+1)}{\Gamma(\lambda-\frac{1}{2})} \times \{1 + \frac{m_s V_z^2}{(2\lambda-3)\kappa T_{\parallel}} + \frac{m_s V_\perp^2}{(2\lambda-3)\kappa T_\perp}\}^{-\lambda-1} \quad . \tag{2.155}$$

It is noted that the above modified distribution function becomes a two-temperature Maxwellian if we let the parameter λ tend to infinity.

Corresponding expressions of the growth rate are obtained by substituting Eqs.(2.153) ∿ (2.155) into Eq.(2.136) and are given as follows:

i) case (a),

$$\gamma_k = \sum_s \frac{\pi}{|k|} \sqrt{\frac{m_s}{2\pi\kappa T_{\parallel}}} \exp(-\frac{m_s V_R^2}{2\kappa T_{\parallel}}) \frac{\Pi_s^2(\omega_r+\epsilon_s\Omega_s)}{\partial D/\partial\omega_r} (A - \frac{\epsilon_s\Omega_s}{\omega_r+\epsilon_s\Omega_s}) \quad , \tag{2.156}$$

ii) case (b),

$$\gamma_k = \sum_s \frac{4V_T^3}{(V_R^2+V_T^2)^3} \frac{\Pi_s^2(\omega_r+\epsilon_s\Omega_s)}{\partial D/\partial\omega_r|k|} \frac{\kappa}{m_s} \{T_\perp - \frac{\epsilon_s\Omega_s}{\omega_r+\epsilon_s\Omega_s} \frac{m_s}{2\kappa}(V_R^2+V_T^2)\} \quad , \tag{2.157}$$

iii) case (c),

$$\gamma_k = \sum_s \pi \sqrt{\frac{m_s}{(2\lambda-3)\pi\kappa T_{\parallel}}} \frac{1}{|k|} \frac{\Gamma(\lambda)}{\Gamma(\lambda-\frac{1}{2})} \frac{1}{\{1+\frac{m_s V_R^2}{(2\lambda-3)\kappa T_{\parallel}}\}^{\lambda}} \frac{\Pi_s^2(\omega_r+\epsilon_s\Omega_s)}{\partial D/\partial\omega_r} \quad . \tag{2.158}$$

Thus, in a case where ions are regarded as an immobile background, the conditions for the cyclotron instability to grow at a given frequency ω_r are

$$A \equiv \frac{T_\perp}{T_{\parallel}} \geq \frac{\Omega_e}{\Omega_e-\omega_r} \quad , \tag{2.159}$$

for cases of (a) and (c), and

$$T_{\perp} \geq \frac{\Omega_e}{\Omega_e - \omega_r} \frac{m_e}{2K} \left\{ \frac{(\Omega_e - \omega_r)^2}{k^2 (\omega_r)} + \frac{KT_{\parallel}}{m_e} \right\} , \tag{2.160}$$

for case (b). It is noticed, however, that the condition for the loss cone distribution function Eq.(2.151) is written as

$$\frac{(n_o+1)T_{\perp}}{T_{\parallel}} \geq \frac{\Omega_e}{\Omega_e - \omega_r} . \tag{2.161}$$

Eq.(2.159) is the well known condition for the cyclotron instability to grow (Stix[25]; Cornwall[80]; Hultquvist[81]). In either case considered above, a strong anisotropy in temperature is necessary for the appearance of an unstable frequency range around $f_H/2$ where discrete VLF emissions are often observed. It should, however, be noticed that these conditions are correct only for the distribution functions considered above. The necessary and sufficient conditions for the wave to grow at a given frequency are, really, not to be describable by the concept of the "temperature anisotropy", because the temperature is by itself only a measure of the macroscopic quantity of the plasma, while the wave growth or damping should be determined by the local gradient of the distribution function around the resonance velocity in phase space.

Numerical calculations of the wave growth rate in the linear approximation are made in order to apprehend the dependence of the cyclotron instability on the temperature anisotropy of each model distribution function. Figs.48, 49 and 50 are the corresponding results for the two-temperature Maxwellian, the modified Cauchy-Maxwellian and the modified Olbertian distribution, respectively. Except the temperature, parameters at the equator on L ≃ 4 field line in the magnetosphere are adopted in the calculations. From these numerical calculations, the following general conclusions are obtained:

(i) In the cyclotron instability due to the temperature anisotropy, we find out that a maximum growth rate appears at a frequency a little below the cutoff frequency above which the wave damps away. This characteristic gives a good explanation of one of the characteristics of WTE-H, summarized in Chapter I, i.e., WTE-H is always

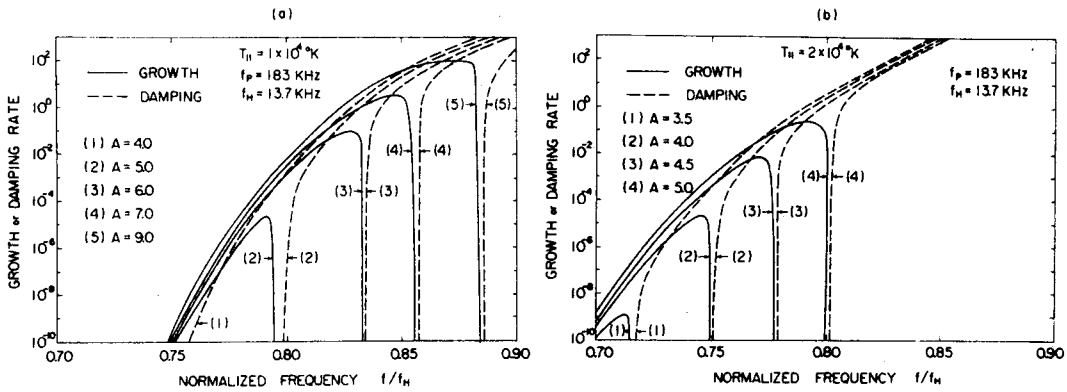

Fig.48 Growth and Damping Rate of Whistler Mode Cyclotron Instability for Two-Temperature Maxwellian Distribution.

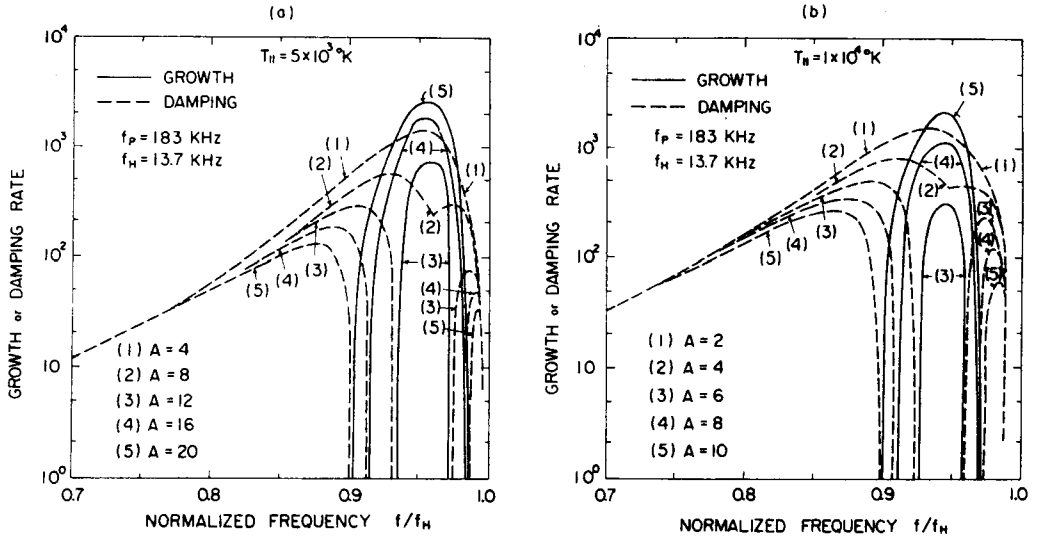

Fig.49 Growth and Damping Rate of Whistler Mode Cyclotron Instability for Modified Cauchy-Maxwellian Distribution.

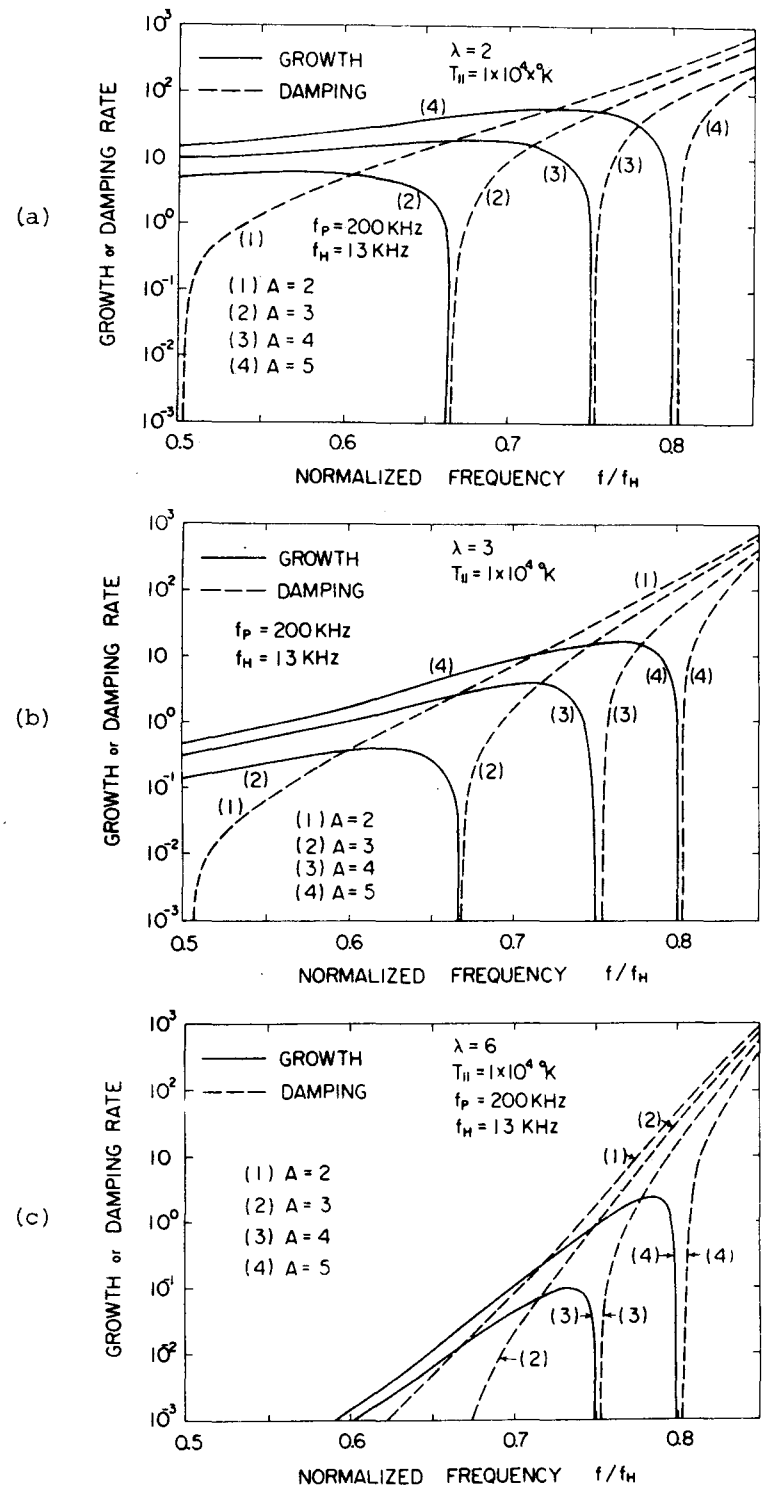

Fig.50 Growth and Damping Rate of Whistler Mode Cyclotron Instability for Modified Olbert Distribution.

triggered around the whistler cutoff frequency.

(ii) However, for the explanation of a narrow band structure of WTE-H, the modified Cauchy distribution and the modified Olbert distribution with small λ are out of question. Even the two-temperature Maxwellian and the modified Olbertian with large λ are not proper to explain it under the plasma parameters of the present interest in the magnetosphere.

(iii) And yet no model distribution functions adopted here are explicable for the observed frequency characteristics that the emissions are most frequently generated at $f \simeq \frac{1}{2} f_H$, since they cannot give a sufficiently large growth rate around $\frac{1}{2} f_H$ unless an unrealistic large parallel temperature is introduced, keeping the temperature anisotropy $A \simeq 2$. (cf. Eq.(2.159))

Thus it can be inferred from a comparison of the observed characteristics of the VLF emissions with the results of linear analysis of the cyclotron instability that such simple distribution functions as considered in the above can not represent the magnetospheric plasma, especially for its high energy tail. These calculations, however, will be useful for the understanding of various physical processes in various plasmas other than the magnetospheric plasma.

5.5 Characteristics of the Instability for the Postulated Triple-Structured Distribution Function in the Magnetosphere

5.5.1 Observed Plasma Distribution in the Magnetosphere

In this section, for applying the cyclotron instability to discrete VLF emissions, we are going to use a more realistic model for the distribution function of the magnetospheric plasma than those considered previously. As already mentioned and summarized in Section 1.3 in Chapter I, recent satellite data (Serbu & Maier[18,19]; Hess[21]) show that the magnetospheric plasma is well described by the sum of two Maxwellian distribution functions. One is a thermal component with a temperature of $2 \sim 5$eV and a number density of $400 \sim 550$ cm^{-3} just inside the plasmapause which is located around $L = 3 \sim 5$ according to K_p condition. The other is a high energy component, which we call here "quasithermal"

plasma, with a temperature of 10 ∿ 50eV and a number density of about 1 per cent of the thermal component. This quasithermal plasma is supposed to be due to the particles diffused from the plasma sheet observed by Sagalyn & Smiddy[82] in the region of L ≃ 3 ∿ 5 in the magnetosphere.

On the other hand, as a transient phenomenon around L ≃ 4 equatorial plane in the magnetosphere, relatively high low-energy electrons with peak differential intensities at E = 100 ∿ 200eV have been observed (Frank[23]; Schield & Frank[22]) as mentioned in Section 1.3 in Chapter I. Their density sometimes attains even to 1 percent of the thermal component. Though a distribution function which describes these transient electrons is indistinct, it can be inferred taking account of the observed narrow band characteristics of the discrete VLF emissions that the distribution must be of a beam shape around the resonance velocity because otherwise a rather wide band structure of emissions can only be expected.

We, therefore, consider the following "triple-structured" loss cone distribution function as a more realistic model for the magnetospheric electrons around L ≃ 4 equatorial plane.

$$g_e(V_\perp, V_z) = \frac{N_e}{\pi}\sqrt{\frac{m_e}{2\pi\kappa}} \sum_{j=T,Q,B} \frac{\eta_j}{T_{j\parallel}\Gamma(n_j+1)} \left[\frac{m_e}{2\kappa T_{j\perp}}\right]^{n_j+1}$$

$$\times V_\perp^{2n_j} \exp\left[- \frac{m_e(V_z - \delta_{jB}V_B)^2}{2\kappa T_{j\parallel}} - \frac{m_e V_\perp^2}{2\kappa T_{j\perp}} \right] , \qquad (2.162)$$

where suffixes T, Q and B stand for thermal, quasithermal and transient beam electrons respectively, η_j shows a relative density of each component to a total density, n_j is a measure of anisotropy of the loss cone distribution and δ_{ij} is Kronecker's delta function. A schematic illustration of the present model distribution function is given in Fig.51.

5.5.2 Growth and Damping Rate and Comparison with Characteristics of VLF Emissions

Substituting Eq.(2.162) into Eq.(2.136) of the expression for γ_k, we can easily calculate frequency characteristics of the whistler mode cyclotron instability for the "triple-structured" plasma distribution function as depicted in Fig.52. The plasma parameters used in the above

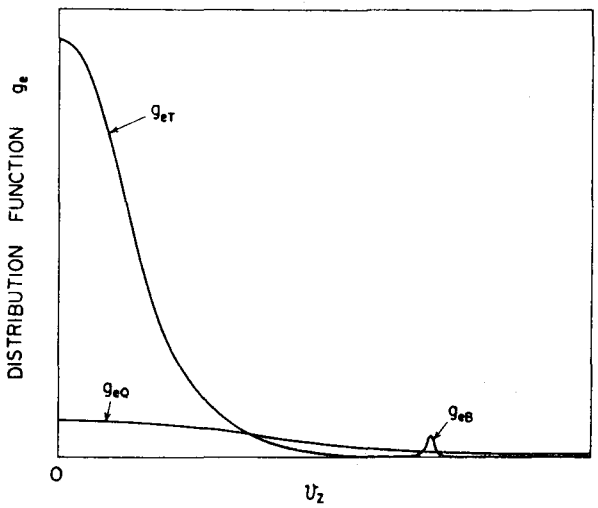

Fig.51 Schematic Illustration of the Model Distribution Function for the Magnetospheric Electrons.

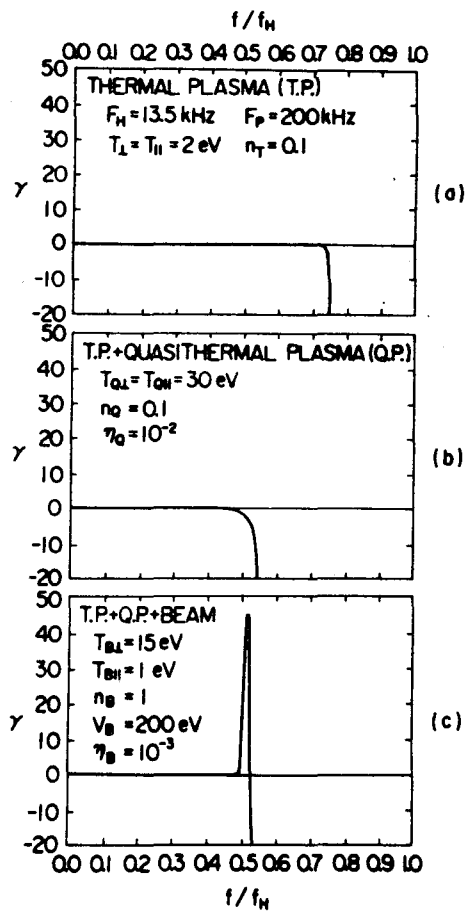

Fig.52 Frequency Characteristics of Whistler Mode Cyclotron Instability for the Model "Triple-Structured" Loss Cone Distribution Function.

calculation are applicable to the L ≃ 4 equatorial region as summarized in Section 1 in Chapter I; e.g., Fig.52(a) is for the plasma composed only of the thermal plasma with f_p = 200kHz, $T_{T\perp}$= $T_{T\parallel}$= 2eV and n_T= 0.1. It is obvious from this figure that a strong cyclotron damping exists only in the frequency range $f > 0.75f_H$, though the cutoff frequency f_c above which γ_k becomes negative (damping sense) is given analytically from Eq.(2.161) by

$$\frac{f_c}{f_H} = 1 - \frac{T_{T\parallel}}{(n_T+1)T_{T\perp}} = 1 - \frac{1}{1.1} = 0.09 \quad .$$

Similar quantitative calculations for the thermal temperature up to 5eV show that a strong cyclotron damping appears only in the frequency range $f > 0.7f_H$ and waves with frequencies below $0.7f_H$ are hardly damped and are marginally stable, i.e. they can propagate without damping in the magnetospheric plasma. This is physically natural because number density of the resonant electrons, which interact with waves in the frequency range $f < 0.7f_H$, is very few in such a low temperature plasma as T ∿ 2 to 5eV.

In Fig.52(b), a very little quantity of the quasithermal plasma with temperature of the order of 20 ∿ 50eV is added to the thermal plasma. Though the quantity η_Q is taken as 1 %, the frequency characteristics of the cyclotron damping or instability change markedly. In this case, waves with frequencies higher than about $0.5f_H$ are heavily damped out by the cyclotron damping. Dependence of this feature on the temperature of the quasithermal plasma is shown in Fig.53 for plausible values of T_Q= ($T_{Q\parallel}$= $T_{Q\perp}$=) 20, 30, 40, and 50eV. From these figures, we could conclude that the frequency characteristics of the cyclotron damping are scarcely different from that in Fig.52(b) for the temperature of the quasithermal plasma actually observed in the magnetosphere. It is interesting that the whistler cutoff frequency around $0.5f_H$ is explicable by the above cyclotron damping which has been alternatively explained by the duct theory (Smith[83,84]). Scarf[55], Liemohn & Scarf[56] and Guthart[57] so far attempted to explain the whistler cutoff by the cyclotron damping due to the thermal plasma and obtained the result that a necessary temperature was unrealistically high for the magnetospheric thermal plasma,

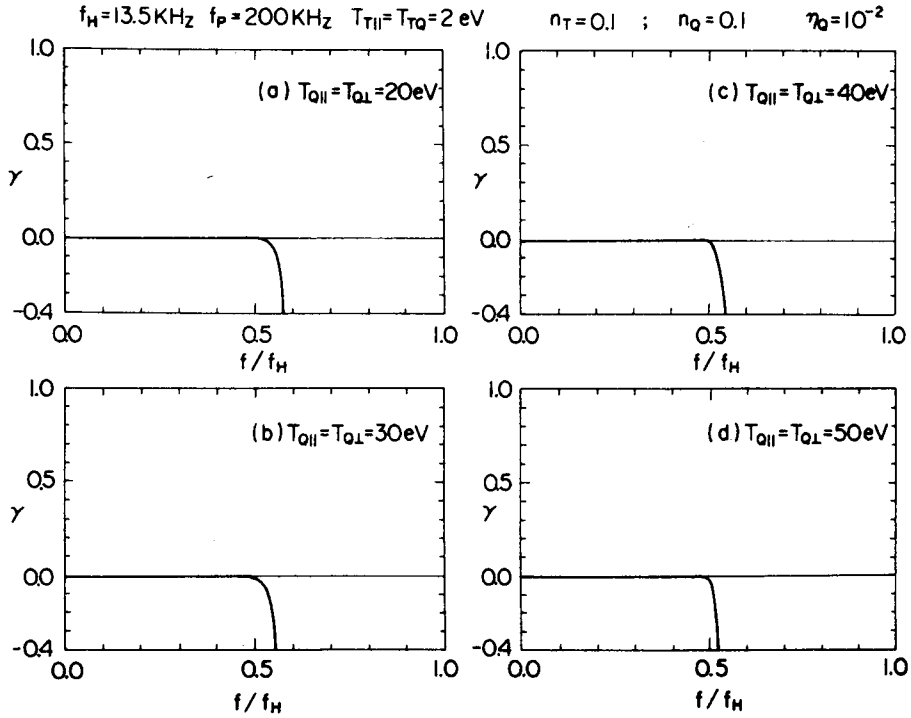

Fig.53 Frequency Characteristics of the Cyclotron Damping of the Whistler Mode Waves in the Plasma Composed of Both Thermal and Quasithermal Electrons.

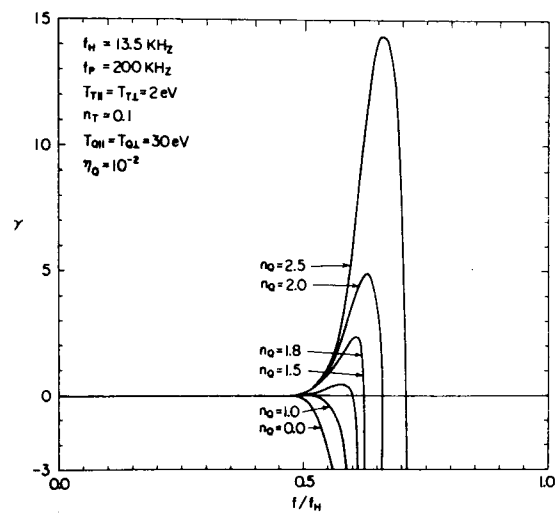

Fig.54 Frequency Characteristics of the Cyclotron Instability Excited by the Temperature Anisotropy of the Quasithermal Plasma.

because they assumed that the medium was expressed by a simple Maxwellian distribution. Thus a coexistence of the quasithermal and thermal plasmas is found to remove the above difficulty. It is, however, noticed that the frequency above which the strong cyclotron damping occurs is much affected by the plasma parameter $P = \Pi_e/\Omega_e$ since it is the main factor which controls the resonance velocity V_R as seen in Eq.(2.150). In the region of the present concern in the magnetosphere, the parameter P is large enough to yield a sufficient growth or damping rate around the frequency of $0.5f_H$.

There is a possibility that the cyclotron instability is excited by the plasma composed only of thermal and quasithermal particles, if the temperature anisotropy of the quasithermal plasma is suitably large. The growth rate vs. frequency for such a plasma is shown in Fig.54, in which only the quantity n_Q is changed as a parameter. Such an instability, however, will not be preferable for the reasons that the band width of the excited spectrum is larger than that of the usually observed discrete VLF emissions, and that the frequency of the most unstable waves in the instability lies in the frequency range higher than $0.6f_H$.

We are now going to discuss the cyclotron instability due to the coexistence of the transient beamy electrons with the thermal and the quasithermal electrons. In such a plasma, the frequency characteristics of the instability are illustrated in Fig.52(c). A sharp and narrow band structure of the excited waves due to the instability is seen near the frequency around $0.5f_H$ as well as a strong cyclotron damping in the frequency range $f \gtrsim 0.5f_H$. These features can well explain the observed WTE-H characteristics as summarized in Section 2.2.2 in Chapter I even when the beam relative density η_B is as small as 10^{-3}.

Dependencies of the frequency of the maximum growth rate upon the beam perpendicular temperature $T_{B\perp}$, the beam anisotropic index n_B and the beam bulk energy V_B are shown in Figs.55(a), (b), (c) and (d), respectively. It follows from these figures that the beam perpendicular temperature and the anisotropic index scarcely affect the frequency of the maximum growth rate, but control only the magnitude of the maximum growth rate. The bulk energy, on the other hand, of the beam electrons, which lies in the range of $V_B \lesssim 200$eV, has an influence both on the frequency and the magni-

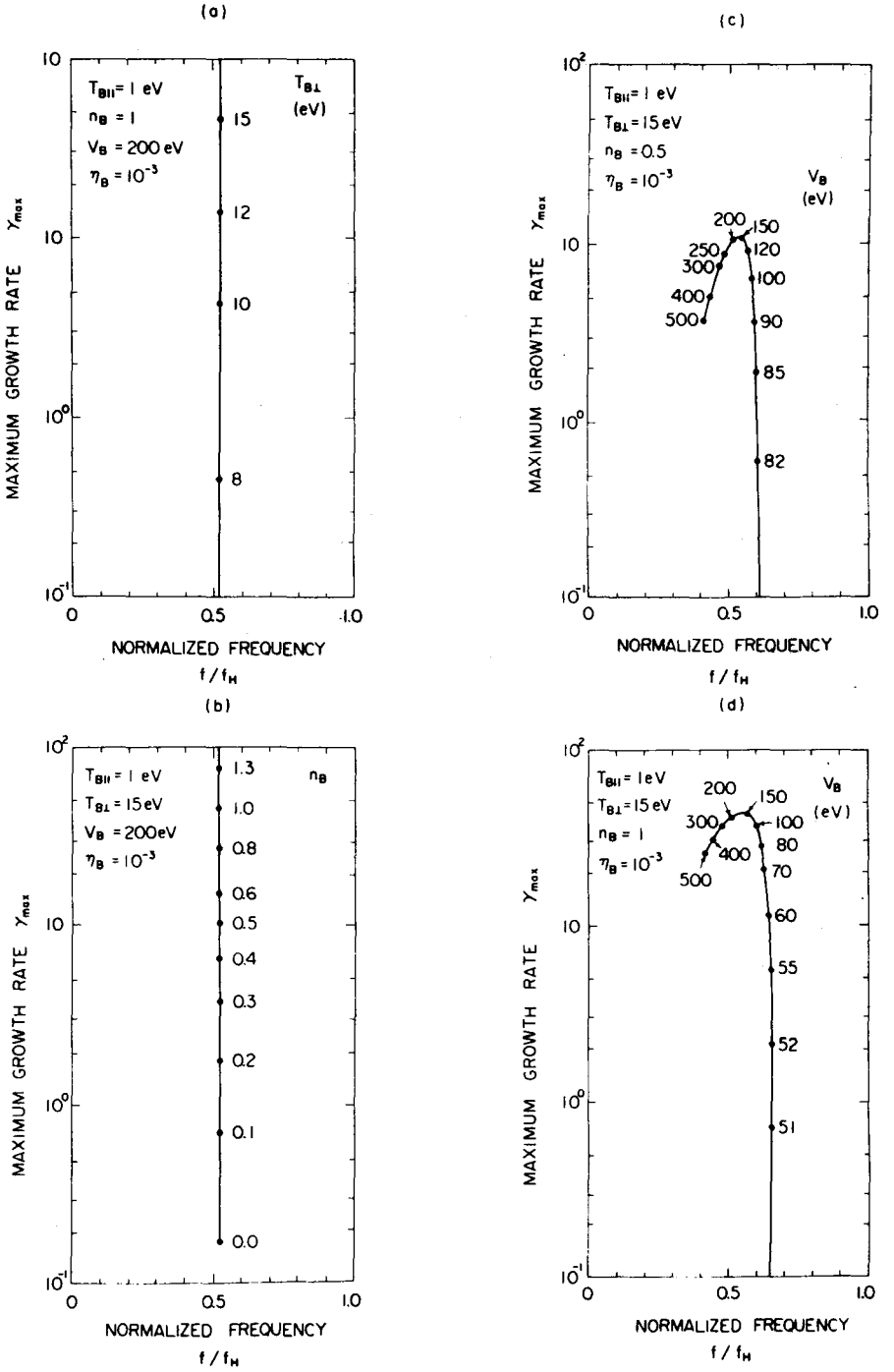

Fig.55 Dependence of the Maximum Growth Rate of Whistler Mode Cyclotron Instability upon Beam Parameters in the Model Distribution Function Eq.(2.162). Parameters of thermal and quasithermal plasma are the same as those given in Figs.52(a) and (b).

tude of the maximum growth rate. It should be noted that the resultant frequency and magnitude of the maximum growth rate under the magnetospheric circumstance of the present interest are just explicable for the observed characteristics of WTE, from (1) to (3) in Section 2.2.2 in Chapter I, if we take the observed parameters of the bulk energy V_B from 100eV up to 400eV.

From these characteristics of the instability due to the co-existence of the beam, the quasithermal and the thermal electrons, and from their transient properties, it can be well concluded that a generation mechanism of WTE-H is attributed to the whistler mode cyclotron instability in the "triple-structured" loss cone distribution function considered here in the magnetospheric plasma.

5.6 Discussion and Conclusions

In this section, we have surveyed the cyclotron instability in the whistler mode due mainly to the temperature anisotropy. The treatment of the instability is based upon the Vlasov-Maxwell equations, which are analyzed by the usual perturbation (linear) scheme to yield an analytic expression for the growth and/or damping rate for any distribution functions as far as $|\gamma_k| \ll \omega_r$. It, then, makes it possible for us to grasp many features of the instability. One example is that the instability conveniently called "due to temperature anisotropy" is not necessarily controlled by the macroscopic quantity of temperature but by the local gradient of the distribution function around the resonance velocity. Another example is that the whistler mode waves are most unstable usually at the equatorial plane on each geomagnetic field line.

Frequency characteristics of the instability are quantitatively calculated for various model distribution functions. It is found that the excitation of the narrow band VLF emissions should not be attributed to the instability in such simple model distribution functions as the bi-Maxwellian, modified Cauchy or modified Olbertian and that a simple criterion of the instability by the sign of γ_k leads to the improper understanding of the wave growth and damping. The growth or damping is a problem of the quantity.

The "triple-structured" loss cone distribution function is, then, shown to explain successfully most of the features of the whistler triggered emissions (WTE-H).

Apart from the explanation of the natural phenomena such as VLF emissions, we could get much information from the quantitative calculations about the behavior of the whistler mode cyclotron instability. We have confirmed throughout the present investigation that quantitative investigations are necessary and important instead of the so-called hand-wave qualitative investigations.

Chapter III

NONLINEAR ANALYSIS OF WHISTLER MODE CYCLOTRON INSTABILITY AND ITS APPLICATION TO VLF EMISSIONS —— QUASILINEAR VLASOV TREATMENT —— [50]

§1. Introduction

In the previous Chapter II, we have developed a linear analysis of the whistler mode cyclotron instability. As a natural extension of the theoretical investigation, a nonlinear treatment is required for the more complete understanding of the instability. In the problems of VLF emissions, for example, many important features ——— such as the temporal change of the frequency of the emission, the quenching process of the instability itself, and the unclarified process of triggering of a rather strong instability by the triggering whistler mode waves ——— still remain unclarified and are not thought to be clarified within the linear theory. It was, therefore, eagerly desired to take into account the nonlinear effects in the wave-particle interaction theory of VLF emissions.

Nonlinear interactions are mainly classified into two kinds; one is a wave-wave nonlinear interaction, while the other is a resonant wave-particle nonlinear interaction. Recently the former problem of the nonlinear wave-wave couplings between the whistler mode waves was investigated (Harker & Crawford[85]) resulting in a conclusion which is not in favor of the generation of VLF emissions. This is due to the dispersion characteristics of the whistler mode waves. In a relatively high frequency range in the whistler mode, the wave-wave couplings are small within the approximation of the three wave process, because of the nondecay characteristics of the dispersion (see, Kadomtsev[86]). On the contrary, the latter resonant interaction plays a fundamental role in the case of the whistler mode waves. If the wave under consideration ——— either the triggering or the excited wave ——— has

a considerable amplitude, reaction of the wave to the resonant particles becomes unnegligible and the background distribution function itself is deformed by such a nonlinear effect.

In the case of the interaction in which the frequency spread of resonance is infinitesimally small, the reaction is well described by the quasilinear theory. The main feature of the quasilinear theory is to describe the instability by the instantaneous homogeneous distribution function $g_e(\vec{V},t)$ which undergoes a slow change due to the nonlinear kinetic effects associated with the resonant interaction. In this Chapter III, we concern ourselves about the nonlinearity of the whistler mode cyclotron instability within the framework of the quasilinear theory.

A quasilinear treatment was first contrived for the study of the weak turbulence of the electrostatic waves (Vedenov, Velikov & Sagdeev[87]; Drummond & Pines[44]). The quasilinear treatments of the electromagnetic mode instability were subsequently developed recently (Shapiro & Schevchenko[88,89]; Andronov & Trakhtengertz[90]; Bass, Fainberg & Shapiro[91]; Kennel & Engelman[92]; Watanabe[93]; Sizonenko & Stepanov[94]; Lerche[95]; Wu[96]; Momota & Terashima[97] etc.). The basic principle of the quasilinear theory has been well established and its standard technique is now available.

General arguments on the cyclotron interaction for both electromagnetic and electrostatic instabilities were made by Kennel & Engelman[92]. In the present paper, however, main concern lies in the application to VLF emissions which propagate almost along the geomagnetic field lines in the whistler mode. Therefore, the quasilinear theory only for the whistler mode cycloron instability would be more effective in grasping the physical process in the instability and the emission process. Such a problem was once attacked by Engel[98] but it was restricted to a rather special case of relatively low frequency whistler mode waves, i.e., of the waves with $\omega_r << \Omega_e$. Engel's work stimulated Kennel & Petschek[42] to study a relation between the low frequency whistler mode waves and the precipitating particles from the magnetosphere.

In our present case, however, frequencies of the VLF phenomena of interest are relatively high around $0.5\ f_H$. Therefore, a similar problem should be attacked without such a frequency restriction.

Before entering into a mathematical formulation of the quasilinear theory, we first discuss in Section 2 the physical processes of the whistler mode quasilinear instability. In this section, we will derive a fundamental equation for the temporal change of the background distribution function $\partial g_{sr}/\partial t$ from the basic physical relations without complex mathematical manipulations.

In Section 3, a mathematical formulation of the whistler mode quasilinear cyclotron instability is developed along the standard way hitherto established. A set of the basic equations of the whistler mode quasilinear cyclotron instability will be obtained, which enables us to discuss the characteristics of the whistler mode instability in the nonlinear regimes. A discussion on the characteristics of the electromagnetic whistler mode instability is also made in the same section stressing a point on the frequency change of the maximum growth rate of the whistler mode cyclotron instability.

Using the quasilinear set of equations, computer calculations on the temporal development of the instability are performed in order to trace the evolution of the emissions produced by the instability. Section 4 is devoted to the description of the method of computations and the discussions of the numerical results. Two different kinds of computations were done; one is to trace the evolution of the instability which is initially set to grow spontaneously with a considerable growth rate by giving proper plasma parameters; the other is, on the other hand, to see the change of the growth rate by the incoming whistler mode waves with a relatively strong intensity. The former is, essentially, a stabilization problem which corresponds to the phenomenon of WTE-H. The latter is the problem of the triggering of the instability due to the triggering wave by changing the distribution function through the quasilinear effect. It corresponds to a model of ASE.

In Section 5, a physical consideration is made on the relevancy between the phenomena of triggered VLF emissions and the quasilinear effect of the whistler mode cyclotron instability. In Section 6, as another application of the quasilinear self-exciting cycle of the wave-particle interaction in the magnetosphere which was proposed by Kennel & Petschek[42], a morphological study is made. We clarified there what is the responsible wave in the K-P cycle in the magnetosphere.

§2. Physical Picture of Whistler Mode Quasilinear Cyclotron Instability

2.1 Principle of the Quasilinear Theory

An essential point for the quasilinear theory is that the nonlinearity is taken into account only in a slow deformation of the background distribution function due to the action of the excited waves by the instability. Each harmonic wave in the whistler mode with a certian frequency ω_r and a wave number k is assumed to exist independently of each other. Therefore they always interact only with the particles which satisfy the linear resonance condition of

$$\omega_r - kV_z + \varepsilon_s\Omega_s = 0 \quad . \tag{3.1}$$

Each harmonic satisfies the dispersion equation

$$D(\omega_r,k) = c^2k^2 - \omega_r^2 + \sum_s \frac{\omega_r \Pi_s^2}{\omega_r + \varepsilon_s\Omega_s} = 0 \quad , \tag{3.2}$$

which is derived by the same procedure as in the linear theory described in Chapter II except the point that the distribution function $g_s(V_\perp, V_z, t)$ is a slowly varying function of time. In other words the results of the linear analysis are to be applicable at any time by using an instantaneous value of the background distribution function.

2.2 Physical Reduction of the Quasilinear Equations

In this section, we derive an expression for the rate of the temporal change of the background distribution function from the basic physical laws. We could grasp the physical picture and essence of the whistler mode quasilinear cyclotron instability by such a physical derivation.

As mentioned in the previous section 2.1, each harmonic wave can exist independently of each other so that the wave energy density W_w is given by the following summation

$$W_w = \sum_k \left(\varepsilon_{wave} + \varepsilon_{T\perp} + \varepsilon_{Tz} \right) , \tag{3.3}$$

where ε_{wave} is the field energy density of a harmonic wave, and given by

$$\varepsilon_{wave} = \frac{1}{2}\mu_o H_k^2 + \frac{1}{2}\varepsilon_o E_k^2 \quad , \tag{3.4}$$

in which the suffix k denotes the harmonic index with a wave number k. $\varepsilon_{T\perp}$ and ε_{Tz} are the kinetic energy densities of the coherent motion of thermal particles associated with the wave in the directions perpendicular and parallel to the external magnetic field (z-direction), respectively. In the case of the purely transverse whistler mode waves, the coherent motion is limited in the plane perpendicular to the wave vector $\vec{k} = k\hat{z}$ so that $\varepsilon_{Tz} = 0$. The kinetic energy of the coherent motion $\varepsilon_{T\perp}$ is easily calculated by

$$\varepsilon_{T\perp} = \sum_s \frac{1}{2} N_s m_s \langle v_T^2 \rangle = \sum_s \frac{1}{2} \frac{\Pi_s^2}{(\omega_r + \varepsilon_s \Omega_s)^2} \varepsilon_o E_k^2 \quad , \tag{3.5}$$

where

$$\langle v_T^2 \rangle = \frac{q_s^2}{m_s^2} \frac{E_k^2}{(\omega_r + \varepsilon_s \Omega_s)^2} \quad , \tag{3.6}$$

is obtained from the linearized equation of motion under the influence of $\vec{E}_k$. Substitution of Eqs.(3.4) and (3.5) into Eq.(3.3) with the use of the Maxwell equations yields

$$W_w = \sum_k \left\{ 1 + \frac{c^2 k^2}{\omega_r^2} + \sum_s \frac{\Pi_s^2}{(\omega_r + \varepsilon_s \Omega_s)^2} \right\} \varepsilon_k \quad , \tag{3.7}$$

where

$$\varepsilon_k = \frac{1}{2} \varepsilon_o E_k^2 \quad , \tag{3.8}$$

is the electric field energy density of the k-th harmonic wave. While ω_r and k satisfy the dispersion equation (3.2), we finally get

$$W_w = - \sum_k \frac{\partial D / \partial \omega_r}{\omega_r} \varepsilon_k \quad . \tag{3.9}$$

The time derivative of ε_k is given by

$$\frac{d\varepsilon_k}{dt} = 2\gamma_k \varepsilon_k \quad , \tag{3.10}$$

where the growth rate γ_k has the same form as that in the linear theory

(Eq.(2.136) in Chapter II) except that the background distribution function is now a function of time. Since the integration in Eq.(2.136) over V_z is mainly contributed by particles with velocities around the resonance velocity V_R as clarified in the physical picture of the linear cyclotron instability (Section 2 in Chapter II), we could replace the velocity distribution $g_s(V_\perp,V_z)$ by $g_{sr}(V_\perp,V_z,t)$. The range of the integration over V_z can be conveniently changed from $(-\infty,\infty)$ to $(V_R-\Delta V_R, V_R+\Delta V_R)$, where ΔV_R is a measure of the spread of the resonance. Thus we can write down the growth rate expression in the quasilinear treatment as

$$\gamma_k(t) = \sum_s \frac{\pi^2}{N_s} \frac{\varepsilon_s \Omega_s \Pi_s^2}{\partial D/\partial \omega_r} \int_{V_R-\Delta V_R}^{V_R+\Delta V_R} dV_z \int_0^\infty dV_\perp V_\perp^2 \, \delta(\omega_r - kV_z + \varepsilon_s \Omega_s) \nabla_v g_{sr}(V_\perp,V_z,t). \tag{3.11}$$

We can now ready to calculate the time derivative of the distribution function $g_{sr}(V_\perp,V_z,t)$. The energy conservation for the sum of the wave energy density W_w and the kinetic energy density of the resonant particles $\langle W_p \rangle$ yields

$$\frac{d\langle W_p \rangle}{dt} = - \frac{dW_w}{dt} \quad , \tag{3.12}$$

where $\langle\ \rangle$ denotes an average over the velocity distribution function. The kinetic energy $\langle W_p \rangle$ is conveniently divided into the energy densities in the directions perpendicular and parallel to the static magnetic field as

$$\langle W_p \rangle = \varepsilon_{r\perp} + \varepsilon_{rz} \quad , \tag{3.13}$$

where

$$\varepsilon_{r\perp} = \sum_s \frac{1}{2} m_s \int_0^{2\pi} d\phi \int_{V_R-\Delta V_R}^{V_R+\Delta V_R} dV_z \int_0^\infty V_\perp dV_\perp V_\perp^2 g_{sr}(V_\perp,V_z,t)$$

$$= \sum_s m_s \pi \int_{V_R-\Delta V_R}^{V_R+\Delta V_R} dV_z \int_0^\infty dV_\perp V_\perp^2 \, V_\perp g_{sr}(V_\perp,V_z,t) \quad , \tag{3.14}$$

and

$$\varepsilon_{rz} = \sum_s \frac{1}{2} m_s \int_0^{2\pi} d\phi \int_{V_R-\Delta V_R}^{V_R+\Delta V_R} dV_z \int_0^\infty V_\perp dV_\perp V_z^2 g_{sr}(V_\perp,V_z,t)$$

$$= \sum_s m_s \pi \int_{V_R-\Delta V_R}^{V_R+\Delta V_R} dV_z \int_0^\infty dV_\perp \, V_z^2 \, V_\perp g_{sr}(V_\perp, V_z, t) \quad . \tag{3.15}$$

Substituting Eqs.(3.13) and (3.9) into Eq.(3.12) with the use of Eq.(3.10), we get

$$\frac{d\varepsilon_{r\perp}}{dt} + \frac{d\varepsilon_{rz}}{dt} = 2 \sum_k \frac{\partial D/\partial \omega_r}{\omega_r} \gamma_k \varepsilon_k \quad . \tag{3.16}$$

Thus we have obtained the total energy change of the resonant particles. As for the energy distribution of the total kinetic energy into the perpendicular and parallel directions, we make an assumption that the energy distribution is made independently of each other in each harmonic. The resonant particles in each harmonic diffuse in the velocity space according to the following relation (Brice[38,39]) as shown in the physical picture in Chapter II by Eqs.(2.5) and (2.6).

$$\frac{\Delta W_{p\perp}}{\Delta W_{p\parallel}} = \frac{\omega_r - kV_z}{kV_z} = -\frac{\varepsilon_s \Omega_s}{\omega_r + \varepsilon_s \Omega_s} \quad . \tag{3.17}$$

As a sum of the energy distribution rate in each harmonic, the following distribution into the perpendicular and parallel directions is possible.

$$\frac{d\varepsilon_{r\perp}}{dt} = 2 \sum_k \frac{-\varepsilon_s \Omega_s}{\omega_r + \varepsilon_s \Omega_s + (-\varepsilon_s \Omega_s)} \frac{\partial D/\partial \omega_r}{\omega_r} \gamma_k \varepsilon_k$$

$$= -2 \sum_k \frac{\varepsilon_s \Omega_s \partial D/\partial \omega_r}{\omega_r^2} \gamma_k \varepsilon_k \quad , \tag{3.18}$$

$$\frac{d\varepsilon_{rz}}{dt} = 2 \sum_k \frac{\omega_r + \varepsilon_s \Omega_s}{\omega_r + \varepsilon_s \Omega_s + (-\varepsilon_s \Omega_s)} \frac{\partial D/\partial \omega_r}{\omega_r} \gamma_k \varepsilon_k$$

$$= 2 \sum_k \frac{(\omega_r + \varepsilon_s \Omega_s) \partial D/\partial \omega_r}{\omega_r^2} \gamma_k \varepsilon_k \quad . \tag{3.19}$$

Substituting the expression Eq.(3.11) for γ_k into Eqs.(3.18) and (3.19), we finally obtain

$$\frac{d\varepsilon_{r\perp}}{dt} = -2 \sum_s \sum_k \frac{\pi^2}{N_s} \frac{\Omega_s^2 \Pi_s^2}{\omega_r^2} \varepsilon_k \int_{V_R-\Delta V_R}^{V_R+\Delta V_R} dV_z \int_0^\infty dV_\perp \, V_\perp^2 \delta(\omega_r - kV_z + \varepsilon_s \Omega_s) \nabla_v g_{sr} \, , \tag{3.20}$$

and

$$\frac{d\varepsilon_{rz}}{dt} = 2 \sum_s \sum_k \frac{\pi^2}{N_s} \frac{\Omega_s^2 \Pi_s^2}{\omega_r^2} \varepsilon_k \int_{V_R-\Delta V_R}^{V_R+\Delta V_R} dV_z \int_0^\infty dV_\perp V_\perp^2 \frac{kV_z}{\varepsilon_s \Omega_s} \delta(\omega_r - kV_z + \varepsilon_s \Omega_s) \nabla_v g_{sr} \ . \tag{3.21}$$

If we compare Eqs.(3.20) and (3.21) with the time derivatives of Eq.(3.14) and (3.15), we can get the expression for $\partial g_{sr}/\partial t$. It is, however, necessary to make a little more mathematical manipulation before the comparison. Let us consider the following integrations.

$$I_1 = \int_{V_R-\Delta V_R}^{V_R+\Delta V_R} dV_z \int_0^\infty dV_\perp [\ V_\perp^2 \nabla_v Q(V_\perp, V_z)\ ] \ , \tag{3.22}$$

$$I_2 = \int_{V_R-\Delta V_R}^{V_R+\Delta V_R} dV_z \int_0^\infty dV_\perp [\ V_z^2 \nabla_v Q(V_\perp, V_z)\ ] \ , \tag{3.23}$$

where the operater ∇_v is defined by Eq.(2.137) in Chapter II, and $Q(V_\perp, V_z)$ is an arbitrary function which satisfies the conditions

$$Q(\infty, V_z) = 0 \ , \quad \text{in order of } o(V_\perp^{-n}) \ ; \ n > 2 \ , \tag{3.24}$$

$$Q(V_\perp, V_z = V_R \pm \Delta V_R) = 0 \ . \tag{3.25}$$

After some integration by parts with the use of the conditions Eqs.(3.24) and (3.25), the integrations I_1 and I_2 reduce to

$$I_1 = \int_{V_R-\Delta V_R}^{V_R+\Delta V_R} dV_z \{V_\perp^2 Q\Big|_{V_\perp=0}^{V_\perp=\infty} - 2V_\perp Q\} - \int_0^\infty dV_\perp \frac{kV_\perp^3}{\varepsilon_s \Omega_s} Q\Big|_{V_z=V_R-\Delta V_R}^{V_z=V_R+\Delta V_R}$$

$$= -2 \int_{V_R-\Delta V_R}^{V_R+\Delta V_R} dV_z \int_0^\infty dV_\perp \ V_\perp Q \ , \tag{3.26}$$

$$I_2 = \int_{V_R-\Delta V_R}^{V_R+\Delta V_R} dV_z V_z^2 Q\Big|_{V_\perp=0}^{V_\perp=\infty} - \int_0^\infty dV_\perp \{ \frac{kV_\perp}{\varepsilon_s \Omega_s} V_z^2 Q\Big|_{V_z=V_R-\Delta V_R}^{V_z=V_R+\Delta V_R} - 2\frac{kV_z}{\varepsilon_s \Omega_s} V_\perp Q\}$$

$$= 2 \int_{V_R-\Delta V_R}^{V_R+\Delta V_R} dV_z \int_0^\infty dV_\perp \frac{kV_z}{\varepsilon_s \Omega_s} V_\perp Q \ , \tag{3.27}$$

respectively. If we regard that

$$Q(V_\perp,V_z) = V_\perp \delta(\omega_r - kV_z + \varepsilon_s\Omega_s)\nabla_v g_{sr} \quad , \tag{3.28}$$

the function $Q(V_\perp,V_z)$ satisfies the conditions Eqs.(3.24) and (3.25). Consequently Eqs.(3.20) and (3.21) reduce to the more convenient forms for the comparison mentioned before.

$$\frac{d\varepsilon_{r\perp}}{dt} = \sum_s \sum_k \frac{\pi^2}{N_s} \frac{\Omega_s^2 \Pi_s^2}{\omega_r^2} \varepsilon_k \int_{V_R-\Delta V_R}^{V_R+\Delta V_R} dV_z \int_0^\infty dV_\perp V_\perp^2 [\nabla_v \{V_\perp \delta(\omega_r - kV_z + \varepsilon_s\Omega_s)\nabla_v g_{sr}\}] \quad , \tag{3.29}$$

$$\frac{d\varepsilon_{rz}}{dt} = \sum_s \sum_k \frac{\pi^2}{N_s} \frac{\Omega_s^2 \Pi_s^2}{\omega_r^2} \varepsilon_k \int_{V_R-\Delta V_R}^{V_R+\Delta V_R} dV_z \int_0^\infty dV_\perp V_z^2 [\nabla_v \{V_\perp \delta(\omega_r - kV_z + \varepsilon_s\Omega_s)\nabla_v g_{sr}\}] \quad . \tag{3.30}$$

The evolution of the background velocity distribution $g_{sr}(V_\perp,V_z,t)$ is determined by comparing Eq.(3.29) and d/dt{Eq.(3.14)} and/or Eq.(3.30) and d/dt{Eq.(3.15)}. The result is

$$\frac{\partial g_{sr}}{\partial t} = \frac{\pi}{N_s m_s} \sum_k \frac{\Omega_s^2 \Pi_s^2}{\omega_r^2} \frac{\varepsilon_k}{V_\perp} \nabla_v \{V_\perp \delta(\omega_r - kV_z + \varepsilon_s\Omega_s)\nabla_v g_{sr}\} \quad . \tag{3.31}$$

It coincides with Eq.(3.83) which will be derived by a more tedious mathematical manipulation of the Vlasov-Maxwell equations in the next section.

2.3 Physical Consideration

We have so far derived intuitively the expression of the evolution of the background distribution function which is the most fundamental equation in the quasilinear instability. From the above procedure, we can extract some physical pictures of the quasilinear cyclotron instability. They are in brief:

1) The growth or damping process is just the same as that in the linear instability (see Section 2 in Chapter II) except that the distribution function itself changes slowly with time.
2) The resonance width in the velocity space is infinitesimally small, i.e., the resonance factor is described by the delta function

$\delta(\omega_r - kV_z + \varepsilon_s \Omega_s)$. Consequently a wave of a certain frequency ω_r and a wave number k always interacts only with the resonant particles with $V_R = (\omega_r + \varepsilon_s \Omega_s)/k$.

3) The evolution of the background distribution function is brought about so as to satisfy the energy conservation law of the total system.

4) The energy distribution is made in such a way that only the perpendicular energy density $\varepsilon_{r\perp}$ of the resonant particles decreases or increases, while all the other energy densities such as the wave field energy density ε_{wave}, the wave kinetic energy density $\varepsilon_{T\perp}$ and the parallel energy density of the resonant particles ε_{rz} increase or decrease according to whether the waves grow up or damp away. This can be easily understood by looking at the signs of the r.h.s. of Eqs.(3.18),(3.19) and the following equations.

$$\frac{d\varepsilon_{T\perp}}{dt} = 2 \sum_s \frac{\Pi_s^2}{(\omega_r + \varepsilon_s \Omega_s)^2} \gamma_k \varepsilon_k \ , \tag{3.32}$$

$$\frac{d\varepsilon_{wave}}{dt} = 2 \sum_k \left(1 + \frac{c^2 k^2}{\omega_r^2}\right) \gamma_k \varepsilon_k \ . \tag{3.33}$$

5) Consequently, the energy source for the growth of whistler mode waves by the instability is the kinetic energy in the direction perpendicular to $\vec{B}_o$ of the resonant particles which is decreased by the growing of the wave until a quasilinear stabilization of the instability is brought about.

6) In this case, the resonant particles diffuse in the velocity space according to Eq.(3.17) which determines the diffusion lines in the velocity space.

§3. Quasilinear Theory of Whistler Mode Cyclotron Instability

3.1 Model and Basic Equations

A set of the basic equations of the quasilinear theory of the whistler mode cyclotron instability is also obtainable in the standard mathematical way hitherto established.

In this section, we consider the quasilinear instability in the whistler mode waves which propagate along the external magnetic field $\vec{B}_o = B_o \hat{z}$ in an infinite, collisionless and homogeneous plasma. The waves are assumed to be purely transverse. The situation is set to be quite the same as the model in the linear treatment in Chapter II (cf. Fig.43). Basic equations in this case are also the Vlasov equation

$$\frac{\partial F_s}{\partial t} + \vec{V}\cdot\frac{\partial F_s}{\partial \vec{r}} + \frac{q_s}{m_s}\left(\vec{E} + \vec{V}\times\vec{B} + \vec{V}\times\vec{B}_o\right)\cdot\frac{\partial F_s}{\partial \vec{V}} = 0 \quad , \tag{3.34}$$

and the Maxwell equations.

As usually done in the standard method of the quasilinear theory, we divide the distribution function $F_s(V_\perp, V_z, z, t)$ into a slowly varying homogeneous part and a rapidly oscillating, spatially wavy part as

$$F_s(V_\perp, V_z, z, t) = g_s(V_\perp, V_z, t) + f_s(V_\perp, V_z, z, t) \ . \tag{3.35}$$

After expanding $\vec{E}, \vec{B}$ and f_s into the Fourier series as

$$\vec{E} = \sum_k \vec{E}_k \, e^{ikz}, \qquad \vec{B} = \sum_k \vec{B}_k \, e^{jkz} \quad , \tag{3.36}$$

$$f_s = \sum_{\substack{k \\ k\neq 0}} f_{sk} \, e^{jkz} \quad , \tag{3.37}$$

the Vlasov equation (3.34) is reduced to

$$\frac{\partial f_{sk}}{\partial t} + jkV_z f_{sk} + \frac{q_s}{m_s}(\vec{V}\times\vec{B}_o)\cdot\frac{\partial f_{sk}}{\partial \vec{V}}$$

$$= -\frac{q_s}{m_s}(\vec{E}_k + \vec{V}\times\vec{B}_k)\cdot\frac{\partial g_s}{\partial \vec{V}} - \frac{q_s}{m_s}\sum_{k'}{}' \, (\vec{E}_{k-k'} + \vec{V}\times\vec{B}_{k-k'})\cdot\frac{\partial f_{sk'}}{\partial \vec{V}} \quad , \tag{3.38}$$

and

$$\frac{\partial g_s}{\partial t} + \frac{q_s}{m_s}\vec{V}\times\vec{B}_o\cdot\frac{\partial g_s}{\partial \vec{V}} = -\frac{q_s}{m_s}\sum_{k'}{}'' \, (\vec{E}_{-k'} + \vec{V}\times\vec{B}_{-k'})\cdot\frac{\partial f_{sk'}}{\partial \vec{V}} \quad , \tag{3.39}$$

where $\sum'$ and $\sum''$ are taken over $k' \neq 0, k$ and $k' \neq 0$ respectively. The second term in the r.h.s. of Eq.(3.38) denotes the non-resonant mode-mode couplings. Since it was clarified (Harker & Crawford[85]) that

the mode-mode couplings do not play an important role in the whistler mode cyclotron instability, we assume that the second term in the r.h.s. of Eq.(3.38) can be neglected. Then the basic equations of the quasi-linear cyclotron instability become

$$\frac{\partial f_{sk}}{\partial t} + jkV_z f_{sk} + \frac{q_s}{m_s}(\vec{V}\times\vec{B}_o)\cdot\frac{\partial f_{sk}}{\partial \vec{V}} = -\frac{q_s}{m_s}(\vec{E}_k + \vec{V}\times\vec{B}_k)\cdot\frac{\partial g_s}{\partial \vec{V}} \quad , \tag{3.40}$$

$$\frac{\partial g_s}{\partial t} + \frac{q_s}{m_s}\vec{V}\times\vec{B}_o\cdot\frac{\partial g_s}{\partial \vec{V}} = -\frac{q_s}{m_s}\sum_{k'}''(\vec{E}_{-k'} + \vec{V}\times\vec{B}_{-k'})\cdot\frac{\partial f_{sk'}}{\partial \vec{V}} \quad , \tag{3.41}$$

and

$$jk\hat{z}\times\vec{E}_k = -\frac{\partial \vec{B}_k}{\partial t} \quad , \tag{3.42}$$

$$jk\hat{z}\times\vec{B}_k = \mu_o\sum_s q_s\int \vec{V} f_{sk}\, d\vec{V} + \frac{1}{c^2}\frac{\partial \vec{E}_k}{\partial t} \quad . \tag{3.43}$$

Eqs.(3.40),(3.42) and (3.43) are the same set of basic equations of the linear theory except that $g_s(\vec{V},t)$ is a slowly changing function of time. Consequently Eqs.(3.40), (3.42) and (3.43) can be solved by assuming

$$f_{sk},\ \vec{E}_k \text{ and } \vec{B}_k \propto e^{-j\omega t}, \tag{3.44}$$

provided the real part of ω is much greater than the reciprocal of the characteristic time of the change of the background distribution function g_s. The solution of $f_{sk\omega}$, where $f_{sk} = f_{sk\omega}\exp\{-j\omega t\}$, is given by

$$f_{sk\omega} = -\frac{q_s}{m_s\varepsilon_s\Omega_s} e^{-j\frac{\omega-kV_z}{\varepsilon_s\Omega_s}\phi}\int^{\phi}(\vec{E}_k + \vec{V}\times\vec{B}_k)\cdot\frac{\partial g_s}{\partial \vec{V}} e^{j\frac{\omega-kV_z}{\varepsilon_s\Omega_s}\phi'} d\phi' \quad , \tag{3.45}$$

which reduces to Eq.(2.123) in Chapter II. It is again written here as

$$f_{sk\omega} = \frac{q_s}{jm_s}\Bigg[\frac{\frac{\partial g_s}{\partial V_z}}{\omega-kV_z}E_{kz} + \frac{(1-\frac{kV_z}{\omega})\frac{\partial g_s}{\partial V_\perp} + \frac{kV_\perp}{\omega}\frac{\partial g_s}{\partial V_z}}{\omega - kV_z + \varepsilon_s\Omega_s}\frac{e^{j\phi}}{\sqrt{2}}E_{k-} + \frac{(1-\frac{kV_z}{\omega})\frac{\partial g_s}{\partial V_\perp} + \frac{kV_\perp}{\omega}\frac{\partial g_s}{\partial V_z}}{\omega - kV_z - \varepsilon_s\Omega_s}\frac{e^{-j\phi}}{\sqrt{2}}E_{k+}\Bigg]. \tag{3.46}$$

On the other hand, Eq.(3.41) can be expressed in terms of $f_{sk\omega}$, E_{k-}, E_{k+} and E_{kz} as

$$\frac{\partial g_s}{\partial t} = -\frac{q_s}{m_s} \mathrm{Re}\Big[\sum_k \Big\{ \Big(1-\frac{kV_z}{\tilde{\omega}}\Big) \frac{E_{k+}e^{+j\phi} + E_{-k-}e^{-j\phi}}{\sqrt{2}} \hat{r}$$

$$+ \Big(1-\frac{kV_z}{\tilde{\omega}}\Big) \frac{E_{k+}e^{+j\phi} - E_{-k-}e^{-j\phi}}{\sqrt{2}} \hat{\phi} + \Big(E_{-kz} + \frac{kV_\perp}{\tilde{\omega}} \frac{E_{-k+}e^{+j\phi} + E_{-k-}e^{-j\phi}}{\sqrt{2}} \hat{z}\Big\}$$

$$\cdot \Big\{ \frac{\partial f_{sk\omega}}{\partial V_\perp} \hat{r} + \frac{\partial f_{sk\omega}}{V_\perp \partial \phi} \hat{\phi} + \frac{\partial f_{sk\omega}}{\partial V_z} \hat{z} \Big\} \Big] \quad , \tag{3.47}$$

where $\hat{r}$, $\hat{\phi}$ and $\hat{z}$ are the unit vectors in the directions of $\vec{V}_\perp$, $\vec{V}_\perp \times \vec{B}_o$ and $\vec{B}_o$ respectively and $\tilde{\omega}$ and E_{-k} are the complex conjugate of ω and E_k respectively, and Re[ ] means the real part of the quantity in the bracket. Eqs.(3.42) and (3.43) are simply expressed as

$$\hat{z} \times \vec{E}_k = \frac{\omega}{k} \vec{B}_k \quad , \tag{3.48}$$

$$k\hat{z} \times \vec{B}_k = -j\mu_o \sum_s q_s \int \vec{V} f_{sk} d\vec{V} - \frac{\omega}{c^2} \vec{E}_k \quad . \tag{3.49}$$

Eqs.(3.46), (3.47), (3.48) and (3.49) are the basic equations for the quasilinear cyclotron instability.

3.2 Derivation of the Set of Equations for the Whistler Mode Quasilinear Cyclotron Instability

Since we consider the purely transverse whistler mode waves which propagate along the external magnetic field, we can assume that

$$E_{k+} = E_{kz} = 0 \quad , \tag{3.50}$$

in Eqs.(3.46) and (3.47) so that

$$f_{sk\omega} = \frac{q_s}{jm_s} \frac{G_s}{\omega - kV_z + \varepsilon_s \Omega_s} \frac{e^{j\phi}}{\sqrt{2}} E_k \quad , \tag{3.51}$$

$$\frac{\partial g_s}{\partial t} = -\frac{q_s}{m_s} \mathrm{Re}\Big[\sum_k \Big\{ \Big(1-\frac{kV_z}{\tilde{\omega}}\Big) \frac{e^{-j\phi}}{\sqrt{2}} E_k^* \hat{r} - \Big(1-\frac{kV_z}{\tilde{\omega}}\Big) \frac{e^{-j\phi}}{\sqrt{2}} E_k^* \hat{\phi}$$

$$+\frac{kV_\perp}{\tilde{\omega}}\frac{e^{-j\phi}}{\sqrt{2}}E_k^*\hat{z}\}\cdot\{\frac{\partial f_{sk\omega}}{\partial V_\perp}\hat{r}+\frac{\partial f_{sk\omega}}{V_\perp\partial\phi}\hat{\phi}+\frac{\partial f_{sk\omega}}{\partial V_z}\hat{z}\}] \quad , \tag{3.52}$$

where

$$G_s \equiv \frac{\partial g_s}{\partial V_\perp}+\frac{\omega}{k}\left(V_\perp\frac{\partial g_s}{\partial V_z}-V_z\frac{\partial g_s}{\partial V_\perp}\right) \quad , \tag{3.53}$$

and E_k^* is the complex conjugate of E_k which is short for E_{k-}. Substituting Eq.(3.51) into Eq.(3.52), we find out

$$\frac{\partial g_s}{\partial t}=\mathrm{Re}[j\frac{q_s^2}{2m_s^2}\sum_k E_kE_k^*\{(1-\frac{kV_z}{\tilde{\omega}})\frac{\frac{\partial G_s}{\partial V_\perp}+\frac{G_s}{V_\perp}}{\omega-kV_z+\varepsilon_s\Omega_s}+\frac{kV_\perp}{\tilde{\omega}}\frac{\partial}{\partial V_z}(\frac{G_s}{\omega-kV_z+\varepsilon_s\Omega_s})\}] \quad , \tag{3.54}$$

for the temporal change of the background distribution function.

Replacing ω by $\omega_r+j\gamma_k$, we pick up the real part of the quantity in the bracket in Eq.(3.54) and obtain the following expression after some tedious manipulations (see Appendix B)

$$\frac{\partial g_s}{\partial t}=\frac{1}{N_sm_s}\sum_k\frac{\Pi_s^2}{\omega_r^2}\varepsilon_k\frac{\gamma_k}{(\omega_r-kV_z+\varepsilon_s\Omega_s)^2+\gamma_k^2}$$

$$\times\{C_1\frac{\partial^2 g_s}{\partial V_\perp^2}+C_2\frac{\partial^2 g_s}{\partial V_z^2}+C_3\frac{\partial^2 g_s}{\partial V_\perp\partial V_z}+C_4\frac{\partial g_s}{\partial V_\perp}+C_5\frac{\partial g_s}{\partial V_z}\} \quad , \tag{3.55}$$

where

$$C_1=(\omega_r-kV_z)^2 \quad , \tag{3.56}$$

$$C_2=k^2V_\perp^2 \quad , \tag{3.57}$$

$$C_3=2kV_\perp(\omega_r-kV_\perp) \quad , \tag{3.58}$$

$$C_4=\frac{1}{V_\perp}\{(\omega_r-kV_z)^2-\frac{2k^2V_\perp^2\varepsilon_s\Omega_s(\omega_r-kV_z+\varepsilon_s\Omega_s)}{(\omega_r-kV_z+\varepsilon_s\Omega_s)^2+\gamma_k^2}\} \quad , \tag{3.59}$$

$$C_5=2k\{\varepsilon_s\Omega_s+2(\omega_r-kV_z)+\frac{k^2V_\perp^2(\omega_r-kV_z+\varepsilon_s\Omega_s)}{(\omega_r-kV_z+\varepsilon_s\Omega_s)^2+\gamma_k^2}\} \quad , \tag{3.60}$$

or equivalently

$$\frac{\partial g_s}{\partial t} = \frac{1}{N_s m_s} \sum_k \frac{\Pi_s^2}{\omega_r^2} \varepsilon_k \left[\frac{1}{V_\perp} \frac{\partial}{\partial V_\perp} \{ V_\perp \frac{\gamma_k}{(\omega_r - kV_z + \varepsilon_s \Omega_s)^2 + \gamma_k^2} [(\omega_r - kV_z)^2 \frac{\partial g_s}{\partial V_\perp} \right.$$

$$+ kV_\perp \{ \varepsilon_s \Omega_s + 2(\omega_r - kV_z) \} \frac{\partial g_s}{\partial V_z}] \} - \frac{\partial}{\partial V_z} \{ kV_\perp \frac{\gamma_k}{(\omega_r - kV_z + \varepsilon_s \Omega_s)^2 + \gamma_k^2}$$

$$\left. \times (\varepsilon_s \Omega_s \frac{\partial g_s}{\partial V_\perp} - kV_\perp \frac{\partial g_s}{\partial V_z}) \} \right] \quad , \tag{3.61}$$

where

$$\varepsilon_k = \frac{1}{2} \varepsilon_o |E_k|^2 \quad , \tag{3.62}$$

is the energy density of the electric field of the wave.

The growth rate $\gamma_k(t)$ is also reducible by the same procedure as in the linear theory (see Appendix A). The result is

$$\gamma_k(t) = \sum_s \frac{\pi^2}{N_s} \frac{\varepsilon_s \Omega_s \Pi_s^2}{\partial D / \partial \omega_r} \int_{-\infty}^{\infty} dV_z \int_0^{\infty} dV_\perp \, V_\perp^2 \delta(\omega_r - kV_z + \varepsilon_s \Omega_s) \nabla_v g_s(\vec{V}, t) \quad . \tag{3.63}$$

The electric field energy density changes with time according to

$$\frac{\partial \varepsilon_k}{\partial t} = 2 \gamma_k \varepsilon_k \quad , \tag{3.64}$$

and the dispersion relation between ω_r and k is also the same as that of the linear theory

$$D(\omega_r, k) = c^2 k^2 - \omega_r^2 + \sum_s \frac{\omega_r \Pi_s^2}{\omega_r + \varepsilon_s \Omega_s} = 0 \quad . \tag{3.65}$$

We thus have the complete set of the quasilinear cyclotron instability, which describes the dispersion relation between ω_r and k, the growth rate $\gamma_k(t)$ and the evolution of the distribution function $\partial g_s(\vec{V}, t)/\partial t$. They are Eqs.(3.65), (3.63) and (3.61) or (3.55), respectively.

In order to grasp a more clear meaning of the set of the quasilinear equations, we make a little more mathematical manipulation as shown in the following. As is done frequently in the problem of the wave-particle resonant interactions, it is informative to divide the plasma

particles into two parts, i.e., the resonant particles and the thermal (or non-resonant) particles. The resonant particles are those which satisfy the condition $\omega_r - kV_z + \varepsilon_s \Omega_s = 0$ and are known to play a fundamental role in the wave-particle interaction as shown in the physical picture of the cyclotron instability in Chapter II. On the other hand, the thermal particles play another role to sustain the wave in the plasma and usually do not contribute as a source of the instability.

As for the thermal particles, the conditions

$$|kV_z|, \ |kV_\perp| \ll \omega_r, \ |\omega_r + \varepsilon_s \Omega_s| \quad , \tag{3.66}$$

are well satisfied and therefore we obtain the following equation,

$$\frac{\partial g_{sT}}{\partial t} = \frac{1}{N_s m_s} \sum_k \frac{\Pi_s^2}{(\omega_r + \varepsilon_s \Omega_s)^2} \gamma_k \varepsilon_k \frac{1}{V_\perp} \frac{\partial}{\partial V_\perp} \left(V_\perp \frac{\partial g_{sT}}{\partial V_\perp} \right) \quad , \tag{3.67}$$

where the subscript T of g_{sT} means the thermal part of the particle distribution function. It follows from this equation that the instability results in a diffusion of the thermal particles so as to increase the $V_\perp$ component in the velocity space. This corresponds physically to the fact that the wave growth in the whistler mode should be accompanied with the increase of the mean thermal velocity $\sqrt{\langle V_\perp^2 \rangle}$ in order to supply the increase of the perpendicular current $\vec{J}_\perp$ which maintains the wave. This can be also understood by the following calculation. Since the thermal kinetic energy densities $\varepsilon_{T\perp}$ and ε_{Tz} in the directions perpendicular and parallel to the propagation vector, which are associated with the wave, are expressed as

$$\varepsilon_{T\perp} \equiv \sum_s \frac{1}{2} m_s \int_0^{2\pi} d\phi \int_{-\infty}^{\infty} dV_z \int_0^{\infty} V_\perp dV_\perp \, V_\perp^2 g_{sT}(\vec{V}, t) \quad , \tag{3.68}$$

$$\varepsilon_{Tz} \equiv \sum_s \frac{1}{2} m_s \int_0^{2\pi} d\phi \int_{-\infty}^{\infty} dV_z \int_0^{\infty} V_\perp dV_\perp \, V_z^2 g_{sT}(\vec{V}, t) \quad , \tag{3.69}$$

we can investigate whether these energies increase or decrease when the distribution function changes according to Eq.(3.67) due to the quasilinear effect. Namely

$$\frac{d\varepsilon_{T\perp}}{dt} = \sum_s \sum_k \frac{\pi\Pi_s^2}{N_s} \frac{\gamma_k \varepsilon_k}{(\omega_r+\varepsilon_s\Omega_s)^2} \int_{-\infty}^{\infty} dV_z \int_0^{\infty} dV_\perp \, V_\perp^2 \frac{\partial}{\partial V_\perp}\left(V_\perp \frac{\partial g_{sT}}{\partial V_\perp}\right) \quad , \tag{3.70}$$

$$\frac{d\varepsilon_{Tz}}{dt} = \sum_s \sum_k \frac{\pi\Pi_s^2}{N_s} \frac{\gamma_k \varepsilon_k}{(\omega_r+\varepsilon_s\Omega_s)^2} \int_{-\infty}^{\infty} dV_z \int_0^{\infty} dV_\perp \, V_z^2 \frac{\partial}{\partial V_\perp}\left(V_\perp \frac{\partial g_{sT}}{\partial V_\perp}\right) \quad . \tag{3.71}$$

Integration by parts over $V_\perp$ gives

$$\frac{d\varepsilon_{T\perp}}{dt} = \sum_s \sum_k \frac{1}{N_s} \frac{2\Pi_s^2}{(\omega_r+\varepsilon_s\Omega_s)^2} \gamma_k \varepsilon_k \int_0^{2\pi} d\phi \int_{-\infty}^{\infty} dV_z \int_0^{\infty} V_\perp dV_\perp g_{sT} \quad , \tag{3.72}$$

$$\frac{d\varepsilon_{Tz}}{dt} = 0 \quad . \tag{3.73}$$

In the above calculation, we have assumed

$$V_\perp^3 \frac{\partial g_{sT}}{\partial V_\perp} = V_\perp^2 \frac{\partial g_{sT}}{\partial V_\perp} = V_\perp \frac{\partial g_{sT}}{\partial V_\perp} = 0 \quad (\text{ as } V_\perp \to \infty) . \tag{3.74}$$

If we neglect the contribution of the resonant particles to the total particle number density of the plasma, i.e.,

$$\frac{1}{N_s} \int_0^{2\pi} d\phi \int_{-\infty}^{\infty} dV_z \int_0^{\infty} V_\perp dV_\perp g_{sT} \simeq 1 \quad , \tag{3.75}$$

Eq.(3.72) reduces to

$$\frac{d\varepsilon_{T\perp}}{dt} = \sum_s \sum_k \frac{2\Pi_s^2}{(\omega_r+\varepsilon_s\Omega_s)^2} \gamma_k \varepsilon_k \quad , \tag{3.76}$$

$$= \sum_s \sum_k \frac{\Pi_s^2}{(\omega_r+\varepsilon_s\Omega_s)^2} \frac{d\varepsilon_k}{dt} \quad , \tag{3.76}'$$

$$= \frac{d}{dt} \left(\sum_s \sum_k \frac{\Pi_s^2}{(\omega_r+\varepsilon_s\Omega_s)^2} \varepsilon_k \right) \quad . \tag{3.76}''$$

Eq.(3.76)' indicates that the thermal energy density in the perpendicular direction increases when the wave grows up and vice versa. Another expression Eq.(3.76)" makes us recognize that the expression of the rate of change of the perpendicular energy density $\varepsilon_{T\perp}$ deduced from the

integration of the quasilinear equation becomes quite coincident with that calculated by the cold plasma linear theory, if we note that the quantity in the parenthesis in Eq.(3.76)" is equivalent to the kinetic energy density Eq.(3.5). Eq.(3.73) implies that the parallel kinetic energy density of the thermal particles does not change in the case of the instability or damping of the purely transverse whistler mode waves. This is a physically natural result since no motions of the thermal particles in the parallel direction are associated in that case.

On the other hand, the rate of deformation of the distribution function of the resonant particles $g_{sr}(\vec{V},t)$ with subscript r is to be obtained by simplifying Eq.(3.55) with the use of the linear resonace condition as

$$\omega_r - kV_z + \varepsilon_s\Omega_s = 0 \quad . \tag{3.77}$$

It can be shown that the products between the factor

$$d(\omega_r - kV_z + \varepsilon_s\Omega_s) \equiv \frac{\gamma_k}{(\omega_r - kV_z + \varepsilon_s\Omega_s)^2 + \gamma_k^2} \quad , \tag{3.78}$$

and each coefficient C_i (i=1∿5) in Eq.(3.55) have a sharp peak at the resonance velocity $V_R = (\omega_r + \varepsilon_s\Omega_s)/k$ under the assumption of $|\gamma_k| \ll \omega_r$, since the velocity gradients in Eq.(3.55) are all smooth functions of V_z around V_R. Therefore we can well approximate the function, defined by Eq.(3.78), by the so called delta function. In this procedure, however, a careless operation leads to an erroneous result. An analytic continuation should be carefully used as follows;

$$\lim_{\gamma_k \to 0} d(\omega_r - kV_z + \varepsilon_s\Omega_s) = \lim_{\gamma_k \to 0} \mathrm{Re}\left[j\frac{1}{\omega - kV_z + \varepsilon_s\Omega_s}\right]$$

$$= \lim_{\gamma_k \to 0} \left[-\frac{1}{V_z}\,\mathrm{Re}\left\{j\frac{1}{k - (\omega_r + \varepsilon_s\Omega_s)/V_z - j(\gamma_k/V_z)}\right\}\right]$$

$$= \begin{cases} \dfrac{1}{V_z}\dfrac{\gamma_k/V_z}{\{k - (\omega_r + \varepsilon_s\Omega_s)/V_z\}^2 + (\gamma_k/V_z)^2}\,P \quad , & \text{for } \gamma_k > 0 \ , \\ \dfrac{1}{V_z}\dfrac{\gamma_k/V_z}{\{k - (\omega_r + \varepsilon_s\Omega_s)/V_z\}^2 + (\gamma_k/V_z)^2}\,P + \dfrac{1}{|V_z|}2\pi\delta\left(k - \dfrac{\omega_r + \varepsilon_s\Omega_s}{V_z}\right) \quad , & \text{for } \gamma_k \leq 0, \end{cases}$$

$$= \begin{cases} \pi \frac{1}{|V_z|} \delta\left(k - \frac{\omega_r + \varepsilon_s \Omega_s}{V_z}\right) , & \text{for } \gamma_k > 0 . \\ -\pi \frac{1}{|V_z|} \delta\left(k - \frac{\omega_r + \varepsilon_s \Omega_s}{V_z}\right) + \frac{1}{|V_z|} 2\pi\delta\left(k - \frac{\omega_r + \varepsilon_s \Omega_s}{V_z}\right) = \pi \frac{1}{|V_z|} \delta\left(k - \frac{\omega_r + \varepsilon_s \Omega_s}{V_z}\right) , & \text{for } \gamma_k \leq 0 . \end{cases}$$

(3.79)

Thus the following approximation

$$d(\omega_r - kV_z + \varepsilon_s \Omega_s) \simeq \pi \delta(\omega_r - kV_z + \varepsilon_s \Omega_s) , \tag{3.80}$$

is valid for both cases of $\gamma_k > 0$ and $\gamma_k \leq 0$. For the resonant particles we thus have

$$\frac{\partial g_{sr}}{\partial t} = \frac{1}{N_s m_s} \sum_k \frac{\Omega_s^2 \Pi_s^2}{\omega_r^2} \frac{\varepsilon_k}{V_\perp} \left(\frac{\partial}{\partial V_\perp} - \frac{kV_\perp}{\varepsilon_s \Omega_s} \frac{\partial}{\partial V_z}\right)$$

$$\times [V_\perp d(\omega_r - kV_z + \varepsilon_s \Omega_s) \left(\frac{\partial g_s}{\partial V_\perp} - \frac{kV_\perp}{\varepsilon_s \Omega_s} \frac{\partial g_s}{\partial V_z}\right)] . \tag{3.81}$$

Expressing by the operator ∇_v, defined by Eq.(2.137) in Chapter II, Eq.(3.81) is reduced to

$$\frac{\partial g_{sr}}{\partial t} = \frac{1}{N_s m_s} \sum_k \frac{\Omega_s^2 \Pi_s^2}{\omega_r^2} \frac{\varepsilon_k}{V_\perp} \nabla_v \{V_\perp d(\omega_r - kV_z + \varepsilon_s \Omega_s) \nabla_v g_{sr}\} , \tag{3.82}$$

or furthermore using Eq.(3.80),

$$\frac{\partial g_{sr}}{\partial t} = \frac{\pi}{N_s m_s} \sum_k \frac{\Omega_s^2 \Pi_s^2}{\omega_r^2} \frac{\varepsilon_k}{V_\perp} \nabla_v \{V_\perp \delta(\omega_r - kV_z + \varepsilon_s \Omega_s) \nabla_v g_{sr}\} . \tag{3.83}$$

It is noticed again that Eq.(3.83) coincides with Eq.(3.31) which is reduced from the physical consideration independently.

Eq.(3.83) for the resonant particles and Eq.(3.67) for the thermal particles are useful in the analytic discussion but for numerical computations of the quasilinear evolution of the cyclotron instability,

another expression is convenient and preferable. Approximating the summation over k by the integral in Eq.(3.55), we have

$$\frac{\partial g_{sr}}{\partial t} = \frac{L_c}{2N_s m_s} \Omega_s^2 \Pi_s^2 \int dk \frac{\varepsilon_k}{\omega_r^2(k) V_\perp} \nabla_v \{ \frac{V_\perp}{|V_z|} \delta(k - \frac{\omega_r + \varepsilon_s \Omega_s}{V_z}) \nabla_v g_{sr} \quad , \qquad (3.84)$$

or equivalently

$$\frac{\partial g_{sr}}{\partial t} = \frac{L_c}{2N_s m_s} \frac{\Omega_s^2 \Pi_s^2}{\omega_r^2(V_z)} \frac{\varepsilon_k(V_z)}{V_\perp}$$

$$\times [\frac{\partial^2 g_{sr}}{\partial V_\perp^2} + \frac{k^2 V_\perp^2}{\Omega_s^2} \frac{\partial^2 g_{sr}}{\partial V_z^2} - \frac{2kV_\perp}{\varepsilon_s \Omega_s} \frac{\partial^2 g_{sr}}{\partial V_z \partial V_\perp} + \frac{1}{V_\perp} \frac{\partial g_{sr}}{\partial V_\perp} - \frac{2k}{\varepsilon_s \Omega_s} \frac{\partial g_{sr}}{\partial V_z}]_{k=(\omega_r + \varepsilon_s \Omega_s)/V_z} \quad , \qquad (3.85)$$

where L_c is a characteristic length of the plasma system under consideration. It should be noticed that ω_r and ε_k are expressed as a function of V_z through the resonance condition Eq.(3.77).

3.3 Characteristics of the Electromagnetic Whistler Mode Quasilinear Cyclotron Instability

We now discuss shortly the characteristics of the electromagnetic whistler mode cyclotron instability on the quasilinear stage. In case of one-dimensional plasma waves, it is well known that the distribution function g_{sr} reaches a quasistatic state called a "plateau" as time elapses. In case of the TEM waves like whistler mode waves, the diffusion of the resonant particles takes place in the two-dimensional velocity space and hence is much complicated. Rowlands et. al.[99] treated these TEM wave problems, and reduced them into one-dimensional diffusion equations along the characteristic lines in the velocity space. They suggested that a treatment similar to those for plasma waves seems to be possible for our TEM wave problems. However, it is found by a careful argument in the present thesis that there are some difficulties in a simple extension of the one-dimensional quasilinear treatment to the present whistler mode cyclotron instability.

One of the main difficulties arises from the fact that the quasi-

static asymptotic state of the distribution function does not coincide with the marginal state which is defined by $\gamma_k = 0$. It is because the excited wave spectrum and the corresponding growth rate in the whistler mode cyclotron instability generally have a form as schematically depicted in Fig.56. As seen in the figure, the wave spectrum is limited in a narrow frequency band so that a diffusion of the resonant particles takes place strongly in a limited corresponding V_z-space (see B-region in Fig.57). In the V_z-space corresponding to the wave damping through the relation of a linear resonance condition, the diffusion takes place in the inverse direction. (see A-region in Fig.57) The distribution function, however, hardly suffers a deformation in this region because the waves rapidly damp away unless the waves imposed to the plasma are strong enough at the corresponding frequencies.

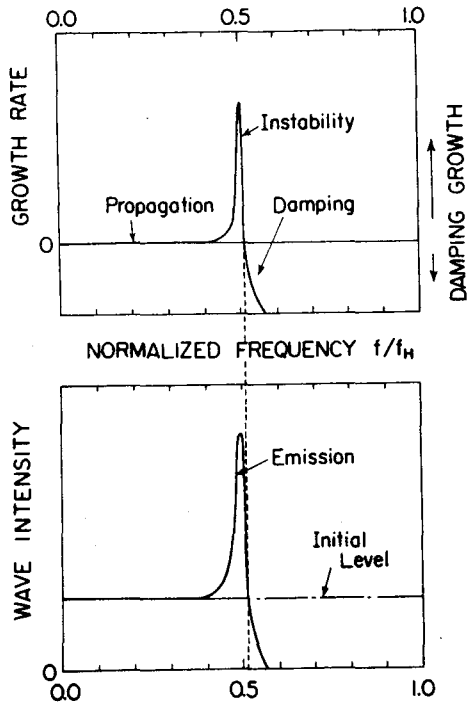

Fig.56 Schematic Illustration of Characteristics of Whistler Mode Cyclotron Instability

Therefore, a strong distortion appears in the velocity distribution function due to the inverse diffusions on both sides of $V_z = V_{zc}$ (see Fig.57) which corresponds to the frequency where γ_k changes its sign from growing to damping. Consequently it may be inferred analytically that the distribution function reaches to the marginal state, which gives $\gamma_k = 0$, except in the region of $|V_z| \leq |V_{zc}|$. The marginal state distribution function can be calculated by setting $\gamma_k = 0$.

From Eq.(3.63), a solution to

$$\left(\frac{\partial}{\partial V_\perp} - \frac{kV_\perp}{\varepsilon_s \Omega_s} \frac{\partial}{\partial V_z} \right) g_s = 0 \quad , \tag{3.86}$$

yields (see Appendix C)

$$g_{s,marg}(V_\perp, V_z) = \frac{N_s m_s}{2\pi K T_\perp} \frac{\exp\left[- \frac{m_s}{kT_\perp} \left\{ \frac{V_\perp^2}{2} + \varepsilon_s \Omega_s \int^{V_z} \frac{du}{k(u)} \right\} \right]}{\int_{-\infty}^{\infty} \exp\left[- \frac{m_s \varepsilon_s \Omega_s}{KT_\perp} \int^{V_z} \frac{du}{k(u)} \right] dV_z} \quad . \tag{3.87}$$

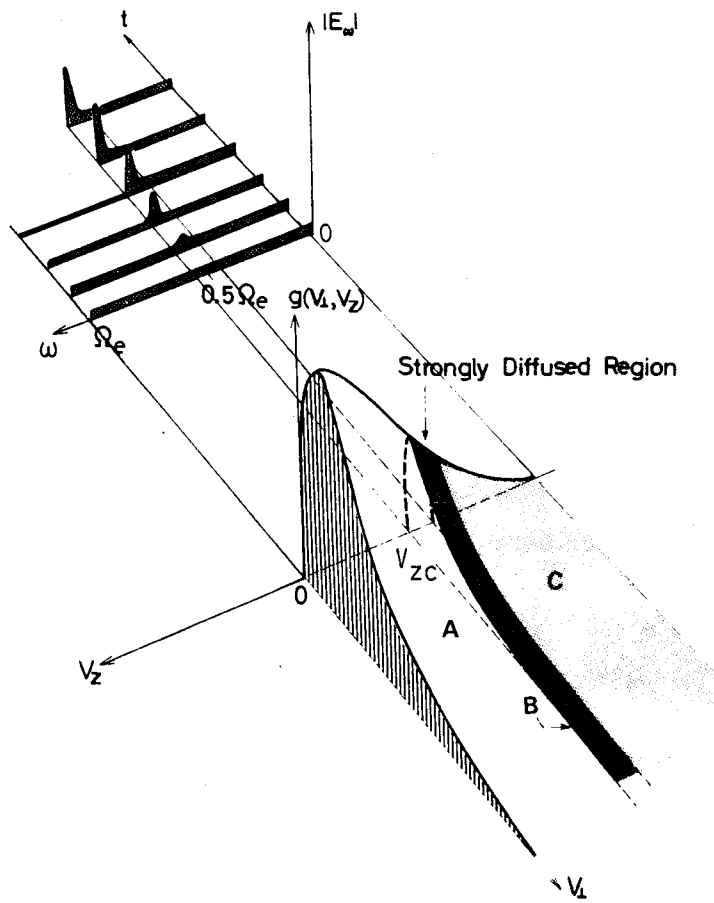

Fig.57 Schematic Illustration of the Reacted Region in the Phase Space of the Distribution Function due to the Excited Waves. Region A suffers a diffusion only on the initial stage of the interaction, whereas region C hardly suffers a diffusion because of the marginal feature ($\gamma_k \simeq 0$) in the corresponding frequency range. Region B is a strongly diffused region.

In the above calculation, we have used the linear resonance condition Eq.(3.77) in order to get $k = k(V_z)$. It is interesting to note that the marginal distribution function is the Maxwellian in the perpendicular direction. The shape in the V_z-direction of $g_{s,marg}$, i.e.,

$$S_s(V_z) \equiv \exp[-\frac{m_s \varepsilon_s \Omega_s}{KT_\perp} \int^{V_z} \frac{du}{k(u)}] = \exp[-\frac{m_s \varepsilon_s \Omega_s}{KT_\perp} \int^{V_z} \frac{udu}{\omega_r(u)+\varepsilon_s\Omega_s}] \quad , \tag{3.88}$$

is computed for electrons and illustrated in Fig.58 with parameters P and $T_\perp$, where $S_s(V_z)$ is normalized to unity. It is noted that $\omega_r(V_z)$ is to be calculated by the simultaneous equations of Eqs.(3.77) and (3.65).

Another interesting feature of the whistler mode cyclotron instability is the frequency change of the excited waves. The frequency range of the wave growth is formally determined from Eq.(2.159) as

$$\omega_r \leq \frac{A-1}{A} \Omega_e \quad , \tag{3.89}$$

where $A = T_\perp / T_{||}$ and is expressed by the macroscopic temperature. However, the growth rate itself is not essentially determined by such a macroscopic quantity but is delicately related to the local shape of the distribution function, i.e., the velocity gradients of the distribution function at the resonance velocity, as clarified in Section 2 in Chapter II. Therefore Eq.(3.89) is only a measure of the frequency range of the initial wave growth. The fine deformation around V_{zc}, which corresponds to a frequency a little higher than that showing the initial maximum growth rate, affects the frequency-time characteristics of the excited waves on the nonlinear stage.

Furthermore, it is easily considered that the distribution function suffers a strong deformation when a wave with a narrow frequency band is applied since the strong diffusion in this case is limited in the corresponding narrow V_z-space. This may lead to a drastic change of of the growth rate through an abrupt change of the velocity gradient of the distribution function.

Thus the nonlinear behavior of the whistler mode cyclotron instability will exhibit an interesting but peculiar evolution. Computer

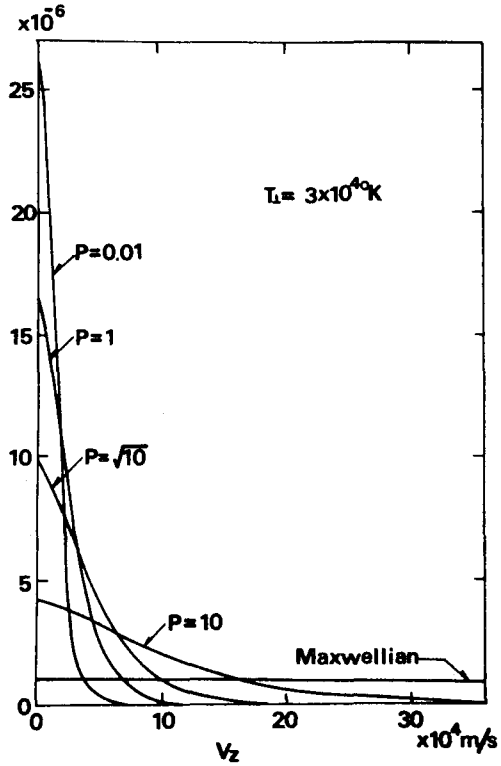

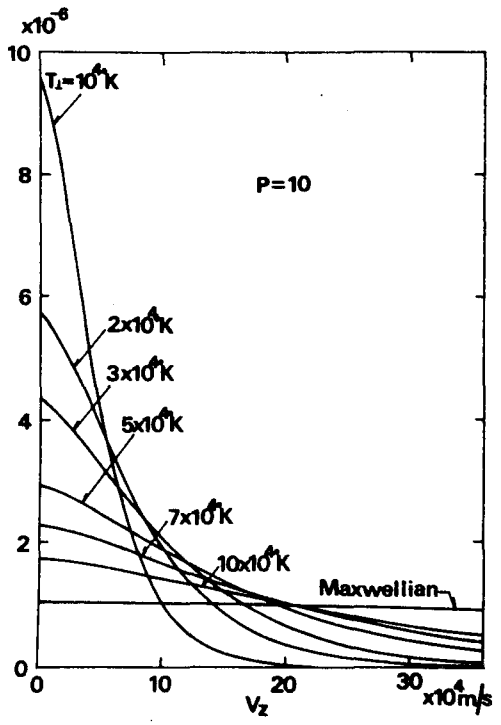

Fig.58 Calculated Marginal State Distribution Functions. For comparison a Maxwellian distribution function with $T_{||} = 3\times10^{4}$°K is also given in the figures.

tracings of the evolution of the instability are, therefore, much informative. In the next section, we will show the results of such computations.

§4. Computer Calculation of Quasilinear Evolution of the Whistler Mode Cyclotron Instability

4.1 Model and Method of Computation

We have seen in Section 5 in Chapter II that the initial stage of the generation of WTE-H in the magnetosphere is well explained by the linear theory of whistler mode cyclotron instability. However, the subsequent temporal behavior of those emissions and the generation mechanism of ASE etc. are not to be explained by the linear theory. These phenomena are essentially related to the nonlinear process of the whistler mode cyclotron instability. Regarding to this point, a mathematical description of the quasilinear cyclotron instability was given in the previous Section in this Chapter. Though it is possible to discuss a qualitative behavior of the cyclotron instability by considering the set of basic quasilinear equations ——— Eqs.(3.63), (3.64), (3.65),(3.67) and (3.83) ——— , quantitative investigations on the temporal evolution of the instability and the excited wave spectrum etc. are difficult without the help of the numerical computations. These numerical analyses would serve for the understanding of the hitherto unknown process of the actual phenomena in the magnetosphere. In this Section, we attempt to trace the quasilinear evolution of the whistler mode cyclotron instability by an electronic computer. The computation is performed with the aim of pursuing the temporal evolutions of the instability such as —— the amplitude change of the excited waves, the frequency shift of the excited waves, the growth rate change due to the wave pumping and the resultant change of the plasma distribution function ——.

Within the quasilinear regimes, waves of different frequencies affect each other only through the deformation of the distribution function around their own resonance velocity. Relation between the wave frequency and the corresponding resonance velocity V_R is determined by the simultaneous equations of the resonance condition Eq.(3.77) and

the dispersion equation (3.65). An illustration of this relation is given in the (ω_r, k, V_z) three-dimensional space in Fig.59. Therefore, when waves in some frequency bands are excited or imposed, the distribution function begins to be deformed at the corresponding velocity region. This relation has already been depicted in Fig.57. In this figure, we know that when an emission around 0.5 f_H grows up with time, a part of the distribution function indicated as "strongly diffused region" suffers a strong diffusion and its velocity gradients change to some extent, which, in turn, causes a change of the frequency of the maximum growth rate. It is noticed in this process that though the absolute amount of the deformation of the distribution function at the resonance region is very small, the velocity gradients suffer much distortion

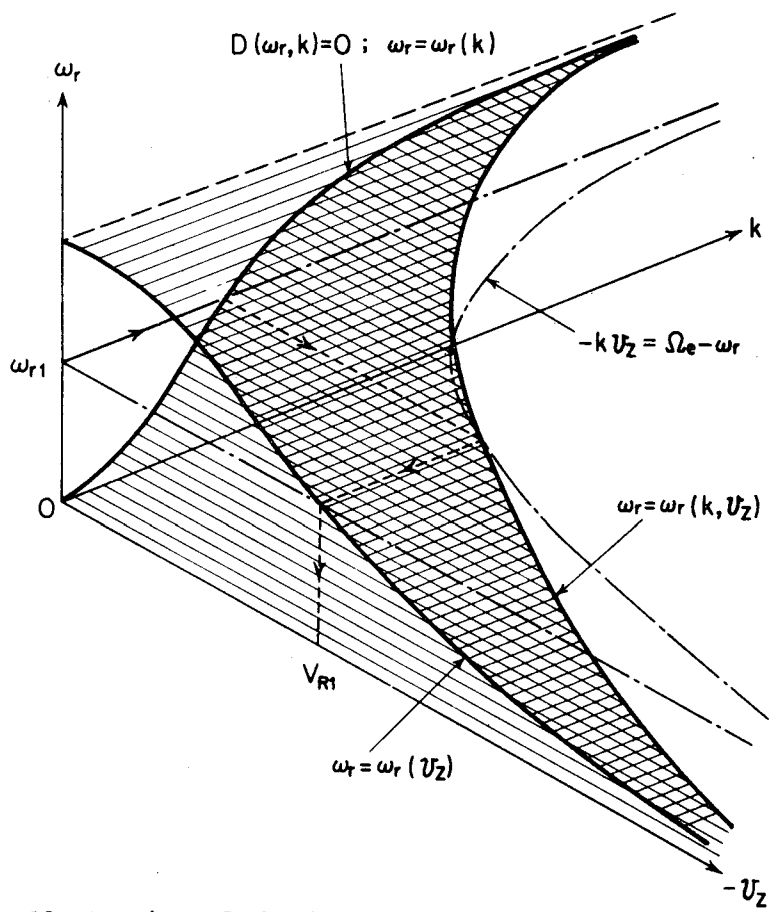

Fig.59 Illustration of Showing a Relation between Resonance Velocity and Corresponding Frequency in the Whistler Mode.

which results effectively in the change of the magnitude and the frequency of the maximum growth rate.

An extensive computation was carried out using the basic set of quasilinear equations (3.63) for γ_k calculation, (3.64) for the change of the wave amplitude and (3.85) for the evolution of the resonance part of the distribution function. Two cases are taken into consideration; one is corresponding to a spontaneous instability, which is caused by the strongly anisotropic distribution function, and the other is to a wave-triggered instability, which is caused by the change of the distribution function due to the incoming wave so as to give a large amount of the growth rate. The former is supposed to simulate the generation and the subsequent frequency change of the whistler triggered emissions, WTE-H. The latter, on the other hand, corresponds to the simulation of the generation process of the artificially stimulated emissions, ASE.

As was mentioned before, the evolution problem of the present instability should be treated in the two-dimensional velocity space so that the computation becomes much more laborious than that of the one-dimensional plasma wave problem. The spectrum of the excited waves is, however, fortunately narrow as would be expected from the linear analysis in Chapter II. Consequently the necessary information about the background distribution function $g_{er}(V_\perp, V_z, t)$ for the resonant electrons could be reduced to the values on the lattice points of the number of 6×10^4 in the $V_\perp - V_z$ two-dimensional velocity space.

Main flow of the computation is as follows. After giving necessary initial values such as the thermal plasma parameters (Π_e and Ω_e), the initial wave intensity ε_{wave} and the distribution function $g_{er}(V_\perp, V_z)$, the program enters into the main loop. First a numerical integration of the growth rate expression (3.63) is performed and $\gamma_k(t)$ is determined. Then the increment $\Delta\varepsilon_{wave}$ of the wave intensity $\varepsilon_{wave}(\omega_r, t)$ is calculated by Eq.(3.64). Finally the increment $\Delta g_{er}(V_\perp, V_z, t)$ is determined by Eq.(3.85). In this process, the differentiations of g_{er} with regard to the velocity are necessary. They are calculated by the usual difference method with a special contrivance of the differentiation at the end points in the velocity space by the use of the Newton's backward or forward difference formula. After computing other desired informations from the new distribution function $g_{er} = g_{er} + \Delta g_{er}$,

we come back to the entrance of the main loop. Throughout the computation, the energy conservation law of

$$\frac{d}{dt}\left(W_w + \varepsilon_{r\perp} + \varepsilon_{rz} \right) = 0 \quad , \tag{3.90}$$

is monitored for the check of the accumulation of numerical errors.

4.2 Computation of the Evolution of Spontaneous Instability

A first computation was carried out with an initial plasma distribution function represented by Eq.(2.162), i.e., the "triple - structured" loss cone distribution function. Plasma parameters used in the computation are the same as shown in Fig.52, i.e.,

$$\begin{aligned} &f_H=13.5\text{kHz}, && f_p=200\text{kHz}, && \\ &T_{T\perp}=T_{T\parallel}=2\text{eV}, && n_T=0.1 \ , && \\ &T_{Q\perp}=T_{Q\parallel}=30\text{eV}, && n_Q=0.1, && \eta_Q=10^{-2}, \\ &T_{B\perp}=15\text{eV}, \ T_{B\parallel}=1\text{eV}, && n_B=1.0, && \eta_B=10^{-3}, \quad V_B=200\text{eV} \ . \end{aligned} \tag{3.91}$$

Applied initial signals were like a white noise, but were assumed to be composed of many discrete frequency components, and the intensity was chosen as 100 μV/m. In making the assumption of the signal intensity, we had whistlers in the magnetosphere in mind.

Waves of different frequencies with the same initial intensity start to change their amplitude according to the frequency characteristics of the corresponding growth rates on the initial stage of evolution, then some time later, quasilinear reactions begin to appear in the distribution function. A measure of the time T_o after when the quasilinear theory becomes effective is of the order of minimum growing time, i.e., $T_o \sim 1/\gamma_{max}$ (Sagdeev & Galeev[100]), which is about 20 msec in the present situation. A simple illustration of the way for the application of the linear and quasilinear theories to the present simulation is given in Fig.60.

The results of the computation are shown in Figs.61 and 62. Fig. 61 shows the evolution of the frequency dependence of the growth rate of the whistler mode cyclotron instability, in which the quantity $T_H = 1/f_H$ is the period of the cyclotron motion of electrons. As a

general tendency of the quasilinear effect, a growth rate decreases with increasing time. This tendency is observed in Fig.61 prominently around the peak of the growth rate. This is due to the fact that the quasilinear effect appears first at a frequency of the strongest amplitude.

Another and important numerical result is that the frequency of the maximum growth rate shifts to the higher frequency as time elapses. This tendency comes from the abrupt change of the velocity gradients of the distribution function at the boundary velocity $V_z = V_{zc}$ that divides the velocity regions into those corresponding to the cyclotron instability and damping (see Fig.57). In the velocity region below the boundary velocity V_{zc}, which is indicated by "A" in Fig.57, the resonant particles diffuse in the sense that the perpendicular velocity $V_\perp$ increases with decreasing $|V_z|$. In the velocity region corresponding to the rather abruptly growing instability indicated by "B", the particles begin to diffuse in the opposite sense, i.e., of decreasing $V_\perp$ and increasing $|V_z|$. Consequently the growth rate near the cutoff frequency (a frequency given by $\gamma_k=0$) does not decrease but on the contrary increases locally as seen in Fig.61. This process is physically identical to that used by Kimura[26] to explain the offset phenomenon of ASE. This may be the physical background of the frequency shift of the peak growth rate in the quasilinear effect

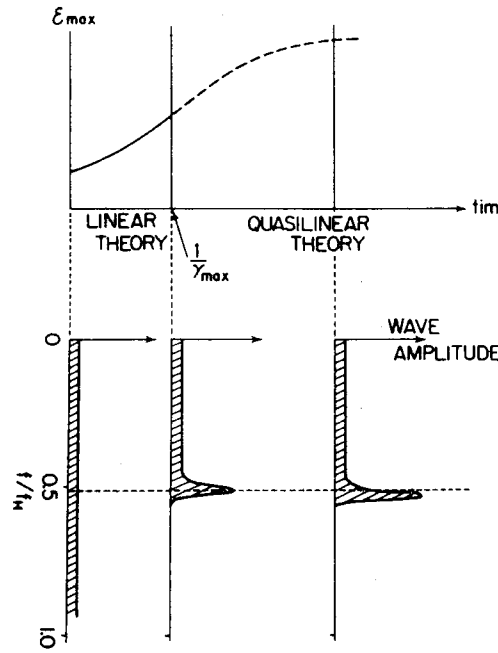

Fig.60 Applicable Time of Linear and Quasilinear Theories in the Computer Calculation.

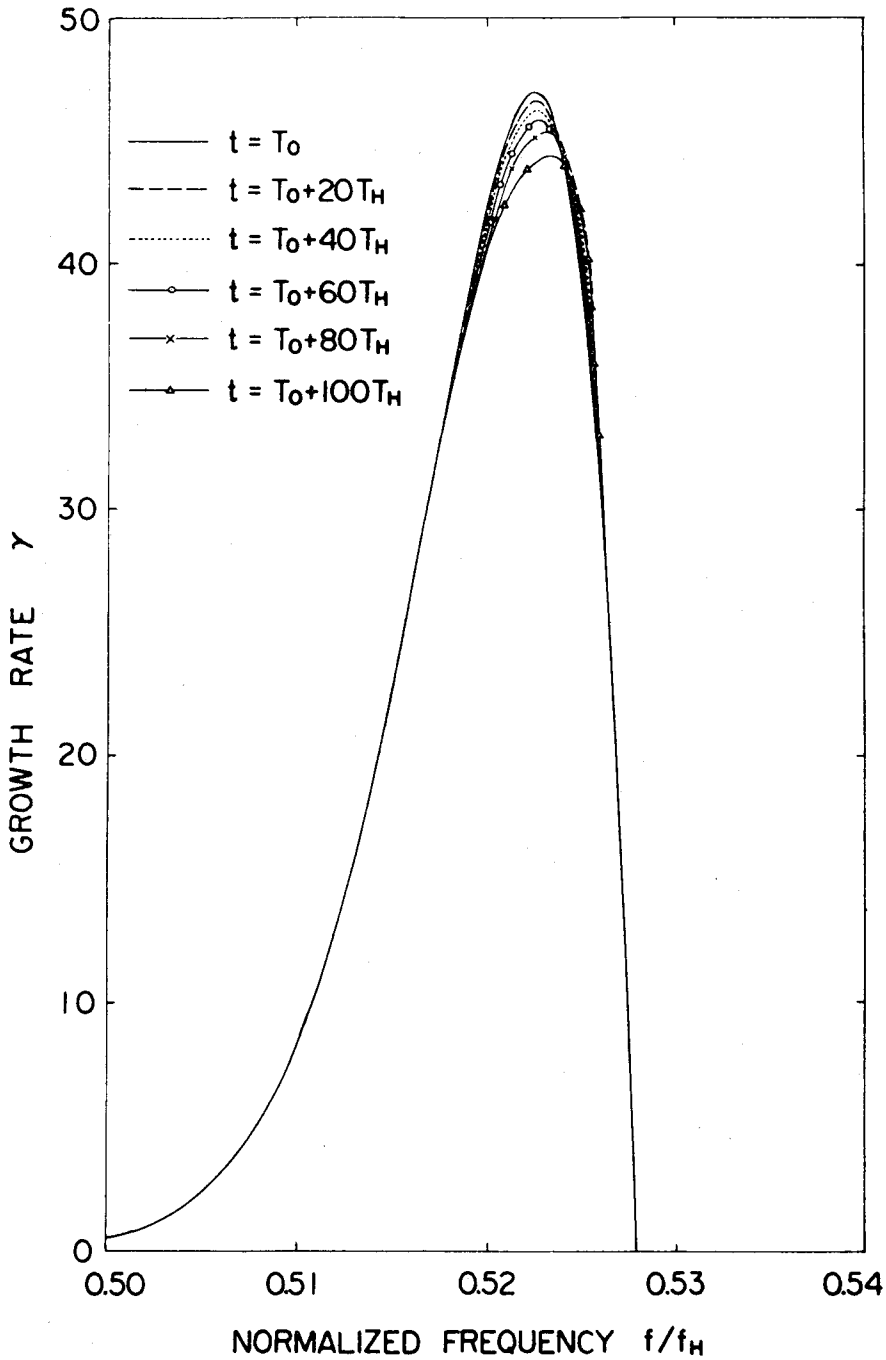

Fig.61 Evolution of Spontaneous Whistler Mode Cyclotron Instability. The figure shows a reduction of the growth rate together with a frequency shift of the peak growth rate due to a quasilinear effect.

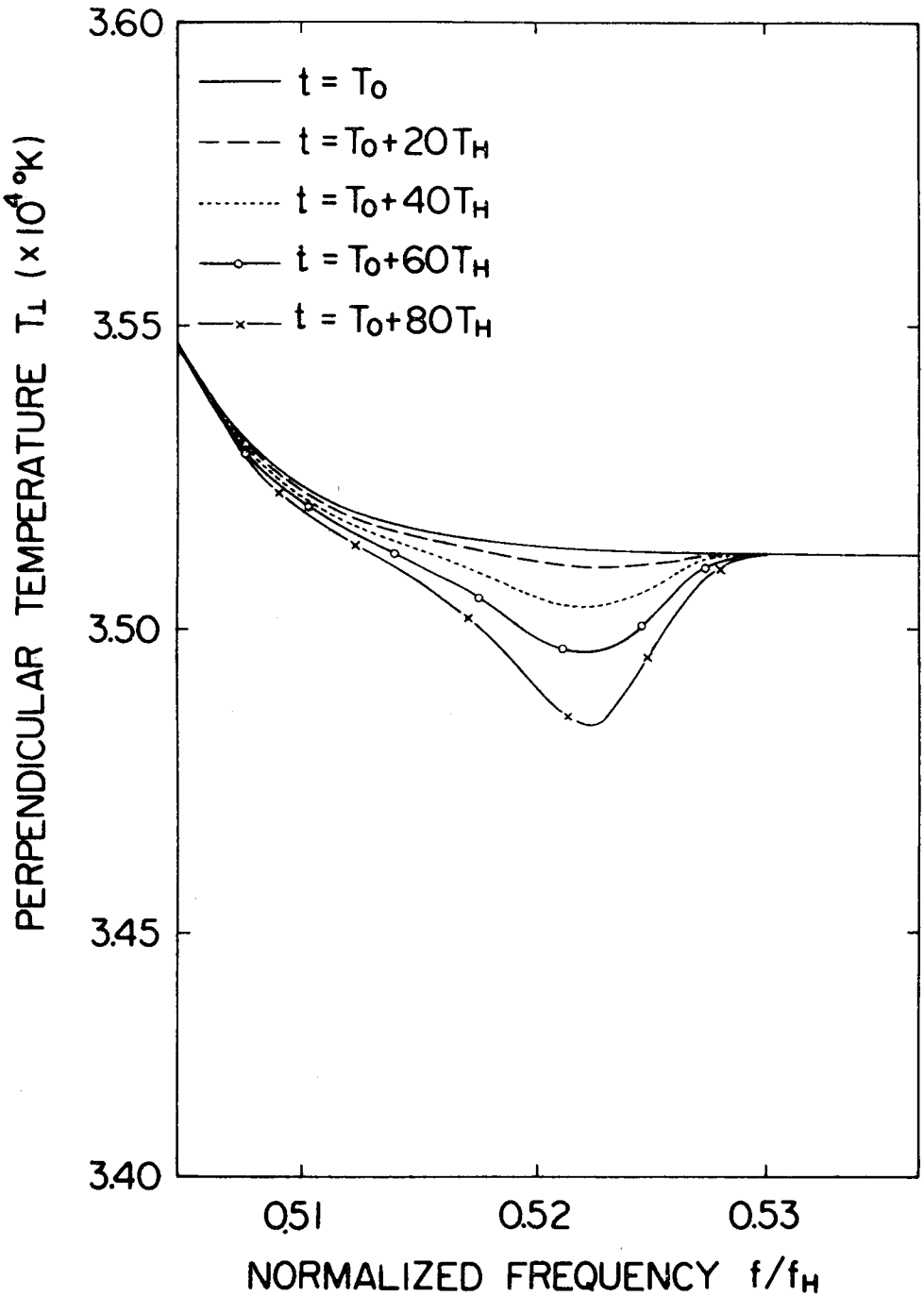

Fig.62 Corresponding Change of Perpendicular Temperature $T_\perp$ due to the Quasilinear Effect.

of the present spontaneous instability. Since the maximum growth rate shifts to higher frequency as time elapses, a peak intensity of the excited emission accordingly moves to higher frequency. It is, however, noticed that this frequency shift is a very slow phenomenon and its increment is small as seen in the result of computation, Fig.61.

Fig.62 shows a corresponding change of the perpendicular temperature $T_\perp$ due to the quasilinear diffusion. In this figure, $T_\perp$ is plotted vs. frequency using the relation between V_z and ω_r as shown in Fig.59. The perpendicular temperature, in this figure, is defined by

$$T_\perp(V_z,t) = T_\perp(\omega_r,t) = \frac{\int_0^\infty V_\perp^3 g_e(V_\perp,V_z,t)\,dV_\perp}{\int_0^\infty V_\perp g_e(V_\perp,V_z,t)\,dV_\perp} \quad . \tag{3.92}$$

In the frequency range corresponding to the wave growth ($0.51f_H \sim 0.53f_H$ in Fig.62), the perpendicular temperature decreases as time elapses. Thus we again recognize that the source of the present instability is the perpendicular kinetic energy of the resonant particles as clarified by the physical consideration of the quasilinear instability in Section 2.2 of this Chapter, i.e., by Eq.(3.18). In the frequency range corresponding to the cyclotron damping ($f > 0.53f_H$ in Fig.62), an increase of the perpendicular temperature is expected qualitatively but actually it is negligibly small as seen in Fig.62. This is due to the fact that the initial wave intensity is as small as 100 μV/m and hence quickly becomes zero by the strong cyclotron damping.

We believe that these results are much informative to consider the quantitative evolution of the whistler mode cyclotron instability, especially in application to the generation mechanism of various emissions by the present instability.

4.3 Computation of the Evolution of Wave-Triggered Instability

A second computation was performed to see what happens on the nonlinear stage when a whistler mode wave with a narrow frequency spectrum is transmitted into a weakly unstable plasma. The conditions here were set up to enable us to search for the generation mechanism of ASE which has not been clarified so far.

The plasma distribution function is again chosen as the "triple-structured" loss cone distribution function, Eq.(2.162). In this case, such plasma parameters are selected so as that the growth rate of the whistler mode cyclotron instability is enough small. They are

f_H=13.5kHz, f_p=200kHz ,
$T_{T\perp}=T_{T\parallel}$=2eV, n_T=0.1 ,
$T_{Q\perp}=T_{Q\parallel}$=30eV, n_Q=0.1, $\eta_Q=10^{-2}$,
$T_{B\perp}$=10eV, $T_{B\parallel}$=1eV, n_B=0.5, $\eta_B=10^{-3}$, V_B=200eV .

The intensity of the injected triggering wave is taken as 100 μV/m for one case and 1 mV/m for the other case.

Figures 63 and 64 show the results of computations on the evolution of the growth rate for the intensity of the triggering wave, 100 μV/m and 1 mV/m respectively. In both cases, the plasma parameters are the same and the maximum growth rate at the initial stage is $\gamma_{max} \sim 0.2$. The shaded rectangular parts indicate the spectra of the triggering wave.

It is observed that there appear horns in the growth rate curve as time elapses. Of course, the growth rate as a whole except the part of horns is reduced due to the usual quasilinear effect. These horns are observed to grow up most at the upper boundary of the frequency band of the triggering wave, whereas there also appears a small amount of change at the lower boundary. These phenomena newly found are quite different from the usual quasilinear effect as treated in the previous computation of the case of the spontaneous instability. Such peculiar changes of the growth rate, however, are to be expected analytically from the essential characteristics of quasilinear effect as explained below. When a wave packet with a certain frequency band is transmitted into a plasma, plasma particles with the resonance velocity $V_R = V_R(\omega_r)$ start to suffer a strong diffusion in the velocity space with increasing $V_\perp$ and decreasing V_z so that a warp appears in the distribution function at the boundary of the strongly diffused and the normally stable regions, which produces an abrupt change of the growth rate at the corresponding frequency. It is, however, noticed that these horns in the growth rate will be softened when spontaneous emissions from the plasma are taken into account (Sato[101]) or when the triggering wave has a more roundish shape than a rectangular form.

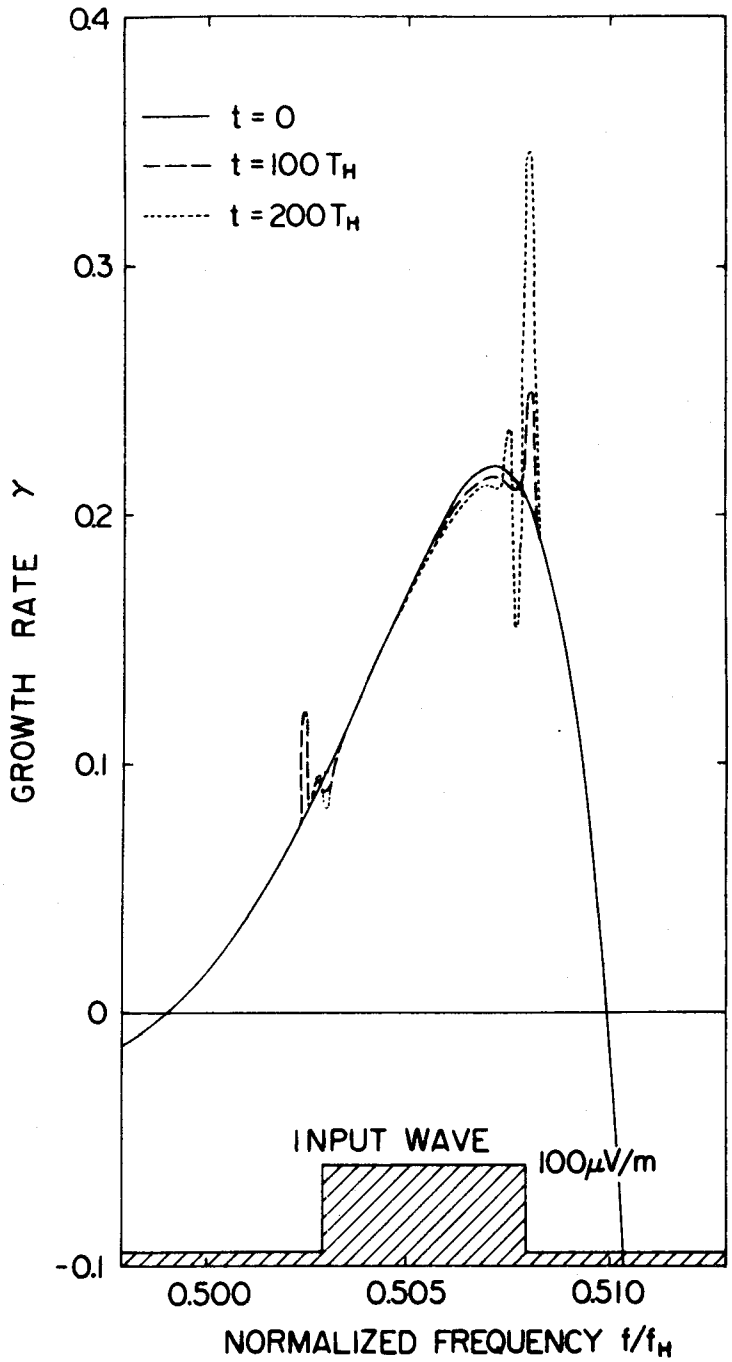

Fig.63 A Temporal Change of the Growth Rate in a Weakly Unstable Plasma due to the Effect of a Triggering Wave (I). Intensity of the triggering wave is taken as 100 μV/m.

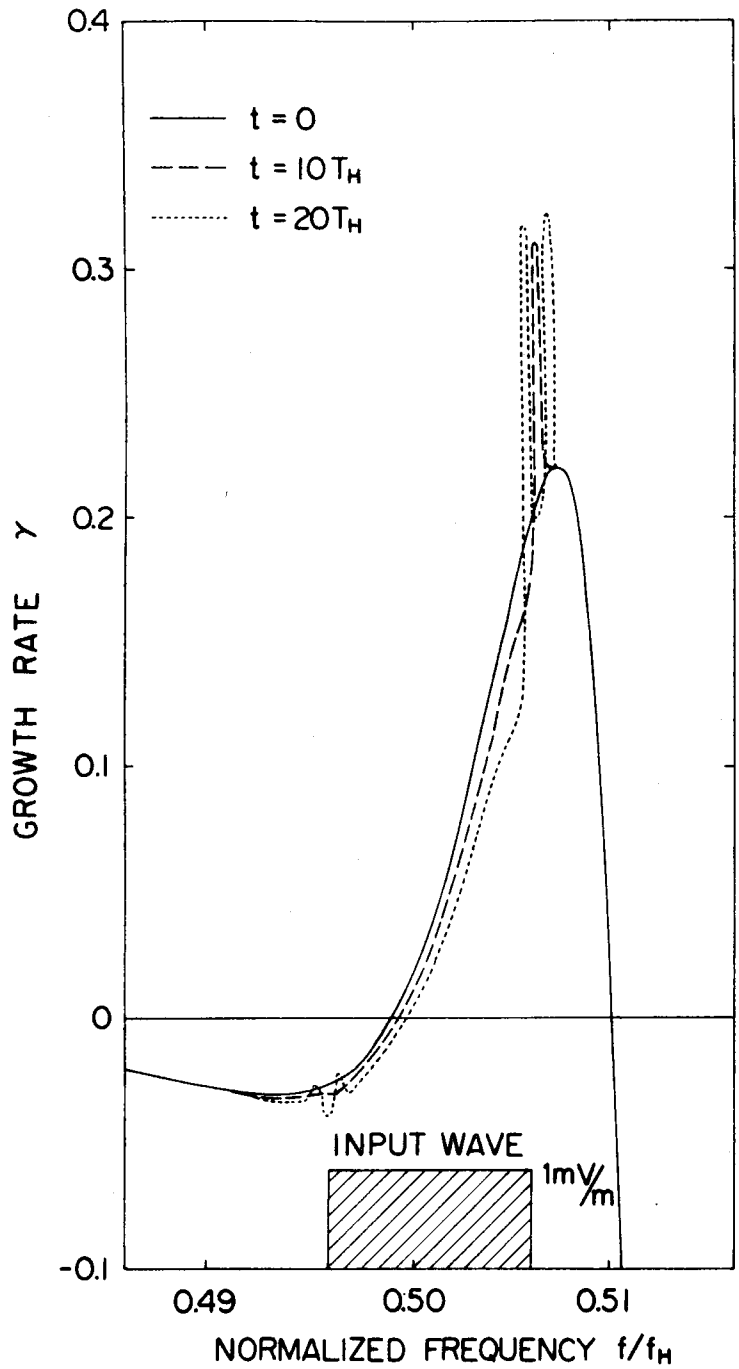

Fig.64 A Temporal Change of the Growth Rate in a Weakly Unstable Plasma due to the Effect of a Triggering Wave (II). Intensity of the triggering wave is taken as 1 mV/m.

It is also observed in both Figs.63 and 64 that the horn splits into double peaks (horns) in the γ-f curves to some extent as time elapses. This is what cannot be expected analytically from the theory. This branching of the peak growth rate may be closely related to the phenomenon of the branching emissions as frequently observed in ASE.

§5. Relevancy between Triggered VLF Emissions and Quasilinear Whistler Mode Cyclotron Instability

It is now possible to consider the generation mechanisms of triggered discrete VLF emissions in the magnetosphere based on the quantitative results of the linear and quasilinear calculations already mentioned.

5.1 Spontaneous Quasilinear Cyclotron Instability and WTE-H

We have already shown that almost all of the characteristics of WTE-H can be well understood by the linear whistler mode cyclotron instability in the plasma described by the "triple - structured" loss cone distribution function. However, the remaining features of WTE-H, the items (4) and (5) mentioned in Section 2.2 in Chapter I, are clearly related with the nonlinear behavior of the causative instability.

The first one, item (4), is that the emission frequency hardly changes but has a tendency to rise slowly. The result of the numerical computation, Fig.61, showed the characteristics which are just fit for those of WTE-H. The second one, item (5), characterizing the long life of emissions is certainly related to the slow decrease of the growth rate for typical intensities of the whistler mode waves in the magnetospheric plasma. It is, however, natural to consider that a cause of the extinction of the emission WTE-H may lie in another factor such as an abrupt change of the background plasma distribution function by some external forces.

Thus, we can conclude that the whistler triggered emissions around the whistler cutoff frequency, WTE-H, are generated by the cyclotron instability when the following two conditions are satisfied:

(a) In a region in the magnetosphere, the medium plasma has a velocity distribution function such as described by Eq.(2.162) which ex-

hibits a considerable growth rate around $f \sim 0.5 f_H$.

(b) A whistler mode wave with intensity higher than a certain level propagates through the above region in the magnetosphere.

If the condition (a) is not satisfied, which means that the plasma is composed only of thermal and quasithermal particles, usual nose whistler cutoffs around $f \sim 0.5 f_H$ are to be observed. On the other hand, the condition (b) requires that the triggering noise should have a certain level because the growth rate is not sufficient for the thermal noise to be rapidly grown up to the observable intensity level of emissions. It is noticed that whistlers do not stimulate the instability, but only play a role of a donor of the "seed" of emissions in this case.

5.2 Wave-Triggered Quasilinear Cyclotron Instability and ASE

Characteristics of ASE have been summarized in Section 2.2 in Chapter I, all of which cannot be understood within the linear theory of the cyclotron instability. It was also demonstrated recently (Harker & Crawford[85]) that even by a nonlinear treatment of mode-mode couplings in the whistler mode waves, the characteristics of ASE were not explained. The most prominent feature of ASE, which is a difficulty in the theories considered earlier is that the time delay of the excited wave is strongly dependent on the intensity and duration of the triggering wave. Such a peculiar feature may closely related to the quasilinear effect. When a triggering wave packet with a narrow frequency spectrum comes into the weakly unstable plasma, the velocity distribution is deformed by the triggering wave through the cyclotron damping process, resulting in a sufficient growth rate for the generation of the triggered emissions. From Eq.(3.83), we know that the amount of change in the particle velocity distribution, Δg_{er} is proportional both to the wave intensity ε_k and to the characteristic time $\Delta\tau$, i.e.,

$$\Delta g_{er} \propto \varepsilon_k \cdot \Delta\tau \quad . \tag{3.93}$$

When a intensity of the triggering wave is small, then it takes a long time to make the velocity distribution much deform to provide a sufficient growth rate, and vice versa.

In the previous section, it was demonstrated how the growth rate of the instability, which is initially weakly unstable, changes with time when a narrow band triggering wave is imposed on the plasma. The results are summarized in Figs.63 and 64. Using the characteristics shown in these figures, we will discuss the relevancy between ASE and the present ASE theory, which is ascribed to the wave-triggered quasilinear cyclotron instability in the whistler mode.

The time delay of an excitation of ASE is well explained by the computed results. It is observed that the appearance of the horns in the γ-f curves takes place at an earlier time in Fig.64 (the case of E = 1mV/m) than in Fig.63 (the case of E = 100μV/m) according to the initial intensity of the triggering wave. The numerical result on this point coincides well with the prediction by Eq.(3.93). Therefore it is understood that ASE is triggered even with a low power transmitter (Kimura[31]) if the triggering wave continues patiently to change the particle distribution.

The offset phenomenon in ASE can be explained as follows. In case where the frequency f of a triggering wave is slightly lower than the cutoff frequency f_c where $\gamma_k = 0$, a triggering occurs at higher frequency than f as seen in Figs.63 and 64. This is the offset. However, if f is very close to f_c, the offset is thought to be small because the frequency of the excited emission cannot exceed the cutoff frequency.

A tendency of ASE being most often triggered at about $f_H/2$ (Carpenter[28]) is explained as follows. In the computation in the previous section, a frequency of the triggering wave is chosen around the frequency of the maximum growth rate as seen in Figs.63 and 64. However, if the frequency of the triggering wave is chosen in the frequency range corresponding to the cyclotron damping, no particular change in the growth rate γ will take place unless the intensity of the triggering signal is extremely strong. On the contrary, when the frequency of the triggering wave is smaller than the frequency of the maximum growth rate, little quasilinear effect will be observed because the growth rate at that frequency is initially exponentially small as seen in the linear calculation. It means that the number of resonant particles itself is too small for the growth rate to attain the necessary amount. Therefore, the tendency of ASE triggered around $f_H/2$ is closely related to the characteristics

of triggering around $f_H/2$ of WTE-H which was explained fairly well by the linear analysis in Section 5.5 in Chapter II.

Thus we can conclude that a quasilinear behavior of the wave-triggered whistler mode cyclotron instability plays an important role for the generation of ASE in the magnetosphere.

5.3 Summary of Explicability of WTE-H and ASE

We have hitherto investigated the linear and quasilinear theories of the whistler mode cyclotron instability and their application to the magnetospheric VLF problem. It may be convenient to summarize here the explicability of discrete VLF triggered emissions by the theory. The summary is given in Table 3.

Table 3 Explicability of WTE-H and ASE by the Linear and Quasilinear Instability in the Whistler Mode

Species	Characteristics	Linear Theory	Quasilinear Theory
WTE-H	$f \simeq f_{cut}$	O	
	$f_H/2$	O	
	Narrow band	O	
	Generation condition	O	
	Frequency change		O
	Quenching		Δ
ASE	$f_H/2$	O	O
	Generation condition	O	O
	Time delay		O
	Time × intensity		O
	Frequency branching		O
	Quenching		Δ

§6. Generation Mechanism of Background Hiss of Polar Chorus

6.1 Introduction to KP Cycle in the Magnetosphere

A steady self-exciting cycle of low frequency whistler mode waves due to the quasilinear interaction with high energy electrons was proposed by Kennel & Petschek[42] (hereafter called KP) in order to estimate the upper limit of trapped electron fluxes in the magnetosphere. Though their main concern was to estimate the limit of trapped particles by the quasilinear diffusion due to the cyclotron instability, their steady interaction cycle theory is also useful to study a generation mechanism of VLF emissions which have a steady characteristic.

The steady self-exciting cycle of low frequency whistler mode waves is schematically summarized in Fig.65. We term this closed cycle as "KP cycle". The growth rate γ for this instability is given by KP[42] as

$$\gamma = \pi\Omega_e (1 - \frac{\omega_r}{\Omega_e})^2 \eta (A_p - \frac{\omega_r}{\Omega_e - \omega_r}) \quad , \tag{3.94}$$

where

$$\eta = 2\pi \frac{\Omega_e - \omega_r}{|k| N_e} \int_0^\infty V_\perp dV_\perp g_e(V_\perp, V_z = V_R) \quad , \tag{3.95}$$

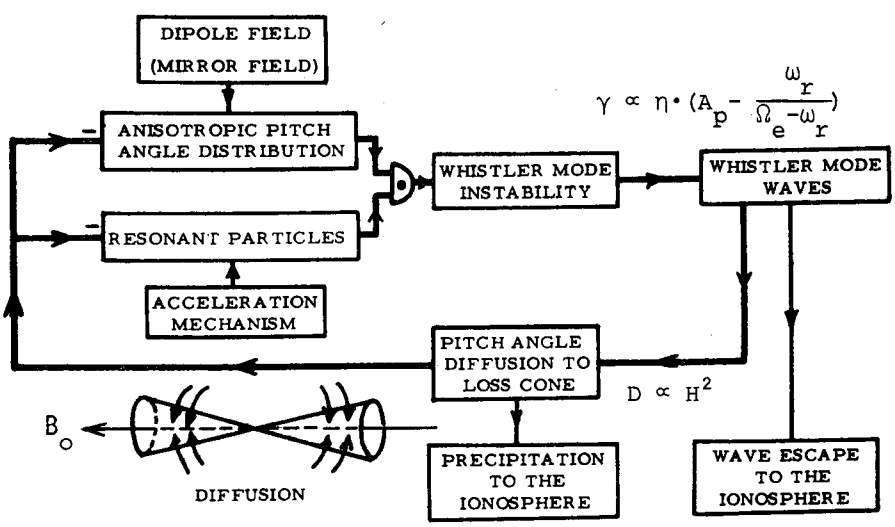

Fig.65 Schematic Summary of Self-Exciting Cycle (KP Cycle) of Low Frequency Whistler Mode Waves ($\omega_r << \Omega_e$) in the Magnetosphere.

is a fraction of the resonant electrons and

$$A_p = \frac{\int_0^\infty V_\perp dV_\perp \tan\alpha \frac{\partial g_e}{\partial \alpha}}{2\int_0^\infty V_\perp dV_\perp g_e} \Bigg|_{V_z = V_R} , \tag{3.96}$$

is a measure of the pitch angle anisotropy of electrons and α is a pitch angle. The expression Eq.(3.94) is also derived under the following limit

$$\omega_r << \Omega_e , \tag{3.97}$$

from the general expression Eq.(2.136) (see Appendix D). It is noticed that there is a relation between the temperature anisotropic factor A and the pitch angle anisotropic factor A_p defined by Eq.(3.96) as

$$A_p = A - 1 . \tag{3.98}$$

A brief explanation of the KP cycle is as follows. Since the magnetic field has a shape of a mirror field in the magnetosphere, the pitch angle distribution of the resonant particles show
tropy. If these resonant particles are always created in the interaction region in the magnetosphere by a certain unknown acceleration mechanism, then a whistler mode cyclotron instability grows up and as a result, whistler mode waves are generated. These waves, in turn, affect the particle distribution function by the quasilinear effect through a pitch angle diffusion process. Consequently we can observe both the waves and the high energy resonant electrons which penetrate the ionosphere and are precipitated into the loss cone of the mirror field of the earth, respectively. Thus a loss cone anisotropic distribution initially supposed can be maintained and a steady cycle is completely formed as long as the supply of the resonant particles continues (see Fig.65).

A measure of the pitch angle anisotropy A_p was estimated as a steady state solution of the KP cycle by KP[42]. They estimated A_p for a case of the weakly turbulent pitch angle diffusion, namely a case of the wave-particle interaction which gives a weakly unstable waves ($\gamma \simeq 0$), assuming that the contributing waves are such low frequency whistler mode waves as $\omega_r << \Omega_e$. The resultant formula that they obtained was

$$A_p \sim 1/2\{\ln(1/\alpha_L)\} , \tag{3.99}$$

where α_L is the loss cone angle of the interaction region. It should be noticed that another solution of A_p for a wave-particle interaction in the magnetosphere may exist if the frequency constraint Eq.(3.97) is released. However, as pointed out by KP[42], this constraint (3.97) is necessary to explain the similarity between the energy spectra of electrons at 1000km height and in the equatorial plane on the same field line in the magnetosphere. This is easily understood if we remind Eq.(3.17), as

$$\frac{\Delta W_{p\perp}}{\Delta W_{p\parallel}} = \frac{\Omega_e}{\omega_r - \Omega_e} \simeq -1 \quad , \tag{3.100}$$

under the assumption of $\omega_r << \Omega_e$. In this case

$$\Delta W_p = \Delta W_{p\perp} + \Delta W_{p\parallel} \simeq 0 \quad , \tag{3.101}$$

so that the total kinetic energy of the resonant electrons does not change though the pitch angle diffusion process is taken place in the wave-particle interaction of the KP cycle.

In the rest part of the present section, we estimate the wave cutoff frequency and A_p using the plausible plasma parameters in the magnetosphere, and will present a semi-morphological study in order to clarify what type of VLF emissions actually contributes to such KP cycle in the magnetosphere.

6.2 Quantitative Extraction of Characteristics of Responsible VLF Waves to the KP Cycle

The interaction region of the KP cycle was a priori presumed to lie in the equatorial plane in the paper by KP[42], but it is well supported as clarified in Section 3.3 in Chapter II. Therefore, a loss cone angle α_L and the corresponding anisotropic factor A_p through Eq.(3.99) are computable as a function of the geocentric distance. Fig.66 is an illustration of the results. Solid lines are those estimated for a dipole model of the earth's magnetic field, while the dashed lines are those for a compressed model by the solar wind (see for example, Mead[102]). Since the upper cutoff frequency $\omega_c = 2\pi f_c$ of the unstable whistler mode waves is determined from Eq.(3.94) as

$$\omega_c = \frac{A_p}{A_p + 1} \Omega_e \quad , \tag{3.102}$$

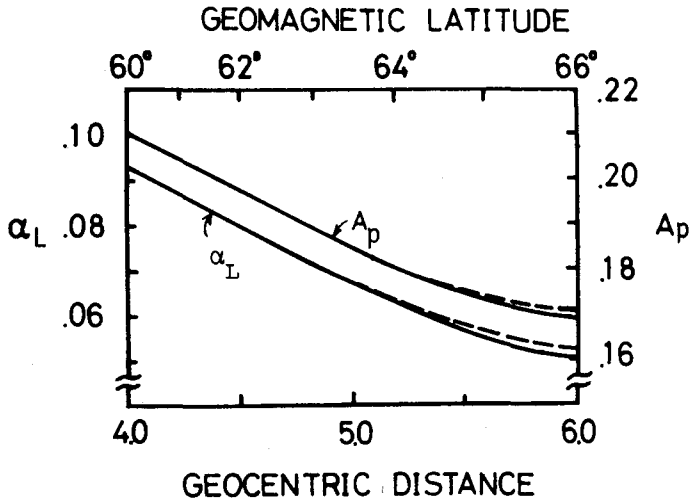

Fig.66 Loss Cone Angle α_L and the Pitch Angle Anisotropic Factor A_p as a Function of Geocentric Distance.

Fig.67 Upper Cutoff Frequency of the Whistler Mode Waves Generated by the KP Cycle as a Function of Geocentric Distance.

$$f_c \left(= \frac{f_{H\min}}{1 + 1/A_p}\right)$$

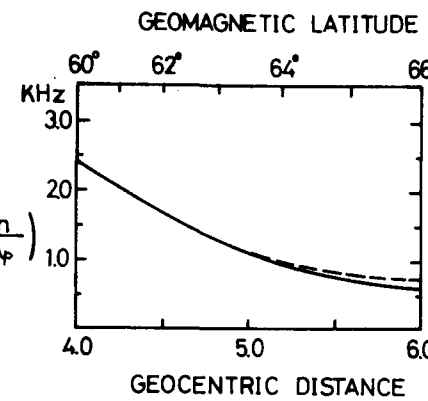

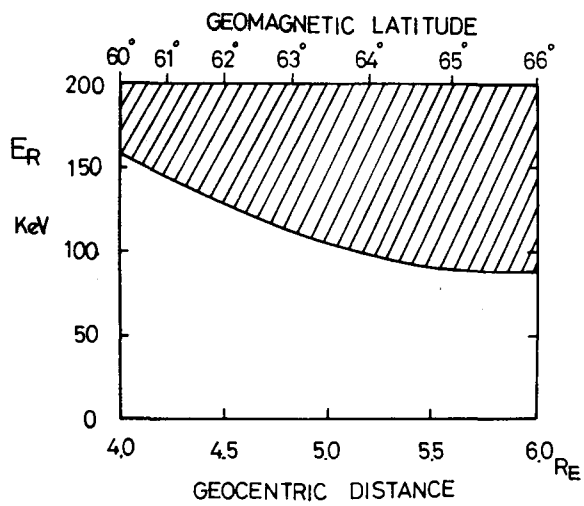

Fig.68 Energy Range of Resonant Electrons with the Whistler Mode Waves in the KP Cycle.

it is also possible to depict f_c as a function of the geocentric distance. It is illustrated for both dipole and distorted models for the magnetic field in Fig.67. We thus know, from the figure, that the upper cutoff frequency f_c of the responsible whistler mode waves to the KP cycle should fall between 0.6kHz and 2.4kHz, i.e.,

$$0.6\text{kHz} \leq f_c \leq 2.4\text{kHz} \quad , \tag{3.103}$$

if the generation region lies between L = 4 and L = 6 in the equatorial plane.

The equation for the energy of the resonant electrons E_R was given by KP[42] as

$$E_R = \frac{1}{2} mV_R^2 = \frac{\Omega_e}{\omega_r} \left(1 - \frac{\omega_r}{\Omega_e}\right)^3 \frac{\frac{1}{2}\mu_o H_o^2}{N_e} \quad , \tag{3.104}$$

where $H_o = B_o/\mu_o$ is the intensity of the geomagnetic field and N_e is the electron number density in the interaction region. This equation also follows after Eq.(2.149). Using this equation, the lower limit of the energy of the resonant electrons, which corresponds to the higher limit of the wave frequency f_c, is to be estimated by adopting the dipole field model and an electron density profile calculated by a diffusive-equilibrium model (Angerami[14]). Noting that the interaction region of such type lies outside the plasmapause (Carpenter[12]), the energy range of the resonant electrons is calculated as shown in Fig.68.

Thus, the characteristics of the VLF emissions generated by the KP cycle should be the followings:

1) They should have a rather continuous character than a discrete one because it is ascribed to the steady state cycle.
2) They should have a frequency band lower than the upper cutoff frequency shown in Fig.67. Namely their maximum frequency is around 0.6kHz to 2.4kHz when their generation region lies between L = 4 and L = 6 in the equatorial plane in the magnetosphere.
3) Their diurnal variation must have close relation with the precipitation pattern of electrons with the energy shown in Fig.68. The corresponding energy of the electrons which couple with these waves of $f \leq f_c$ through the cyclotron resonance is, on the average,

higher than 100keV. Therefore the polar graph of their diurnal variation must resemble the precipitation pattern of harder electrons (E > 40keV) which was elegantly summarized by Hartz & Brice[103] and indicated by "dots" in Fig.69.

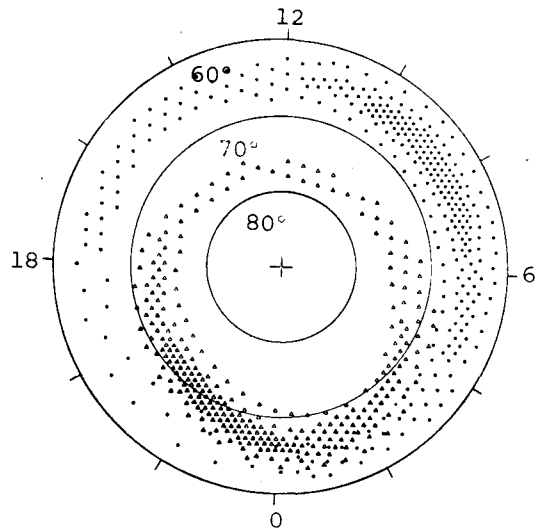

Fig.69 An Idealized Auroral Particle Precipitation Pattern (Hartz & Brice[103])

6.3 Morphological Study of Polar Chorus and Precipitated Hard Electrons

Among various VLF emissions, we sought what kind of emissions is responsible to the KP cycle based on theoretically predicted characteristics as summarized above. A conclusion is that the background hiss of "polar chorus" is such a type of VLF emissions. A similar problem was also investigated by Brice[104] but his argument on the mid-latitude hiss does not satisfy the above summarized characteristics. One example of the frequency spectrum of the polar chorus is shown in Fig.70 taking from the Helliwell's Atlas. As seen in the figure, polar chorus shows actually a fairly steady char-

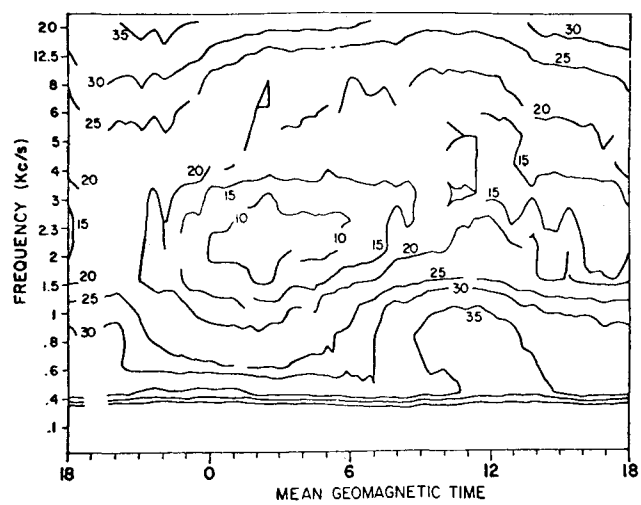

Fig.71 The Diurnal Variation of the Average Peak VLF Emission Intensity in Decibels Relative to $10^{-18}Wm^{-2}Hz^{-1}$ as a Function of Observing Frequency (Morozumi & Helliwell[105])

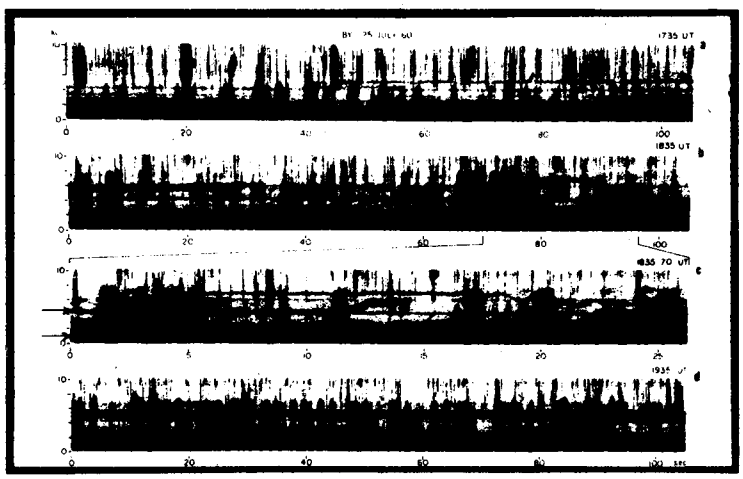

(a)

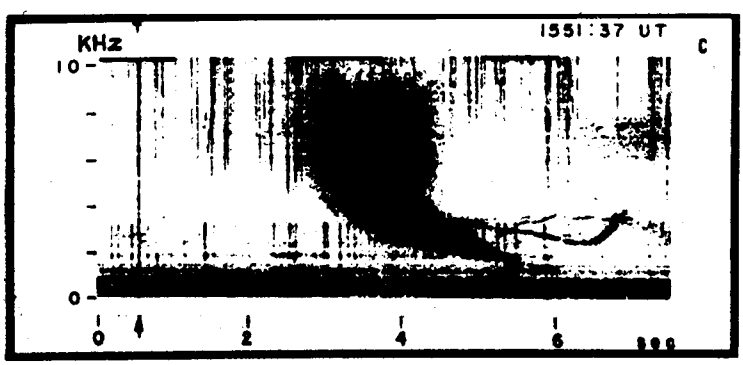

(b)

Fig.70 Examples of Polar Chorus and its Background Hiss. Polar chorus in the spectrum is the emission that appears continuously below 1.5kHz or so.

(from Helliwell[8])

acter, i.e., it accompanies with hiss as its background. The upper cutoff f_c falls in the vicinity of 1.5kHz.

The diurnal variation of the average intensity of VLF emissions is presented by Morozumi & Helliwell[105], as indicated in Fig.71. The figure shows that the polar chorus, which has a maximum intensity in the frequency range between 0.6kHz and 2.4kHz in the geomagnetic local time 1100 hours. This upper cutoff frequency of polar chorus (or rigorously its background hiss) agrees quite well with the theoretically predicted value of Eq.(3.103).

The diurnal variation of polar chorus accompanied with its background hiss is checked using the Helliwell's Atlas[8]. The result is plotted in the polar graph and illustrated in Fig.72. As easily understood, the polar graph of polar chorus exhibits a good agreement with the precipitation pattern of harder electrons (shown by dots in Fig.69).

From the above discussion, it is well concluded that the waves or VLF emissions responsible to the KP cycle are the background hiss of polar chorus.

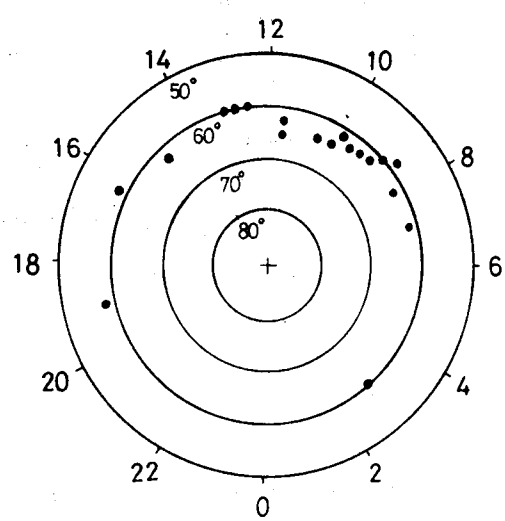

Fig.72 Diurnal Variation of the Background Hiss of Polar Chorus.

§7. Discussion and Conclusions

It is the purpose of this chapter to describe the nonlinear behavior of the whistler mode cyclotron instability with a view of applying the theoretical analyses to VLF wave problems in the magnetosphere.

In case of the whistler mode waves, major nonlinear effects come from the resonant kinetic effects associated with the wave-particle interactions, since the nonlinear wave-wave interaction is known to play no significant role in the whistler mode waves. As one of the effective treatments of the wave-particle interactions, a quasilinear treatment of the whistler mode cyclotron instability has been investigated as a natural extension of the linear cyclotron instability in the whistler mode. A usual quasilinear formulation was used about a fine deformation of the distribution function. It is interesting, however, to note that a set of quasilinear equations are reducible not from the Vlasov equation but only from a physical consideration about the essential points of the quasilinear theory. Such a mathematical and independent physical derivation of the basic set of quasilinear equations have served much to understand the underlying physical process and to know the limitation of the quasilinear treatment. The quasilinear treatment is essentially the same as the linear treatment. It is modified from the linear theory so as to satisfy the conservation law of energy in the sum of the wave and particle energies by correcting a shape of the distribution function. The basic philosophy about the resonance is still the same as in the linear theory, i.e., the resonance is also thought to be described by the delta function $\delta(\omega_r - kV_z + \varepsilon_s \Omega_s)$.

It should be emphasized that a careful consideration is necessary in the electromagnetic mode (including the whistler mode) quasilinear instability. It was shown that the excited wave spectrum of whistler mode waves changed with time in addition to the growth rate reduction (stabilization) as a usual quasilinear effect. A consideration was also made on the difference in the appearance of the quasilinear effects between the following two cases; a spontaneous cyclotron instability and a wave-triggered cyclotron instability.

Regarding with the last points mentioned above, extensive numerical

computations of the two-dimensional problem were carried out on the nonlinear evolution of the whistler mode cyclotron instability, yielding necessary information of the time-dependent characteristics of the instability. The computations were performed for the above two cases; one to trace a temporal behavior of fairly unstable cyclotron instability (spontaneous instability) and the other to see what happens on the nonlinear stage, when a wave of a narrow frequency band with a considerable intensity is transmitted into a weakly unstable plasma. The second case is intended to simulate the triggered emissions. The results of both cases are much informative and help us not only to ascertain the physical and analytical considerations but also to get much informations which can be obtained only by the computer experiment.

Applications of these analyses and the numerical computations on the quasilinear behavior of the whistler mode cyclotron instability to the elucidation of the generation mechanism of triggered discrete VLF emissions are then discussed. The conclusions deduced from our investigations are as follows. The whistler triggered emissions around the whistler cutoff are generated by a spontaneous cyclotron instability. In this case, whistlers do not play as a triggering wave but play as a donor of the "seed" of the emissions. The tendency of slow rising frequency is also well explained by the quasilinear evolution of the instability. On the other hand, a triggering process of the artificially stimulated emissions, ASE, is also found to be explicable by the quasilinear change of the distribution function. The result of the numerical computation was useful to understnad the process of triggering of the instability. It is clarified that ASE are, different from WTE-H, essentially "triggered" emissions. It is, however, noticed that our present analyses for the interaction in the homogeneous plasma did not clarify the mechanism of a large amount of the frequency change of ASE.

A detailed physical consideration as well as quantitative investigations of the quasilinear behavior of the whistler mode cyclotron instability made in the present chapter is believed to contribute more or less to the better understanding of the instability and a mysterious process of generation of the triggered emissions. Of course, however, we should well recognize the limitation of the applicability of the quasilinear

theory which comes from many restrictions and assumptions made in the course of the derivation and formulation of the basic equations. The most severe problem may come from the breakdown of the δ-function description of the resonance. It becomes difficult to treat a problem of the wave-particle interaction between a monochromatic wave and resonant particles. In this case, it is obviously unnatural to treat the resonance by the δ-function, i.e., it is meaningless to consider the change of the distribution function only at $V_z = V_R(\omega_r)$. In such a problem, another method of investigation other than the quasilinear treatment is necessary.

Another aspect of the quasilinear theory of the whistler mode cyclotron instability was noticed in the last section of the present chapter. Apart from the problem previously treated, a steady interaction between particles and waves with continuous low frequency band had been considered by Kennel & Petschek[42]. In this case, a marginal instability, i.e., a weakly unstable instability plays a main role. The KP theory was reviewed for the generation of VLF noises and it was clarified that there was a kind of emissions responsible to the KP cycle, that is the background hiss of polar chorus.

Thus we may well conclude that the quasilinear processes of the whistler mode cyclotron instability play a fundamental and important role in the magnetospheric VLF phenomena of both continuous and discrete emissions.

Chapter IV

NONLINEAR ANALYSIS OF WHISTLER MODE WAVE-PARTICLE INTERACTIONS BETWEEN MONOCHROMATIC WAVE AND PARTICLES ——— SINGLE PARTICLE APPROACH ———

§1. Introduction

There have been enthusiastic studies on problems of the cyclotron interaction between energetic electrons and the whistler mode waves, especially regarding with the generation theory of VLF emissions in the magnetosphere. Though the basic laws describing the problems are very simple, the problems have hardly been solved elegantly even in the case of an interaction in a homogeneous plasma. This is partly because of the nonlinearity involved and partly because of the self-consitent condition between the wave field and the particle distribution function. Two extreme methods, therefore, have been so far conventionally employed for this wave-particle interaction problem. One is the small amplitude approximation theory which assumes that particle trajectories are only perturbed from the zero-order orbits. The growth and/or damping rate are thus obtained by using the zero-order background distribution function. This is the well established linear theory (Stix[25]). In Chapter II, we have investigated in some detail the cyclotron instability in the whistler mode along this method of linear theory. The other is the large amplitude theory in which the wave amplitude is assumed to be so large that the particles are trapped in the wave field and their distribution function is deformed to much extent with remaining the wave amplitude almost constant (O'Neil[106]; Al'tshul & Karpman[107]). Problems of the trapped particles, the amplitude oscillations and the electron bunching in the klystron are studied by this latter method.

A rigorous treatment of the problem of the wave-particle interaction, however, should take account of both the change of the wave field and

the particle distribution function. In a weak nonlinear system, a quasilinear approach is developed for waves with a rather wide band spectrum (Drummond & Pines[44]; Vedenov, Velikov & Sagdeev[87]). As an application of the quasilinear theory to the VLF emission problem, some studies have been performed (Matsumoto & Kimura[50]). In Chapter III, we have presented a qualitative and quantitative investigation on the whistler mode cyclotron instability within the quasilinear theory and have gained some fruitful results. However, for a problem of the nonlinear interaction between a monochromatic wave and particles, such a quasilinear treatment is not valid because a basic assumption of the linear resonance condition expressed by the delta function is unnatural as mentioned in the last part of Chapter III. An alternative self-consistent approach should, then, be used for such a problem.

As a first step for the settlement of the problem, the exact nonlinear trajectories of electrons in a given monochromatic electromagnetic wave field have been extensively solved (Bell[41]; Roberts & Buchsbaum[108]; Laird & Knox[109]; Lutomirski & Sudan[110]; Mamiya[111]; Dungey[112]; Ashour-Abdalla[113]), and it was pointed out that a phase-bunching or phase trapping was important and essentially different from the case of the electrostatic waves. It should, however, be noticed that the exact solutions of the nonlinear equation of motion of electrons in a given electromagnetic field are meaningless because a resonant current due to the phase bunching will soon alter the original wave field. Then a feedback of the resonant current to the original field is taken into account. This feedback effect is sensitive in the sense that the direction of the wave magnetic and electric field vectors are quickly affected by the resonant current even when their magnitude is not altered so much.

This chapter deals with the nonlinear properties of the wave-particle interaction based upon a single particle approach. Though this approach is very primitive, it is easily extended from the linear treatment (Section 2.2 in Chapter II) to the nonlinear category. In this method, a velocity spread of the resonant particles can be involved so that the method is useful especially for a problem of the interaction between the monochromatic wave and particles, which cannot be treated rigorously by the usual quasilinear theory.

In Section 2, we begin with a survey of the behavior of electrons

which is resonant with a whistler mode wave of a frequency f and of a considerable intensity. Numerical and topological analyses will be made in the course of the present study (Mamiya[109]; Hashimoto[112]; Matsumoto, Hashimoto & Kimura[54]). Also a note on the difference of the concepts of the phase trapping and the phase bunching is described.

In Section 3, a "phase bunching" due to the wave fields is treated. The concept of the phase bunching in the wave-particle interaction in the whistler mode was first construed by Brice[38,39] and it was adopted recently in the theories of VLF emissions by many authors (Helliwell[29]; Sudan & Otto[46]; Dysthe[47]; Nunn[48]).

It is pointed out in the present section that a phase bunching can be classified by its mechanism into two types:

(a) One is the phase bunching due to a parallel acceleration by the Lorentz force $-e\vec{V}_{\perp}\times\vec{B}_{w}$, where $\vec{B}_{w}$ and $\vec{V}_{\perp}$ are the wave magnetic field and the velocity component of an electron perpendicular to the external magnetic field $\vec{B}_{o}$. This type of bunching is called $\vec{V}_{\perp}\times\vec{B}_{w}$-phase bunching hereafter.

(b) The other is the phase bunching due to a perpendicular acceleration by the Lorentz force $-e\vec{V}_{z}\times\vec{B}_{w}$ where $\vec{V}_{z}$ is a velocity component parallel to $\vec{B}_{o}$. We call this type $\vec{V}_{z}\times\vec{B}_{w}$-phase bunching.

The phase bunching dealt by Brice is the former type. Based upon the above classification, we present a physical interpretation of the mechanism of each type of phase bunching.

We will especially pay attention on the resultant resonant currents due to the phase bunching and some formulation of the resonant current is given in Section 4.

The bunching process in the actual interaction, however, is governed by two types of accelerations mentioned above. Hence numerical computations are carried out in Section 5 on the time-behavior of the phase and the magnitude of the perpendicular velocity vector for various initial values of the particle velocity. The time-evolution of the resonant currents is calculated using the above phase-time solutions for assumed various plasma distribution functions.

In the last Section 6, the numerical results will be compared with those analytically obtained in Section 3 and 4. The importance of the $\vec{V}_{z}\times\vec{B}_{w}$-phase bunching in the self-consistent model of the interaction is

stressed there.

§2. Nonlinear Trajectories of Electrons in a Monochromatic Whistler Mode Wave

2.1 Model and Basic Equations

In order to trace a trajectory of an electron in a propagating whistler mode wave, nonlinear equation of motion of the electron in the wave field is used. A model is set so as to be able to deal with VLF wave phenomena observed in the magnetosphere. Therefore, a simple situation is considered of the interaction between energetic electrons and a purely transverse and monochromatic wave propagating in a homogeneous, magnetoactive and collisionless plasma. In this case it is assumed that the electrons do not affect the propagating wave fields. A feedback of the motion of these electrons to the wave field will be discussed later. Neglecting the relativistic effects, the nonlinear set of equations of motion is written

$$\frac{dV_\perp}{dt} = -\frac{eE_w}{m}\left(1-\frac{V_z}{V_{ph}}\right)\sin\phi \quad , \tag{4.1}$$

$$\frac{dV_z}{dt} = -\frac{eE_w}{m}\frac{V_\perp}{V_{ph}}\sin\phi \quad , \tag{4.2}$$

$$\frac{d\phi}{dt} = \Omega_e - \omega_r\left(1-\frac{V_z}{V_{ph}}\right) - \frac{eE_w}{m}\left(1-\frac{V_z}{V_{ph}}\right)\frac{\cos\phi}{V_\perp} \quad , \tag{4.3}$$

in the rest frame or

$$\frac{dV_\perp}{dt} = -\Omega_1 V_z \sin\zeta \quad , \tag{4.4}$$

$$\frac{dV_z}{dt} = \Omega_1 V_\perp \sin\zeta \quad , \tag{4.5}$$

$$\frac{d\zeta}{dt} = \Omega_e + kV_z - \Omega_1\frac{V_z}{V_\perp}\cos\zeta \quad , \tag{4.6}$$

in the wave frame, respectively, where $\Omega_1 = eB_w/m$, and $\zeta(= kz+\theta)$ is the angle between $\vec{V}_\perp$ and $\vec{B}_w$ as shown in Fig.73. ϕ in Eqs.(4.1) ∿ (4.3) is related with ζ by

$$\phi = \zeta + \pi \quad . \tag{4.7}$$

Eqs.(4.1) to (4.3) are first used by Bell[41] and Eqs.(4.4) to (4.6) are used by Lutomirski & Sudan[110] and Sudan & Otto[46]. Derivation of these equations are given in Appendix E. In this section, topologically shown are the electron trajectories in the phase space, which are numerically computed by the use of the basic equations (4.1) to (4.3). While Eqs.(4.4) to (4.6) are used in the analysis of phase bunching because of their physical simplicity.

2.2 Topological Analysis

Before giving the solution of the electron trajectories as a function of time t, a topological or state plane representation is presented in advance in this section. By this representation a qualitative aspect of the solution as well as some quantitative informations would be shown.

2.2.1 Equilibrium Curves in $V_\perp - V_z$ Plane

A point in the phase space $(V_\perp, V_z, \phi)$ at which all of the time derivatives in the basic set of equations of motion, Eqs.(4.1) to (4.3), vanish is a singular point for the given simultaneous equations. Physically such a point represents an equilibrium state of the system under consideration. From Eqs.(4.1) to (4.3), we can find two functional relations between $V_\perp$ and V_z, which satisfy the condition of singular points for two particular values of ϕ as

$$V_z = - V_{ph} \frac{\Omega_e - \omega_r - (eE_w/mV_\perp)}{\omega_r + (eE_w/mV_\perp)} \quad , \qquad \text{for } \phi = 0 \ , \tag{4.8}$$

and

$$V_z = - V_{ph} \frac{\Omega_e - \omega_r + (eE_w/mV_\perp)}{\omega_r + (eE_w/mV_\perp)} \quad , \qquad \text{for } \phi = \pi \ . \tag{4.9}$$

The curves in Fig.74 corresponding to Eqs.(4.8) and (4.9) may be termed as "equilibrium curves". In this figure, the so-called Liapunov's criterion

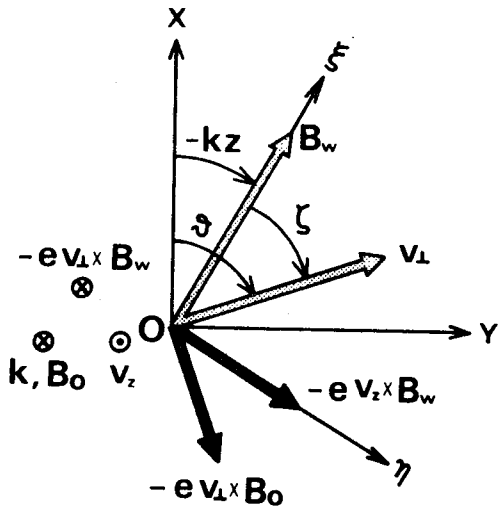

Fig.73 Wave Frame Coordinate and Three Lorentz Forces Acting on an Electron Running Antiparallel to $\vec{k}$.

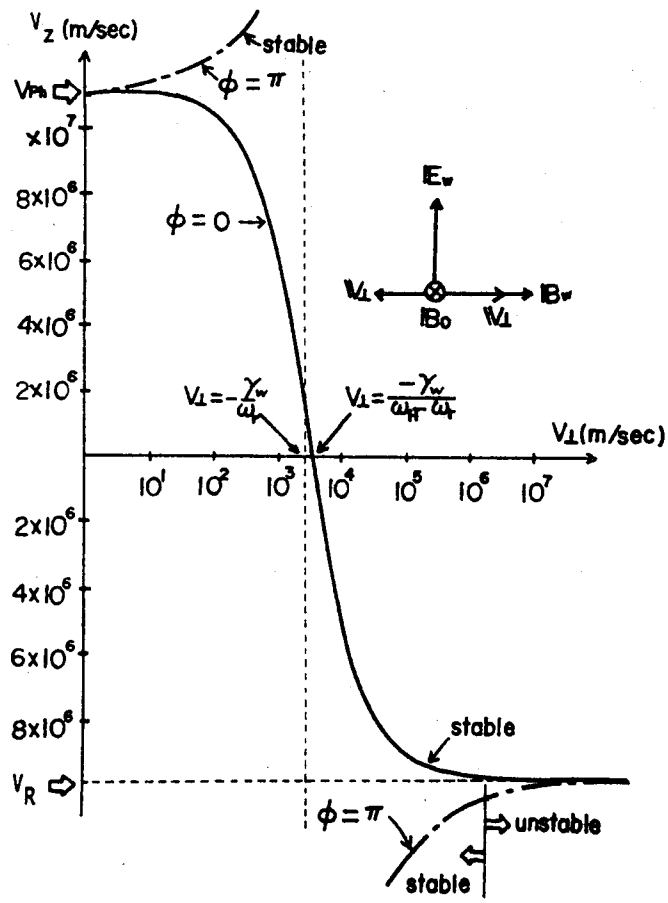

Fig.74 Equilibrium Curves for the Nonlinear Set of Equations of Motion of Electrons in the Field of a Whistler Mode Wave. γ_w in the figure is defined as $\gamma_w = -eE_w/m$. The result of Liapunov's criterion is also shown.

for the singular points (Mamiya[111]) is also shown.

As mentioned before, all the variables on the equilibrium curves remain constant. This is physically due to the fact that the total force seen by an electron with the equilibrium velocity $(V_\perp, V_z, \phi)$ vanishes. However, if the electron moves out from the stable equilibrium point, it is expected that the electron begins to oscillate due to a periodic change of force. The range of such a motion in the phase space depends on the initial condition.

It is noticed that the conditions for equilibrium coincide with the linear resonance condition,

$$\omega_r - kV_z - \Omega_e = 0 \quad , \tag{4.10}$$

if we tend $V_\perp$ to infinity. The transition from Eqs.(4.8) and (4.9) to Eq.(4.10) is obviously made by the condition

$$\frac{eE_w}{mV_\perp} << \Omega_e \quad . \tag{4.11}$$

Therefore a large $V_\perp$ or an enough small value of E_w makes it possible to neglect the nonlinear effect on the equilibrium conditions. As seen in Fig.74, the equilibrium conditions have another limit if we tend $V_\perp$ to zero. The limit is

$$V_z = V_{ph} \quad . \tag{4.12}$$

This is nothing but the expression for the longitudinal resonance, i.e., the condition for Landau resonance or Cerenkov radiation.

We can thus know that there exist two kinds of equilibrium state in the motion of electrons in the field of a whistler mode wave. One of them is always stable, the other is partly stable. The equiliblium conditions have two limits $V_z = V_R$ (< 0) and $V_z = V_{ph}$ (> 0) as $V_\perp \to \infty$ and $V_\perp \to 0$, respectively. Physically, the equilibrium conditions mentioned here approache to the linear resonance condition of the cyclotron and the Landau resonances as the motion of the electrons becomes purely circular or longitudinal.

2.2.2 State Plane Analysis

In this section, we consider the motion of electrons in the phase

space. Since the phase space is three dimensional, it may be more convenient to express the motion by two state planes. In our case, $(V_\perp - V_z)$ plane and $(\phi - V_\perp)$ plane are adopted. On each plane, it is found out (Bell[41]) that there exists a constant of motion as

$$C_1 = V_\perp^2 + (V_{ph} - V_z)^2 \quad , \tag{4.13}$$

on the $(V_\perp - V_z)$ plane and

$$C_2 = \pm V_{ph}\Omega_e\sqrt{C_1 - V_\perp^2} - \frac{1}{2}\omega_r V_\perp^2 - \frac{eE_w}{m} V_\perp \cos\phi \quad , \tag{4.14}$$

on the $(\phi - V_\perp)$ plane. Therefore, we can easily find a locus of the motion of electrons in each phase space. Examples of the computation of loci on the $(V_\perp - V_z)$ plane and the corresponding $(\phi - V_\perp)$ plane and illustrated in Fig.75. In the figure, C_1 is taken as a parameter and four kinds of C_1; C_{11}, C_{12}, C_{13} and C_{14} in increasing order are given.

From Fig.75, we can well extract the following prominent features in the nonlinear trajectories of electrons in the phase space. In the $(V_\perp - V_z)$ plane, electrons move along a circle determined by Eq.(4.13) so as to satisfy an energy conservation law in the wave frame. Different from $(V_\perp - V_z)$ plane, $(\phi - V_\perp)$ plane gives much more informations. As seen in the figure, there appears a "focus" around the corresponding equilibrium point indicated by dots or open circles. We thus know that some electrons with proper initial values are trapped in a limited phase ϕ around $\phi = 0$ and $\phi = \pi$. Of course, there also exists a separatrix, out of which electrons are not phase-trapped. This is the "phase trapping" appearing in the motion of electrons in the TEM wave which corresponds to a "potential trapping" in the case of the longitudinal plasma wave problem.

2.3 Phase Trapping and Phase Bunching

By the topological analysis, we have shown that there exists a phase-trapping in the problem of nonlinear motion of electrons in a TEM wave. The concept of the phase trapping is not original but there have been some works regarding with this subject recently as mentioned in the introduction of this chapter. It should be, however, noticed that most of papers dealing with the subject investigate the problem only in the phase space like done in the above. Therefore, as a natural result, we could not know

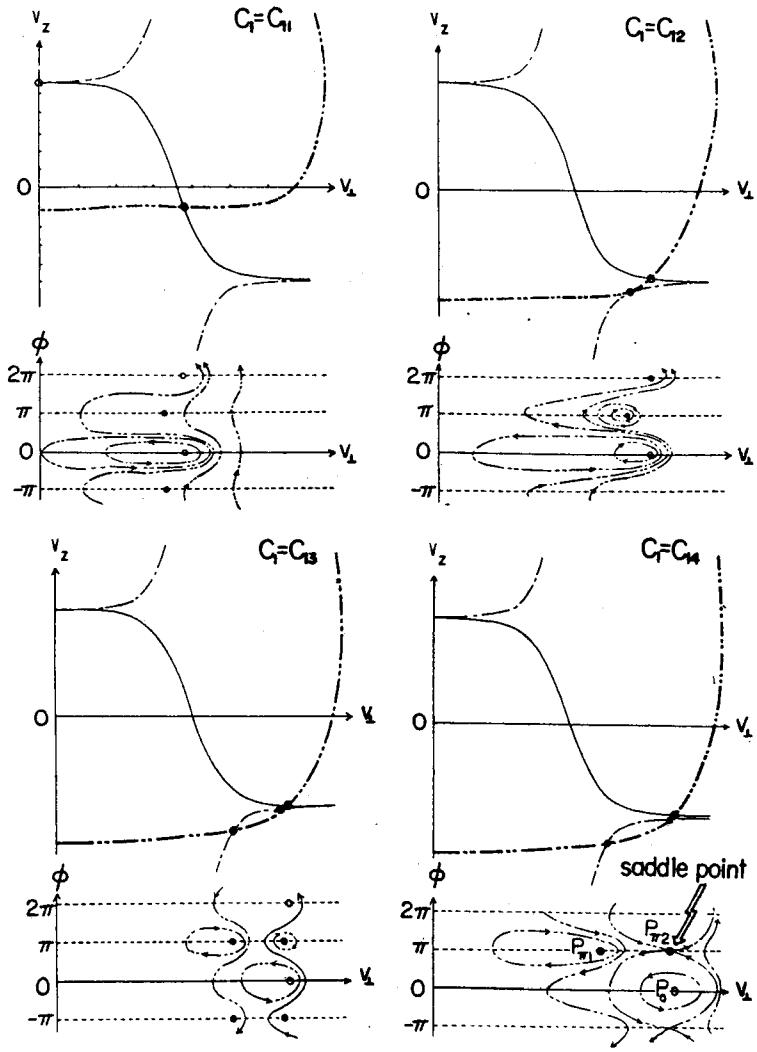

Fig.75 Characteristics of the Loci in the State Plane with C_1 Fixed to C_{11}, C_{12}, C_{13} and C_{14} in increasing order.

$V_\perp$ in the abscissa is measured in logarithmic scale so that the circle of Eq.(4.13) is much deformed.

how electrons behave temporally along these trajectories in the phase space or planes. Namely it is not considered rigorously when the phases of electrons are bunched as a function of time. Really, it is not expected that phases of phase-trapped electrons are bunched for a certain period. On the contrary, we could not say that phases of electrons out of the

separatorix, i.e., of non-phase-trapped electrons do not gather around together each other as time elapses. Consequently, the reaction to the original electromagnetic wave due to the resonant current formed by the electron motions is not simple. Then, the behavior of the phase ϕ of each electron as a function of time and its initial velocity is important. Though all electrons on the same locus on the phase plane experience the same trajectory but the instantaneous position on the locus is different for each electron, depending upon the different initial positions in the phase plane, i.e., different initial velocities.

Therefore, the concept of "phase bunching" should be introduced instead of the concept of "phase trapping" when a temporal behavior of each electron is of an interest. The terminologies of "phase bunching" and "phase trapping" should, thus, be used separately. Their physical meanings are quite different from each other.

§3. Two Types of Phase Bunching[54]

In this section, we will elucidate the characteristics of the phase bunching of electrons by a propagating whistler mode wave. As mentioned previously, we should inquire after a solution of the basic set of equations (4.1) to (4.3) or Eqs.(4.4) to (4.6) as an explicit function of time. These basic equations are, however, nonlinear so that we could not analytically obtain the exact solution. Therefore in this section we will consider two extreme cases by making proper assumptions. The exact solutions will be given later which were solved by a computer. For simplicity of both mathematical manipulation and physical consideration, we adopt the basic equations in the wave frame expressed by Eqs.(4.4) to (4.6) in this section.

3.1 $\vec{V}_\perp \times \vec{B}_w$-Phase Bunching*

In this section, we consider a special case in which the initial value $V_{\perp o}$ (the subscript o indicates initial values hereafter) of the perpendicular speed $V_\perp$ of the electron is so large that the change of $V_\perp$ can be

*) This type of the phase bunching is sometimes called "nonlinear phase bunching", but it is not proper because a linear treatment is possible as seen in the text in the case that $V_{\perp o}$ is large enough.

neglected and the third term in the r.h.s. of Eq.(4.6) can also be neglected comparing with the other terms. Thus the basic equations, in this case, become

$$V_\perp \simeq V_{\perp o} \quad , \tag{4.15}$$

$$\frac{dV_z}{dt} = \Omega_1 V_{\perp o} \sin\zeta \quad , \tag{4.16}$$

$$\frac{d\zeta}{dt} = \Omega_e + kV_z \quad . \tag{4.17}$$

Since the solution $\zeta = \zeta(t)$ of Eqs.(4.15) to (4.17) oscillates around $\zeta = \pi$, a transformation of ζ into ϕ which is equal to $\zeta + \pi$, is convenient, then

$$\frac{d\phi}{dt} = \Omega_e + kV_z \equiv k(V_z - V_R) \quad , \tag{4.18}$$

$$\frac{dV_z}{dt} = -\Omega_1 V_{\perp o} \sin\phi \equiv -kV_{\perp o} V_w \sin\phi \quad , \tag{4.19}$$

where $V_R = -\Omega_e/k$ is the resonance velocity in the wave frame and $V_w = \Omega_1/k$. Eliminating V_z from Eq.(4.18) and Eq.(4.19), we obtain the differential equation for ϕ as

$$\frac{1}{2}\left(\frac{d\phi}{dt}\right)^2 - k^2 V_{\perp o} V_w \cos\phi = \text{const.} \quad , \tag{4.20}$$

which is of the same form as the well known differential equation for a large amplitude pendulum motion.

The solution of Eq.(4.20) is then given by

$$\sin\frac{\phi}{2} = \sin\frac{\phi_m}{2}\, sn\left[\, sgn(V_{zo}-V_R)\, k\sqrt{V_{\perp o} V_w}\; t + Sn^{-1}\left(\frac{\sin\frac{\phi_o}{2}}{\sin\frac{\phi_m}{2}}\right)\right] \quad , \tag{4.21}$$

$$\text{for } 0 \leq |\phi_o| \leq \phi_{oL} \quad ,$$

or

$$\sin\frac{\phi}{2} = sn\left[\, sgn(V_{zo}-V_R)\, k\sqrt{V_{\perp o} V_w}\; Ct + Sn^{-1}\left(\sin\frac{\phi_o}{2}\right)\right] \quad , \tag{4.22}$$

$$\text{for } \phi_{oL} \leq |\phi_o| \leq \pi \quad ,$$

where sgn(0) ≡ 1 and sn[x] is the Jacobi function,

$$\phi_{oL} = \begin{cases} \cos^{-1}\{ \dfrac{(V_{zo}-V_R)^2}{2V_{\perp o}V_w} - 1\} & ; \text{ when } (V_{zo}-V_R)^2 \leqq 4V_{\perp o}V_w \ , \\ 0 & ; \text{ when } (V_{zo}-V_R)^2 \leqq 4V_{\perp o}V_w \ , \end{cases} \tag{4.23}$$

$$C = \sqrt{\sin^2\frac{\phi_o}{2} + \frac{(V_{zo}-V_R)^2}{4V_{\perp o}V_w}} \ . \tag{4.24}$$

The solutions (4.21) and (4.22) correspond to the case of the phase trapping and that of the phase rotation respectively. ϕ_m in Eq.(4.21) means the maximum amplitude of the phase oscillation of the phase-trapped electrons and is determined by

$$\phi_m = 2 \sin^{-1}C \ . \tag{4.25}$$

$Sn^{-1}(u)$ is the principal value of the inverse Jacobi function, i.e., $-K \leqq Sn^{-1}(u) \leqq K$ where K is the complete elliptic integral of the first kind. The modulus k_m of the sn-function in Eq.(4.21) and Eq.(4.22) determines the period of the phase oscillation by $k_m = C$ for the phase-trapped electrons in case of Eq.(4.21) and that of the phase rotation by $k_m = 1/C$ in case of Eq.(4.22).

Using the solutions (4.21) and (4.22), we can clarify some characteristics of the $\vec{V}_\perp \times \vec{B}_w$-phase bunching. In this procedure, we may have a more clear understanding by discussing the behavior of the resonant electrons, which are defined by $V_{zo} = V_R$, and the quasiresonant electrons, which are defined by $V_{zo} \gtrless V_R$, separately.

The resonant electrons are all phase trapped regardless of the initial phase angle ϕ_o since $\phi_m = |\phi_o|$ from Eq.(4.24) and Eq.(4.25), and $\phi_{oL} = \pi$ from Eq.(4.23). Using the relations $Sn^{-1}(\pm 1) = \pm K$ and $sn(u+2K) = -sn(u)$, the solution for the resonant electrons is simply expressed as

$$\sin\frac{\phi}{2} = \sin\frac{\phi_o}{2}\ sn[\ k\sqrt{V_{\perp o}V_w}\ t + K\ ] \ , \tag{4.26}$$

which indicates that the phase-time behavior is symmetric around $\phi = 0$ with the period T_o given by

$$T_o = 4K(\sin\frac{\phi_o}{2}) \Big/ k\sqrt{V_{\perp o}V_w} \ . \tag{4.27}$$

Thus the resonant electrons with same $V_{\perp o}$ are phase-bunched toward $\phi = 0$ as time elapses. However, the periods of the individual resonant electrons with different initial phase angles ϕ_o are different from each other as known from Eq.(4.27) and K vs. ϕ_o curve shown in Fig.76 so that an effective phase bunching is not to be expected. A vague phase bunching around $\phi = 0$ (or $\zeta = \pi$) is realized at a bunching time T_B, which is approximately given by $T_B \simeq T_o/4$, i.e.,

$$T_B \simeq \frac{2}{k\sqrt{V_{\perp o} V_w}} \quad . \tag{4.28}$$

A schematic illustration is depicted in Fig.77(b). It should be noticed that an efficiency of the phase bunching decreases in the next bunching period because the difference of the period becomes remarkable as time elapses.

The quasiresonant electrons, on the other hand, are classified into the phase-trapped electrons and the phase-rotating electrons according to the values of $V_{\perp o}$, V_{zo} and ϕ_o through Eqs.(4.21) to (4.23). All of the quasiresonant electrons satisfying the condition $|V_{zo}-V_R| \geqq 2\sqrt{V_{\perp o} V_w}$ are not phase-trapped but are phase-rotating regardless of the initial phase angle ϕ_o (or ζ_o). The quasiresonant electrons, which satisfy $|V_{zo}-V_R| \leqq 2\sqrt{V_{\perp o} V_w}$ and $|\phi_o| \leqq \phi_{oL}$ are phase-trapped, while those satisfying $|V_{zo}-V_R| \leqq 2\sqrt{V_{\perp o} V_w}$ and $|\phi_o| \geqq \phi_{oL}$ are phase-rotating. The period of the phase-trapped electrons is longer for larger $|\phi_o|$, while that of the phase-rotating electrons, on the contrary, becomes shorter for larger $|\phi_o|$. A symmetry around $\phi = 0$ of the ϕ-t curves as seen for the resonant electrons does not exist in this case. Noting the characteristics mentioned above, we can depict a schematic illustration of the phase behavior for the quasiresonant electrons with $V_{zo} > V_R$ and $V_{zo} < V_R$ as shown in Fig.77 (a) and (c) respectively. As easily understood, an efficiency of the phase bunching of the quasiresonant electrons is almost the same as that of the resonant electrons. The bunching angle, of course, departs from $\phi = 0$ for the quasiresonant electrons.

As discussed in the above, the $\vec{V}_\perp \times \vec{B}_w$-phase bunching is not so effective that the resultant resonant current is not expected to amount to a large value.

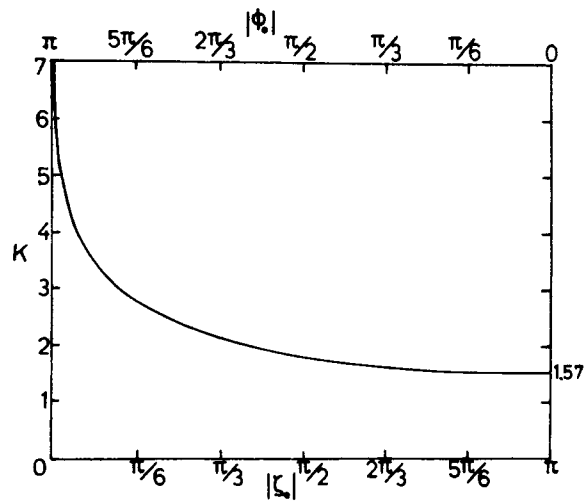

Fig.76 Complete Elliptic Integral (K) vs. Initial Phase Angle. The period T_o of the $\vec{V}_\perp \times \vec{B}_w$-phase bunching is given by $T_o = 4K/k\sqrt{V_{\perp o} V_w}$.

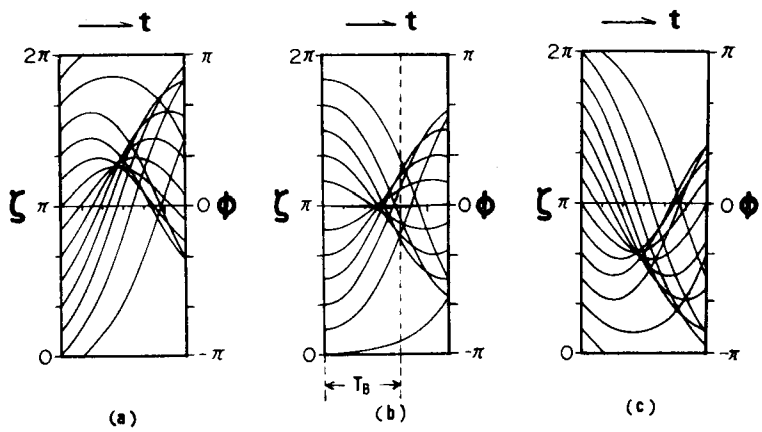

Fig.77 Schematic Illustration of the Phase Change due to $\vec{V}_\perp \times \vec{B}_w$-Phase Bunching;
(a) $V_{zo} > V_R$, (b) $V_{zo} = V_R$, (c) $V_{zo} < V_R$.

3.2 $\vec{V}_z \times \vec{B}_w$-Phase Bunching

In this section, we consider another case in which $V_{\perp o}$ is so small that the change of V_z by the Lorentz force $-e\vec{V}_\perp \times \vec{B}_w$ is negligible, i.e., $V_z \simeq V_{zo}$. Under this first-order approximation, the basic equations become

$$\frac{dV_\perp}{dt} = -\Omega_l V_{zo}\sin\zeta \equiv -kV_{zo}V_w\sin\zeta \quad , \tag{4.29}$$

$$\frac{d\zeta}{dt} = \Omega_e + kV_{zo} - \Omega_l\frac{V_{zo}}{V_\perp}\cos\zeta \equiv k(V_{zo} - V_R) - \frac{kV_{zo}V_w}{V_\perp}\cos\zeta \quad , \tag{4.30}$$

or equivalently

$$\frac{d}{dt}(V_\perp e^{j\zeta}) - jk(V_{zo} - V_R)V_\perp e^{j\zeta} = -jkV_{zo}V_w \quad . \tag{4.31}$$

Solutions of Eq.(4.31) are

$$V_\xi \equiv V_\perp\cos\zeta = \frac{V_{zo}V_w}{V_{zo}-V_R}\{1-\cos k(V_{zo}-V_R)t\} + V_{\perp o}\cos\{k(V_{zo}-V_R)t+\zeta_o\} \quad , \tag{4.32}$$

$$V_\eta \equiv V_\perp\sin\zeta = -\frac{V_{zo}V_w}{V_{zo}-V_R}\sin k(V_{zo}-V_R)t + V_{\perp o}\sin\{k(V_{zo}-V_R)t+\zeta_o\} \quad , \tag{4.33}$$

where V_ξ and V_η are the components of $\vec{V}_\perp$ in the directions of ξ axis and η axis shown in Fig.73. From Eq.(4.32) and Eq.(4.33), we get the expression for the temporal change of both $V_\perp$ and the phase angle ζ as follows.

$$\zeta = \tan^{-1}\left[\frac{V_{\perp o}\sin\{k(V_{zo}-V_R)t+\zeta_o\} - \frac{V_{zo}V_w}{V_{zo}-V_R}\sin k(V_{zo}-V_R)t}{V_{\perp o}\cos\{k(V_{zo}-V_R)t+\zeta_o\} + \frac{V_{zo}V_w}{V_{zo}-V_R}\{1-\cos k(V_{zo}-V_R)t\}}\right] , \tag{4.34}$$

and

$$V_\perp = \left[\,(V_{zo}V_w St)^2 - 2V_{zo}V_w\sin\{\frac{k(V_{zo}-V_R)}{2}t+\zeta_o\}St + V_{\perp o}^2\,\right]^{1/2} \quad , \tag{4.35}$$

where $S \equiv 2\sin\{k(V_{zo}-V_R)t/2\}/k(V_{zo}-V_R)t$ is the sampling function.
It should be noticed that the approximation made here is equivalent to the linear calculation discussed by Stix[25] except for $V_{\perp o} \neq 0$.

Using these solutions Eqs.(4.34) and (4.35), we can show characteris-

tics of this second type of phase bunching.

The phase change of the resonant electrons are described by

$$\zeta = \tan^{-1}\{ \tan\zeta_o - \frac{kV_wV_R}{V_{\perp o}\cos\zeta_o} t \} \quad , \tag{4.36}$$

which shows that ζ-t curves are symmetric around $\zeta = \pi/2$ and that all of the resonant electrons with different initial phase angle ζ_o are phase-bunched within the range of $|\zeta-\pi/2| < \Delta\zeta$ in a time T_B determined by

$$T_B = \frac{V_{\perp o}}{kV_w|V_R|} \tan\left(\frac{\pi}{2} - \Delta\zeta \right) \quad . \tag{4.37}$$

This bunching time is much shorter than that of the $\vec{V}_\perp \times \vec{B}_w$-phase bunching. For a numerical example, in the case that the resonant electrons with $V_{\perp o} = 10^4$m/s interact with a whistler mode wave of f = 10kHz, E = 1mV/m propagating through a plasma of f_p = 180kHz and f_H = 20kHz, we get $T_B \sim 8.5T$ for $\Delta\zeta = 2°$, while $T_B \sim 30T$ in the case that $V_{\perp o} = 10^7$m/s, where T is the period of the wave. A schematic illustration of the $\vec{V}_z \times \vec{B}_w$-phase bunching of the resonant electrons is given in Fig.78.

The change of $V_\perp$ of the resonant electrons is, given by

$$V_\perp = \sqrt{(V_wV_Rt - V_{\perp o}\sin\zeta_o)^2 + V_{\perp o}^2\cos^2\zeta} \quad , \tag{4.38}$$

which means that $V_\perp$ increases almost linearly with time. This is caused by the first-order approximation made in the above. When $V_\perp$ increases to much extent, the neglected Lorentz force $-e\vec{V}_\perp \times \vec{B}_w$ cannot be neglected since the phases are bunched around $\zeta = \pi/2$ at that time. Then a perturbation V_{z_1}, a difference of V_z from V_{zo}, should be taken into account.

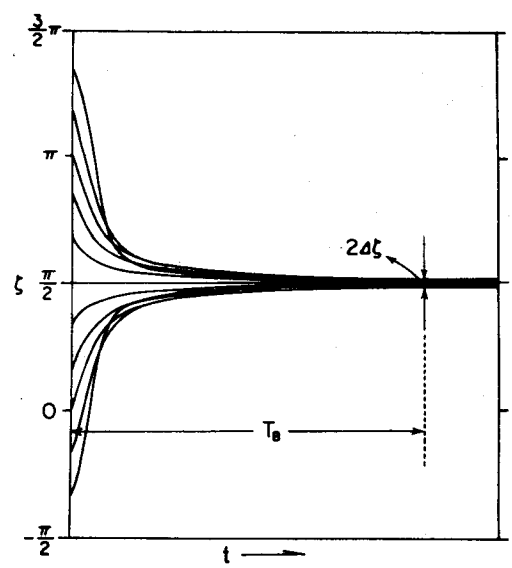

Fig.78 Schematic Illustration of the $\vec{V}_z \times \vec{B}_w$-Phase Bunching of Resonant Electrons.

When V_z changes from V_{zo}, a sum of the first and the second terms in Eq. (4.6) is most affected since we consider the nearly resonant electrons with $V_{zo} \simeq V_R$. Therefore, making a correction of V_{z1} only in the second term in Eq.(4.6), we get the following second-order approximation.

$$\frac{dV_\perp}{dt} = - kV_w V_{zo} \sin\zeta \quad , \tag{4.39}$$

$$\frac{dV_{z1}}{dt} = kV_w V_\perp \sin\zeta \quad , \tag{4.40}$$

$$\frac{d\zeta}{dt} = k(V_{zo}-V_R) + kV_{z1} - \frac{kV_{zo}V_w}{V_\perp} \cos\zeta \quad . \tag{4.41}$$

From these equations, we get

$$V_{z1} = - \frac{V_\perp^2 - V_{\perp o}^2}{2V_{zo}} \quad , \tag{4.42}$$

$$V_\perp \cos\zeta - V_{\perp o}\cos\zeta_o = \frac{V_\perp^2 - V_{\perp o}^2}{4V_{zo}V_w}\{ 2(V_{zo}-V_R) + V_{z1} \} \quad . \tag{4.43}$$

When $V_\perp$ is increased so as to satisfy $V_\perp >> V_{\perp o}$, Eq.(4.43) is well approximated for the resonant electrons as

$$V_\perp \cos\zeta - V_{\perp o}\cos\zeta_o = - \frac{V_\perp^4}{8V_w V_R^2} \quad . \tag{4.44}$$

Therefore, when the bunched phase angle ζ changes from $\pi/2$ due to a change of V_z so as to satisfy $|\cos\zeta| >> V_{\perp o}/V_\perp$, the second term in Eq.(4.44) can be neglected to yield

$$V_\perp = - 2(V_w V_R^2 \cos\zeta)^{1/3} \quad , \tag{4.45}$$

which shows that the bunched phase angle ζ changes so as to satisfy $\cos\zeta < 0$, i.e., to the direction, $\zeta=\pi$. Thus $V_\perp$ does not increase indefinitely with time but reaches a maximum value $V_{\perp max}$ given by

$$V_{\perp max} = 2(V_w V_R^2)^{1/3} \quad , \tag{4.46}$$

when $\zeta = \pi$. The perturbation V_{z1} is also maximized at the same time as

$$V_{z1} = 2(V_w^2 V_R^4 V_{zo}^{-3})^{1/3} \tag{4.47}$$

$$\simeq 2(V_w^2 V_R)^{1/3} \quad . \tag{4.47)'}$$

It should be noticed that a time-behavior of all resonant electrons is described universally by Eq.(4.45) and Eq.(4.46) regardless of their initial phase angles ζ_o and their initial perpendicular velocities $V_{\perp o}$. In Fig.79, a result of the rigorous numerical computation for different $V_{\perp o}$ is shown in the $V_\perp$-ζ polar coordinates. The end points of each trajectory in the figure show the $(V_\perp, \zeta)$ values at the same instance.

As for the quasiresonant electrons which satisfies $|V_{zo}-V_R| >> |V_{z1max}|$ or equivalently

$$|(V_{zo} - V_R)/V_R| >> 2(V_w/V_R)^{2/3} \quad , \tag{4.48}$$

the perturbation V_{z1} can be neglected so that the first-order approximation is effective. The change of the phase of the quasiresonant electrons is almost the same as the resonant electrons for small t, but is described approximately by

$$\zeta = \frac{k(V_{zo} - V_R)}{2} t + \frac{\pi}{2} \quad , \tag{4.49}$$

after a time when the first terms in both the numerator and the denominator in Eq.(4.34) can be neglected. Noting that $\zeta(t,\zeta_o) = -\zeta\{2\pi/k(V_{zo}-V_R)-t,-\zeta_o\}$ and $V_\perp(t,\zeta_o) = V_\perp\{2\pi/k(V_{zo}-V_R)-t,\zeta_o\}$ from Eqs.(4.34) and (4.35), we know the temporal behavior of $V_\perp$ and ζ of the quasiresonant electrons and their period T_o which is given by

$$T_o = \frac{2\pi}{k(V_{zo} - V_R)} \quad . \tag{4.50}$$

We can thus show a schematic illustration of the phase change for the quasiresonant electrons as shown in Fig.80. The maximum value $V_{\perp max}$ for the quasiresonant electrons which satisfy Eq.(4.48) is given by

$$V_{\perp max} = \frac{\pi V_w}{k} \left|\frac{V_{zo}}{V_{zo} - V_R}\right| \quad . \tag{4.51}$$

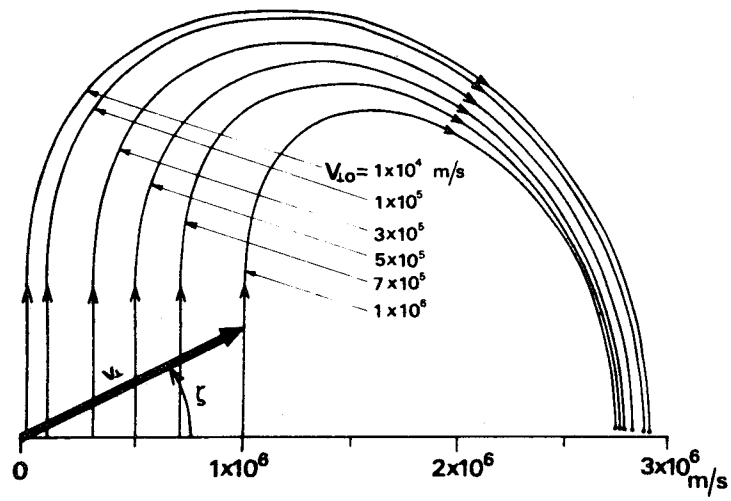

Fig.79 Polar Representation of the Locus of the Perpendicular Velocity $(V_\perp, \zeta)$ in Case of the $\vec{V}_z \times \vec{B}_w$-Phase Bunching.

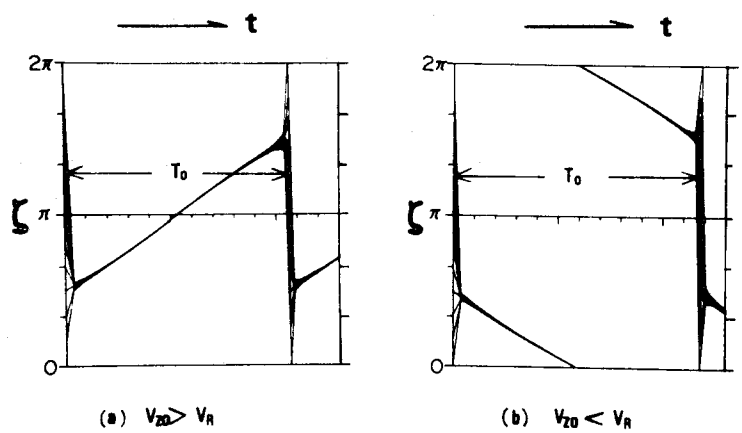

Fig.80 Schematic Illustration of the $\vec{V}_z \times \vec{B}_w$-Phase Bunching of Quasiresonant Electrons.

As clarified above, the $\vec{V}_z \times \vec{B}_w$-phase bunching is much more effective than the $\vec{V}_\perp \times \vec{B}_w$-phase bunching. Therefore, the resonant current is formed to much extent by the $\vec{V}_z \times \vec{B}_w$-phase bunching though $V_\perp$ is not large enough initially. The bunching angle due to this new type of the phase bunching is initially $\zeta = \pi/2$ and then changes slowly. Namely the resonant and the quasiresonant electrons are initially phase-bunched in the direction perpendicular to $\vec{B}_w$ and then the bunched phases and the perpendicular speed change slowly.

3.3 Discussion and Physical Interpretation

In the previous section, we have investigated a time behavior of an approximate solution of the nonlinear set of equations of motion. In spite of the mathematical approximation, it has been found that there are two types of phase-bunching. Furthermore, we can recognize that a simple drawing of the loci of trajectories in the phase space could not suggest the existence of these two types of phase bunching.

These bunchings are physically interpreted as follows. In the wave frame, forces acting on the electron are three Lorentz forces, $-e\vec{V}_\perp \times \vec{B}_o$, $-e\vec{V}_\perp \times \vec{B}_w$ and $-e\vec{V}_z \times \vec{B}_w$ as illustrated in Fig.73. The first Lorentz force $-e\vec{V}_\perp \times \vec{B}_o$ causes the cyclotron motion of the electron and corresponds to the first term in the r.h.s. of Eq.(4.6). The second Lorentz force $-e\vec{V}_\perp \times \vec{B}_w$ accelerates the electron in the direction parallel to $\vec{B}_o$ and changes V_z through Eq.(4.5) which, in turn, results in the phase change mainly by the second term in the r.h.s. of Eq.(4.6). The electron is accelerated along z-axis until the condition $\zeta = \pi$ is satisfied when the Lorentz force $-e\vec{V}_\perp \times \vec{B}_w$ vanishes. It should be noticed that even when ζ becomes π, the phase ζ continues to change through Eq.(4.6). Therefore, if $V_\perp$ is initially enough large, the third term in the r.h.s. of Eq.(4.6) can be neglected, which yields a result of oscillation of the phase ζ through an acceleration and decceleration of electrons along z axis. Consequently if the other Lorentz force $-e\vec{V}_z \times \vec{B}_w$ is negligibly small compared with the present Lorentz force $-e\vec{V}_\perp \times \vec{B}_w$, electrons which have initially random phases are phase-bunched in the antiparallel direction to the wave magnetic field $\vec{B}_w$. This is the qualitative physical interpretation for $\vec{V}_\perp \times \vec{B}_w$-phase bunching which was also discussed by Brice.

The third Lorentz force $-e\vec{V}_z \times \vec{B}_w$ is also responsible for changing the phase since it accelerates electrons in the plane perpendicular to $\vec{B}_o$ yielding the change of both the direction and the magnitude of the vector $V_\perp$. This effect is expressed by the third term in the r.h.s. of Eq.(4.6). In this case, the phase ζ changes until the condition $\zeta = \pi/2$ is satisfied, when $\vec{V}_\perp$ becomes parallel to the Lorentz force $-e\vec{V}_z \times \vec{B}_w$ so that the phase ζ can not be changed by this force. Therefore, the electrons are forced to be phase-bunched in the direction perpendicular to $\vec{B}_w$ by this acceleration, if the other Lorentz force $-e\vec{V}_\perp \times \vec{B}_w$ is to be neglected. This is the physical interpretation of another type of $\vec{V}_z \times \vec{B}_w$-phase bunching.

§4. Resonant Currents due to Phase Bunching

We have seen that the resonant and quasiresonant electrons with initially random phases are phase-bunched by the wave magnetic field, which, then, produces a resonant current. As discussed in the previous section, a contribution of electrons with small $V_{\perp o}$ is of the same order as that of electrons with large $V_{\perp o}$ since the $\vec{V}_z \times \vec{B}_w$-phase bunching is much more efficient than the $\vec{V}_\perp \times \vec{B}_w$-phase bunching. When, furthermore, a distribution function with respect to $V_{\perp o}$ is taken into account, the contribution of the $\vec{V}_\perp \times \vec{B}_w$-phase bunching to the resonant current becomes lesser since a population of the electrons decreases, generally, as $V_{\perp o}$ increases. We, therefore, show an approximate expression of the resonant current in this section by assuming that a perpendicular temperature $T_\perp$ of the nearly resonant electrons is so low that most of the resonant and quasiresonant electrons suffer from the $\vec{V}_z \times \vec{B}_w$-phase bunching. A more general calculation of the resonant current is to be shown by a numerical computation, which will be given in the next section.

As a distribution function $g_e(V_{\perp o}, V_{zo} \simeq V_R, \zeta_o)$ of the nearly resonant electrons may be symmetric around B_o, we can assume $\partial g_e/\partial \zeta_o = 0$, i.e., $g_e = g_e(V_{\perp o}, V_{zo})$. The resonant current density is, then, expressed as

$$J_i(t) = \frac{-N_e e \int_0^{2\pi} d\zeta_o \int_0^\infty V_{\perp o} dV_{\perp o} \int dV_{zo}\, g_e(V_{\perp o}, V_{zo}) v_i}{\int_0^{2\pi} d\zeta_o \int_0^\infty V_{\perp o} dV_{\perp o} \int_{-\infty}^{\infty} dV_{zo}\, g_e(V_{\perp o}, V_{zo})} , \qquad (4.52)$$

where the suffix i refers to ξ and η, N is the total electron number density and the integration over V_{zo} is taken around $V_{zo} = V_R$.

Substituting Eqs.(4.32) and (4.33) into Eq.(4.52), we get the following expressions after the integration over ζ_o.

$$J_\xi = - N_e e\Omega_1 \frac{\int dV_{zo} g_{eo}(V_{zo}) \frac{1-\cos(\Omega_e + kV_{zo})t}{\Omega_e + kV_{zo}} V_{zo}}{\int_{-\infty}^{\infty} g_{eo}(V_{zo}) dV_{zo}} \quad , \tag{4.53}$$

$$J_\eta = N_e e\Omega_1 \frac{\int dV_{zo} g_{eo}(V_{zo}) \frac{\sin(\Omega_e + kV_{zo})t}{\Omega_e + kV_{zo}} V_{zo}}{\int_{-\infty}^{\infty} g_{eo}(V_{zo}) dV_{zo}} \quad , \tag{4.54}$$

where $g_{eo}(V_{zo})$ is the integrated distribution function of $g_e(V_{\perp o}, V_{zo})$ over $V_{\perp o}$, i.e.,

$$g_{eo}(V_{zo}) = \int_0^\infty V_{\perp o} dV_{\perp o} g_e(V_{\perp o}, V_{zo}) \quad . \tag{4.55}$$

Transforming a variable V_{zo} to s through

$$\begin{aligned} s &= \Omega_e + kV_{zo} \quad , \\ ds &= kdV_{zo} \quad , \end{aligned} \tag{4.56}$$

Eqs.(4.53) and (4.54) can be expressed as

$$J_\xi = \frac{N_e e\Omega_e \Omega_1}{k} \frac{\int_{-\Delta s}^{\Delta s} g_{eo}(s) \frac{1-\cos(st)}{s} ds}{\int_{-\infty}^{\infty} g_{eo}(s) ds} \quad , \tag{4.57}$$

$$J_\eta = - \frac{N_e e\Omega_e \Omega_1}{k} \frac{\int_{-\Delta s}^{\Delta s} g_{eo}(s) \frac{\sin(st)}{s} ds}{\int_{-\infty}^{\infty} g_{eo}(s) ds} \quad , \tag{4.58}$$

where an approximation that

$$s - \Omega_e \simeq - \Omega_e \quad , \tag{4.59}$$

is made for electrons with $V_{zo} \simeq - \Omega_e/k$ ($\equiv V_R$), and Δs is the resonance width. Since the functions except $g_{eo}(s)$ in the integrands in Eqs.(4.57) and (4.58) are both peaky functions around $s = 0$, $g_{eo}(s)$ is approximately

expressed by the first two terms of the Taylor expansion as

$$g_{eo}(s) = g_{eo}(0) + \frac{dg_{eo}}{ds}\Big|_{s=0} s \quad . \tag{4.60}$$

Substituting Eq.(4.60) into Eqs.(4.57) and (4.58) and eliminating odd functions from the integrands, we get the following expressions.

$$J_\xi = \frac{N_r e\Omega_e \Omega_1}{k^2} \frac{dg_{eo}(s=0)}{ds} \int_{-\Delta s}^{\Delta s} \{1-\cos(st)\} ds \quad , \tag{4.61}$$

$$J_\eta = -\frac{N_r e\Omega_e \Omega_1}{k^2} g_{eo}(s=0) \int_{-\Delta s}^{\Delta s} \frac{\sin(st)}{s} ds \quad , \tag{4.62}$$

where

$$N_r \equiv \frac{\int_{-\Delta s}^{\Delta s} g_{eo}(s) ds}{\int_{-\infty}^{\infty} g_{eo}(s) ds} \quad , \tag{4.63}$$

is the number density of resonant electrons which have a parallel velocity V_{zo} of

$$-\frac{\Omega_e + \Delta s}{k} \leq V_{zo} \leq -\frac{\Omega_e - \Delta s}{k} \quad . \tag{4.64}$$

Noting that

$$\frac{dg_{eo}}{ds}\Big|_{s=0} = \frac{1}{k} \frac{dg_{eo}(V_R)}{dV_{zo}} = -\frac{\Omega_e}{V_R} \frac{dg_{eo}}{dV_{zo}}(V_R) \quad , \tag{4.65}$$

integration of Eqs.(4.61) and (4.62) yields the following final expressions.

$$J_\xi(t) = N_r e \frac{\Omega_1}{\Omega_e} V_R^2 \frac{dg_{eo}}{dV_{zo}}(V_R)(2\Delta V_R)\{1 - \frac{\sin(k\Delta V_R t)}{k\Delta V_R t}\} \quad , \tag{4.66}$$

$$J_\eta(t) = -2N_r e \frac{\Omega_1}{\Omega_e} V_R \, g_{eo}(V_R) V_R Si(k\Delta V_R t) \quad , \tag{4.67}$$

where

$$Si(x) = \int_0^x \frac{\sin x}{x} dx \quad , \tag{4.68}$$

and ΔV_R is the spread of resonance velocity.

If the following approximation

$$k\Delta V_R t \ll 1 \quad , \tag{4.69}$$

is possible, Eqs.(4.66) and (4.67) are simply represented as

$$J_\xi(t) = \frac{N_r e}{3}\frac{\Omega_1}{\Omega_e} k^2 V_R^2 \frac{dg_{eo}}{dV_{zo}}(V_R)(\Delta V_R)^3 t^2 \quad , \tag{4.70}$$

$$J_\eta(t) = -2N_r e \frac{\Omega_1}{\Omega_e} k V_R g_{eo}(V_R) V_R \Delta V_R t \quad . \tag{4.71}$$

As seen in the expressions J_ξ and J_η start to increase parabolically and linearly with time, respectively.

It should be noticed that the expressions Eqs.(4.66) and (4.67) are only effective in a short time after the interaction begins since we used the results Eqs.(4.32) and (4.33) for V_ξ and V_η which are derived from the first-order (linear) approximation as mentioned in the previous section. Thus we can conclude that a resonant current flows first in the η-direction perpendicular to $\vec{B}_w$ unless a gradient $dg_{eo}/dV_{zo}\big|_{V_{zo}=V_R}$ is much steep.

Transforming the coordinate (ξ,η) into (x,y) by

$$J_x(z,t) = J_\xi \cos kz + J_\eta \sin kz \quad , \tag{4.72}$$

$$J_y(z,t) = -J_\xi \sin kz + J_\eta \cos kz \quad , \tag{4.73}$$

we can get the feedbacked magnetic fields H_{fx} and H_{fy} as

$$H_{fx} = \int J_y dz \quad , \tag{4.74}$$

$$H_{fy} = \int -J_x dz \quad , \tag{4.75}$$

where it is assumed that $\vec{H}_f$ is again a plane field. Substituting Eqs.(4.72) and (4.73) into Eqs.(4.74) and (4.75),

$$H_{fx} = \frac{J_\xi}{k}\cos kz + \frac{J_\eta}{k}\sin kz \quad , \tag{4.76}$$

$$H_{fy} = -\frac{J_\xi}{k}\sin kz + \frac{J_\eta}{k}\cos kz \quad , \tag{4.77}$$

and

$$H_f^2 = H_{fx}^2 + H_{fy}^2 = \frac{1}{k^2}\left(J_\xi^2 + J_\eta^2 \right) \quad . \tag{4.78}$$

We thus can estimate the feedbacked field intensity due to the resonant current which is brought about by the $\vec{V}_z \times \vec{B}_w$-phase bunching. However, it should be noticed that this result is effective only in the early stage of the interaction.

§5. Numerical Computation of Nonlinear Phase Bunching and Resonant Currents

5.1 Efficiency of Phase Bunching

A rigorous numerical computation of the nonlinear basic equations (4.4) to (4.6) is performed for various $V_{\perp o}$, V_{zo} and ζ_o in order to see a behavior of the phase and the perpendicular velocity $V_\perp$ and the parallel velocity V_z. An observation is also made on the formation of the resonant current for each initial speed $(V_{\perp o}, V_{zo})$. Selecting 36 different values of the initial phase ζ_o uniformly distributing between $\zeta_o = 0$ to 2π for each fixed parameter $(V_{\perp o}, V_{zo})$, a calculation of

$$I_\xi(V_{\perp o}, V_{zo}, t) = - e \sum_{i=1}^{36} V_{\perp i} \cos\zeta_i \ , \tag{4.79}$$

$$I_\eta(V_{\perp o}, V_{zo}, t) = - e \sum_{i=1}^{36} V_{\perp i} \sin\zeta_i \ , \tag{4.80}$$

is made for $0 \leq t \leq 200T$ where suffix i refers to different electrons with different initial phases ζ_o. For the velocity parameters, three kinds of V_{zo} were selected as $V_{zo} < V_R$, $V_{zo} = V_R$ and $V_{zo} > V_R$ and $V_{\perp o}$ was chosen as five values of $V_{\perp o} = 10^4$, 10^5, 10^6, 5×10^6 and 10^7 m/s. The results of the computation are shown in Fig.81 on the phase change and in Fig.82 on the change of I_ξ and I_η for 15 combined parameters $(V_{\perp o}, V_{zo})$. Plasma and wave parameters used in the computation were typical values of the whistler mode waves propagating in the magnetosphere. These values are given in the figure captions.

As seen in Fig.81, the $\vec{V}_z \times \vec{B}_w$-phase bunching is brought with high efficiency for small $V_{\perp o}$, and $\vec{V}_\perp \times \vec{B}_w$-phase bunching is, on the contrary, seen for large $V_{\perp o}$. A transient change from the $\vec{V}_z \times \vec{B}_w$-phase bunching

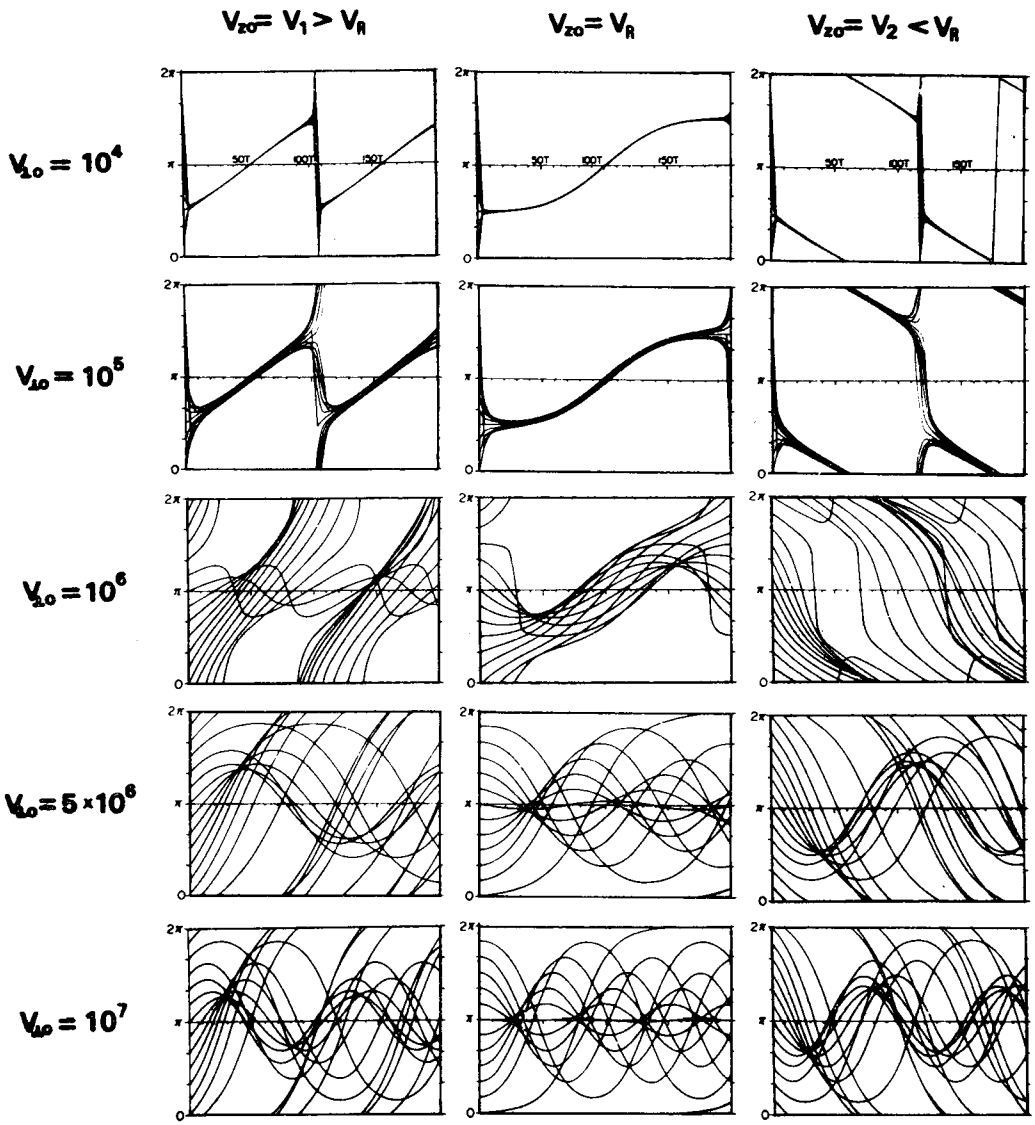

Fig.81 Phase Change with Time for Various Initial Speeds ($V_{\perp o}$,V_{zo}). Computations were done for $0 \leq t \leq 200T$ under the following parameters; f_p = 180kHz, f_H = 20kHz, $f \equiv 1/T$ = 10kHz, $V_R = -3.328 \times 10^7$m/s, $V_1 = -3.314 \times 10^7$m/s and $V_2 = -3.344 \times 10^7$m/s. Plottings are made for 12 different initial angles, one in every $\pi/6$ in each figure.

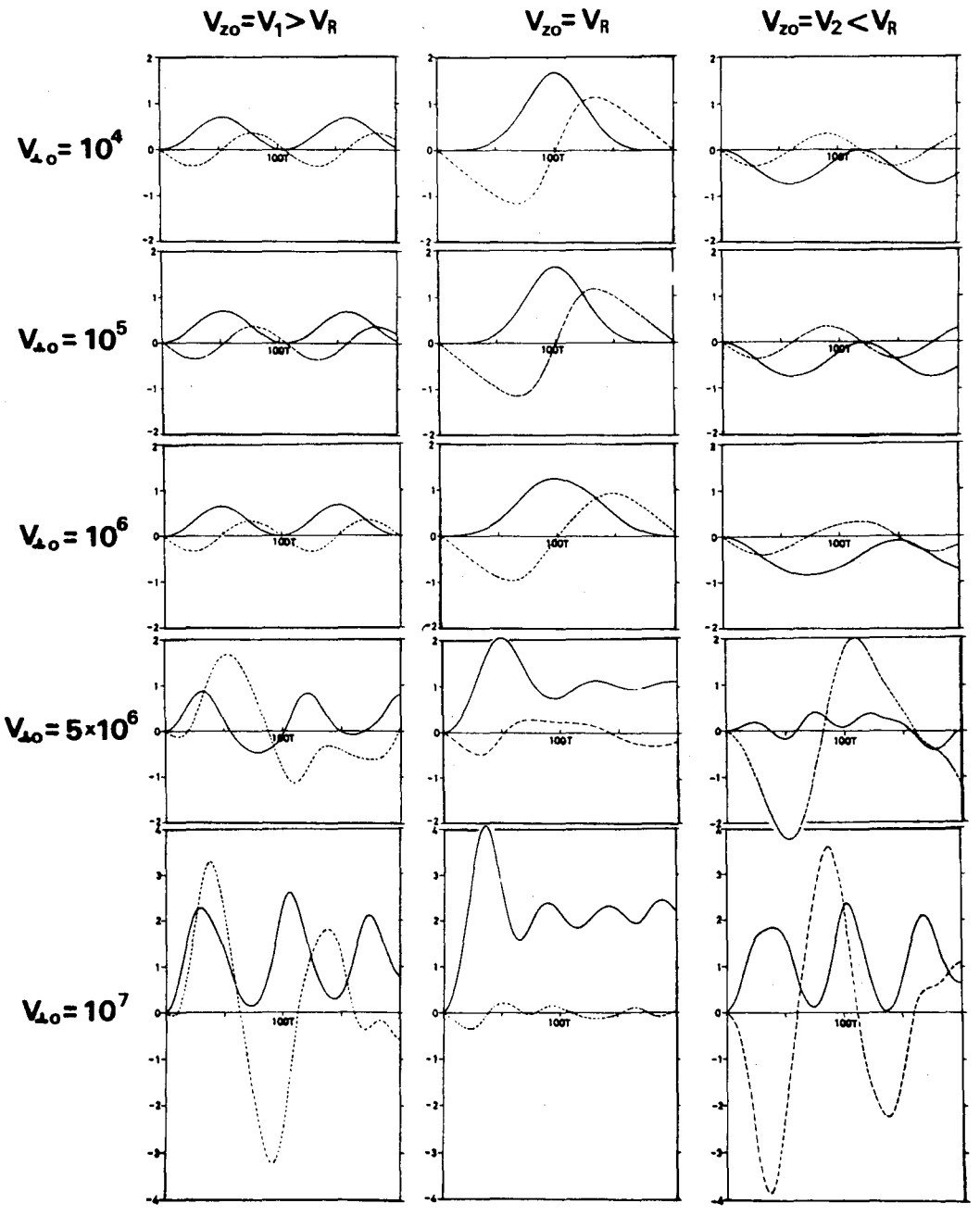

Fig.82 Corresponding Resonant Current due to the Phase Bunching in Fig.81. Solid and dashed lines indicate I_ξ and I_η, respectively.

to the $\vec{V}_\perp \times \vec{B}_w$-phase bunching is also observed. Specific characteristics of each phase bunching seen in Fig.81 coincide well with those discussed by analytical speculations in the previous section. Fig.82 indicates a corresponding resonant current formed by 36 electrons due to the phase bunching. Comparing the cases of $V_{\perp o} = 10^4$m/s and of $V_{\perp o} = 10^7$m/s, we can confirm the low efficiency of the $\vec{V}_\perp \times \vec{B}_w$-phase bunching since the resonant current by the $\vec{V}_\perp \times \vec{B}_w$-phase bunching is only 2 to 4 times that by the $\vec{V}_z \times \vec{B}_w$-phase bunching in spite of the 1000 times initial values of $V_{\perp o}$. It is interesting to note that the time-behaviors of the resonant currents I_ξ and I_η do not depend upon $V_{\perp o}$ for $V_{\perp o} = 10^4$ to 10^6m/s and show a resonant character. Namely I_i $(i=\xi,\eta)$ is maximum at $V_{zo} = V_R$ and decreases as V_{zo} departs from V_R with increasing its period. As predicted analytically, I_η precedes I_ξ for small t in the case of small $V_{\perp o}$. On the contrary, in the case of $V_{\perp o} = 5\times10^6$ and 10^7m/s, the perpendicular current $I_\perp = (I_\xi^2 + I_\eta^2)^{1/2}$ does not show a peaky resonant character since I_η becomes minimum at $V_{zo} = V_R$ though I_ξ shows a broad resonant character. It should be noticed that the current due to the $\vec{V}_\perp \times \vec{B}_w$-phase bunching shows a nonperiodic behavior as seen in the case of $V_{\perp o} = 5\times10^6$ and 10^7m/s in Fig.80. This is due to the fact that the period of each electron differs from each other since the period is dependent on the initial phases ζ_o.

5.2 Computation of Resonant Current due to Phase Bunching

Taking a velocity distribution function $H_e(V_{\perp o})$ as a loss cone distribution function given by

$$H_e(V_{\perp o}) = \frac{N_e}{\pi\Gamma(n+1)}\left(\frac{m}{2\kappa T_\perp}\right)^{n+1} V_{\perp o}^{2n} \exp\left(-\frac{mV_{\perp o}^2}{2\kappa T_\perp}\right) , \tag{4.81}$$

a numerical integration over $V_{\perp o}$ on the resonant current was performed by calculating the nonlinear equations of motion (4.3) to (4.6) for 30 values of $V_{\perp o}$ ($V_{\perp o} = 10^4$ to 10^7m/s) and 12 values of ζ_o, where the parameter n indicates an anisotropic index and Γ is the gamma function. The result of the computation of

$$\delta J_i(V_{zo},t) = \frac{2\pi}{12}\int_0^\infty V_{\perp o} dV_{\perp o} H_e(V_{\perp o})\ I_i(V_{\perp o},V_{zo},t) , \quad (i=\xi,\eta) \tag{4.82}$$

is shown in Fig.83, where $g_e(V_{\perp o}, V_{zo}) = H_e(V_{\perp o}) \cdot G_e(V_{zo})$. Calculations were done for a parameter of $T_\perp = 10^4$°K and n = 0. Comparing Fig.83 with Fig.82, we can conclude that a contribution of the $\vec{V}_\perp \times \vec{B}_w$-phase bunching is little for a perpendicular temperature of the order of 10^4°K. It is also interesting to note that the component of the resonant current parallel to $\vec{B}_w$, δJ_ξ (shown by solid lines in the figure), changes its sign as V_{zo} passes V_R, while the component δJ_η perpendicular to $\vec{B}_w$ does not show a change of sign on both sides of the resonance velocity V_R. Therefore, an integration over V_{zo}, which gives the final real resonant current density formed by the nonlinear wave-particle interaction, will result in a tendency that the resonant current flows initially in the direction perpendicular to $\vec{B}_w$. This means that a current formation is strongly controlled by the $\vec{V}_z \times \vec{B}_w$-phase bunching at least in the first stage of the interaction. The integration over V_{zo} is performed by calculationg $\delta J_i(V_{zo}, t)$ for 11 different

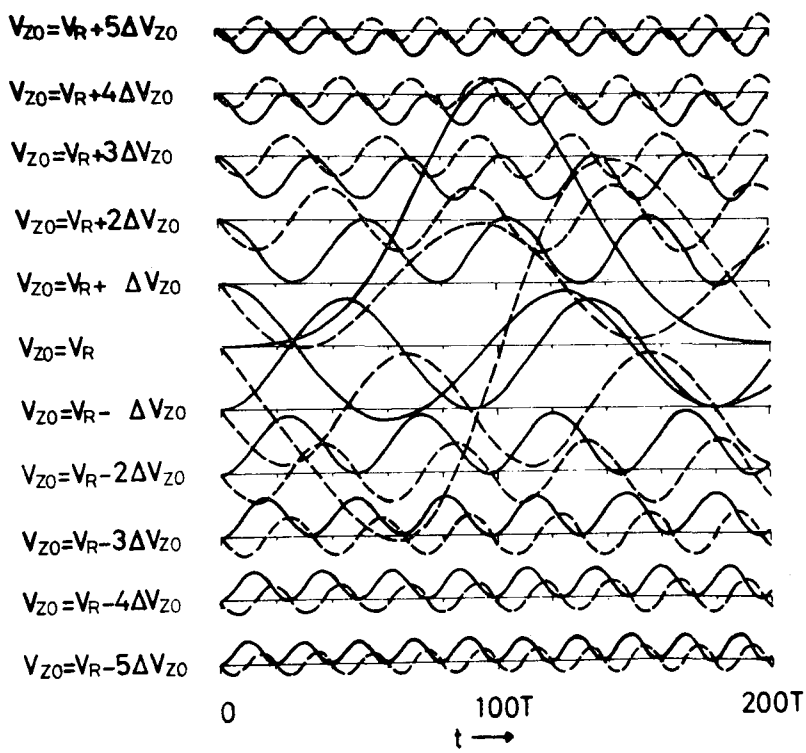

Fig.83 Integrated Resonant Current $\delta J_i(V_{zo}, t)$ over $V_{\perp o}$ $(i=\xi,\eta)$ under the Maxwell Distribution Function. Solid and dashed lines correspond to δJ_ξ and δJ_η, respectively.

values of V_{zo} within ±5 % around V_R. Computations were carried out by assuming a shifted Maxwellian distribution function for nearly resonant electrons as

$$G_e(V_{zo}) = \{\frac{m}{2\pi K T_{||}}\}^{\frac{1}{2}} \exp\{-\frac{m(V_{zo}-V_B)^2}{2K T_{||}}\} \quad . \tag{4.83}$$

The final results of the integration

$$J_i(t) = \int_{V_R-\Delta V_R}^{V_R+\Delta V_R} dV_{zo}\, G_e(V_{zo})\, \delta J_i(V_{zo},t) \quad , \qquad (i=\xi,\eta) , \tag{4.84}$$

were shown in Fig.84 for three cases of $V_R < V_B$, $V_R = V_B$ and $V_R > V_B$ by varying the perpendicular temperature $T_\perp$ as $T_\perp = 10^4$°K, 5×10^4°K and 10^5°K in each case. As seen in Fig.84, J_ξ and J_η increase initially parabolically and linearly with time respectively, as shown by the analytical calculation Eq.(4.70) and Eq.(4.71). The maximum value of J_η is of the same order as that of J_ξ. This means physically that the resonant current J_η plays a more important role than the resonant current J_ξ in a self-consistent nonlinear theory because J_η reaches its maximum value earlier than J_ξ. This is the case when we consider an interaction between energetic electrons and a whistler mode wave propagating in the magnetospheric plasma with $T_\perp$ of the order of 10^4 to 10^5°K. This tendency was also confirmed by a further calculation in which the parameter n in the distribution function Eq.(4.81) is changed from 0 to unity, i.e., when the distribution function is changed from the Maxwellian to the loss cone distribution. The results are depicted in Fig.85.

§6. Discussion and Conclusions

In this chapter, we have investigated physically some of the characteristics of the phase bunching of electrons due to the interaction with a whistler mode wave, which is believed to be essential in the generation mechanism of the VLF emissions triggered by a monochromatic wave. The nonlinear motion of electrons in a large amplitude electromagnetic wave has been studied so far mainly in the phase domain yielding a concept of the phase trapping similar to the potential trapping in the electrostatic

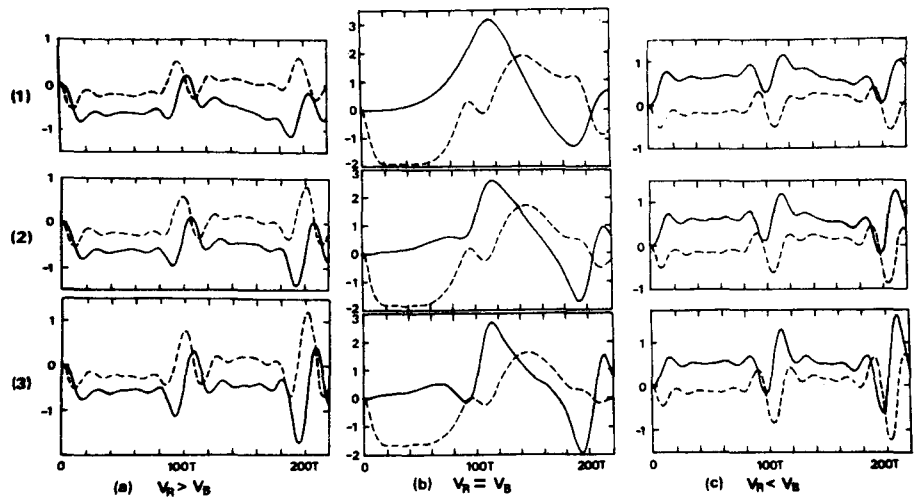

Fig.84 Temporal Behavior of Resonant Current $J_\xi(t)$ and $J_\eta(t)$ —(I)—.
Distribution function is taken as Maxwellian.
(1) $T_\perp = 1\times10^{4}$°K, (2) $T_\perp = 5\times10^{4}$°K, (3) $T_\perp = 1\times10^{5}$°K.

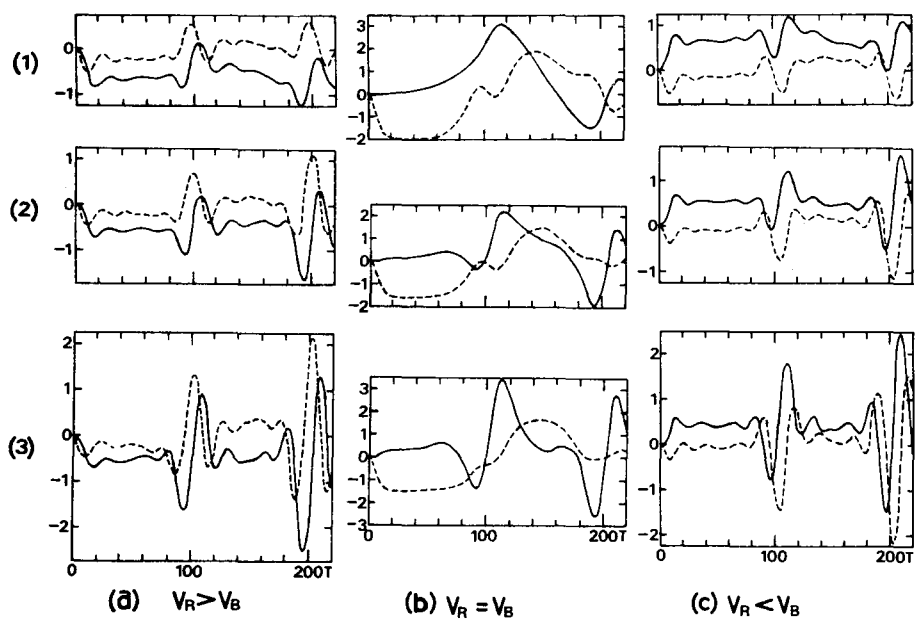

Fig.85 Temporal Behavior of Resonant Current $J_\xi(t)$ and $J_\eta(t)$ —(II)—.
Distribution function is taken as a loss cone distribution function with n = 1.
(1) $T_\perp = 1\times10^{4}$°K, (2) $T_\perp = 5\times10^{4}$°K, (3) $T_\perp = 1\times10^{5}$°K.

case. The concept of the phase bunching is similar to that of the phase trapping but is different in the sense that it deals with the temporal behavior of phases and of its resultant resonant currents. We have investigated both of the phase-trapping by a topological study and the phase-bunching by solving the nonlinear equations of motion analytically with some assumptions as well as numerically. As a result, we have realized a significant difference between the concept of the phase-trapping and that of the phase-bunching.

We have also shown that the phase bunching due to the whistler mode wave can be classified by its mechanism into two types and both are explained physically and analytically. They are termed as $\vec{V}_{\perp} \times \vec{B}_{w}$-phase bunching and $\vec{V}_{z} \times \vec{B}_{w}$-phase bunching according to the main force leading to the phase bunching, respectively. The former is that proposed by Brice[38,39], and the latter is newly pointed out in the present chapter. Numerical computations were carried out on the change of the phase and the perpendicular velocity of resonant electrons with verious initial velocities. By taking a plasma distribution function into account, resonant currents due to the phase bunching were calculated, and it is pointed out that the second type of phase bunching is more important for the usual distribution functions.

In the theory of the trapped particle instability, the nonlinear orbits of electrons determined by the original wave are, so far, used to search for an instability condition and the growth rate in such a system. However, we think that such a method is not to be applicable to the case that emissions newly generated by the instability grow up to the same order of amplitude as that of the original wave and the nonlinear orbits themselves are modified strongly by the newly generated wave field.

On the other hand, as an extention of the analysis presented in this chapter, there is a method which is to trace the time evolution of the total wave field by taking account of a feedback by the resonant currents or charges formed by the nearly resonant particles that, in turn, are governed by the instantaneous total wave field. When a time evolution of the wave field is slow comparing with the wave frequency, it may be possible to find analytical expressions for the change of the wave field and its frequencies, though this analysis will be accompanied with considerable difficulties. It is also possible to do a computer simulation experiment on this problem. Though both approaches are very much interesting,

they will be given in the future. In such a theory and a computer simulation, there exists a case in which the second type of the phase bunching pointed out in the present chapter plays an essential role.

Chapter V

DISCUSSION AND CONCLUDING REMARKS

§1. Summary and Conclusions

In this thesis, we have made a theoretical investigation on the linear and nonlinear wave-particle interactions in the whistler mode with a view to applying it to the problem of the magnetospheric wave phenomena, especially VLF emissions.

In Chapter II, linear analyses of the whistler mode cyclotron instability have been made on three main problems.

Firstly, a whistler mode beam cyclotron instability has been studied quantitatively with a special attention on its convective characteristics. After the idea originally proposed by Kimura[26] that the drifting mechanism of the moving oscillator which generates VLF emissions could be attributed to this convective beam cyclotron instability, a frequency change of the generated emissions has been numerically calculated using the obtained drift velocity of the instability region. The calculated frequency spectra show a good agreement with the observed spectra of VLF emissions.

Secondly, we have investigated on the propagation velocity of waves in the plasma-beam system which manifests a whistler mode beam cyclotron instability. In this system, a dispersion equation gives an abnormal group velocity which exceeds the light speed for some frequency range. Numerical computations have been carried out on the response of a signal in the system in real time and space by the inverse Fourier-Laplace transformation method. From the results, we have clarified some characteristics of the wave propagation in such an abnormally dispersive and unstable medium. It is found that the most unstable wave grows up and propagates with a velocity which is smaller than c if a terminated current source is imposed to the system. This velocity changes temporally depending on the amplitude from an initial group velocity of an unperturbed

whistler mode wave in a beamless plasma to a final group velocity which is determined on the modified whistler mode branch for a frequency giving a maximum growth rate on the dispersion curve.

Thirdly, a whistler mode instability due to an anisotropic distribution function is quantitatively investigated assuming various distribution functions which are plausible in the magnetosphere. It was clarified that prominent features of the whistler triggered emissions are well explained by the whistler mode cyclotron instability due to the anisotropic "triple-structured" loss cone distribution function composed of thermal, quasithermal and beam plasmas.

In Chapter III, a nonlinar analysis of the whistler mode cyclotron instability has been investigated by the quasilinear treatment. We have shown that a basic set of quasilinear equations for the whistler mode cyclotron instability is quite derivable only by a physical consideration on the essential point of the quasilinear theory. A proposal is then made for the explanation of the generation mechanism of the triggered emissions by this quasilinear cyclotron instability. Based upon this idea, two dimensional numerical computations have been performed in order to simulate both the whistler triggered emissions (WTE-H) and the artificially stimulated emissions (ASE). Both of the results have satisfactorily explained the peculiar features of the WTE-H and ASE which could not be explained by the linear theory. We are now convinced that such a quasilinear effect as considered in the present thesis plays an essential role in the process of the wave-particle interactions in the magnetosphere.

In Chapter IV, a study has been given on the nonlinear interaction between particles and a whistler mode monochromatic wave. The nonlinear behavior of individual electrons in the wave field and the resultant resonant currents have been investigated both analytically and numerically. It has been emphasized that the so-called phase bunching is different rigorously from the phase trapping. It has also been shown that the phase bunching can be classified into two types by its mechanism. One is the $\vec{V}_\perp \times \vec{B}_w$-phase bunching which was first pointed out by Brice[38,39] and the other is the $\vec{V}_z \times \vec{B}_w$-phase bunching which is newly pointed out in the present thesis. It has been shown that the $\vec{V}_z \times \vec{B}_w$-phase bunching plays an important role when a perpendicular temperature of plasma is of the

order of 10^5°K or below in the magnetospheric circumstances.

In conclusion, several quantitative aspects of the whistler mode wave-particle interactions have been clarified in both linear and nonlinear regimes. They are, then, applied successfully to the elucidation of the generation mechanisms and characteristics of VLF emissions in the magnetosphere. We hope that this work would contribute more or less to the development of the magnetospheric physics and the plasma physics.

§2. Suggestions for the Experiments Related with the Present Work

Though there have been many theoretical works including the present thesis about the whistler mode wave-particle interactions, only a few corresponding experiments have so far been made. One reason is that a laboratory experiment is inconvenient to treat VLF electromagnetic wave phenomena, because the size of the experimental equipment is too small compared with the wave length. The other reason is that the radiation efficiency of antennas is very small for low or very low frequency electromagnetic waves so that a big antenna should be built on the ground if we wish to do a more controlled experiment in the VLF range similar to the transmitter-receiver system actually yielding the ASE phenomena. In spite of these difficulties, experimental works are eagerly desired and hence some suggestions on future experiments both in space and laboratory will be mentioned briefly below.

2.1 Experiments in Space

Controlled experiments in the midst of the space plasma using space vehicles like the Alouette topside sounder are recommended and some rocket and satellite experiments have already been performed. In the satellite REXS (Radio Exploration Satellite) which was lauched on August 19 in 1972, and was named "Denpa", an active experiment named CIE (Cyclotron Instability Experiment) was on board which is one of our projects of an artificial triggering of the whistler mode cyclotron instability by a pulse transmission at frequencies below the cyclotron frequency in the vicinity of the satellite or at the equator on the geomagnetic line of force passing

through the satellite. This project unfortunately ended on the third day after lauching by unexpected troubles in the satellite, but some interesting data for three days were obtained although they will not be given here and will be published in another place (Kimura, Matsumoto & Miyatake[115]). REXS-CIE was a primitive and preparatory active experiment and a more cultivated active experiment is strongly recommended in order to collect many informations on the nonlinear cyclotron instabilities. In this case, however, another important point should be kept in mind, that is, electrostatic instabilities may be excited in addition to the electromagnetic whistler mode instability at the same time.

2.2 Experiments in the Laboratory

If it is possible to make an experiment of the whistler mode wave-particle interactions in the laboratory, it is no doubt that it contributes much to the progress of the subject. Experiments in actual space plasmas have several advantages such as a vast scale and a comparatively stable state of the plasma but on the contrary have a disadvantage that there is a rare chance of experiments and many restrictions are involved which come from the instrumentation on board. In order to overcome this disadvantage, it is desired to contrive a laboratory experiments on the whistler mode instability. Though there are a few experiments on the propagation of the whistler mode waves, there has been no experiments on the wave-particle interactions in the whistler mode as far as we know. A planning and design on such an experiment is now under progress (Matsumoto, Kimura & Mamiya[116]; Hashimoto, Matsumoto, Kimura & Kawashima[117]). We are very much anxious for a success of such an experiment.

§3. Suggestions for Further Theoretical Works

In the present thesis, we have studied only a simple case of the interaction between whistler mode waves which propagate along the external

magnetic field and particles in the homogeneous plasma. As an extension of the study, inhomogeneity of the background plasma and an oblique propagation to the external magnetic field should be taken into account. Though these two factors make the problem much more complicated than the present work, it is desirable to perform an investigation from linear to nonlinear stages.

As a directly extended work for a more deep understanding of ASE or triggering of the instability, it is hopeful to do a computer simulation based upon the discussion given in Chapter IV. It will give us many informations that could not be obtained by the quasilinear computations which are based on the delta-function model of resonance.

Appendix A

Derivation of the Dispersion Equation and the Growth rate in the Whistler Mode

Though it is well known how to derive the dispersion equation and the expression for the growth rate in the linear theory, we present the procedure here for completeness.

The basic equations are the Vlasov and the Maxwell equations which are written as

$$\frac{\partial F_s}{\partial t} + \vec{V}\cdot\frac{\partial F_s}{\partial \vec{r}} + \frac{q_s}{m_s}\{\vec{E} + \vec{V}\times(\vec{B}_o + \vec{B})\}\cdot\frac{\partial F_s}{\partial \vec{V}} = 0 \quad , \tag{A1}$$

and

$$\nabla\times\vec{E} = -\frac{\partial \vec{B}}{\partial t} \quad , \tag{A2}$$

$$\nabla\times\vec{B} = \mu_o\sum_s q_s\int\vec{V}\,F_s d\vec{V} + \frac{1}{c^2}\frac{\partial\vec{E}}{\partial t} \quad . \tag{A3}$$

We divide the velocity distribution function $F_s(\vec{V},\vec{r},t)$ into the zero-order homogeneous part $g_s(\vec{V})$ and the first-order perturbation $f_s(\vec{V},\vec{r},t)$ as

$$F_s(\vec{V},\vec{r},t) = g_s(\vec{V}) + f_s(\vec{V},\vec{r},t) \quad . \tag{A4}$$

Regarding $\vec{E}$, $\vec{B}$ and f_s as the first-order perturbations, we get the following linearized set of equations.

$$\frac{\partial f_s}{\partial t} + \vec{V}\cdot\frac{\partial f_s}{\partial \vec{r}} + \frac{q_s}{m_s}(\vec{V}\times\vec{B}_o)\cdot\frac{\partial f_s}{\partial \vec{V}} = -\frac{q_s}{m_s}\{\vec{E} + \vec{V}\times\vec{B}\}\cdot\frac{\partial g_s}{\partial \vec{V}} \quad , \tag{A5}$$

$$\nabla\times\vec{E} = -\frac{\partial\vec{B}}{\partial t} \quad , \tag{A6}$$

$$\nabla\times\vec{B} = \mu_o\sum_s q_s\int\vec{V}\,f_s d\vec{V} + \frac{1}{c^2}\frac{\partial\vec{E}}{\partial t} \quad . \tag{A7}$$

We now make an assumption that all of the perturbations are expressed as a sum of the normal plane waves propagating in the z-direction along $\vec{B}_o$. Namely,

$$(f_s, \vec{E}, \vec{B}) = \sum_k (f_{sk\omega}, \vec{E}_k, \vec{B}_k) e^{-j\omega(k)t+jkz} \quad . \tag{A8}$$

Then

$$\frac{\partial f_{sk\omega}}{\partial \phi} + j\frac{\omega - kV_z}{\varepsilon_s \Omega_s} f_{sk\omega} = \frac{q_s}{m_s \varepsilon_s \Omega_s} (\vec{E}_k + \vec{V} \times \vec{B}_k) \cdot \frac{\partial g_s}{\partial \vec{V}} \quad , \tag{A9}$$

$$\vec{B}_k = \frac{k}{\omega} \hat{z} \times \vec{E}_k \quad , \tag{A10}$$

$$k \hat{z} \times \vec{B}_k + \frac{\omega}{c^2} \vec{E}_k = - j\mu_o \sum_s q_s \int \vec{V} f_{sk\omega} d\vec{V} \quad . \tag{A11}$$

Eliminating $\vec{B}_k$ by Eq.(A10), Eqs.(A9) and (A11) become

$$\frac{\partial f_{sk\omega}}{\partial \phi} + j \frac{\omega - kV_z}{\varepsilon_s \Omega_s} f_{sk\omega} = \frac{q_s}{m_s \varepsilon_s \Omega_s} \{ \vec{E}_k (1 - \frac{kV_z}{\omega}) + \frac{k}{\omega} (\vec{E} \cdot \vec{V}) \hat{z} \} \cdot \frac{\partial g_s}{\partial \vec{V}} \quad , \tag{A12}$$

$$(c^2k^2 - \omega^2)\vec{E}_k - c^2k^2 E_{kz} \hat{z} = j\frac{\omega}{\varepsilon_o} \sum_s q_s \int \vec{V} f_{sk\omega} d\vec{V} \quad . \tag{A13}$$

In the coordinate of $(\hat{r}, \hat{\phi}, \hat{z})$, where $\hat{r}$, $\hat{\phi}$ and $\hat{z}$ are the unit vectors in the directions of $\vec{V}_\perp$, $\vec{V}_\perp \times \vec{B}_o$ and $\vec{B}_o$ respectively, we may well assume generally that the $g_s(\vec{V})$ is symmetry around $\vec{B}_o$, i.e.,

$$\frac{\partial g_s}{\partial \phi} = 0 \quad . \tag{A14}$$

Writing in terms of the components in this coordinate, Eqs.(A12) and (A13) become

$$\frac{\partial f_{sk\omega}}{\partial \phi} + j\frac{\omega - kV_z}{\varepsilon_s \Omega_s} f_{sk\omega} = \frac{q_s}{m_s \varepsilon_s \Omega_s} [E_{kr} (1 - \frac{kV_z}{\omega}) \frac{\partial g_s}{\partial V_\perp} + (E_{kz} + \frac{kV_\perp}{\omega} E_{kr}) \frac{\partial g_s}{\partial V_z}] \quad , \tag{A15}$$

$$\sqrt{2}\ (c^2k^2 - \omega^2) E_{k-} = j\frac{\omega}{\varepsilon_o} \sum_s q_s \int V_\perp e^{-j\phi} f_{sk\omega} d\vec{V} \quad , \tag{A16}$$

$$\sqrt{2}\ (c^2k^2 - \omega^2) E_{k+} = j\frac{\omega}{\varepsilon_o} \sum_s q_s \int V_\perp e^{+j\phi} f_{sk\omega} d\vec{V} \quad , \tag{A17}$$

$$-\omega^2 E_{kz} = j\frac{\omega}{\varepsilon_o} \sum_s q_s \int V_z f_{sk\omega} d\vec{V} \quad , \tag{A18}$$

where the component in the $\hat{r}$-direction of $\vec{E}_k$ is

$$E_{kr} = E_{kx}\cos\phi + E_{ky}\sin\phi = \frac{1}{\sqrt{2}} \left(E_{k-}e^{+j\phi} + E_{k+}e^{-j\phi} \right) , \tag{A19}$$

in which

$$E_{k+} = \frac{1}{\sqrt{2}} \left(E_{kx} + jE_{ky} \right) , \tag{A20}$$

$$E_{k-} = \frac{1}{\sqrt{2}} \left(E_{kx} - jE_{ky} \right) . \tag{A21}$$

The solution of the linear differential equation (A15) is given by

$$f_{sk\omega} = e^{-j\frac{\omega-kV_z}{\varepsilon_s\Omega_s}\phi} \int^{\phi} \frac{q_s}{m_s\varepsilon_s\Omega_s} \left[\left\{ \left(1- \frac{kV_z}{\omega}\right) \frac{\partial g_s}{\partial V_\perp} + \frac{kV_\perp}{\omega} \frac{\partial g_s}{\partial V_z} \right\} \frac{e^{+j\phi'}}{\sqrt{2}} E_{k-} \right.$$

$$\left. + \left\{ \left(1- \frac{kV_z}{\omega}\right) \frac{\partial g_s}{\partial V_\perp} + \frac{kV_\perp}{\omega} \frac{\partial g_s}{\partial V_z} \right\} \frac{e^{-j\phi'}}{\sqrt{2}} E_{k+} + \frac{kV_\perp}{\omega} \frac{\partial g_s}{\partial V_z} E_{kz} \right] e^{j\frac{\omega-kV_z}{\varepsilon_s\Omega_s}\phi'} d\phi' . \tag{A22}$$

Integrating over ϕ', we obtain

$$f_{sk\omega} = \frac{q_s}{jm_s} \left[\frac{\left(1- \frac{kV_z}{\omega}\right) \frac{\partial g_s}{\partial V_\perp} + \frac{kV_\perp}{\omega} \frac{\partial g_s}{\partial V_z}}{\omega-kV_z+\varepsilon_s\Omega_s} \frac{e^{j\phi}}{\sqrt{2}} E_{k-} + \frac{\left(1- \frac{kV_z}{\omega}\right) \frac{\partial g_s}{\partial V_\perp} + \frac{kV_\perp}{\omega} \frac{\partial g_s}{\partial V_z}}{\omega-kV_z-\varepsilon_s\Omega_s} \right.$$

$$\left. \times \frac{e^{-j\phi}}{\sqrt{2}} E_{k+} + \frac{\frac{\partial g_s}{\partial V_z}}{\omega-kV_z} E_{kz} \right] . \tag{A23}$$

In the case of the purely transverse whistler mode (i.e., R-polarized) waves,

$$E_{kz} = E_{k+} = 0 , \tag{A24}$$

so that Eq.(A23) is simply expressed as

$$f_{sk\omega} = \frac{q_s}{jm_s} \frac{\left(1- \frac{kV_z}{\omega}\right) \frac{\partial g_s}{\partial V_\perp} + \frac{kV_\perp}{\omega} \frac{\partial g_s}{\partial V_z}}{\omega-kV_z+\varepsilon_s\Omega_s} \frac{e^{j\phi}}{\sqrt{2}} E_{k-} . \tag{A25}$$

Substituting Eq.(A25) into Eq.(A16), we find the following relation.

$$\left[c^2k^2 - \omega^2 - \sum_s \frac{\omega q_s^2}{m_s \varepsilon_o} \int_0^{2\pi} d\phi \int_{-\infty}^{\infty} dV_z \int_0^{\infty} V_\perp^2 dV_\perp \frac{(1 - \frac{kV_z}{\omega}) \frac{\partial g_s}{\partial V_\perp} + \frac{kV_\perp}{\omega} \frac{\partial g_s}{\partial V_z}}{\omega - kV_z + \varepsilon_s \Omega_s} \right] E_{k-} = 0 \ . \tag{A26}$$

We, thus, find the dispersion equation in the integral form for the whistler mode waves as

$$c^2k^2 - \omega^2 - \sum_s \frac{2\pi\omega \Pi_s^2}{N_s} \int_{-\infty}^{\infty} dV_z \int_0^{\infty} V_\perp^2 dV_\perp \frac{(1 - \frac{kV_z}{\omega}) \frac{\partial g_s}{\partial V_\perp} + \frac{kV_\perp}{\omega} \frac{\partial g_s}{\partial V_z}}{\omega - kV_z + \varepsilon_s \Omega_s} = 0. \tag{A27}$$

Integration by parts over $V_\perp$ in Eq.(A27) gives a furthermore simple form of

$$c^2k^2 - \omega^2 - \sum_s \frac{\pi\omega \Pi_s^2}{kN_s} \int_{-\infty}^{\infty} dV_z \frac{2H_{s1}(V_z) + \frac{k}{\omega} H_{s2}(V_z)}{V_z - V} = 0 \ , \tag{A28}$$

where

$$H_{s1}(V_z) = \int_0^{\infty} V_\perp \, g_s \, dV_\perp \ , \tag{A29}$$

$$H_{s2}(V_z) = \int_0^{\infty} V_\perp^2 \left(V_z \frac{\partial g_s}{\partial V_\perp} - V_\perp \frac{\partial g_s}{\partial V_z} \right) dV_\perp \ , \tag{A30}$$

$$V = \frac{\omega + \varepsilon_s \Omega_s}{k} \ . \tag{A31}$$

We now consider the analytic process to get the dispersion equation $D(\omega_r, k) = 0$ between the real frequency ω_r and the wave number k and the expression of the growth rate γ_k. By writing

$$\omega = \omega_r + j\gamma_k \ , \tag{A32}$$

where ω_r and γ_k are the real quantities, we make an assumption that

$$|\gamma_k| \ll \omega_r \ . \tag{A33}$$

Under this assumption, we get to the first order of γ_k ,

$$\frac{1}{\omega} \simeq \frac{1}{\omega_r}\left(1 - j\frac{\gamma_k}{\omega_r}\right) , \tag{A34}$$

$$\frac{1}{\omega^2} \simeq \frac{1}{\omega_r^2}\left(1 - j\frac{2\gamma_k}{\omega_r}\right) , \tag{A35}$$

and

$$\int_{-\infty}^{\infty} \frac{H_{si}(V_z)}{V_z - V} dV_z = P\int_{-\infty}^{\infty} \frac{H_{si}(V_z)}{V_z - V_R} dV_z \mp \frac{\pi\gamma_k}{k} H'_{si}(V_R)$$

$$+ j\left[\pm\pi H_{si}(V_R) + \frac{\gamma_k}{k} P\int_{-\infty}^{\infty} \frac{H'_{si}(V_z)}{V_z - V_R} dV_z\right] , \quad (i = 1,2) \tag{A36}$$

where

$$V_R = \frac{\omega_r + \epsilon_s \Omega_s}{k} , \tag{A37}$$

is the resonance velocity, P denotes the principal part of the integral and the prime means a differentiation with respect to V_z. In the above expansion in Eq.(A36), we have used the Dirac-Plemelj formula as

$$\lim_{y\to 0} \frac{1}{z-(x\pm jy)} = P\frac{1}{z-x} \pm \pi j\delta(z-x) , \quad (y>0) , \tag{A38}$$

where x, y and z are real quantities. The sign + and - in the expansion Eq.(A36) correspond to the case of $k > 0$ and $k < 0$, respectively.

Substituting Eqs.(A34) to (A36) into (A28), we can resolve the dispersion equation equation into the real and imaginary parts as

$$c^2k^2 - \omega_r^2 - \sum_s \frac{\pi\omega_r \Pi_s^2}{kN_s}\left[2P\int_{-\infty}^{\infty} \frac{H_{s1}(V_z)}{V_z - V_R} dV_z + \frac{k}{\omega_r} P\int_{-\infty}^{\infty} \frac{H_{s2}(V_z)}{V_z - V_R} dV_z\right.$$

$$\left. \pm 2\pi\gamma_k\left\{\frac{H_{s1}(V_R)}{\omega_r} - \frac{H'_{s1}(V_R)}{k}\right\} \pm \frac{k}{\omega_r}\pi\gamma_k\left\{\frac{2H_{s2}(V_R)}{\omega_r} - \frac{H'_{s2}(V_R)}{k}\right\}\right] = 0, \tag{A39}$$

and

$$2c^2k^2\gamma_k + \sum_s \frac{\pi\omega_r \Pi_s^2}{kN_s}\left[\pm 2\pi H_{s1}(V_R) \pm \pi\frac{k}{\omega_r} H_{s2}(V_R) + \frac{2\gamma_k}{k} P\int_{-\infty}^{\infty} \frac{H'_{s1}(V_z)}{V_z - V_R} dV_z\right.$$

$$\left. + \frac{\gamma_k}{\omega_r} P\int_{-\infty}^{\infty} \frac{H'_{s2}(V_z)}{V_z - V_R} dV_z - \frac{2\gamma_k}{\omega_r} P\int_{-\infty}^{\infty} \frac{H_{s1}(V_z)}{V_z - V_R} dV_z - \frac{2k\gamma_k}{\omega_r^2} P\int_{-\infty}^{\infty} \frac{H_{s2}(V_z)}{V_z - V_R} dV_z\right] = 0 . \tag{A40}$$

We may well drop the first order term in γ_k leaving the zero-order quantities and obtain

$$c^2k^2 - \omega_r^2 - \sum_s \frac{\pi\omega_r \Pi_s^2}{kN_s} \left[2P\int_{-\infty}^{\infty} \frac{H_{s1}(V_z)}{V_z - V_R} dV_z + \frac{k}{\omega_r} P\int_{-\infty}^{\infty} \frac{H_{s2}(V_z)}{V_z - V_R} dV_z \right] = 0 \quad . \tag{A41}$$

Substituting Eq.(A41) into Eq.(A40), we find,

$$\gamma_k = \frac{- \sum_s \frac{\pi^2 \Pi_s^2}{|k| N_s} \left[2H_{s1}(V_R) + \frac{k}{\omega_r} H_{s2}(V_R) \right]}{2 + \sum_s \frac{\pi \Pi_s^2}{kN_s\omega_r} \left[2P\int_{-\infty}^{\infty} \frac{H_{s1}(V_z)}{V_z - V_R} dV_z + \frac{2\omega_r}{k} P\int_{-\infty}^{\infty} \frac{H'_{s1}(V_z)}{V_z - V_R} dV_z + P\int_{-\infty}^{\infty} \frac{H'_{s2}(V_z)}{V_z - V_R} dV_z \right]} \quad . \tag{A42}$$

Now we must evaluate the principal value of the above integrals. If the function $H_{s1}(V_z)$, i.e., $g_s(V_\perp, V_z)$ is such that the contribution to the integral from the range

$$|V_z| > |V_R| \quad , \tag{A43}$$

is negligibly small, then we get after some appropriate integrations by parts and the Taylor expansion of the denominator of Eq.(A42) as

$$P\int_{-\infty}^{\infty} \frac{H_{s1}(V_z)}{V_z - V_R} dV_z = - \frac{N_s}{2\pi V_R} \left\{ 1 + \frac{\langle V_z \rangle}{V_R} + \frac{\langle V_z^2 \rangle}{V_R^2} + \cdots\cdots \right\} \quad , \tag{A44}$$

$$P\int_{-\infty}^{\infty} \frac{H'_{s1}(V_z)}{V_z - V_R} dV_z = \frac{N_s}{2\pi V_R^2} \left\{ 1 + \frac{2\langle V_z \rangle}{V_R} + \frac{3\langle V_z^2 \rangle}{V_R^2} + \cdots\cdots \right\} \quad , \tag{A45}$$

$$P\int_{-\infty}^{\infty} \frac{H_{s2}(V_z)}{V_z - V_R} dV_z = \frac{N_s}{\pi} \left\{ \frac{\langle V_z \rangle}{V_R} + \frac{\langle V_z^2 \rangle}{V_R^2} + \cdots \right\} - \frac{N_s}{2\pi} \left\{ \frac{\langle V_\perp^2 \rangle}{V_R^2} + \cdots\cdots \right\} \quad , \tag{A46}$$

$$P\int_{-\infty}^{\infty} \frac{H'_{s2}(V_z)}{V_z - V_R} dV_z = - \frac{1}{\pi V_R} \left\{ \frac{\langle V_z \rangle}{V_R} + \frac{2\langle V_z^2 \rangle}{V_R^2} - \frac{\langle V_\perp^2 \rangle}{V_R^2} + \cdots\cdots \right\} \quad , \tag{A47}$$

where $\langle\rangle$ denotes the averaged quantity and $\cdots\cdots$ shows higher order terms than $\langle V_\ell^3 \rangle / V_R^3$ $(\ell = z, \perp)$.

Substituting these estimations to the second order of $\langle V_\ell \rangle / V_R$ ($\ell = z, \perp$) into Eqs.(A41) and (A42), we finally find

$$c^2k^2 - \omega_r^2 + \sum_s \frac{\omega_r \Pi_s^2}{\omega_r + \varepsilon_s \Omega_s} \left[1 - \frac{\varepsilon_s \Omega_s k \langle V_z \rangle}{\omega_r (\omega_r + \varepsilon_s \Omega_s)} - \frac{\varepsilon_s \Omega_s k^2}{\omega_r (\omega_r + \varepsilon_s \Omega_s)^2} \right.$$

$$\left. \times \left\{ \langle V_z^2 \rangle - \frac{\omega_r + \varepsilon_s \Omega_s}{\varepsilon_s \Omega_s} \frac{1}{2} \langle V_\perp^2 \rangle \right\} \right] = 0 \quad , \tag{A48}$$

and

$$\gamma_k = - \frac{\sum_s \frac{\pi^2 \Pi_s^2}{|k| N_s} \left[2H_{s1}(V_R) + \frac{k}{\omega_r} H_{s2}(V_R) \right]}{2 - \sum_s \frac{\varepsilon_s \Omega_s \Pi_s^2}{\omega_r (\omega_r + \varepsilon_s \Omega_s)^2} \left[1 + \frac{2\langle V_z \rangle}{V_R} + \frac{3\langle V_z^2 \rangle}{V_R^2} - \frac{\omega_r + \varepsilon_s \Omega_s}{\varepsilon_s \Omega_s} \frac{\langle V_\perp^2 \rangle}{V_R^2} \right]} \quad . \tag{A49}$$

In the case of the rest plasma, i.e.,

$$\langle V_z \rangle = 0 \quad , \tag{A50}$$

Eqs.(A48) and (A49) are written

$$c^2k^2 - \omega_r^2 - \sum_s \frac{\omega_r \Pi_s^2}{\omega_r + \varepsilon_s \Omega_s} - \sum_s \frac{k^2 \varepsilon_s \Omega_s \Pi_s^2}{(\omega_r + \varepsilon_s \Omega_s)^3} \frac{\kappa}{m_s} \left(T_{\parallel} - \frac{\omega_r + \varepsilon_s \Omega_s}{\varepsilon_s \Omega_s} T_\perp \right) = 0 , \tag{A51}$$

and

$$\gamma_k = - \frac{\sum_s \frac{\pi^2 \Pi_s^2}{|k| N_s} \left[2H_{s1}(V_R) + \frac{k}{\omega_r} H_{s2}(V_R) \right]}{\left\{ 2 - \sum_s \frac{\varepsilon_s \Omega_s \Pi_s^2}{\omega_r (\omega_r + \varepsilon_s \Omega_s)^2} \right\} \left\{ 1 - \frac{3 \sum_s \frac{\varepsilon_s \Omega_s \Pi_s^2}{(\omega_r + \varepsilon_s \Omega_s)^2} \frac{\kappa}{m_s V_R^2} \left(T_{\parallel} - \frac{2}{3} \frac{\omega_r + \varepsilon_s \Omega_s}{\varepsilon_s \Omega_s} T_\perp \right)}{2 - \sum_s \frac{\varepsilon_s \Omega_s \Pi_s^2}{\omega_r (\omega_r + \varepsilon_s \Omega_s)^2}} \right\}} \quad , \tag{A52}$$

where

$$T_{\parallel} \equiv \frac{m_s \langle V_z^2 \rangle}{\kappa} \quad , \quad \text{and} \quad T_\perp \equiv \frac{m_s \langle V_\perp^2 \rangle}{2\kappa} \quad . \tag{A53}$$

In the limit of $T_\perp$, $T_{\parallel} \to 0$, Eqs.(A51) and (A52) become the well known expressions as

$$D(\omega_r,k) \equiv c^2k^2 - \omega_r^2 + \sum_s \frac{\omega_r \Pi_s^2}{\omega_r+\varepsilon_s\Omega_s} = 0 \quad , \tag{A54}$$

and

$$\gamma_k = - \frac{\sum_s \frac{\pi^2\Pi_s^2}{|k|N_s} \left[2H_{s1}(V_R) + \frac{k}{\omega_r} H_{s2}(V_R) \right]}{2 - \sum_s \frac{\varepsilon_s\Omega_s\Pi_s^2}{\omega_r(\omega_r+\varepsilon_s\Omega_s)^2}} \quad , \tag{A55}$$

or equivalently

$$\gamma_k = + \sum_s \frac{\pi^2}{N_s} \frac{\varepsilon_s\Omega_s\Pi_s^2}{\partial D/\partial\omega_r} \int_{-\infty}^{\infty} dV_z \int_0^{\infty} dV_\perp V_\perp^2 \delta(\omega_r - kV_z + \varepsilon_s\Omega_s) \left(\frac{\partial g_s}{\partial V_\perp} - \frac{kV_\perp}{\varepsilon_s\Omega_s} \frac{\partial g_s}{\partial V_z} \right), \tag{A56}$$

where we noticed

$$\int_{-\infty}^{\infty} dV_z \ \delta(\omega_r - kV_z + \varepsilon_s\Omega_s) = |k| \quad , \tag{A57}$$

and

$$\begin{aligned}
&2H_{s1}(V_R) + \frac{k}{\omega_r} H_{s2}(V_R) \\
&= 2\int_0^{\infty} V_\perp g_s(V_\perp, V_R) dV_\perp + \frac{k}{\omega_r} \int_0^{\infty} V_\perp^2 \left(V_z \frac{\partial g_s}{\partial V_\perp} - V_\perp \frac{\partial g_s}{\partial V_z} \right) dV_\perp \Big|_{V_z = V_R} \\
&= - \int_0^{\infty} V_\perp^2 \frac{\partial g_s}{\partial V_\perp} dV_\perp \Big|_{V_z=V_R} + \frac{k}{\omega_r} \int_0^{\infty} V_\perp^2 \left(V_z \frac{\partial g_s}{\partial V_\perp} - V_\perp \frac{\partial g_s}{\partial V_z} \right) dV_\perp \Big|_{V_z=V_R} \\
&= \int_0^{\infty} V_\perp^2 \frac{\partial g_s}{\partial V_\perp} \left(\frac{kV_z - \omega_r}{\omega_r} \right) dV_\perp \Big|_{V_z=V_R} - \int_0^{\infty} V_\perp^2 \frac{kV_\perp}{\omega_r} \frac{\partial g_s}{\partial V_z} dV_\perp \Big|_{V_z=V_R} \\
&= \frac{\varepsilon_s\Omega_s}{\omega_r} \int_0^{\infty} V_\perp^2 dV_\perp \left(\frac{\partial g_s}{\partial V_\perp} - \frac{kV_\perp}{\varepsilon_s\Omega_s} \frac{\partial g_s}{\partial V_z} \right) \Big|_{V_z=V_R} \quad ,
\end{aligned} \tag{A58}$$

and

$$\frac{\partial D}{\partial \omega_r} = - \omega_r \left\{ 2 - \sum_s \frac{\varepsilon_s\Omega_s\Pi_s^2}{(\omega_r+\varepsilon_s\Omega_s)^2} \right\} \quad . \tag{A59}$$

Appendix B

Derivation of Eqs.(3.55) to (3.61)

In this appendix, we show a tedious calculation of the derivation of Eqs.(3.55) to (3.61) from Eq.(3.54). Eq.(3.54) is written as

$$\frac{\partial g_s}{\partial t} = \mathrm{Re}\left[j \frac{q_s^2}{2m_s^2} \sum_k E_k E_k^* I \right] , \tag{B1}$$

where

$$I \equiv \left(1 - \frac{kV_z}{\tilde{\omega}}\right) \frac{\frac{\partial G_s}{\partial V_\perp} + \frac{G_s}{V_\perp}}{\omega - kV_z + \varepsilon_s \Omega_s} + \frac{kV_\perp}{\tilde{\omega}} \frac{\partial}{\partial V_z} \left(\frac{G_s}{\omega - kV_z + \varepsilon_s \Omega_s}\right) , \tag{B2}$$

in which

$$G_s \equiv \frac{\partial g_s}{\partial V_\perp} + \frac{k}{\omega} \left(V_\perp \frac{\partial g_s}{\partial V_z} - V_z \frac{\partial g_s}{\partial V_\perp} \right) . \tag{B3}$$

We should calculate the imaginary part of I. Writing the first and the second terms in the r.h.s. of Eq.(B2) as I_1 and I_2, respectively, i.e.,

$$I_1 \equiv \left(1 - \frac{kV_z}{\tilde{\omega}}\right) \frac{\frac{\partial G_s}{\partial V_\perp} + \frac{G_s}{V_\perp}}{\omega - kV_z + \varepsilon_s \Omega_s} , \tag{B4}$$

$$I_2 \equiv \frac{kV_\perp}{\tilde{\omega}} \frac{\partial}{\partial V_z} \left(\frac{G_s}{\omega - kV_z + \varepsilon_s \Omega_s}\right) , \tag{B5}$$

we proceed calculations of I_1 and I_2 seperately. The procedure is to substitute the relations

$$\frac{1}{\tilde{\omega}} = \frac{1}{\omega_r - j\gamma_k} = \frac{\omega_r}{\omega_r^2 + \gamma_k^2} + j \frac{\gamma_k}{\omega_r^2 + \gamma_k^2} , \tag{B6}$$

and

$$\frac{1}{\omega - kV_z + \varepsilon_s \Omega_s} = \frac{\omega_r - kV_z + \varepsilon_s \Omega_s}{(\omega_r - kV_z + \varepsilon_s \Omega_s)^2 + \gamma_k^2} - j \frac{\gamma_k}{(\omega_r - kV_z + \varepsilon_s \Omega_s)^2 + \gamma_k^2} , \tag{B7}$$

into Eqs.(B4) and (B5) and extract the imaginary parts of I_1 and I_2.

In order to make it easy to trace the calculation, we present here lengthy and redundant calculations of each term appearing in the calculations.

$$G_s = \frac{\partial g_s}{\partial V_\perp} + \frac{k\omega_r}{\omega_r^2+\gamma_k^2}\left(V_\perp\frac{\partial g_s}{\partial V_z} - V_z\frac{\partial g_s}{\partial V_\perp}\right) - j\frac{k\gamma_k}{\omega_r^2+\gamma_k^2}\left(V_\perp\frac{\partial g_s}{\partial V_z} - \frac{\partial g_s}{\partial V_\perp}\right) , \qquad \text{(B8)}$$

$$\frac{\partial G_s}{\partial V_\perp} = \frac{\partial^2 g_s}{\partial V_\perp^2} + \frac{k\omega_r}{\omega_r^2+\gamma_k^2}\left(\frac{\partial g_s}{\partial V_z} + V_\perp\frac{\partial^2 g_s}{\partial V_z\partial V_\perp} - V_z\frac{\partial^2 g_s}{\partial V_\perp^2}\right)$$

$$-j\frac{k\gamma_k}{\omega_r^2+\gamma_k^2}\left(\frac{\partial g_s}{\partial V_z} + V_\perp\frac{\partial^2 g_s}{\partial V_z\partial V_\perp} - V_z\frac{\partial^2 g_s}{\partial V_\perp^2}\right) . \qquad \text{(B9)}$$

Combining Eqs.(B7), (B8) and (B9), we can show

$$\frac{\frac{\partial G_s}{\partial V_\perp} + \frac{G_s}{V_\perp}}{\omega - kV_z + \varepsilon_s\Omega_s} = \frac{1}{(\omega_r - kV_z + \varepsilon_s\Omega_s)^2+\gamma_k^2}\left[\left[\left\{\frac{\partial^2 g_s}{\partial V_\perp^2} + \frac{1}{V_\perp}\frac{\partial g_s}{\partial V_\perp} + \frac{k\omega_r}{\omega_r^2+\gamma_k^2}\left(V_\perp\frac{\partial^2 g_s}{\partial V_z\partial V_\perp}\right.\right.\right.\right.$$

$$\left.\left.\left.\left.-V_z\frac{\partial^2 g_s}{\partial V_\perp^2} + 2\frac{\partial g_s}{\partial V_z} - \frac{V_z}{V_\perp}\frac{\partial g_s}{\partial V_\perp}\right)\right\}(\omega_r - kV_z + \varepsilon_s\Omega_s) - \frac{k\gamma_k^2}{\omega_r^2+\gamma_k^2}\left(V_\perp\frac{\partial^2 g_s}{\partial V_z\partial V_\perp} - V_z\frac{\partial^2 g_s}{\partial V_\perp^2}\right.\right.\right.$$

$$\left.\left.\left.+2\frac{\partial g_s}{\partial V_z} - \frac{V_z}{V_\perp}\frac{\partial g_s}{\partial V_\perp}\right)\right] - j\gamma_k\left[\frac{\partial^2 g_s}{\partial V_\perp^2} + \frac{1}{V_\perp}\frac{\partial g_s}{\partial V_\perp} + \frac{k\omega_r}{\omega_r^2+\gamma_k^2}\left(V_\perp\frac{\partial^2 g_s}{\partial V_z\partial V_\perp} - V_z\frac{\partial^2 g_s}{\partial V_\perp^2}\right.\right.$$

$$\left.\left.+2\frac{\partial g_s}{\partial V_z} - \frac{V_z}{V_\perp}\frac{\partial g_s}{\partial V_\perp}\right) + \frac{k(\omega_r - kV_z + \varepsilon_s\Omega_s)}{\omega_r^2+\gamma_k^2}\left(V_\perp\frac{\partial^2 g_s}{\partial V_z\partial V_\perp} - V_z\frac{\partial^2 g_s}{\partial V_\perp^2} + 2\frac{\partial g_s}{\partial V_z} - \frac{V_z}{V_\perp}\frac{\partial g_s}{\partial V_\perp}\right)\right] .$$

(B10)

From Eqs.(B6) and (B10), we extract the imaginary part of I_1 as

$$\mathrm{Im}\ I_1 = \frac{\omega_r^2+\gamma_k^2-kV_z\omega_r}{\omega_r^2+\gamma_k^2}\,\mathrm{Im}\left(\frac{\frac{\partial G_s}{\partial V_\perp} + \frac{G_s}{V_\perp}}{\omega - kV_z + \varepsilon_s\Omega_s}\right) - \frac{kV_z\gamma_k}{\omega_r^2+\gamma_k^2}\,\mathrm{Re}\left(\frac{\frac{\partial G_s}{\partial V_\perp} + \frac{G_s}{V_\perp}}{\omega - kV_z + \varepsilon_s\Omega_s}\right)$$

$$= -\frac{\gamma_k}{(\omega_r - kV_z + \varepsilon_s\Omega_s)^2+\gamma_k^2}\frac{1}{\omega_r^2+\gamma_k^2}\Big[(\omega_r^2+\gamma_k^2-kV_z\omega_r)\Big[\{1-\frac{kV_\perp(2\omega_r-kV_z+\varepsilon_s\Omega_s)}{\omega_r^2+\gamma_k^2}\}\frac{\partial^2 g_s}{\partial V_\perp^2}$$

$$+\frac{kV_\perp(2\omega_r-kV_z+\varepsilon_s\Omega_s)}{\omega_r^2+\gamma_k^2}\frac{\partial^2 g_s}{\partial V_z\partial V_\perp}+\{1-\frac{kV_z(2\omega_r-kV_z+\varepsilon_s\Omega_s)}{\omega_r^2+\gamma_k^2}\}\frac{1}{V_\perp}\frac{\partial g_s}{\partial V_\perp}$$

$$+\frac{2kV_z(2\omega_r-kV_z+\varepsilon_s\Omega_s)}{\omega_r^2+\gamma_k^2}\frac{1}{V_z}\frac{\partial g_s}{\partial V_z}\Big]+kV_z\Big[\{\omega_r-kV_z+\varepsilon_s\Omega_s-\frac{kV_z(\omega_r^2-kV_z\omega_r+\varepsilon_s\Omega_s\omega_r-\gamma_k^2)}{\omega_r^2+\gamma_k^2}\}$$

$$\times\frac{\partial^2 g_s}{\partial V_\perp^2}+\frac{kV_\perp(\omega_r^2-kV_z\omega_r+\varepsilon_s\Omega_s\omega_r-\gamma_k^2)}{\omega_r^2+\gamma_k^2}\frac{\partial^2 g_s}{\partial V_z\partial V_\perp}+\{\omega_r-kV_z+\varepsilon_s\Omega_s-\frac{kV_z}{\omega_r^2+\gamma_k^2}$$

$$\times(\omega_r^2-kV_z\omega_r+\varepsilon_s\Omega_s\omega_r-\gamma_k^2)\}\frac{1}{V_\perp}\frac{\partial g_s}{\partial V_\perp}+\frac{2kV_z(\omega_r^2-kV_z\omega_r+\varepsilon_s\Omega_s\omega_r-\gamma_k^2)}{\omega_r^2+\gamma_k^2}\frac{1}{V_z}\frac{\partial g_s}{\partial V_z}\Big]\Big] \quad . \tag{B11}$$

On the other hand, regarding with I_2, we know

$$\frac{\partial}{\partial V_z}\left(\frac{G_s}{\omega-kV_z+\varepsilon_s\Omega_s}\right)=\frac{\frac{\partial G_s}{\partial V_z}}{\omega-kV_z+\varepsilon_s\Omega_s}+\frac{kG_s}{(\omega_r-kV_z+\varepsilon_s\Omega_s)^2} \quad . \tag{B12}$$

Substituting Eqs.(B6) and (B7) into Eq.(B12), we get after a tedious calculation,

$$\frac{\partial}{\partial V_z}\left(\frac{G_s}{\omega-kV_z+\varepsilon_s\Omega_s}\right)=\frac{1}{(\omega_r-kV_z+\varepsilon_s\Omega_s)^2+\gamma_k^2}\Big[\Big[\frac{kV_\perp(2\omega_r-kV_z+\varepsilon_s\Omega_s)}{\omega_r^2+\gamma_k^2}\frac{\partial^2 g_s}{\partial V_z^2}$$

$$+\{1-\frac{kV_z(2\omega_r-kV_z+\varepsilon_s\Omega_s)}{\omega_r^2+\gamma_k^2}\}\frac{\partial^2 g_s}{\partial V_z\partial V_\perp}+\{\frac{2kV_\perp(\omega_r-kV_z+\varepsilon_s\Omega_s)}{(\omega_r-kV_z+\varepsilon_s\Omega_s)^2+\gamma_k^2}-\frac{kV_\perp(2\omega_r-kV_z+\varepsilon_s\Omega_s)}{\omega_r^2+\gamma_k^2}$$

$$-\frac{kV_\perp}{\omega_r^2+\gamma_k^2}\frac{kV_z\{(\omega_r-kV_z+\varepsilon_s\Omega_s)^2+2\omega_r(\omega_r-kV_z+\varepsilon_s\Omega_s)-\gamma_k^2\}}{(\omega_r-kV_z+\varepsilon_s\Omega_s)^2+\gamma_k^2}\}\frac{1}{V_\perp}\frac{\partial g_s}{\partial V_\perp}+\frac{kV_\perp}{\omega_r^2+\gamma_k^2}$$

$$\times\frac{kV_z\{(\omega_r-kV_z+\varepsilon_s\Omega_s)^2+2\omega_r(\omega_r-kV_z+\varepsilon_s\Omega_s)-\gamma_k^2\}}{(\omega_r-kV_z+\varepsilon_s\Omega_s)^2+\gamma_k^2}\frac{1}{V_z}\frac{\partial g_s}{\partial V_z}\Big]-j\Big[\frac{kV_\perp(\omega_r^2-kV_z\omega_r+\varepsilon_s\Omega_s\omega_r-\gamma_k^2)}{\omega_r^2+\gamma_k^2}$$

$$\times\frac{\partial^2 g_s}{\partial V_z^2} + \{\omega_r - kV_z + \varepsilon_s\Omega_s - \frac{kV_z(\omega_r^2 - kV_z\omega_r + \varepsilon_s\Omega_s\omega_r - \gamma_k^2)}{\omega_r^2+\gamma_k^2}\}\frac{\partial^2 g_s}{\partial V_z \partial V_\perp} + \{kV_\perp$$

$$\times\frac{(\omega_r - kV_z + \varepsilon_s\Omega_s)^2 - \gamma_k^2}{(\omega_r - kV_z + \varepsilon_s\Omega_s)^2 + \gamma_k^2} - \frac{kV_\perp}{\omega_r^2+\gamma_k^2}\frac{kV_z\{\omega_r(\omega_r - kV_z + \varepsilon_s\Omega_s)^2 - \omega_r\gamma_k^2 - 2\gamma_k^2(\omega_r - kV_z + \varepsilon_s\Omega_s)\}}{(\omega_r - kV_z + \varepsilon_s\Omega_s)^2 + \gamma_k^2}$$

$$- \frac{kV_\perp(\omega_r^2 - kV_z\omega_r + \varepsilon_s\Omega_s\omega_r - \gamma_k^2)}{\omega_r^2+\gamma_k^2}\}\frac{1}{V_\perp}\frac{\partial g_s}{\partial V_\perp} + \frac{kV_\perp}{\omega_r^2+\gamma_k^2}$$

$$\times\frac{\omega_r(\omega_r - kV_z + \varepsilon_s\Omega_s)^2 - \omega_r\gamma_k^2 - 2\gamma_k^2(\omega_r - kV_z + \varepsilon_s\Omega_s)}{(\omega_r - kV_z + \varepsilon_s\Omega_s)^2 + \gamma_k^2}\frac{1}{V_\perp}\frac{\partial g_s}{\partial V_z}\Big]\Big] \quad . \tag{B13}$$

Consequently, we finally obtain

$$\text{Im } I_2 = \frac{kV_\perp}{\omega_r^2+\gamma_k^2}[\gamma_k \text{Re}\{\frac{\partial}{\partial V_z}(\frac{G_s}{\omega - kV_z + \varepsilon_s\Omega_s}\} + \omega_r \text{Im}\{\frac{\partial}{\partial V_z}(\frac{G_s}{\omega - kV_z + \varepsilon_s\Omega_s}\}]. \tag{B14}$$

Adding Eqs.(B11) and (B14) and arranging the coefficients of the derivatives, we could get the result of Eq.(3.55), i.e.,

$$\frac{\partial g_s}{\partial t} = \frac{1}{N_s m_s}\sum_k \frac{\Pi_s^2}{\omega_r^2}\varepsilon_k \frac{\gamma_k}{(\omega_r - kV_z + \varepsilon_s\Omega_s)^2 + \gamma_k^2}[(\omega_r - kV_z)^2\frac{\partial^2 g_s}{\partial V_\perp^2} + k^2V_\perp^2\frac{\partial^2 g_s}{\partial V_z^2}$$

$$+ 2kV_\perp(\omega_r - kV_\perp)\frac{\partial^2 g_s}{\partial V_z \partial V_\perp} + \{(\omega_r - kV_z)^2 - \frac{2k^2V_\perp^2\varepsilon_s\Omega_s(\omega_r - kV_z + \varepsilon_s\Omega_s)}{(\omega_r - kV_z + \varepsilon_s\Omega_s)^2 + \gamma_k^2}\}\frac{1}{V_\perp}\frac{\partial g_s}{\partial V_\perp}$$

$$+ 2kV_z\{\varepsilon_s\Omega_s + 2(\omega_r - kV_z) + \frac{k^2V_\perp^2(\omega_r - kV_z + \varepsilon_s\Omega_s)}{(\omega_r - kV_z + \varepsilon_s\Omega_s)^2 + \gamma_k^2}\}\frac{1}{V_z}\frac{\partial g_s}{\partial V_z} \quad . \tag{B15}$$

The following arrangement makes it possible to rewrite the expression in a more elegant form as Eq.(3.61) in the text.

$$\frac{(\omega_r - kV_z)^2}{(\omega_r - kV_z + \varepsilon_s\Omega_s)^2 + \gamma_k^2}\frac{\partial^2 g_s}{\partial V_\perp^2} + \frac{k^2V_\perp^2}{(\omega_r - kV_z + \varepsilon_s\Omega_s)^2 + \gamma_k^2}\frac{\partial^2 g_s}{\partial V_z^2} + \frac{2kV_\perp(\omega_r - kV_z)}{(\omega_r - kV_z + \varepsilon_s\Omega_s)^2 + \gamma_k^2}$$

$$\times\frac{\partial^2 g_s}{\partial V_z \partial V_\perp} + [\frac{(\omega_r - kV_z)^2}{(\omega_r - kV_z + \varepsilon_s\Omega_s)^2 + \gamma_k^2} - \frac{2\varepsilon_s\Omega_s k^2V_\perp^2(\omega_r - kV_z + \varepsilon_s\Omega_s)}{\{(\omega_r - kV_z + \varepsilon_s\Omega_s)^2 + \gamma_k^2\}^2}]\frac{1}{V_\perp}\frac{\partial g_s}{\partial V_\perp}$$

$$+\left[\frac{2k(2\omega_r-2kV_z+\varepsilon_s\Omega_s)}{(\omega_r-kV_z+\varepsilon_s\Omega_s)^2+\gamma_k^2}+\frac{2k^3V_\perp^2(\omega_r-kV_z+\varepsilon_s\Omega_s)}{\{(\omega_r-kV_z+\varepsilon_s\Omega_s)^2+\gamma_k^2\}^2}\right]\frac{\partial g_s}{\partial V_z}$$

$$=\frac{(\omega_r-kV_z)^2}{(\omega_r-kV_z+\varepsilon_s\Omega_s)^2+\gamma_k^2}\left\{\frac{\partial^2 g_s}{\partial V_\perp^2}+\frac{1}{V_\perp}\frac{\partial g_s}{\partial V_\perp}\right\}+\frac{k(2\omega_r-2kV_z+\varepsilon_s\Omega_s)}{(\omega_r-kV_z+\varepsilon_s\Omega_s)^2+\gamma_k^2}\frac{1}{V_\perp}\left(V_\perp^2\frac{\partial^2 g_s}{\partial V_z\partial V_\perp}\right.$$

$$\left.+2V_\perp\frac{\partial g_s}{\partial V_z}\right)-kV_\perp\frac{\partial}{\partial V_z}\left[\frac{1}{(\omega_r-kV_z+\varepsilon_s\Omega_s)^2+\gamma_k^2}\left(\varepsilon_s\Omega_s\frac{\partial g_s}{\partial V_\perp}-kV_\perp\frac{\partial g_s}{\partial V_z}\right)\right]$$

$$=\frac{(\omega_r-kV_z)^2}{(\omega_r-kV_z+\varepsilon_s\Omega_s)^2+\gamma_k^2}\frac{1}{V_\perp}\frac{\partial}{\partial V_\perp}\left(V_\perp\frac{\partial g_s}{\partial V_\perp}\right)+\frac{k(2\omega_r-2kV_z+\varepsilon_s\Omega_s)}{(\omega_r-kV_z+\varepsilon_s\Omega_s)^2+\gamma_k^2}\frac{1}{V_\perp}\frac{\partial}{\partial V_\perp}\left(V_\perp^2\frac{g_s}{V_z}\right)$$

$$-\frac{\partial}{\partial V_z}\left[\frac{kV_\perp}{(\omega_r-kV_z+\varepsilon_s\Omega_s)^2+\gamma_k^2}\left(\varepsilon_s\Omega_s\frac{\partial g_s}{\partial V_\perp}-kV_\perp\frac{\partial g_s}{\partial V_z}\right)\right]$$

$$=\frac{1}{V_\perp}\frac{\partial}{\partial V_\perp}\left[V_\perp\frac{1}{(\omega_r-kV_z+\varepsilon_s\Omega_s)^2+\gamma_k^2}\left[(\omega_r-kV_z)^2\frac{\partial g_s}{\partial V_\perp}+kV_\perp\{\varepsilon_s\Omega_s+2(\omega_r-kV_z)\}\frac{g_s}{V_z}\right]\right]$$

$$-\frac{\partial}{\partial V_z}\left[kV_\perp\frac{1}{(\omega_r-kV_z+\varepsilon_s\Omega_s)^2+\gamma_k^2}\left(\varepsilon_s\Omega_s\frac{\partial g_s}{\partial V_\perp}-kV_\perp\frac{\partial g_s}{\partial V_z}\right)\right] \qquad \text{(B16)}$$

Appendix C

Derivation of the Marginal State Distribution Function

In this appendix, we inquire after the marginal state velocity distribution function. It is defined as a distribution function which gives $\gamma_k = 0$ for all ω_r. The condition for $\gamma_k = 0$ is given by

$$\nabla_v g_s \equiv \frac{\partial g_s}{\partial V_\perp} - \frac{kV_\perp}{\varepsilon_s \Omega_s} \frac{\partial g_s}{\partial V_z} = 0 \quad . \tag{C1}$$

Noting that k is a function of V_z determined by the following simultaneous equations,

$$\omega_r - kV_z + \varepsilon_s \Omega_s = 0 \quad , \tag{C2}$$

$$c^2k^2 - \omega_r^2 + \sum_s \frac{\omega_r \Pi_s^2}{\omega_r + \varepsilon_s \Omega_s} = 0 \quad , \tag{C3}$$

we get the equation for the marginal state distribution function g_s as

$$\frac{\partial g_s}{\partial V_\perp} = \frac{k(V_z)V_\perp}{\varepsilon_s \Omega_s} \frac{\partial g_s}{\partial V_z} \quad . \tag{C4}$$

We make here an assumption that $g_s(V_\perp, V_z)$ is to be seperable as

$$g_s(V_\perp, V_z) = S_s(V_z) R_s(V_\perp) \quad . \tag{C5}$$

Then Eq.(C4) becomes

$$\frac{1}{V_\perp} \frac{\partial R_s}{\partial V_\perp} S_s(V_z) = \frac{k(V_z)}{\varepsilon_s \Omega_s} R_s(V_\perp) \frac{\partial S_s}{\partial V_z} \quad , \tag{C5}$$

which is resolved to

$$\frac{dR_s}{dV_\perp} = \text{const} \times V_\perp R_s \, , \tag{C6}$$

$$\frac{dS_s}{dV_z} = \text{const} \times \frac{\varepsilon_s \Omega_s}{k(V_z)} S_s(V_z) \quad . \tag{C7}$$

The solution of Eq.(C5) is then

$$g_s(V_\perp, V_z) = C_1 \exp\{C_2 (\frac{1}{2} V_\perp^2 + \varepsilon_s \Omega_s \int^{V_z} \frac{du}{k(u)})\} \, , \tag{C8}$$

where the integration constants C_1 and C_2 should be determined by the restrictions

$$N_s = 2\pi\int_0^\infty V_\perp dV_\perp \int_{-\infty}^\infty dV_z g_s \ , \tag{C9}$$

$$N_s\langle V_\perp^2\rangle \equiv N_s \frac{2\kappa T_\perp}{m_s} = 2\pi\int_0^\infty V_\perp^3 dV_\perp \int_{-\infty}^\infty dV_z g_s \ . \tag{C10}$$

Thus we could obtain the final equation (3.87) in the text.

Appendix D

Derivation of Eq.(3.94) from Eq.(2.136)

As seen in the Appendix A, the growth rate is expressed by Eq.(A55), i.e.,

$$\gamma_k = - \frac{\sum_s \frac{\pi^2 \Pi_s^2}{|k| N_s} \left[2H_{s1}(V_R) + \frac{k}{\omega_r} H_{s2}(V_R) \right]}{2 - \sum_s \frac{\varepsilon_s \Omega_s \Pi_s^2}{\omega_r (\omega_r + \varepsilon_s \Omega_s)^2}} \ . \tag{D1}$$

If we neglect the ion contribution and dropping the subscript k,

$$\gamma = - \frac{\frac{\pi^2 \Pi_e^2}{|k| N_e} \left[2H_{e1}(V_R) + \frac{k}{\omega_r} H_{e2}(V_R) \right]}{2 + \frac{\Omega_e \Pi_e^2}{\omega_r (\omega_r - \Omega_e)^2}} \ , \tag{D2}$$

where, from Eq.(A58)

$$H_{e1}(V_R) + \frac{k}{\omega_r} H_{e2}(V_R)$$

$$= 2\int_0^\infty V_\perp g_e(V_\perp, V_z = V_R) dV_\perp + \frac{kV_R}{\omega_r} \int_0^\infty V_\perp dV_\perp \frac{V_\perp}{V_z} \left(V_z \frac{\partial g_e}{\partial V_\perp} - V_\perp \frac{\partial g_e}{\partial V_z} \right) \Big|_{V_z = V_R} \ . \tag{D3}$$

Introducing a pitch angle α as

$$\tan \alpha = \frac{V_\perp}{V_z} \ , \tag{D4}$$

we know

$$\frac{\partial g_e}{\partial \alpha} = \frac{\partial g_e}{\partial V_z}\frac{\partial V_z}{\partial \alpha} + \frac{\partial g_e}{\partial V_\perp}\frac{\partial V_\perp}{\partial \alpha} = |V|\{-\sin\alpha\frac{\partial g_e}{\partial V_z} + \cos\alpha\frac{\partial g_e}{\partial V_\perp}\} = V_z\frac{\partial g_e}{\partial V_\perp} - V_\perp\frac{\partial g_e}{\partial V_z} \ . \tag{D5}$$

Therefore

$$H_{e1}(V_R) + \frac{k}{\omega_r}H_{e2}(V_R) =$$

$$2\int_0^\infty V_\perp g_e(V_\perp, V_z=V_R)dV_\perp + \frac{\omega_r-\Omega_e}{\omega_r}\int_0^\infty V_\perp dV_\perp \tan\alpha \left.\frac{\partial g_e}{\partial \alpha}\right|_{V_z=V_R} \ . \tag{D6}$$

Under the assumption that $\omega_r << \Omega_e$, the first term in the denominator of Eq.(D2) can well be neglected. Substituting Eq.(D6) into Eq.(D2), we get

$$\gamma = -\frac{\omega_r(\omega_r-\Omega_e)^2}{|k|N_e\Omega_e} \times 2\int_0^\infty V_\perp g_e dV_\perp [\ 1 + \frac{\omega_r-\Omega_e}{\omega_r}A_p\ ]$$

$$= \pi\Omega_e(1-\frac{\omega_r}{\Omega_e})^2 \cdot 2\pi\frac{\Omega_e-\omega_r}{|k|N_e}\int_0^\infty V_\perp g_e dV_\perp [\ A_p - \frac{\omega_r}{\Omega_e-\omega_r}\ ] \ , \tag{D7}$$

where

$$A_p = \frac{\int_0^\infty V_\perp dV_\perp \tan\alpha \dfrac{\partial g_e}{\partial \alpha}}{2\int_0^\infty V_\perp dV_\perp g_e} \ . \tag{D8}$$

Appendix E

Derivation of Nonlinear Equations of Motion in both Laboratory and Wave Frames

In this appendix, a basic equation is given in both lab. and wave frames. Quantities in the wave frame are represented with primes, while those in the lab. frame are expressed without primes.

Nonlinear equation of motion of electrons in the purely transverse electromagnetic (TEM) wave is written as

$$\frac{d\vec{V}}{dt} = -\frac{e}{m}\left(\vec{E}_w + \vec{V}\times\vec{B}_w + \vec{V}\times\vec{B}_o\right) , \tag{E1}$$

where $\vec{E}_w$ and $\vec{B}_w$ are the electric and magnetic field vectors of TEM wave (see Fig.E1). In the wave frame, which moves along $\hat{z}$-axis with the wave phase velocity, quantities are transformed by the Lorentz transformation as

$$\left.\begin{aligned} V'_x &= V_x , \\ V'_y &= V_y , \\ V'_z &= V_z - V_{ph} , \\ x' &= x , \\ y' &= y , \\ z' &= z - V_{ph}t , \\ t' &= t , \\ m' &= m , \\ e' &= e , \\ B'_o &= B_o , \end{aligned}\right\} \tag{E2}$$

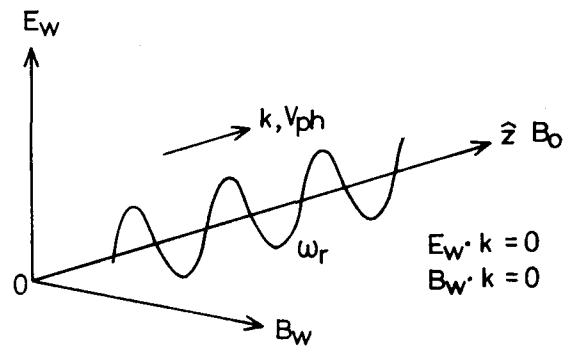

Fig.E1 Situation of a Wave Propagation (Lab. Frame)

if the relativistic effects are neglected. As for the wave fields, the Lorentz transformation gives

$$\vec{E}'_w = \gamma_o\left(\vec{E}_w + \vec{V}_{ph}\times\vec{B}_w\right) , \tag{E3}$$

$$\vec{B}'_w = \gamma_o\left(\vec{B}_w - \frac{\vec{V}_{ph}\times\vec{E}_w}{c^2}\right) , \tag{E4}$$

where

$$\gamma_o = (1-\beta^2)^{-\frac{1}{2}} \quad ; \quad \beta = \frac{V_{ph}}{c} \ . \tag{E5}$$

In case of a monochromatic wave, there exists the following relation

$$\vec{B}_w = \frac{\vec{V}_{ph} \times \vec{E}_w}{V_{ph}^2} \ . \tag{E6}$$

Substituting Eq.(E6) into Eq.(E3), we can show

$$\vec{E}'_w = \gamma_o (\vec{E}_w - \vec{E}_w) = 0 \ . \tag{E7}$$

Furthermore, in the case of a whistler mode wave, the phase velocity is much smaller than c so that the relativistic effects can be well neglected. Replacing γ_o by unity, Eq.(E4) becomes

$$\vec{B}'_w = \vec{B}_w \ . \tag{E8}$$

Thus the nonlinear equation of motion in the <u>wave</u> frame is simply written as

$$\frac{d\vec{V}'}{dt'} = - \frac{e'}{m'} (\vec{V}' \times \vec{B}'_w + \vec{V}' \times \vec{B}_o) \ . \tag{E9}$$

It should be noticed that $\vec{B}'_w$ is a static magnetic field vector with a helical structure in the wave frame. This is easily understood by

$$\begin{aligned} \vec{B}'_w(z',t') &= \vec{B}_w(z,t) \equiv \hat{\vec{B}}_w \, e^{j(\omega_r t - kz)} \\ &= \hat{\vec{B}}'_w \, e^{j\{\omega'_r t' - k'(z' + V_{ph} t')\}} \\ &= \hat{\vec{B}}'_w \, e^{-jk'z'} \ , \end{aligned} \tag{E10}$$

$$\therefore \quad \frac{\partial \vec{B}'_w}{\partial t'} = 0 \ . \tag{E11}$$

A relation between the wave and the laboratory frames is schematically shown in Fig.E2.

We will show below the representations of the equation of motion Eq.(E1) and Eq.(E9) expressed by components in a cylindrical coordinate.

A configuration of the field and velocity vectors in the perpen-

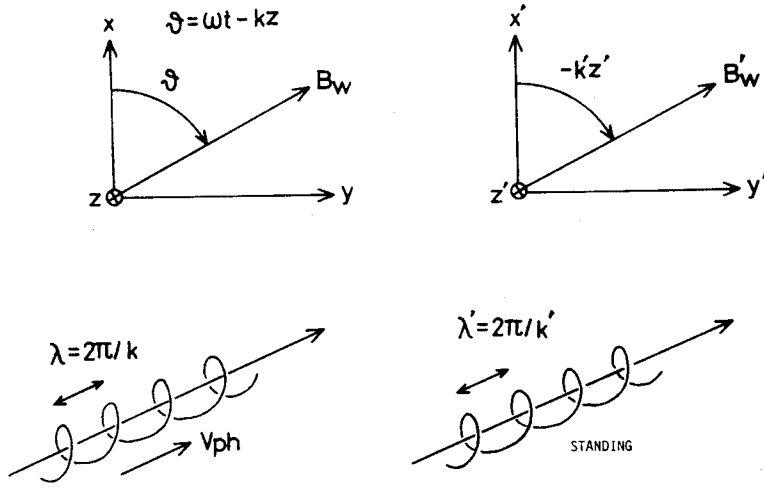

(a) Lab. Frame (b) Wave Frame

Fig.E2 A schematic illustration of a wave structure in the lab. and wave frames. Helices in the figure show the loci of the tip of the magnetic field vector of the wave.

dicular plane to $\vec{B}_o$ is given in Fig.E3 for Lab. frame. From this figure,

$$\left.\begin{aligned}
&\vec{E}_w = E_w \cos(\phi - \tfrac{\pi}{2})\hat{r} - E_w \sin(\phi - \tfrac{\pi}{2})\hat{\theta} \\
&\quad = E_w \sin\phi\ \hat{r} + E_w \cos\phi\ \hat{\theta}\ , \\
&\vec{V}_z \times \vec{B}_w = -V_z B_w \sin\phi\ \hat{r} - V_z B_w \cos\phi\ \hat{\theta}\ , \\
&\vec{V}_\perp \times \vec{B}_o = -V_\perp B_o\ \hat{\theta}\ , \\
&\vec{V}_\perp \times \vec{B}_w = V_\perp B_w \sin(\pi-\phi)\hat{z} = V_\perp B_w \sin\phi\ \hat{z}\ .
\end{aligned}\right\} \qquad \text{(E12)}$$

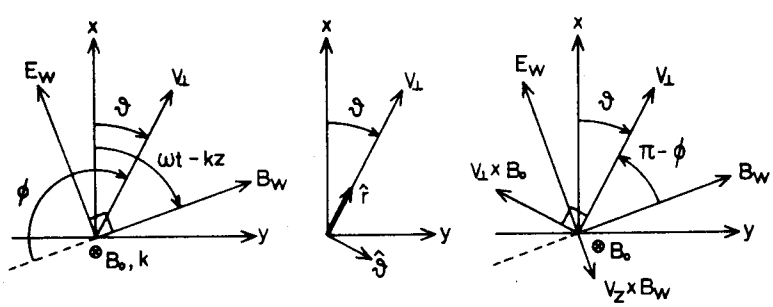

$$\phi + (\omega t - kz - \theta) = 2\pi \qquad d\vec{V}_\perp = dV_\perp \hat{r} + V_\perp d\theta \hat{\theta}$$

Fig.E3 Configuration of the field and velocity Vectors in the Lab. Frame

Therefore

$$\frac{dV_\perp}{dt} = -\frac{e}{m}\left(E_w - V_z B_w\right)\sin\phi \quad , \tag{E13}$$

$$\frac{dV_z}{dt} = -\frac{e}{m} V_\perp B_w \sin\phi \quad , \tag{E14}$$

$$V_\perp \frac{d\theta}{dt} = -\frac{e}{m}\left[\left(E_w - V_z B_w\right)\cos\phi - V_\perp B_o\right] \quad . \tag{E15}$$

While there is a relation

$$\theta = \phi + \omega t - kz - 2\pi \quad , \tag{E16}$$

we get

$$\frac{d\theta}{dt} = \frac{d\phi}{dt} + \omega - kV_z \quad . \tag{E17}$$

Substituting (E17) into (E15)

$$\frac{d\phi}{dt} = -\frac{e}{mV_\perp}\left[\left(E_w - V_z B_w\right)\cos\phi - V_\perp B_o\right] - \omega + kV_z \quad . \tag{E18}$$

Noting

$$B_w = \frac{k}{\omega} E_w \quad , \tag{E19}$$

the basic set of equations in the lab. frame are written as

$$\frac{dV_\perp}{dt} = -\frac{eE_w}{m}\left(1 - \frac{V_z}{V_{ph}}\right)\sin\phi \quad , \tag{E20}$$

$$\frac{dV_z}{dt} = -\frac{eE_w}{m}\frac{V_\perp}{V_{ph}}\sin\phi \quad , \tag{E21}$$

$$\frac{d\phi}{dt} = -\left(\omega - kV_z - \Omega_e\right) - \frac{eE_w}{m}\left(1 - \frac{V_z}{V_{ph}}\right)\frac{\cos\phi}{V_\perp} \quad . \tag{E22}$$

In the wave frame, a configuration of the field and velocity vectors is much simpler and illustrated in Fig.E4. In this circumstance,

$$\begin{aligned} \vec{V}'_\perp \times \vec{B}'_o &= -V'_\perp B'_o \hat{\theta}' \quad , \\ \vec{V}'_z \times \vec{B}'_w &= V'_z B'_w \sin\zeta' \hat{r}' + V'_z B'_w \cos\zeta' \hat{\theta}' \quad , \\ \vec{V}'_\perp \times \vec{B}'_w &= -V'_\perp B'_w \sin\zeta' \hat{z}' \quad . \end{aligned} \tag{E23}$$

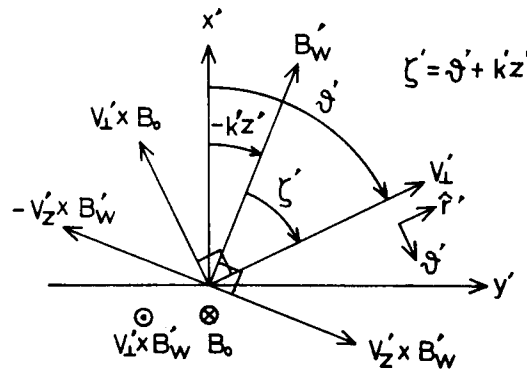

Fig.E4 Configuration of the field and velocity vectors in the wave frame.

Therefore

$$\frac{dV'_\perp}{dt'} = -\frac{e'}{m'} V'_z B'_w \sin\zeta' = -\Omega'_l V'_z \sin\zeta' \quad , \tag{E24}$$

$$\frac{dV'_z}{dt'} = \frac{e'}{m'} V'_\perp B'_w \sin\zeta' = \Omega'_l V'_\perp \sin\zeta' \quad , \tag{E25}$$

$$\frac{d\theta'}{dt'} = -\frac{e'}{m'V'_\perp} (V'_z B'_w \cos\zeta' - V'_\perp B'_o) = \Omega'_e - \frac{V'_z}{V'_\perp} \Omega'_l \cos\zeta' \quad , \tag{E26}$$

while

$$\frac{d\theta'}{dt'} = \frac{d\zeta'}{dt'} - k'\frac{dz'}{dt'} = \frac{d\zeta'}{dt'} - k'V'_z \quad . \tag{E27}$$

From Eqs.(E26) and (E27),

$$\frac{d\zeta'}{dt'} = \Omega'_e + k'V'_z - \Omega'_l V'_z \frac{\cos\zeta'}{V'_\perp} \quad . \tag{E28}$$

Eqs.(E24), (E25) and (E28) are the basic nonlinear set of equations of motion in the wave frame.

REFERENCES

1. King, J. W. and W. S. Newman (ed.), Solar-Terrestrial Physics, Academic Press, 1967.

2. Carovillano, R. L., J. F. McClay and H. R. Radoski (ed.), Physics of the Magnetosphere, D. Reidel Publ. Co., 1967.

3. Williams, D. J. and G. D. Mead (ed.), Magnetospheric Physics, Williams Byrd Press, 1968.

4. McCormac, B. M. (ed.), Particles and Fields in the Magnetosphere, D. Reidel Publ. Co., 1969.

5. Obayashi, T., Space Science —— Solar Terrestrial Physics —— (in Japanese), Shokabo, Tokyo, 1970.

6. Ness, N. F., Solar Wind-Geomagnetic Field Interaction: Quiet Conditions, Chapt.III in Solar-Terrestrial Physics, Ed. King, J.W. and W.S. Newman, Academic Press, 1967.

7. Fairfield, D. H., Average Magnetic Field Configuration of the Outer Magnetosphere, J. Geophys. Res. 73, 7329-7338, 1968.

8. Helliwell, R. A., Whistlers and Related Ionospheric Phenomena, Stanford Univ. Press, Stanford, 1965.

9. McIlwain, C. E., Coordinates for Mapping the Distribution of Magnetically Trapped Particles, J. Geophys. Res. 66, 3681-3691, 1961.

10. Carpenter, D. L., Whistler Evidence of a "Knee" in the Magnetospheric Ionization Density Profile, J. Geophys. Res. 68, 1675-1682, 1963.

11. Angerami, J. J. and D. L. Carpenter, Whistler Studies of the Plasmapause in the Magnetosphere; 2. Electron Density and Total Tube Electron Content near the Knee in the Magnetospheric Ionization, J. Geophys. Res. 71, 711-725, 1966.

12. Carpenter, D. L., Whistler Studies of the Plasmapause in the Magnetosphere: 1. Temporal Variation in the Position of the Knee and Some Evidence on Plasma Motion near the Knee, J. Geophys. Res. 71, 693-709, 1966.

13. Smith, R. L., Properties of the Outer Ionosphere Deduced from Nose Whistlers, J. Geophys. Res. 66, 3709-3716, 1961.

14. Angerami, J. J., A Whistler Study of the Distribution of Thermal Electrons in the Magnetosphere, Tech. Rept. No.3412-7, Stanford Univ., Stanford, Calif., 1966.

15. Harris, K. K., G. W. Sharp and C. R. Chapell, Observation of the Plasmapause from OGO-5, J. Geophys. Res. 75, 219-224, 1970.

16. Gringauz, K. I., Rocket and Satellite Measurements of Ionospheric and Magnetospheric Particle Temperature, Chapt.X in Solar-Terrestrial Physics, Ed. King, J.W. and W.S. Newman, Academic Press, 1967.

17. Evans, J. V., Ground-Based Measurements of Atmospheric and Ionospheric Particle Temperatures, Chapt.IX in Solar-Terrestrial Physics, Ed. King, J.W. and W.S. Newman, Academic Press, 1967.

18. Serbu, G. P. and E. J. R. Maier, Observation from OGO-5 of the Thermal Ion Density and Temperature within the Magnetosphere, J. Geophys. Res. 75, 6102-6113, 1970.

19. Serbu, G. P. and E. J. R. Maier, Low Energy Electrons Measured on IMP2, J. Geophys. Res. 71, 3755-3766, 1966.

20. O'Brien, B. J., Energetic Charged Particles in the Magnetosphere, Chapt.VI in Solar-Terrestrial Physics,Ed. King, J.W. and W.S. Newman, Academic Press, 1967.

21. Hess, W. N., The Radiation Belt and Magnetosphere, Blaisdel Publ. Co., Waltham, Mass., 1968.

22. Schield, M. A. and L. A. Frank, Electron Observation between the Inner Edge of the Plasmasheet and the Plasmasphere, J. Geophys. Res. 75, 5401-5414, 1970.

23. Frank, L. A., Relation of the Plasmasheet, Ring Current, Trapping Boundary and Plasmapause near the Magnetic Equator and Local Midnight, J. Geophys. Res. 76, 2265-2275, 1971.

24. Nicholet, M., Collision Frequency of Electrons in the Terrestrial Atmosphere, Phys. Fluids 2, 95-99, 1959.

25. Stix, T. H., The Theory of Plasma Waves, McGraw-Hill Co. Inc., New York, 1962.

26. Kimura, I., On Observation and Theories of the VLF Emissions, Planet. Space Sci. 15, 1427-1462, 1967.

27. Matsumoto, T., Quasilinear Cyclotron Instability of Whistler Mode Waves in the Magnetospheric Plasma, Master Thesis (supervised by Profs. K. Maeda and I. Kimura), Kyoto Univ., Kyoto, Japan, 1970.

28. Carpenter, D. L., Ducted Whistler-Mode Propagation in the Magnetosphere: A Half Gyrofrequency Upper Intensity Cutoff and Some Associated Wave Growth Phenomena, J. Geophys. Res. 73, 2919-2928, 1968.

29. Helliwell, R. A., A Theory of Discrete VLF Emissions from the Magnetosphere, J. Geophys. Res. 72, 4773-4790, 1967.

30. Matsumoto, H. and S. Miyatake and I. Kimura, Convective Beam Cyclotron Instability and Discrete VLF Emissions in the Magnetosphere, Rept. Ionos. Space Res. Japan 24, 207-221, 1970.

31. Kimura, I., Triggerings of VLF Magnetospheric Noise by a Low Power (∿100 W) Transmitter, J. Geophys. Res. 73, 445-447, 1968.

32. Kimura, I., Amplification of the VLF Electromagnetic Wave by a Proton Beam through the Exosphere —— an Origin of the VLF Emissions ——, Rept. Ionos. Space Res. Japan 15, 171-191, 1961.

33. Neufeld, J. and H. Wright, Instabilities in a Plasma-Beam System Immersed in a Magnetic Field, Phys. Rev. 129, 1489-1507, 1963.

34. Neufeld, J. and H. Wright, Interaction of a Plasma with a "Helical" Electron Beam, ibid 135, A1175-A1189, 1964.

35. Neufeld, J. and H. Wright, Instabilities Produced in a Stationary Plasma by an "Almost Circular Electron Beam", ibid 137, A1076-A1086, 1965.

36. Gendrin, R., Gyroresonance Radiation Produced by Proton and Electron Beams in Different Regions of Magnetosphere, J. Geophys. Res. 70, 5369-5383, 1965.

37. Kimura, I. amd H. Matsumoto, Hydromagnetic Wave Instabilities in a Nonneutral Plasma-Beam System, Radio Sci. 3, 333-343, 1968.

38. Brice, N. M., Discrete VLF Emissions from the Upper Atmosphere, Tech. Rept. No.3412-6, Stanford Univ., Stanford, Calif., 1964.

39. Brice, N. M., An Explanation of Triggered VLF Emissions, J. Geophys. Res. 68, 4626-4628, 1963.

40. Bell, T. and O. Buneman, Plasma Instability in the Whistler Mode Caused by a Gyrating Electron Stream, Phys. Rev. 133, A1300-A1302, 1964.

41. Bell, T., Wave-Particle Gyroresonance Interaction in the Earth's Outer Ionosphere, Tech. Rept. No.3412-5, Stanford Univ., Stanford, Calif., 1964.

42. Kennel, C. F. and H. E. Petschek,Limit on Stably Trapped Particle Fluxes, J. Geophys. Res. 71, 1-28, 1966.

43. Briggs, R. J., Electron Stream Interaction with Plasmas, Research Monograph No.29, M.I.T. Press, 1964.

44. Drummond, W. E. and D. Pines, Nonlinear Stability of Plasma Oscillations, Nucl. Fusion 2, 1049-1057, 1962.

45. Das, A. C., A Mechanism of VLF Emissions, J. Geophys. Res. 73, 7457-7471, 1968.

46. Sudan, R. N. and E. Otto, Theory of Triggered VLF Emissions, J. Geophys. Res. 76, 4463-4476, 1971.

47. Dysthe, K. B., Some Studies of Triggered Whistler Emissions, J. Geophys. Res. 76, 6915-6931, 1971.

48. Nunn, D., A Theory of VLF Emissions, Planet. Space Sci. 19, 1141-1167, 1971.

49. Brinca, A. L., Whistler Side Band Growth due to Nonlinear Wave-Particle Interaction, J. Geophys. Res. 77, 3508-3523, 1972.

50. Matsumoto, H. and I. Kimura, Linear and Nonlinear Cyclotron Instability and VLF Emissions in the Magnetosphere, Planet. Space Sci. 19, 567-608, 1971.

51. Yamazaki, Y., A Theoretical Study on the Responses in Real Space and Time in the Cyclotron Instability (in Japanese), Master Thesis (supervised by Profs. K. Maeda and I Kimura), Kyoto Univ., Kyoto, Japan, 1972.

52. Matsumoto, H., I. Kimura and Y. Yamazaki, Wave Propagation Velocity in the Abnormally Dispersive and Unstable Media, to be published.

53. Matsumoto, H. and I. Kimura, A Note on a Generation Mechanism of Background Hiss of Polar Chorus, Rept. Ionos. Space Res. Japan 24, 223-228, 1970.

54. Matsumoto, H., K. Hashimoto and I. Kimura, Phase Bunching and Resonant Current in the Nonlinear Whistler Mode Interaction, to be published.

55. Scarf, F. L., Landau Damping and Attenuation of Whistlers, Phys. Fluids 5, 6-13, 1962.

56. Liemohn, H. B. and F. L. Scarf, Exospheric Electron Temperatures from Nose Whistler Attenuation, J. Geophys. Res. 67, 1785-1789, 1962.

57. Guthart, H., An Anisotropic Electron Velocity Distribution for the Cyclotron Absorption of Whistlers and VLF Emissions, Radio Sci. 69D, 1403-1415, 1965.

58. Kimura, I., A Review of Theoretical Studies on VLF Emissions, Progress in Radio Science 1960-1963 4, 85-90, 1965.

59. Terashima, Y., Particle Aspect Analyses of Electromagnetic and Electrostatic Instabilities due to Anisotropic Velocity Distributions, Prog. Theor. Phys. 37, 661-681, 1967.

60. Lutomirski, R. F., Physical Model of Cyclotron Damping, Phys. Fluids 13, 149-153, 1970.

61. Hollweg, J.V. and H. J. Völk, Energy and Momentum Exchange in Transverse Plasma Waves, J. Geophys. Res. 76,7527-7541, 1971.

62. Kawai, M., A Basic Theoretical Study of the Cyclotron Type Wave-Particle Interaction, Graduate Thesis (in Japanese),(supervised by Prof. I. Kimura), Kyoto Univ., Kyoto, Japan, 1972.

63. Sturrock, P. A., Kinematics of Growing Waves, Phys. Rev. 112, 1488-1503, 1958.

64. Polovin, R. V., Criteria for Instability and Gain, Soviet Phys. Tech. Phys. 6, 889-895, 1962.

65. Gallet,R. M. and R. A. Helliwell, Origin of "Very-Low-Frequency" Emissions, J. Res. NBS 63D, 21-27, 1959.

66. Dowden, R. L., Doppler-Shifted Cyclotron Radiation from Electrons: A Theory of Very Low Frequency Emissions from the Exosphere, J. Geophys. Res. 67, 1745-1750, 1959.

67. Rayleigh, B., On the Velocity of Light, in Scientific Papers, ed. by J.W. Strutt, Cambridge Univ. Press, 537-540, 1899.

68. Sommerfeld, A., Über die Fortpflanzung des Lichtes in Dispergierenden Medien, Ann. Physik 44, 177-202, 1964.

69. Brillouin, L., Über die Fortpflanzung des Lichtes in Dispergierenden Medien, Ann. Physik 44, 203-240, 1914.

70. Brillouin, L., Wave Propagation and Group Velocity, Academic Press, New York and London, 1960.

71. Hines, C. O., Wave Packets, the Poynting Vector, and Energy Flow: Part I —Nondissipative (Anisotropic) Homogeneous Media, J. Geophys. Res. 56, 63-72, 1951.

72. Hines, C. O., Wave Packets, the Poynting Vector, and Energy Flow: Part II — Group Propagation through Dissipative Isotropic Media, J. Geophys. Res. 56, 197-206, 1951.

73. Hines, C. O., Wave Packets, the Poynting Vector, and Energy Flow: Part III — Packet Propagation through Dissipative Anisotropic Media, J. Geophys. Res. 56, 207-220, 1951.

74. Hines, C. O., Wave Packets, the Poynting Vector, and Energy Flow: Part IV — Poynting and Mcdonald Velocities in Dissipative Anisotropic Media (Conclusion),J. Geophys. Res. 56, 535-544, 1951.

75. Fried, B. D. and S. D. Conte, The Plasma Dispersion Functions, Academic Press, New York, 1961.

76. Scharer, J. E. and A. W. Trivelpiece, Cyclotron Wave Instabilities in a Plasma, Phys. Fluids 10, 591-595, 1967.

77. Sudan, R. N., Plasma Electromagnetic Instabilities, Phys. Fluids 6, 57-61, 1963.

78. Kennel, C. F., Low Frequency Whislter Mode, Phys. Fluids 9, 2190-2202, 1966.

79. Vasyliunas, V. H., A Survey of Low Energy Electrons in the Evening Sectors of the Magnetosphere with OGO-1 and OGO-3, J. Geophys. Res. 73, 2839-2884, 1968.

80. Cornwall, J. M., Cyclotron Instabilities and Electromagnetic Emission in the Ultra-Low Frequency and Very Low Frequency Ranges, J. Geophys. Res. 70, 61-69, 1965.

81. Hultquvist, B., On the Amplification of ELF Emissions by Charged Particles in the Exosphere, with Special Reference to the Frequency Band around Proton Cyclotron Frequency, Planet. Space Sci. 13, 391-401, 1965.

82. Sagalyn, R. C. and M. Smiddy, Electrical Processes in the Nighttime Exosphere, J. Geophys. Res. 69, 1809-1823, 1964.

83. Smith, R. L., The Use of Nose Whistler in the Study of the Outer Ionosphere, Tech. Rept. No.6, Stanford Univ., Stanford, Calif., 1960.

84. Smith, R. L., Propagation Characteristics of Whistlers Trapped in Field-Aligned Columns of Enhanced Radiation, J. Geophys. Res. 66, 3699-3707, 1961.

85. Harker, K.J. and F. W. Crawford, Nonlinear Interaction between Whistlers, J. Geophys. Res. 74, 5029-5040, 1969.

86. Kadomtsev, B. B., Plasma Turbulence, Academic Press, New York, 1965.

87. Vedenov, A. A., E. P. Velikov and R. Z. Sagdeev, Quasilinear Theory of Plasma Oscillations, Nucl. Fusion Suppl. 2, 465-475, 1962.

88. Shapiro, V. D. and V. I. Schevchenko, The Nonlinear Theory of Interaction between Charged Particle Beams and a Plasma in a Magnetic Field, Soviet Phys. JETP 15, 1053-1061, 1962.

89. Shapiro, V. D. and V. I. Shevchenko, Quasilinear Theory of Instability of a Plasma with an Anisotropic Ion Velocity Distribution, Soviet Phys. JETP 18, 1109-1116, 1964.

90. Andronov, A. A. and V. Yu. Trakhtengerz, Instability of One-Dimensional Packets and Absorption of Electromagnetic Waves in a Plasma, Soviet Phys. JETP 18, 698-702, 1964.

91. Bass, F. G., Yu. B. Fainberg and V. D. Shapiro, Quasilinear Theory of a Weakly Turbulent Plasma with Account of Electric Fields, Soviet Phys. JETP 22, 230-233, 1966.

92. Kennel, C. F. and F. Engelman, Velocity Space Diffusion from Weak Plasma Turbulence in a Magnetic Field, Phys. Fluids 9, 2377-2388, 1966.

93. Watanabe, T., Quasilinear Theory of Transverse Plasma Instabilities with Applications to Hydromagnetic Emissions from the Magnetosphere, Can. J. Phys. 44, 815-835, 1966.

94. Sizonenko, V.L. and K. N. Stepanov, Quasilinear Theory of Cerenkov and Cyclotron Damping of Electromagnetic Waves in a Plasma, Soviet Phys. JETP 24, 572-577, 1967.

95. Lerche, I., Quasilinear Theory of Resonant Diffusion in a Magneto-active, Relativistic Plasma, Phys. Fluids 11, 1720-1727, 1968.

96. Wu, C. S., Unified Quasilinear Theory of Weakly Turbulent Plasmas, Phys. Fluids 11, 1733-1744, 1968.

97. Momota, H. and Y. Terashima, Enhanced Particle Losses due to Electron Cyclotron Wave Instability in a Magnetic Mirrors, Nagoya Univ., Japan Res. Rept. No. IPPJ-79, 1968.

98. Engel, R. D., Nonlinear Stability of Extraordinary Wave in a Plasma, Phys. Fluids 8, 939-950, 1965.

99. Rowlands, J., V. D. Shapiro and V. I. Shevchenko, Quasilinear Theory of Plasma Cyclotron Instability, Soviet Phys. JETP 23, 651-660, 1966.

100. Sagdeev, R. S. and A. A. Galeev, Nonlinear Plasma Theory, Revised and Edited by T.M. O'Neil and D.L. Book, Benjamin, New York, 1969.

101. Sato, T., Comments on "Modification of the Quasilinear Theory by Spontaneous Emission of Plasma Waves", Phys. Fluids 13, 3059-3061, 1970.

102. Mead, G. D., Deformation of the Geomagnetic Field by the Solar Wind, J. Geophys. Res. 69, 1181-1195, 1964.

103. Hartz, T. R. and N. M. Brice, The General Pattern of Auroral Particle Precipitation, Planet. Space Sci. 15, 301-329, 1967.

104. Brice, N.M., VLF Radiation and Polar Substorm, Space Res.VIII, 293-302, 1968.

105. Morozumi, H. M. and R. A. Helliwell, A Correlation Study of the Diurnal Variation of Upper Atmosphere Phenomena in the Southern Auroral Zone, Science Rept. No.2, Radio Sci. Labs., Stanford Univ., Stanford, Calif., 1966.

106. O'Neil, T. M., Collisionless Damping of Nonlinear Plasma Oscillations, Phys. Fluids 8, 2255-2262, 1965.

107. Al'tsul, L. M. and V. I. Karpman, Theory of Nonlinear Oscillations in a Collisionless Plasma, Soviet Phys. JETP 22, 361-369, 1966.

108. Roberts, C. S. and S. J. Buchsbaum, Motion of Charged Particle in a Constant Magnetic Field and a Transverse Electromagnetic Wave Propagating along the Field, Phys. Rev. 135, A381-A389, 1964.

109. Laird, M.J. and F. B. Knox, Exact Solution for Charged Particle Trajectories in a Electromagnetic Field, Phys. Fluids 8, 755-756, 1965.

110. Lutomirski, R. F. and R. N. Sudan, Exact Nonlinear Electromagnetic Whistler Modes, Phys. Rev. 147, 156-165, 1966.

111. Mamiya, K., Theory and Experiment on Wave-Particle Interaction in the Whistler Mode, Master Thesis (supervised by Profs. K. Maeda and I, Kimura), Kyoto Univ., Kyoto, Japan, 1969.

112. Dungey, J. W., The Motion of a Charged Particle in the Field of a Whistler Mode Wave Packet, Plasma Waves in Space and in the Laboratory Ed. Thomas and Landmark, vol.1, 407-415, 1969.

113. Ashour-Abdalla, M., Nonlinear Particle Trajectories in a Whistler Wave Packet, Planet. Space Sci. 18, 1799-1812, 1970.

114. Hashimoto, K., A Study on the Nonlinear Interaction between a Whistler Mode Wave and Electron Stream (in Japanese), Master Thesis (supervised by Profs. K. Maeda and I. Kimura), Kyoto Univ., Kyoto, Japan, 1971.

115. Kimura, I., H. Matsumoto and S. Miyatake, A Cyclotron Instability Experiment in Space by the Japanese Scientific Satellite REXS., to be published.

116. Matsumoto, H., I. Kimura and K. Mamiya, Laboratory Simulation Experiment on the Wave-Particle Interaction in the Electromagnetic Mode in the Magnetosphere, Proceedings of Simposium on Space Observations (in Japanese), 162-171, 1968.

117. Hashimoto, K., H. Matsumoto, I. Kimura and N. Kawashima, Simulation Experiment on VLF Triggered Emissions , Proceedings of Simposium on Space Plasma (in Japanese), 1971.

118, Itatani, R., private communication.